OPTIMAL STEERING FOR KINEMATIC VEHICLES WITH APPLICATIONS TO SPATIALLY DISTRIBUTED AGENTS

A Thesis
Presented to
The Academic Faculty

by

Efstathios Bakolas

In Partial Fulfillment
of the Requirements for the Degree
Doctor of Philosophy in the
School of Aerospace Engineering

Georgia Institute of Technology
December 2011

OPTIMAL STEERING FOR KINEMATIC VEHICLES WITH APPLICATIONS TO SPATIALLY DISTRIBUTED AGENTS

Approved by:

Professor Panagiotis Tsiotras,
Committee Chair
School of Aerospace Engineering
Georgia Institute of Technology

Professor Panagiotis Tsiotras, Adviser
School of Aerospace Engineering
Georgia Institute of Technology

Professor Eric Feron
School of Aerospace Engineering
Georgia Institute of Technology

Professor Wassim W. Haddad
School of Aerospace Engineering
Georgia Institute of Technology

Professor Magnus Egerstedt
(ECE Department)
School of Aerospace Engineering
Georgia Institute of Technology

Professor Jeff S. Shamma
(ECE Department)
School of Aerospace Engineering
Georgia Institute of Technology

Date Approved: 9 November 2011

To my parents and my brother.

ACKNOWLEDGEMENTS

I would like to express my deepest gratitude to my advisor Dr. P. Tsiotras for his guidance during my PhD studies. I would also like to express my sincere appreciation to Dr. W. M. Haddad, Dr. E. M. Feron, Dr. J. S. Shamma, and Dr. M. Egerstedt, members of my PhD Disseration committee, for their true interest in evaluating my work.

Furthermore, the financial support by the A. Onassis Public Benefit Foundation, and NASA is gratefully appreciated.

Finally, I owe the greatest debt of gratitude to my parents and my brother for the moral and emotional support during my graduate studies. I dedicate this work to them as a token of appreciation.

TABLE OF CONTENTS

LIST OF FIGURES

SUMMARY

The recent technological advances in the field of autonomous vehicles have resulted in a growing impetus for researchers to improve the current framework of mission planning and execution within both the military and civilian contexts. Many recent efforts towards this direction emphasize the importance of replacing the so-called *monolithic paradigm*, where a mission is planned, monitored, and controlled by a unique global decision maker, with a *network centric paradigm*, where the same mission related tasks are performed by networks of interacting decision makers (autonomous vehicles). In particular, it has been proposed that for a large spectrum of applications, ranging from environmental monitoring, search and rescue operations, distributed surveillance, resource allocation, and tracking of multiple targets, just to mention a few, the use of networks of autonomous vehicles can improve the flexibility and efficiency during the design and execution phases of a mission beyond of what can be achieved using standard, centralized approaches. In this new network-centric paradigm, the vehicles of the network are not constrained to work in isolation but rather, they act as elements in a complex, often spatially distributed network, working in unison by exchanging information to plan and execute a common mission. The interest in applications involving teams of autonomous vehicles is expected to significantly grow in the near future as new paradigms for their use are constantly being proposed for a diverse spectrum of real world applications.

While there is no universal method to address control problems involving networks of autonomous vehicles, there exist a few promising schemes that apply to different specific classes of problems, which have attracted the attention of many researchers from different fields. In particular, one way to extend techniques that

address problems involving a single autonomous vehicle to those involving teams of autonomous vehicles is to use the concept of Voronoi diagram. The Voronoi diagram provides a spatial partition of the environment the team of vehicles operate in, where each element of this partition is associated with a unique vehicle from the team. The partition induces a graph abstraction of the operating space that is in an one-to-one correspondence with the network abstraction of the team of autonomous vehicles; a fact that can provide both conceptual and analytical advantages during mission planning and execution. In this dissertation, we propose the use of a new class of Voronoi-like partitioning schemes with respect to state-dependent proximity (pseudo-) metrics rather than the Euclidean distance or other generalized distance functions, which are typically used in the literature. An important nuance here is that, in contrast to the Euclidean distance, state-dependent metrics can succinctly capture system theoretic features of each vehicle from the team (e.g., vehicle kinematics), as well as the environment-vehicle interactions, which are induced, for example, by local winds/currents. We subsequently illustrate how the proposed concept of state-dependent Voronoi-like partition can induce local control schemes for problems involving networks of spatially distributed autonomous vehicles by examining a sequential pursuit problem of a maneuvering target by a group of pursuers distributed in the plane.

The construction of generalized Voronoi diagrams with respect to state-dependent metrics poses some significant challenges. First, the generalized distance metric may be a function of the direction of motion of the vehicle (anisotropic pseudo-distance function) and/or may not be expressible in closed form. Second, such problems fall under the general class of partitioning problems for which the vehicles' dynamics must be taken into account. The topology of the vehicle's configuration space may be non-Euclidean, for example, it may be a manifold embedded in a Euclidean space. In other words, these problems may not be reducible to generalized Voronoi diagram

problems for which efficient construction schemes, analytical and/or computational, exist in the literature.

This research effort pursues three main objectives. First, we present the complete solution of different steering problems involving a single vehicle in the presence of motion constraints imposed by the maneuverability envelope of the vehicle and/or the presence of a drift field induced by winds/currents in its vicinity. The analysis of each steering problem involving a single vehicle provides us with a state-dependent generalized metric, such as the minimum time-to-go/come. We subsequently use these state-dependent generalized distance functions as the proximity metrics in the formulation of generalized Voronoi-like partitioning problems. The characterization of the solutions of these state-dependent Voronoi-like partitioning problems using either analytical or computational techniques constitutes the second main objective of this dissertation. The third objective of this research effort is to illustrate the use of the proposed concept of state-dependent Voronoi-like partition as a means for passing from control techniques that apply to problems involving a single vehicle to problems involving networks of spatially distributed autonomous vehicles. To this aim, we formulate the problem of sequential/relay pursuit of a maneuvering target by a group of spatially distributed pursuers and subsequently propose a distributed group pursuit strategy that directly derives from the solution of a state-dependent Voronoi-like partitioning problem.

CHAPTER I

INTRODUCTION

1.1 Motivation

The recent theoretical and technological advances in the field of autonomous vehicles have attracted the attention of many researchers from different fields envisioning the design of flexible mission planning and execution architectures involving networks of autonomous vehicles for real world applications within both the military and civilian contexts. It is envisaged that for a large spectrum of applications, ranging from environmental monitoring, search and rescue missions, group pursuit-evasion problems, tracking of multiple targets, as well as surveillance and reconnaissance, the utilization of networks of multiple decision makers/autonomous vehicles (*network-centric paradigm*) in leu of a global decision maker (*monolithic paradigm*) can be beneficial in terms of increasing the flexibility and efficiency during, respectively, the mission planning and execution phases. In particular, on the one hand, missions within the framework of the monolithic paradigm, regardless of whether are carried out by a single vehicle or teams of vehicles are typically planned, monitored, and controlled by a global supervisor. On the other hand, within the network-centric paradigm, a mission is expected to be carried out by a network of autonomous vehicles, where it is understood that each element of this network acts as a decision maker having its own individual objectives that should be compatible with the collective mission objectives of the network. Therefore, in contrast to the traditional monolithic paradigm, where all decisions and control actions are made by a single decision maker, in the new network-centric paradigm, the different elements of the network behave as interconnected subsystems (nodes in a network abstraction of the system), which are operated

by local controllers (algorithms).

Admittedly, the idea of adopting the network-centric paradigm in many real world applications is becoming increasingly popular, primarily among researchers and theoreticians and secondarily among practitioners. The following passage highlights one of the key arguments supporting the use of multiple decision makers rather than a global supervisor in many practical applications

> *...there exist situations in which a problem needs to be solved in a distributed fashion, either because a central controller is not feasible or because one wants to make good use of distributed resources* [187].

We think that one should not take the previous passage as a panacea for every modern application that can be possibly carried out by a network of autonomous vehicles. In particular, we should mention at this point that it is arguable whether techniques and distributed algorithms from the theory of multi-agent systems are applicable to complex engineering systems [119]. We also believe that the previous passage contains some useful insights that we wish to explore as part of this research effort.

Besides the acclaim of the conceptual and analytical/theoretical advantages that the network-centric paradigm offers according to its proponents, the prospective of its implementation in many real world applications is sometimes received with skepticism or even significant criticism. This reluctance to adopt the network-centric paradigm in many practical applications mostly stems from the fact that the design and control of complex engineering systems within a decentralized framework may be, sometimes, more difficult and complex than within a centralized framework. In particular, a network of interacting vehicles constitutes a complex interconnected engineering system whose integral subsystems are governed by local controllers. Therefore, the mission planning and execution within the network-centric paradigm are succumbed by fundamental limitations associated with the design, monitoring and operation of complex interconnected systems, and in particular [206, 207]:

i) their high dimensionality;

ii) the increased levels of uncertainty in their monitoring and operation;

iii) the inadequate propagation of information via the communication channels of the network between its different subsystems.

If we specialize the previously mentioned challenges of generic complex interconnected systems to real-world applications involving networks of autonomous vehicles, we will identify the need to specify protocols and rules under which the vehicles of the network should interact with each other and be assigned tasks and roles in the team (hierarchical decomposition of tasks). In particular, it is also of great importance that the decision making mechanisms adopted by every vehicle of the network adhere to a set of common rules, which are established at the team level, which purport to guarantee that the individual objectives of a vehicle (e.g., the accomplishment of its assigned task) will streamline with the collective mission objectives of the team [3]. It is understood that the utilization of networks of autonomous vehicles becomes more challenging when is furthermore assumed that the communication capabilities of the network are limited; something that places restrictions in the propagation of information among the vehicles of the network through the communication channels of the latter.

Although we acknowledge the potential as well as the limitations of the network-centric paradigm in improving the current trends in the framework of mission planning and execution within both civilian and military contexts, we do not wish to actively participate in the debate of "centralized versus decentralized control." We do wish, however, to highlight the duality inherent to the problem of "decentralized versus centralized control"; something that has been identified within the context of strategic planning and execution of military operations [95]. In simple words, we wish to emphasize that in most practical applications involving interconnected engineering

systems both decentralized and centralized processes need to incorporated in the control architecture. For example, we have previously identified the need for specifying protocols or rules that determine the interaction rules between different vehicles of a network of autonomous vehicles. Admittedly, the design of these protocols involves a centralized process. The existence of underlying centralized processes in the design and implementation of many so-called distributed control architectures proposed in the literature would be later reflected in the solutions of some particular task assignment and control problems involving teams of autonomous vehicles, which we will present later as part of this research effort.

In this dissertation, we are interested in addressing planning, task assignment and control problems for applications involving either a single or teams of autonomous vehicles without necessarily constraint our analysis to neither a solely decentralized nor a centralized framework. Our main motivation is to explore methods that will allow us to extend techniques that apply to problems involving a single vehicle to problems involving multiple vehicles. In the case of a single vehicle, we address different path planning and steering problems in the presence of motion constraints imposed by the maneuverability limitations of the vehicle and/or environment-vehicle interactions induced, for example, by local winds/currents. Subsequently, we extend our analysis to the case of multiple autonomous vehicles. In particular, we assume that each vehicle from a team of autonomous vehicles is equipped with decision making mechanisms allowing it to focus its efforts and/or resources where and when it is necessary. In addition, the vehicles of a team may not be constrained to work in isolation neither from each other nor from their environment. Maintaining high levels of autonomy during the course of a mission is also of critical importance. The mission-level autonomy for a team of autonomous vehicles is strongly related to the ability of each vehicle of the team to cope with unforseen risks as well as to adapt to dynamically changing ambient conditions. For example, the current trend in military operations

is to deploy large numbers of small-size, intelligent robotic aerial vehicles to provide persistent monitoring and battlefield situational awareness. Due to their small size, the UAVs/MAVs are susceptible, for example, to their ambient weather and wind conditions. Therefore a mission of the UAVs/MAVs should be planned such that the UAVs/MAVs are equipped with sufficient fuel resources and decision making mechanisms that will allow them to replan their paths through areas of milder environmental disturbances and lower risk. In this dissertation, we will examine in detail how the vehicle-environment interactions, through, say, the local winds/currents, can either compromise or aid the successful accomplishment of a mission which is purport to be carried out by a team of marine/aerial vehicles. The main tool we utilize to address this kind of problems will be a prototypical partitioning scheme of the state space of each vehicle of the team, which will serve as a means for extending known techniques for dealing with problems involving a single vehicle to those involving multiple vehicles. Before we proceed to a detailed description of the scopes of this research effort, we shall first discuss the motivation behind the use of space partitions for addressing task and role assignment problems involving teams of spatially distributed autonomous vehicles.

1.2 State-Dependent Voronoi Diagram: A New Tool for Problems Involving Teams of Spatially Distributed Autonomous Vehicles

Within the network-centric paradigm, the rules under which the vehicles of the network are assigned roles and tasks should reflect the suitability of each vehicle to accomplish a specific task. Specifically, the hierarchical decomposition of tasks among the subsystems of a multi-vehicle dynamical system should take into account the control/system theoretic properties of each vehicle of the network (say, its maneuverability), the dynamic interactions between the vehicles and their operating environment as well as the communication limitations of the network. In the recent literature,

it has been stressed that the concept of Voronoi diagram can potentially serve as a "vehicle" for designing simple, yet computationally efficient, decentralized control architectures for applications involving teams or networks of spatially distributed vehicles (for a detailed discussion of this approach the reader can refer to [63, 122, 47]). In particular, the Voronoi diagram induces a partition of the operating space of the network. Subsequently, each element of this spatial partition is uniquely assigned to a vehicle from a network of spatially distributed autonomous vehicles. This subset of the operating space of the network serves as the *area of influence* of this particular vehicle of the network, which is subsequently "condensed" into a single node of a graph abstraction of the operating space. The graph abstraction of the operating space is in one-to-one correspondence with the network abstraction of the team of autonomous vehicles. This fact can potentially provide both conceptual and computational advantages to mission planners. For example, it may open the possibility of employing concepts and tools from set and/or graph theoretic control in multi-vehicle problems [34, 130, 131].

The important nuance here is that the characterization of the areas of influence of each vehicle is with respect to the Euclidean distance metric. Thus it is (tacitly) assumed that the Euclidean distance metric is an appropriate figure of merit for partitioning the control architecture for problems involving teams of spatially distributed autonomous vehicles. A key question we want to address, and which has been widely overlooked in the literature, is the following:

> *Is the Euclidean distance the most appropriate metric for partitioning the control architecture for problems involving teams of spatially distributed autonomous vehicles?*

In general, an appropriate metric for problems involving networks of autonomous vehicles need to account for

i) the specific mission objectives,

ii) the structural properties of the network (e.g., communication topology)

iii) the vehicles' control/system theoretic properties (e.g. vehicles' maneuverability),

iv) the environment-vehicle interactions (e.g., drift field in the vicinity of the vehicles).

In this dissertation, it is argued that geometric data structure similar to Voronoi diagrams, but with respect to generalized proximity metrics different than the standard Euclidean distance metric, may encode more critical information for many application scenarios involving teams of distributed autonomous vehicles compared to standard Voronoi diagrams. Figure 1 illustrates a typical application for multi-vehicle dynamical systems that we have in mind. In particular, a team of two UAVs/MAVs, denoted by A_1 and A_2, patrol a given area. Their mission is to attack three targets located at points B, C and D. To simplify the presentation, let us momentarily assume that the wind field is known. One of the questions we wish to address is the following: "Which target(s) each UAV/MAV should attack first?" The typical solution to this problem is to disperse each UAV/MAV to the closest, (in terms of Euclidean distance) target (lhs of Fig. 1). A better choice would have been, however, to direct each vehicle to the target which is the closest to the vehicle in terms of the arrival time (time-to-come) (rhs of Fig. 1). In this simple scenario, the minimum arrival time serves as a"distance" metric which captures the key interactions between each vehicle from the team of autonomous vehicles and its environment (the wind field in this case). This information is succinctly encoded in a Zermelo-Voronoi partition [14] as is illustrated in Fig. 1. In this dissertation, we coin the term Zermelo-Vononoi diagram for the first time in order to describe a Voronoi-like partition with respect to the minimum time-to-go/come for a vehicle traveling in the presence of winds/currents that may

vary both with space and time (a steering problem known as the Zermelo's navigation problem [210]). The Zermelo-Voronoi diagram will provide one of the main cornerstones to address some of the research problems discussed in this dissertation.

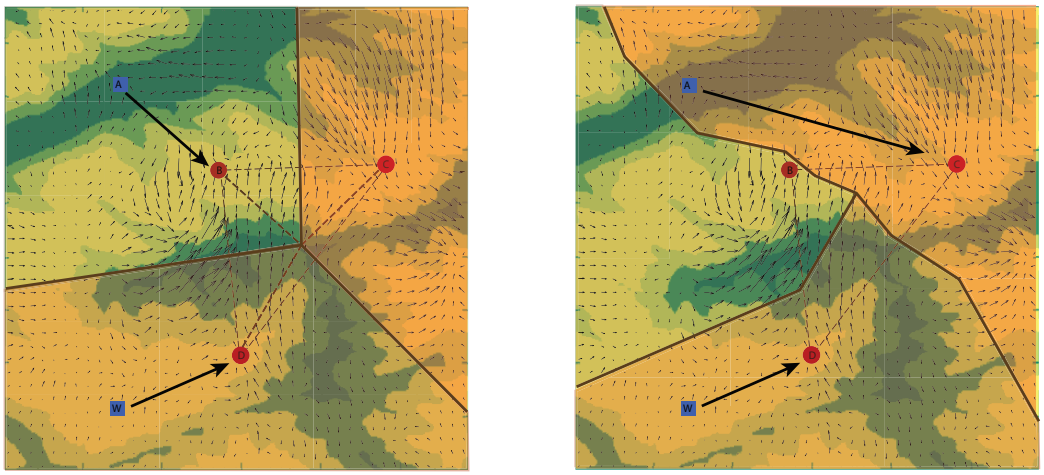

Figure 1: A team of two vehicles A_1 and A_2 are flying in the presence of strong winds, whose aim is to attack three static targets (points $\mathsf{B}, \mathsf{C}, \mathsf{D}$). An efficient distributed control architecture would disperse the vehicles to the targets based on the vehicle/target proximity relations. A standard Voronoi partition uses Euclidean distance (left figure), whereas a Zermelo-Voronoi partition uses minimum time-to-intercept (right figure). The latter is more appropriate for small size UAV/MAVs where the winds can have a large effect on the resulting vehicle trajectories. The only information required for the deployment of the vehicles is the proximity relations between the vehicles and the targets, which are induced, in turn, by the minimum time-to-intercept.

In short, the concept of *time* as a metric is for the previously presented scenario a more appropriate figure of merit for characterizing the notion of proximity between an vehicle and a target than the Euclidean distance. Working with time (a state-dependent concept) as the proximity metric in networked autonomous vehicles has certain ramifications that we will explore as part of this research. This issue has not been addressed in the current literature of multi-vehicle networked systems, where typically proximity relations are solely based on metrics induced from the Euclidean distance [131, 47, 122].

The construction of generalized Voronoi diagrams with respect to the time-to-go/come, as well as other state-dependent concepts such as minimum fuel and control effort, is a difficult task for two reasons. First, the distance metric is not symmetric and/or it may not be expressible in closed form. Second, such problems fall under the general class of partitioning problems for which the vehicles' dynamics must be taken into account[1]. The topology of the vehicle's configuration space may be non-Euclidean, for example, it may be a manifold embedded in a Euclidean space. In other words, these problems may not be reducible to generalized Voronoi Diagram problems, for which efficient construction schemes exist in the literature [141, 6]. For example, the characterization of the minimum time-to-go function for a particular partitioning problem involving networks of vehicles whose kinematics are not trivial may require significant analysis and perhaps computational effort. Therefore, before addressing a particular Voronoi-like partitioning problem with respect to, say, the minimum-time (or other state-dependent metrics), we have to first revisit the minimum-time control problem for a single vehicle and characterize the minimum time-go function (value function of the optimization problem) for arbitrary boundary conditions. In other words, we have to address the so-called time-optimal synthesis problem.

1.3 Goals of this Dissertation

This research effort pursues three main objectives. Our first goal is to address path planning and steering problems that will furnish us state-dependent metrics such as the minimum time-to-go function for arbitrary, prescribed boundary conditions. There are two classes of problems we wish to address as part of this first task. The first class deals with the characterization of the minimum time-to-go function for a vehicle in the presence of motion constraints imposed by the maneuverability envelope of the vehicle and/or the presence of a drift field induced by winds/currents in

[1] A typical example is Voronoi-like partitions for a Dubins vehicle. See [175] for an initial treatment of this problem.

the vicinity of the vehicle. The second class of problems deals with the characterization of the time-to-go function for a vehicle traveling through strong, temporally and spatially varying winds/currents without having global information about them (navigation in an arbitrary and uncertain spatiotemporal drift field). Consequently, the vehicle is not necessarily driven by the minimum-time controller, which is typically a non-causal/anticipative control law that requires global information about all future exogenous inputs acting upon the system. Instead it is driven by non-anticipative controllers that require at most information about the local drift only.

The second goal is to construct abstractions of the operating space of a team of autonomous vehicles by means of state-dependent Voronoi-like partitions, where the proximity relations are determined by a transition cost associated with the solution of different steering problems involving a single vehicle. These pseudo-metrics are purport to serve as more appropriate figures of merit for characterizing the suitability of a vehicle from a team of autonomous vehicles to accomplish a particular task within a partially known environment compared to, say, the Euclidean distance metric, which is typically used in the literature. A typical application would be the characterization of a scheme for distributing a team of UAVs/MAVs or AUVs to carry out, say, environmental monitoring tasks or search and rescue missions while operating under strong wind/currents. The third objective is to use these generalized Voronoi-like partitions as "vehicles" for the design and implementation of local control laws for a number of application scenarios involving teams of spatially distributed autonomous vehicles. Some of the applications that will be explored as part of this research effort is the landing site selection problem for a team of UAVs/MAVs from a given set of landing sites in the presence of strong winds, and problems of pursuit of a maneuvering target by a group of spatially distributed pursuers.

This dissertation identifies and subsequently addresses a key technical challenge

that has not been dealt with so far in the literature. In particular, the intellectual merit of this research effort is the characterization of efficient analytical and/or computational techniques for partitioning the operating environment of teams of autonomous vehicles with respect to state-dependent metrics. It is argued that state-dependent metrics better capture the system theoretic characteristics of each vehicle from a network of autonomous vehicles as well as the vehicle-environment interactions, induced by, say, local winds/currents, than other standard metrics such as the Euclidean distance. Consequently, state-dependent Voronoi-like partitions constitute more appropriate partitioning schemes for application involving teams of spatially distributed vehicles than other standard partitioning techniques available in the literature.

The main argument behind the formulation of this new class of Voronoi-like partitioning problems is that state-dependent metrics, such as the minimum time-to-go, better reflects the system theoretic features of each element of a network of autonomous vehicles than other standard metrics such as the Euclidean distance. Consequently it is argued that state-dependent Voronoi-like partitions encode more relevant information regarding the suitability of a vehicle from a network of autonomous vehicles to accomplish a particular task than a standard Voronoi partition. It is envisioned that this dissertation brings one step closer the realization of real-time, embedded, control systems in applications involving autonomous vehicles.

1.4 Comments on the Structure of the Dissertation

This dissertation is divided into four parts. In particular, the first part of this dissertation (Chapter 2) presents an extensive literature review on topics related to the scopes of this research effort.

The second part of the manuscript, which is comprised of Chapters 3-6, discusses several steering problems involving a single vehicle. Chapters 3, 4, and 5 deal with

variations / extensions of the classical Markov-Dubins problem on shortest paths with curvature constraints. In particular, Chapter 3 and 4 deal with the characterization of the minimum-time paths of a vehicle with Dubins type kinematics in the presence of, respectively, asymmetric steering constraints induced by mechanical failures, and a drift field induced by prevailing local winds/currents. Furthermore, Chapter 5 deals with an extension of the MD problem, when the ensuing path of the vehicle satisfies both curvature and curvature gradient point-wise constraints. In addition, Chapter 6 discusses the problem of guiding an aerial / marine vehicle in the presence of a drift field induced by local winds/currents, which may be uncertain and/or only locally known.

The third part of this dissertation, which includes Chapters 7-9, deals with the complete solution of different Voronoi-like partitioning problems with respect to state-dependent generalized distance functions. Finally, Chapter 10 illustrates the applicability of state-dependent Voronoi-like partitions in problems involving teams of spatially distributed autonomous vehicles by examining a problem of pursuit of a maneuvering target by a group of pursuers. Finally, in the fourth part of this dissertation (Chapter 11), we present possible directions for future research, which build upon the results that will be presented in this dissertation.

1.5 Chapter Description

Next, we give a short description of each chapter of the dissertation.

- **Chapter II: Previous Work**

  Chapter 2 presents an extensive literature review on the following topics: 1) steering problems involving a single vehicle with differential constraints, 2) path planning and navigation in anisotropic media and, in particular, the navigation problem in the presence of a drift field induced by local winds/currents, 3) task assignment and control problems involving teams of autonomous vehicles, 4)

Voronoi-like partitions where time serves as the proximity metric, and 5) group pursuit problems.

- **Chapter III: Optimal Synthesis of the Asymmetric Sinistral/Dextral Markov-Dubins Problem**

  In Chapter 3, we present the complete solution of the synthesis problem of a generalization of the classical Markov-Dubins problem dealing with curvature-constrained, shortest paths in the plane with prescribed initial and terminal positions and tangents, when the lower and upper bounds of the curvature of the path are not necessarily equal. The motivation for this problem stems from vehicle navigation applications, when a vehicle may be biased in taking turns at a particular direction due to, say, hardware failures. After formulating the shortest path problem as a minimum-time problem, a family of extremals which is sufficient for optimality is characterized, and subsequently, the complete analytic solution of the optimal synthesis problem is presented.

- **IV: Optimal Synthesis of the Zermelo-Markov-Dubins Problem in a Constant Drift Field**

  In Chapter 4, we consider the optimal synthesis of the minimum-time steering problem of a vehicle with the kinematics of the Isaacs–Dubins car in the presence of a constant drift field. This minimum-time problem is the combination of two classical optimization problems, namely the Markov–Dubins problem on the characterization of minimum-length planar curves of bounded curvature and the Zermelo's navigation problem on the characterization of minimum-time planar paths of a vehicle with simple integrator kinematics traveling in a drift field. By using standard optimal control tools, we characterize a family of extremal controls that is sufficient for complete controllability and necessary for optimality. Next, we present a semi-analytic scheme for the characterization of a

(nearly) optimal synthesis of the minimum-time problem, and we subsequently compare it with the optimal synthesis of the standard Markov–Dubins problem. Finally, we establish a direct correspondence between the two optimal syntheses by means of a discontinuous set-valued mapping.

- **Chapter V: On the Generation of Nearly Optimal, Planar Paths of Bounded Curvature and Bounded Curvature Gradient**

  In Chapter 5, we present a numerically efficient scheme to generate and subsequently combine a family of path primitives to construct paths of bounded curvature and curvature gradient. The statement of the problem is a generalization of the Markov-Dubins problem to account for more realistic vehicle dynamics. The problem is solved by appropriate concatenations of line segments, circular arcs and pieces of clothoids, which are the path primitives in our scheme. Our analysis reveals that the use of clothoid segments, in addition to line segments and circular arcs, for path generation introduces significant changes on issues such as the path admissibility and length minimality, when compared with the standard Dubins problem.

- **Chapter VI: Feedback Navigation in an Uncertain Flow**

  In Chapter 6, we present several classes of control laws for steering an aerial or marine vehicle, in the presence of a both temporally and spatially varying drift field induced by local winds/currents. The navigation problem is addressed assuming various information patterns about the drift field in the vicinity of the vehicle. In particular, three cases are considered, namely 1) when the vehicle has complete information about the drift, 2) when only the local drift field is partially known, and 3) when the drift field is completely unknown. By first establishing a duality between the navigation problem and a special class of problems of pursuit of a maneuvering target, several navigation schemes are

presented, which are appropriately tailored to the fidelity of the information about the local drift available to the vehicle. The proposed navigation laws are dual to well-known pursuit strategies, such as pure pursuit, parallel guidance/navigation, line-of-sight guidance, motion camouflage, and pursuit with neutralization.

- **Chapter VII: The Zermelo-Voronoi Diagram: A Dynamic Partition Problem**

  Our discussion on state-dependent Voronoi-like partitions starts with Chapter 7, where we discuss in detail a particular class of generalized Voronoi diagrams with respect to the minimum-time of the Zermelo's navigation problem. In particular, we consider a Voronoi-like partitioning problem in the plane for a given finite set of generators, where each element in this partition is uniquely associated with a particular generator in the following sense: A vehicle that resides within a set of the partition at a given time will arrive at the generator associated with this set faster than any other vehicle that resides anywhere outside this set at the same instant of time. The vehicle's motion is affected by the presence of a temporally-varying drift field, which is induced by local winds/currents. As a result, the minimum time to a destination is not equivalent to the minimum distance traveled. This simple fact has important ramifications over the partitioning problem that we examine in detail. In addition, it is shown that this problem can be interpreted as a dynamic Voronoi diagram problem, where the generators are not fixed, but rather they are moving targets to be reached in minimum time. The problem is solved by first reducing it to a standard Voronoi diagram by means of a time-varying coordinate transformation.

- **Chapter VIII: The Zermelo-Voronoi Diagram for a Time-Varying Affine Drift Field**

In Chapter 8, we consider a more general formulation of the Zermelo-Voronoi diagram introduced in Chapter 7. In particular, we assume that the winds/currents induce a time-varying inhomogeneous linear field. The construction of the Voronoi-like partition is based on the efficient propagation of the level sets of the minimum time-to-go function and subsequently, the characterization of a lower envelope of all the cost surfaces associated with each generator of the partition. The proposed approach utilizes the structure of the solution of the Zermelo's navigation problem without resorting to exhaustive numerical techniques.

- **Chapter IX: Optimal Pursuer and Moving Target Assignment using Dynamic Voronoi Diagrams**

  In Chapter 9, we consider a Voronoi-like partitioning problem for a team of spatially distributed pursuers with respect to the minimum capture time of a maneuvering target. Each element of the partition is uniquely associated with a pursuer in the following sense: If a moving target at a given instant of time resides inside a particular member of the partition, then the pursuer associated with this set can intercept this moving target faster than any other pursuer.

- **Chapter X: On the Relay Pursuit of a Maneuvering Target by a Group of Pursuers**

  In Chapter 10, we illustrate how the concept of state-dependent Voronoi-like partition can be utilized to design local control laws for problems involving teams of spatially distributed vehicles by considering a problem of pursuit of a maneuvering target by a group of pursuers distributed in the plane. This group pursuit problem is solved in a distributed way by employing a relay pursuit strategy that derives from the solution of a Voronoi-like partitioning problem with respect to the minimum capture time. With the proposed group pursuit scheme, only one pursuer is assigned the task of capturing the maneuvering

target at each instant of time. During the course of the relay pursuit, the pursuer-target assignment changes dynamically with time in accordance with the (time-varying) proximity relations between the team of pursuers and the target.

- **Chapter XI: Future Research Work**

  Finally, in Chapter 11 we highlight possible directions for future research. Our emphasis is on exploring the possibility of applying the concept state-dependent Voronoi-like partition as a means to design control architectures for addressing problems involving teams of spatially distributed autonomous vehicles.

CHAPTER II

PREVIOUS WORK

2.1 Introduction

In this chapter, we highlight some of the recent advances in different research topics relevant to the scopes of this dissertation. In particular, we review some important contributions from the field of path planning and steering problems involving a single vehicle in the presence of motion constraints with an emphasis on problems of guidance and navigation of aerial and / or marine vehicles. Subsequently, we review some of the available results in the literature on task assignment and distributed control problems involving teams of autonomous vehicles. Finally, we review pursuit-evasion games and we focus on some recent results on group pursuit-evasion problems. Given the vast body of work related to these popular research topics that are available in the literature, our literature review is not meant to be exhaustive but rather indicative of some of the recent trends in the fields related to the scopes of this dissertation.

2.2 Optimal Steering and Guidance of Autonomous Agents with Steering Constraints

2.2.1 The Markov-Dubins Problem and its Variations

Many popular techniques for path planning, guidance and navigation of ground, marine, and aerial vehicles in the literature are based on the assumption that, as a first order approximation, the kinematics of the vehicle can be described by a point mass that traverses paths of bounded curvature with constant forward speed. This simple kinematic model is inherently related to the problem of characterizing curvature-constrained planar paths of minimal-length with prescribed positions and tangents. The origins of the latter problem can be traced back to the end of the nineteenth

century, when the Russian mathematician A. A. Markov posed it for the first time. In 1957, L. E. Dubins generalized the original problem formulation by posing the problem "on curves of minimal length with a constraint on average curvature, and with prescribed initial and terminal positions and tangents" in the n-dimensional Euclidean space. Dubins addressed the planar case of this minimization problem by characterizing a family of six path types that is sufficient for optimality for any set of prescribed boundary conditions in the plane [77]. We shall refer to the problem of finding the shortest, curvature-constrained planar path as the Markov-Dubins (MD) problem, as suggested by Sussmann [198]. The solution of the MD problem is commonly interpreted as the path traversed by a vehicle that travels in the plane with constant (usually unit) speed, and such that the direction of its (forward) velocity vector cannot change faster than a given constant. This simple kinematic model is known in the literature as the Dubins' car although, as highlighted in [146], Dubins never introduced such a kinematic model in his work. It was actually R. Isaacs who first introduced the kinematic model that is widely referred as the Dubins car in the formulation of his classic homicidal chauffeur problem [98, 99]. In this dissertation, we shall refer to this kinematic model as the Isaacs-Dubins (ID) car as suggested by Patsko and Turova [146]. The accessibility/reachability properties of the ID car were first studied by Cockayne and Hall in [59]. In addition, Reeds and Shepp examined a generalization of the MD problem, known as the Reeds and Shepp (RS) problem, when the minimal length path may contain cusps, or equivalently the ID car is allowed to move both forward and backwards with constant speed, (a kinematic model which is known as the Reeds Shepp car) [163]. It is worth mentioning that the ID car and some of its extensions/variations are widely used kinematic models in the field of non-holonomic path planning and control [35, 49, 111].

All the aforementioned results dealing with the characterization of the solution

of the MD problems and some of its variations were based more or less on constructive proofs and ad-hoc methods. These approaches, even though sufficient for the examination of each particular optimization problem, are of limited use as tools for addressing other similar problems. A number of authors during the 1990's argued that the systematic application of optimal control techniques would provide more rigorous proofs to the MD and RS problems along with a more general framework for addressing similar problems in the future. Following this line of argument, Sussmann and Tang [199] and Boissonnat *et al* [39] reformulated the MD and the RS problems as minimum-time problems in $\mathbb{R}^2 \times \mathbb{S}^1$, and they subsequently solved them by employing standard optimal control tools along with geometric control ideas, and provided more general and rigorous proofs, refining the original results of [77] and [163].

An interesting variation of the MD problem is when the motion of the ID car is constrained by both steering constraints as well as the presence of a drift field induced by local winds/currents. The latter steering problem is essentially a combination of the MD problem with the *Zermelo's navigation problem*. In particular, the navigation problem posed by E. Zermelo in the early 1930's, deals with the characterization of the planar minimum-time paths for a vehicle with single integrator kinematics traveling in a flow-field induced by local currents/winds [210]. The Zermelo's navigation problem is a classical optimization problem which is discussed and analyzed in many standard texts in calculus of variations and optimal control [50, 173, 44, 102]. Zermelo solved the navigation problem for the general case of a both temporally and spatially varying drift field using "an extraordinary ingenious method" according to Carathéodory [50]. We shall refer to the combination of these two classical optimization problems as the Zermelo–Markov–Dubins (ZMD) problem. The ZMD problem for the special case of a constant drift field was first posed by McGee and Hedrick in [123]. The authors of [123] examined this special case of the ZMD indirectly, by interpreting the ZMD problem as a minimum-time intercept problem of a non-maneuvering target.

They conjectured that, under some mild modifications, the family of extremals that is sufficient for optimality for the standard MD problem is sufficiently rich to provide feasible paths to the ZMD problem for an arbitrarily pair of boundary configurations. A numerical scheme for the computation of the Dubins-like paths proposed in [123], which may involve the solution of a set of coupled transcendental equations, has been proposed in [200]. A set of decoupled equations that solve the same problem were presented in [15]. In addition, a numerical scheme for the solution of the ZMD problem for a drift field that varies uniformly with time was proposed in [126]. It is worth-mentioning that the equivalent formulation of the ZMD problem as a minimum-time intercept problem of a non-maneuvering target, as discussed in [123], is closely related to the intercept problem addressed by Glizer in [89, 90]. In particular, the author of [89, 90] considered an optimization problem where the hard input constraints were relaxed with the addition of a cost term penalizing the control effort, for which he characterized both exact and simpler approximate solutions in [89] and [90], respectively. It turns out that the ZMD problem is inherently related to another variation of the MD problem, namely the characterization of curvature constrained minimum-length paths in an anisotropic medium [73, 54].

Other variations of the MD problems include 1) characterization of steering laws for the ID car in the presence of polygonal obstacles [203, 87], 2) generalizations and variations of the kinematic model of the ID car [38, 109, 198, 21, 176, 81, 22, 11, 83], and 3) steering laws for an ID car with spatially varying turning constraints [174] and 4) formulation of similar to MD problems in higher dimensional and/or non-Euclidean spaces. In particular, an initial treatment of the three-dimensional version of the MD problem was presented in [196], where some prior conjectures regarding the structure of its extremals [163] were proven wrong. The structure of the optimal solution of a simpler version of the problem introduced in [196] was presented in [57]. In [20] it was argued that some extensions of the results presented in [196, 57] can be used for

the characterization of initial guesses that can expedite the numerical solution of the landing trajectory optimization problem. Some attempts to address generalizations of the MD problem in Riemannian topologies can be found in [135, 134, 56, 188].

One drawback of the aforementioned path planning schemes, which account only for curvature constraints, is that they typically generate paths having discontinuous curvature profiles. In practice, discontinuous curvature profiles induce poor tracking performance [75]. The main source of this poor performance is the latency associated with the steering command inputs of most typical ground vehicles, which, in turn, induces an offset tracking error [105]. Refs. [75, 104] propose schemes to construct curves with continuous curvature profiles, and linear curvature gradients. In [115, 189, 153] an additional global point-wise constraint on the curvature of the path is added to the path problem formulation. Ref. [41] considers the path planning problem with a constraint on the derivative of the curvature. The paths that solve the problem posed in [41] have continuous curvature profiles without, however, necessarily satisfying an explicit upper bound on their curvature that are known a priori. Constraints on both the curvature and the derivative of the curvature of the path are taken into account for the continuous curvature extensions of the MD and the RS problems in [176] and [81], respectively.

Optimal paths of the MD problem and its variations / extensions are often integrated in path planning algorithms, when the latter account for dynamical constraints imposed, in turn, by the dynamics of the vehicle. This can be achieved by appropriately concatenating different Dubins' paths using geometric arguments [29, 8, 9, 64] or by employing a discrete path planner (high level planning) that yields a set of way-points to be locally connected by means of Dubins-like paths (low level planning) [25, 111, 28, 155, 65].

2.2.2 The Weighted Region Problem and Navigation in Anisotropic Media

Path-planning problems with spatially-varying parameters fall under the umbrella of the so-called *weighted region problem* [132, 133, 169, 97]. The weighted region problem, first introduced by Mitchell and Papadimitriou in [132, 133], deals with the characterization of the minimal-length paths from a given point to a prescribed terminal point (or a set of terminal points) assuming that the (obstacle-free) state space is abstracted by a polygonal subdivision. The metric to be minimized along the ensuing path is the weighted Euclidean distance function between successive way points. In [132, 133] is assumed that the distance weight (cost per unit distance) is uniform within each cell of the subdivision. Thus the optimal paths of the problems posed in [132, 133] can be interpreted as the minimum-time paths of a light beam that travels through different isotropic media (where it is understood that the media are the polygonal cells of the subdivision). The optimal paths of the weighted region problem are concatenations of regionally optimal paths, where the concatenations occur along the boundaries of neighboring regions according to Snell's law of refraction [133, 170]. The paper by Rowe and Alexander [169] presents a generalization of the results presented in [133] regarding the characterization of the synthesis of optimal paths to a specific goal destination for the weighted region problem, therein stated as a *map of optimal paths*.

The characterization of minimum-time paths for planning problems where the speed of motion of the agent depends on the direction of motion (anisotropic or directionally weighted problems) are, in general, more challenging compared to isotropic (direction independent) path planning problems. This difficulty arises as a consequence of the fact that the time of travel in an anisotropic medium does not qualify as a distance function given that it does not enjoy, in general, the symmetry property

and / or the triangle inequality. Consequently, standard techniques from the well-studied isotropic problems may not apply to anisotropic problems. An example of a path planning problem with respect to a distance function that is both regionally and directionally weighted is presented in [171]. The approach proposed in [171] is limited to the scopes of the specific problem treated therein, and thus it does not propose a framework to address more general problems. An analytic solution to a more general class of anisotropic path planning problems than the one treated in [171] (albeit non-regionally weighted) was first presented in [179]. In particular, in [179] is demonstrated that the solution of the anisotropic path planning problem in the absence of obstacles is composed of a concatenation of at most two line segments. All the results in [179] are, however, limited to the distance weight being a piece-wise linear function of the direction of motion while the solution of the anisotropic path planning problem for more general weight functions was only conjectured. Some extensions of the results presented in [179] have been proposed in [74].

One technique to reduce the complexity of the weighted anisotropic path planning problem is to assume that the vehicle obeys multi-regional dynamics, that is, the vehicle's motion is governed by different, yet simpler, equations of motion within each region of a given partition of its state space. Since the dynamics of the vehicle within each region are simpler, it is likely that the path-planning problem in this multi-regional formulation admits either an analytic solution, or the construction of the solution by means of numerical schemes is a more tractable problem than the original problem. In particular, the optimal solution depends on n parameters and is a concatenation of $n+1$ locally optimal paths, where n is the number of times the vehicle crosses the common boundary of any two neighboring regions during its progression to the goal destination. These parameters determine essentially the behavior of the optimal path on the boundary of neighboring regions, where the dynamics of the system switch during the progression of the vehicle towards the goal destination [197].

It turns out that standard techniques from the calculus of variations [44] furnish conditions that suffice for the characterization of optimal paths that traverse different regions. The theory of optimal hybrid systems [197, 185] provides an alternative solution to this problem. The hybrid optimal control approach in path planning problems with multi-regional dynamics has been used, for example, in [177, 174].

An anisotropic (direction weighted) path planning problem with many practical applications is the minimum-time navigation of an aerial/marine vehicle in a both temporally and spatially varying drift field induced by the winds/currents in the vicinity of the vehicle. In the absence of obstacles, the latter problem is known as the Zermelo's navigation problem, which, as we have already mentioned, is a classical problem found in many standard texts in calculus of variations and optimal control theory [50, 173, 44, 102]. Semi-analytical and numerical solutions to the minimum-time navigation in the absence of obstacles have been reported in [140, 66, 167, 191], whereas the navigation in the presence of obstacles is considered in [149, 12]. A situation that poses significant challenges to the navigation problem is when the local drift field exceeds the control authority of the vehicle. In the latter case, the vehicle is not a small-time controllable system [24]. Consequently, there may exist directions of motion that are not feasible [50, 12, 191]. An important observation common in all the aforementioned references dealing with the navigation problem, is that the agent has a priori, perfect and global information about the drift field.

2.3 Task Assignment and Control of Spatially Distributed Teams of Autonomous Agents

There is a plethora of results in the literature that deal with task assignment, control, and estimation problems involving spatially distributed multi-agent systems. One particular class of problems that receive an increasing amount of attention is the so-called *sensor coverage* problem. The sensor coverage problem is a special class of the placement problem, which deals with the characterization of an optimal,

in some sense, distribution of a network of (static or moving) sensors. The performance index that is typically employed in this class of problems encodes the notion of "maximizing" the collective amount of information gathered locally by the sensors of the network. Characteristic examples is the measurement of a scalar field, such as the temperature or the salinity levels of a river. Sensor coverage problems involving mobile sensor networks are typically dealt with by planning paths towards "information-rich" areas of the environment, based on spatially distributed motion and estimation architectures [157, 202, 67]. Another popular approach for coverage problems is to employ different variations of the *Lloyd algorithm* [116] as suggested in [63, 62, 61]. In [63, 62, 61] a network of mobile sensors are steered to locations that generate a centroidal tessellation of the area that is desired to be "covered." This is achieved by constructing a time-evolving sequence of Voronoi partitions that eventually converge to the desired centroidal Voronoi partition. The convergence properties of the Lloyd algorithm are examined, for example, in [76]. Some preliminary results introducing a framework for addressing more general distributed estimation problems is presented in [143], where the so-called distributed Kalman filtering problem is proposed and solved. In [211], some of the ideas presented in [143] are extended/tailored to the (scalar) field estimation problem to be carried out by a network of vehicles. A different approach for estimating a spatially-varying field is presented in [121, 120], where Voronoi partitions along with adaptive estimation schemes are employed.

Motion coordination constitutes a class of distributed control/task assignment problems involving multi-agent systems which receive an increasing amount of attention. The roots of this class of problems can be traced in the inspirational work of Reynolds on steering behaviors of autonomous mobile agents [165, 166]. References [165, 166] discusses a large spectrum of motion coordination problems involving multi-agent systems, ranging from flocking, leader following, containment, motion

alignment, cohesion, and separation, to mention a few. In a typical motion coordination problem, within the control/system theoretic framework, the members of a network of autonomous vehicles coordinate their motion strategies such that a global objective, at the kinetic level, is met. For example, a team of robots may coordinate their motions such that their directions of motion are aligned with the motion of an agent of elevated status in the network hierarchy (leader). Motion coordination algorithms for teams of non-holonomic vehicles have been presented in [68, 103, 114, 180, 181]. Multi-vehicle control problems in the presence of a flow-field have been examined in [145, 94, 148]. A special class of motion coordination problems are the so-called *rendezvous problems*, where the global objective is that all the vehicles of the network should meet with each other at a common configuration in their state space. There is a plethora of results in the area of rendezvous problems. The interested reader may refer to [100, 142, 136, 71, 164, 160, 55, 47, 131] and references therein. Motion coordination for UAV applications have been discussed, for example, in [125, 27, 124, 117]. Another class of task assignments problems involving networks of autonomous vehicles, and in particular, robotic networks, is the dynamic vehicle routing problem [48, 147].

A significant body of work in the field of multi-agent systems deals with more general schemes for addressing broader classes of task assignment and distributed control problems. Some of the proposed approaches are based on techniques and ideas from game theory, mixed integer linear programming (MILP) as well as utility theory [101, 3, 187]. In particular, [3] proposes a utility-based game-theoretic framework for addressing vehicle-target assignment problems for teams comprised of self-interested (non-cooperative) autonomous vehicles (agents) which manage to achieve collective team objectives when their decision making strategies are induced by properly designed utility functions. The work in [79] presents a cooperative scheme for task assignment problems for UAV applications based on potential field methods.

A scheme for addressing target allocation problems for a teams of UAVs based on mixed integer-linear programming (MILP) techniques is proposed in [107].

The results in many of the aforementioned approaches are contingent upon a number of standing assumptions. For example, in many cases, it is assumed that the interactions of the environment with the agents are negligible. This fact places restrictions on the applicability of these approaches in many real-world applications. In addition, the more general task assignment schemes usually come with a heavy computational load; something that makes their applicability in mission scenarios that require real-time decision making schemes doubtful. As it will be shown later in this dissertation, there exist task assignment and control problems involving teams of spatially distributed autonomous agents, which, owing to their structure, admit more direct and computationally efficient solutions.

2.4 Voronoi-like Partitions with Respect to Time

The "Dirichlet-Voronoi Diagram," which was first introduced by Dirichlet in 1850 [72], and subsequently generalized by Voronoi in 1908 [205], constitutes a fundamental geometric data structure that along with its extenions/variations have found a large number of applications in different fields, including computer graphics, computer vision, computational geometry, locational optimization, pattern analysis, robotics and, more recently, autonomous agents and mobile sensor networks [86, 76, 36, 84, 40, 110, 63, 61]. Dirichlet-Voronoi Diagrams, known also as "Voronoi Diagrams/Tessellations" or "Thiessen Polygons,"[1] describe a special partition of a topological space, which is equipped with a generalized distance function. Each element of the partition, which is known as the Dirichlet domain or Voronoi cell, is uniquely associated with an element from a given point-set which "generates" the partition, known as the set of *Voronoi generators*. The rule that assigns a Voronoi cell to a particular generator

[1]Henceforth, we shall use the term "Voronoi Diagrams" which is the most commonly used terminology.

is the following: For every point x that belongs to the Voronoi cell associated with a particular generator, the latter is the closest point of the set of generators to the point x . We shall refer to the partitioning problem of a subspace of the n-dimensional Euclidean space with respect to the Euclidean distance as the *standard Voronoi Diagram* problem, and as the *generalized Voronoi Diagram* problem otherwise. A detailed treatment of the Voronoi Diagram problem for a plethora of "distance" functions and topologies can be found in [40, 141, 6] and the references therein.

There are not many results in the literature that deal with partitioning problems with respect to generalized metrics such as time. A partitioning problem with respect to the minimum time-to-come for a small ship in the presence of currents has been examined in [194]. In particular, Ref. [194] treats a generalized Voronoi-like partitioning problem with respect to the minimum time-to-come for a small ship traversing a constant flow river. The approach presented in [194], which deals with a single vehicle scenario, is, however, of limited scope since it is based on geometric constructive arguments that only apply to the case of a constant drift field. An extension of the problem treated in [194] is presented in [139, 140], where the drift is assumed to be spatially-varying (albeit stationary). The approaches in [139, 140] are purely computational/numerical and one of their main drawbacks is that they do not take advantage of the structure of the solution of the associated min-time problem. Furthermore the applicability of the approaches presented in [194, 139, 140] is contingent upon the standing assumptions that 1) the spatial distribution of the currents is time-invariant and, in addition, 2) the spatial distribution is a priori known to the operator of the ship. These assumptions do not hold in many real world applications.

Another class of Voronoi-like partitioning problems, where although time does not necessarily serve as the proximity metric, it plays a key role in the solution of the partitioning problem, is the so-called *dynamic partitioning* problem or *dynamic Voronoi diagram* problem [141]. In particular, the dynamic partitioning problem deals with

a Voronoi-like partitioning problem where the Voronoi generators are moving points rather than stationary points [141, 168, 69, 70, 2, 85]. One of the most fundamental questions in the framework of dynamic partitioning problems is the characterization of the proximity relations between the moving generators and the points in the plane as time evolves. In contrast to the standard Voronoi partitioning problem, where all generators are stationary, the solution of the dynamic partitioning problem consists of a *sequence* of time-evolving Voronoi diagrams. A diagram of this time-evolving data structure at a particular instant of time is a standard Voronoi diagram with respect to the positions of the moving Voronoi generators at that time.

The work of Devillers et al. [69, 70] highlights an interesting aspect of dynamic partitioning problems. In particular, [69, 70] deals with the following problem: Given a set of n postmen (moving targets) that move along prescribed rays with constant speed, a set of n dogs (pursuers) going after the postmen, find the rule that assigns each dog to each postman, under the assumption that every dog is faster than every postmen. The main challenge of this problem comes from the fact that any question regarding the proximity relations between pursuers and moving targets has to be addressed with respect to a generalized distance function, in this case the minimum interception time, rather than the usual Euclidean distance, as with the standard Voronoi partition. The main drawback of the approach in [69, 70] is that the targets, which are constrained to travel slower than their pursuers, are moving along straight lines with constant speed. Thus in the scenarios considered in [69, 70] one deals with a problem of *pursuit-with-anticipation*, that is, the future decisions and actions of a target are perfectly anticipated by its pursuers. In more realistic application scenarios, however, a moving target will not announce its future positions and actions to its pursuers; on the contrary, the target may employ an evading strategy in response to the actions of its pursuers to delay or even avoid capture.

2.5 Pursuit Evasion Games and the Group Pursuit Problem

Problems of pursuit-evasion have a long history. For an interesting discussion on the historical background of problems of this kind, the reader may refer to [138]. The pioneering work of Isaacs [99] on differential games for two strictly competitive players, which extended the theory of zero-sum games from classical game theory [118] to problems with dynamic constraints, provided a powerful framework for addressing problems of pursuit-evasion in a systematic way. The approach of Isaacs has received a significant amount of criticism due to the fact that is based on rather non-rigorous arguments, and more importantly, because it associates the solution of a differentiable game with the solution of a HJB-like equation (the min-max extension of the HJB equation known as the Isaacs equation); something that limits its applicability in many practical problems (see the discussion in [96, 93, 82]). Bergovitz [30] proposed a framework for addressing differential games for two competitive players based on variational techniques. Based on Bergovitz's framework, Ho et al [96] addressed pursuit-evasion games with quadratics costs for players with linear dynamics by employing standard linear optimal control techniques. Problems of pursuit-evasion with nonlinear dynamics, such as planar pursuit-evasion problems in the presence of curvature constraints are considered hard problems that require a rather detailed analysis and whose solutions exhibit interesting phenomena (e.g., existence of singular surfaces [99]). Two famous pursuit-evasion problems with curvature constraints is the Isaacs' homicidal chauffeur problem [99, 128] and the two cars problem [129]. Solvability conditions for pursuit-evasion games with curvature constraints in two and three dimensions are provided in [58] and [172], respectively.

It is worth-noting that the work of both Isaacs and Bergovitz deals with games between only two (strictly competitive) players. The extension of the work by Isaacs and Bergovitz in the case of multiple players are discussed in [151] and [51, 193],

respectively. In particular, [193] extends the results of [96] to pursuit-evasion games with quadratic costs and linear dynamics by adopting the theory of non-zero sum games from classical game theory, and explores the existence of different solutions to the pursuit-evasion problem based on different solution concepts from game theory, such as Nash equilibria and Pareto optima. Problems of pursuit-evasion for multiple players, the so-called group pursuit-evasion games [158, 159, 156, 154, 23, 152, 33], bring into play the possibility of characterizing solutions where multiple pursuers and/or evaders can negotiate with each other. In this case, group pursuit-evasion games fall into the category of cooperative differential games, which is a rather emergent but not sufficiently mature field [209]. The case of both multiple pursuers and targets is a hard problem for which very few results are available in the literature. For example, [23] discusses the solvability conditions for a problem of group pursuit-evasion, where a group of pursuers aim to capture all the evaders, whereas the goal of the evaders is to save at least one evader from being captured.

A special case of the group pursuit-evasion problem, which has received a significant amount of attention in the literature, is when a group of pursuers go after a single evader. This problem in the case when the players have single integrator dynamics was introduced in [159]. The problem introduced in [159] was extended by Pontryagin for players with higher order linear dynamics in [156] (known as the Pontryagin's example in group pursuit problems). A different approach to the group pursuit problem with a unique evader, which is based on a terminal payoff function, was proposed in [162]. More recent extensions of this problem can be found in [108, 32, 152, 33]. In particular, [108] discusses a group pursuit problem with one evader in a discrete time framework where all the players can move equally fast and the objective of the pursuers is that at least one of them will capture the evader ("soft" capture). The solution of the group pursuit problem presented in [108] builds upon the techniques presented in [184], where a novel solution to a variation of the classical "lion and man

problem" is addressed. A group pursuit problem with a single evader in a continuous time framework is examined in [33]. In particular, Ref. [33] discusses a cooperative solution to a group pursuit problem where the motion of all players are described by single integrator kinematics and the objective is that all the pursuers capture simultaneously the evader. In addition, Ref. [32, 152] discuss a group pursuit problem where the motion of all players are described by higher order linear dynamics and the game terminates when at least one pursuer captures the evader ("soft" capture). One main drawback of the aforementioned approaches is that they do not take into account any form of communication constraints in the propagation of information among the team of pursuers (all-to-all communication topology). Hence the validity of the solvability conditions is under the assumption of possibly centralized pursuit strategies. Other recent treatments of the group pursuit problem of a single evader, when the players have either non-holonomic or single integrator dynamics, can be found in [42, 43, 92, 106]. The discussion in [42, 43, 92, 106] focuses on the characterization of pursuit strategies rather than solvability conditions. In most cases, however, these pursuit strategies due to the significant complexity of the group-pursuit problem are based on ad-hoc and suboptimal methods. For example, the pursuit strategies in [42] are inspired by pursuit schemes observed in the behavior of biological systems.

CHAPTER III

OPTIMAL SYNTHESIS OF THE ASYMMETRIC SINISTRAL / DEXTRAL MARKOV-DUBINS PROBLEM

The material presented in this chapter builds upon the results presented in [10, 18].

3.1 Introduction

In this chapter, we consider the problem of finding curvature-constrained, planar paths of minimum-length with prescribed positions and tangents when the lower and upper bounds of the curvature are not necessarily equal. The motivation for this problem stems from vehicle navigation applications when the maneuverability of the vehicle when taking a left or a right turn is asymmetric. A typical case would be an UAV with a damaged aileron as shown in [78]. Henceforth, we shall refer to this generalization of the standard MD problem as the Asymmetric, Sinistral/Dextral[1] Markov-Dubins problem (ASDMD for short). We formulate the ASDMD problem as a minimum-time problem, and we investigate its (time-) optimal synthesis, that is, a) we characterize a family of extremal controls that is sufficient for optimality; b) we provide a state-feedback minimum-time control scheme; and finally c) we compute analytically the level sets of the minimum-time. Additionally, the synthesis problem of the ASDMD when the tangent of the curve at the terminal position is free is also considered, leading us to the analytic characterization of the set of points that can be reached by curves that satisfy asymmetric curvature constraints.

[1]The term sinistral (dextral) means "inclined to left (right)" [1].

3.2 Kinematic Model and Problem Formulation

We consider a vehicle whose motion is defined by the following kinematic equations

$$\dot{x} = \cos\theta, \qquad \dot{y} = \sin\theta, \qquad \dot{\theta} = u/\rho, \tag{1}$$

where (x, y) are the Cartesian coordinates of a reference point of the vehicle, θ is the direction of motion of the vehicle, u is the control input and ρ is a positive constant. We assume that the set of admissible control inputs $\mathcal{U}$ consists of all measurable functions u over $[0, T]$, where $t > 0$, with $u \in U_\delta := [-\delta, 1]$, where $\delta \in (0, 1]$. If we let $\varrho := \rho/\delta$, then it follows that ρ and ϱ are the minimum turning radii for counterclockwise and clockwise turns, respectively. The case $U_\delta = [-1, \delta]$ can be treated similarly. We call the system described by (1) and input value set U_δ the asymmetric, sinistral/dextral Isaacs-Dubins (ASDID) car.

It is a well-known fact that the standard ID car is completely controllable [199]. Next, it is shown that the ASDID car is also completely controllable. The controllability of the ASDID is established by proving that the equations (1) with input value set $U'_\delta = [-\delta, \delta] \subset U$ define a completely controllable system. It suffices to note that the system (1) with input value set U'_δ is the standard ID car with minimum turning radius ϱ (for both left and right turns), which is a completely controllable system.

It is worth-noting that the assumption that $\delta \in (0, 1]$, which guarantees that 0 is an interior of the input value set, can be actually relaxed, and it can be assumed instead that $\delta \in [0, 1]$ (in this case the vehicle cannot take right turns). A proof of the complete controllability in this case, which is based on solely geometric arguments, can be found in [10].

Next, we formulate the following minimum-time problem with fixed initial and terminal boundary conditions for the system (1).

Problem 1. *Given the system described by equations (1) and the cost functional*

$$J(u) = \int_0^{T_\mathrm{f}} 1 \, \mathrm{d}t = T_\mathrm{f}, \tag{2}$$

where T_f *is the free final time and* $\mathsf{x} : [0, T_\mathrm{f}] \mapsto \mathbb{R}^2 \times \mathbb{S}^1$ *with* $\mathsf{x} = (x, y, \theta)$ *is the trajectory generated by the control* $u \in \mathcal{U}$*, determine the control input* $u^* \in \mathcal{U}$ *such that*

i) The trajectory $\mathsf{x}^* : [0, T_\mathrm{f}] \mapsto \mathbb{R}^2 \times \mathbb{S}^1$ *generated by the control* u^* *satisfies the boundary conditions*

$$\mathsf{x}^*(0) = (0, 0, 0), \qquad \mathsf{x}^*(T_\mathrm{f}) = (x_\mathrm{f}, y_\mathrm{f}, \theta_\mathrm{f}). \tag{3}$$

ii) The control u^* *minimizes the cost functional* $J(u)$ *given in (2).*

To show the existence of an optimal solution to Problem 1, one can apply Filippov's theorem on minimum-time problems with prescribed initial and terminal states [53], leading to the following proposition.

Proposition 1. *The minimum-time Problem 1 with boundary conditions* (3) *has a solution for all* $(x_\mathrm{f}, y_\mathrm{f}, \theta_\mathrm{f}) \in \mathbb{R}^2 \times \mathbb{S}^1$.

3.3 Analysis of the ASDMD Minimum-Time Problem

In this section, we characterize the structure of the optimal paths using a similar approach as in [199, 201]. To this end, consider the Hamiltonian $\mathcal{H} : \mathbb{R}^2 \times \mathbb{S}^1 \times \mathbb{R}^3 \mapsto \mathbb{R}$ of Problem 1, which is defined by

$$\mathcal{H}(\mathsf{x}, \mathsf{p}, u) = p_0 + p_1 \cos\theta + p_2 \sin\theta + p_3 u/\rho, \tag{4}$$

From Pontryagin Maximum Principle (PMP), it follows that if x^* is a minimum-time trajectory generated by the control u^*, then there exists a scalar $p_0^* \in \{0, 1\}$ and an absolutely continuous function $\mathsf{p}^* : [0, T_\mathrm{f}] \mapsto \mathbb{R}^3$, where $\mathsf{p}^* = (p_1^*, p_2^*, p_3^*)$, known as the costate, such that

i) $\|\mathsf{p}^*(t)\| + |p_0^*|$ does not vanish for all $t \in [0, T_\mathrm{f}]$,

ii) $\mathsf{p}^*(t)$ satisfies for almost all $t \in [0, T_\mathrm{f}]$ the canonical equation $\dot{p}^* = -\partial\mathcal{H}(\mathsf{x}^*, \mathsf{p}^*, u^*)/\partial\mathsf{x}$, which for the system (1) reduces to

$$\dot{p}_1^* = 0, \quad \dot{p}_2^* = 0, \quad \dot{p}_3^* = p_1^* \sin\theta^* - p_2^* \cos\theta^*, \tag{5}$$

iii) $\mathsf{p}^*(T_\mathrm{f})$ satisfies the transversality condition associated with the free final-time Problem 1

$$\mathcal{H}(\mathsf{x}^*(T_\mathrm{f}), \mathsf{p}^*(T_\mathrm{f}), u^*(T_\mathrm{f})) = 0. \tag{6}$$

Because the Hamiltonian does not depend explicitly on time, it follows from (6) that

$$\mathcal{H}(\mathsf{x}^*(t), \mathsf{p}^*(t), u^*(t)) = 0, \tag{7}$$

for almost all $t \in [0, T_\mathrm{f}]$, which furthermore implies, by virtue of (37), that

$$-p_0^* = p_1^*(0)\cos\theta^* + p_2^*(0)\sin\theta^* + p_3^* u^*/\rho. \tag{8}$$

Furthermore, the optimal control u^* satisfies

$$\mathcal{H}(\mathsf{x}^*(t), \mathsf{p}^*(t), u^*(t)) = \min_{v\in[-\delta,1]} \mathcal{H}(\mathsf{x}^*(t), \mathsf{p}^*(t), v), \tag{9}$$

for almost every $t \in [0, T_\mathrm{f}]$. It follows that

$$u^*(t) = \begin{cases} +1, & \text{if} \quad p_3^*(t) < 0, \\ v \in [-\delta, 1], & \text{if} \quad p_3^*(t) = 0, \\ -\delta, & \text{if} \quad p_3^*(t) > 0. \end{cases} \tag{10}$$

Using similar arguments as in [199, 201] one can show the following proposition.

Proposition 2. *The optimal control u^* of Problem 1 belongs necessarily to U^*, where*

$$\mathsf{U}^* := \{\{\mathsf{u}^\pm, 0, \mathsf{u}^\pm\}, \{\mathsf{u}^\pm, 0, \mathsf{u}^\mp\}, \{\mathsf{u}^\pm, \mathsf{u}^\mp, \mathsf{u}^\pm\}\}, \quad \mathsf{u}^+ := 1, \quad \mathsf{u}^- := -\delta. \tag{11}$$

Proposition 2 implies that the time-optimal paths of Problem 1 are necessarily concatenations of at most three segments, namely two bang arcs denoted by b^- (along which $u^* = -\delta$) and b^+ (along which $u^* = 1$), respectively, and a singular arc, denoted as s (along which $u^* = 0$). Note that b^- and b^+ arcs correspond to circular arcs of radius ϱ and ρ respectively, whereas a singular arc s corresponds to a straight line segment. It follows that a minimum-time paths of Problem 1 has necessarily one the following structures

i) $\mathsf{b}^-_\alpha \mathsf{s}_\beta \mathsf{b}^-_\gamma$, $\mathsf{b}^+_\alpha \mathsf{s}_\beta \mathsf{b}^+_\gamma$, $\mathsf{b}^-_\alpha \mathsf{s}_\beta \mathsf{b}^+_\gamma$ and $\mathsf{b}^+_\alpha \mathsf{s}_\beta \mathsf{b}^-_\gamma$,

ii) or $\mathsf{b}^+_\alpha \mathsf{b}^-_\beta \mathsf{b}^+_\gamma$ and $\mathsf{b}^-_\alpha \mathsf{b}^+_\beta \mathsf{b}^-_\gamma$,

where the subscripts α, β, γ denote the duration of motion along the first, second, and third path segment, respectively.

Proposition 2 provides us with six families of paths that suffice to connect any pair of prescribed initial and terminal configurations in $\mathbb{R}^2 \times \mathbb{S}^1$ similarly to the solution of the standard MD problem. Although we have significantly reduced the family of candidate paths that solve Problem 1, no information regarding the switching times is yet available. In particular, an analysis over the switching times will allow us to significantly refine the family of the extremals before we proceed further to the synthesis problem.

To this end, let us consider an open interval $\mathcal{I} \subset [0, T_\mathrm{f}]$ for which $p_3^*(t) \neq 0$ for all $t \in \mathcal{I}$. The restriction of the optimal control u^* on $\mathcal{I}$ is a piecewise constant function which jumps at most twice, and $u^*(t) \in \{-\delta, +1\}$ for all $t \in \mathcal{I}$. By virtue of (5) and (40), for any subinterval $\mathcal{I}_\mathsf{b}$ of $\mathcal{I}$ where u^* is constant, p_3^* satisfies

$$\ddot{p}_3^* = -\left(\frac{u^*}{\rho}\right)^2 p_3^* - \frac{u^* p_0^*}{\rho}, \tag{12}$$

for all $t \in \mathcal{I}_{\mathsf{b}}$. The general solution of (43) and its derivative for all $t \in \mathcal{I}$ are given by

$$p_3^*(t) = C_1 \cos\frac{u^* t}{\rho} + C_2 \sin\frac{u^* t}{\rho} - \frac{\rho p_0^*}{u^* t}, \tag{13}$$

$$\dot{p}_3^*(t) = \frac{C_2 u^*}{\rho}\cos\frac{u^* t}{\rho} - \frac{C_1 u^*}{\rho}\sin\frac{u^* t}{\rho}, \tag{14}$$

where C_1, C_2 are real constants. It follows readily that

$$\left(\frac{\rho\dot{p}_3^*(t)}{u^*}\right)^2 + \left(p_3^*(t) + \frac{\rho p_0^*}{u^*}\right)^2 = C_1^2 + C_2^2, \quad t \in \mathcal{I}_{\mathsf{b}}. \tag{15}$$

The phase portrait of $(p_3^*, \dot{p}_3^*\rho)$ is illustrated in Fig. 2 for the normal case ($p_0^* = 1$) and in Fig. 3 for the abnormal case ($p_0^* = 0$). In contrast to the standard MD, the phase portrait of $(p_3^*, \dot{p}_3^*\rho)$ is not symmetric w.r.t. the axis $p_3 = 0$ (compare for example, with Ref. [201]).

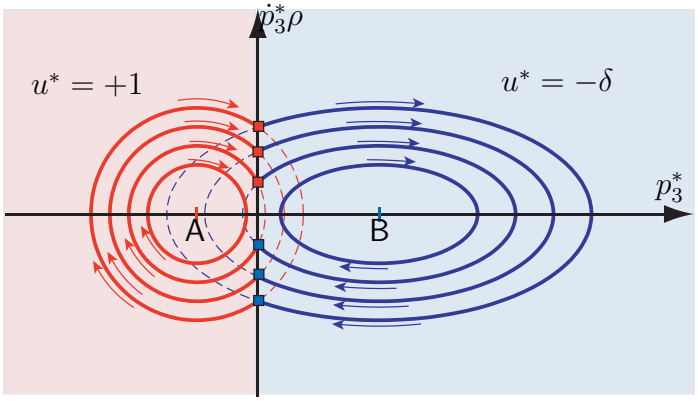

Figure 2: Phase portrait of $(p_3^*, \dot{p}_3^*\rho)$. Normal case $p_0^* = 1$.

Proposition 3. *An* $\mathsf{b}_\alpha^-\mathsf{b}_\beta^+\mathsf{b}_\gamma^-$ $\left[\mathsf{b}_\alpha^+\mathsf{b}_\beta^-\mathsf{b}_\gamma^+\right]$ *path with* $\min\{\alpha,\beta,\gamma\} > 0$ *corresponds to an optimal trajectory of Problem 1 only if*

i) $\beta \in (\pi\rho, 2\pi\rho)$, $\quad\left[\beta \in (\pi\varrho, 2\pi\varrho)\right]$

ii) $\max\{\alpha,\gamma\} \le \varepsilon(\delta,\beta)$, *where*

$$\varepsilon(\delta,\beta) = 2\pi\varrho + 2\varrho\ \mathrm{atan}\left(\delta\tan\frac{\beta}{2\rho}\right), \quad \left[\varepsilon(\delta,\beta) = 2\pi\rho + 2\rho\ \mathrm{atan}\left(\delta^{-1}\tan\frac{\beta}{2\varrho}\right)\right], \tag{16}$$

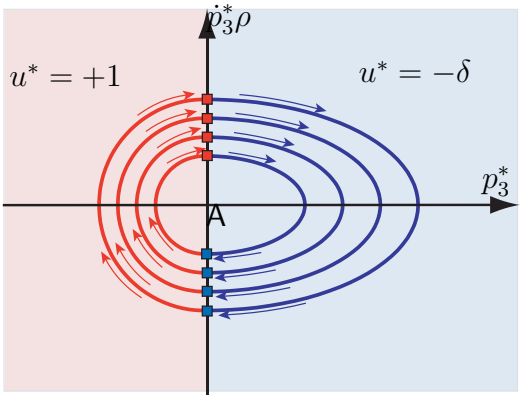

Figure 3: Phase portrait of $(p_3^*, \dot{p}_3^*\rho)$. Abnormal case $p_0^* = 0$.

iii) $\min\{\alpha, \gamma\} < (\beta - \pi)\varrho, \quad \big[\min\{\alpha, \gamma\} < (\beta - \pi)\rho\big].$

Proof. We consider an $\mathsf{b}_\alpha^-\mathsf{b}_\beta^+\mathsf{b}_\gamma^-$ path. The case of an $\mathsf{b}_\alpha^+\mathsf{b}_\beta^-\mathsf{b}_\gamma^+$ path can be treated similarly. First, we consider the abnormal case $p_0^* = 0$. It follows from Fig. 3 that a point in the $(p_3^*, \rho\dot{p}_3^*)$ plane stays in the half plane $p_3 \leq 0$ for exactly $\beta = \pi\rho$ units of time, which is the time required for a particle with coordinates $(p_3^*, \rho\dot{p}_3^*)$ to travel half of the circumference of a circle centered at the origin with constant angular speed $\omega = 1/\rho$. However, using the same geometric argument as in Lemma 23 in [199] we can show that the resulting path with $\beta = \pi\rho$ is not optimal. Hence, all optimal extremals of $\mathsf{b}_\alpha^-\mathsf{b}_\beta^+\mathsf{b}_\gamma^-$ type must be normal.

We therefore let $p_0^* = 1$ in (12)-(15). In Fig. 4, we observe that the phase portrait of $(p_3^*, \rho\dot{p}_3^*)$ consists of a circle centered at A, denoted as C_A and an ellipse centered at B, denoted as E_B, in the $p_3^* < 0$ and $p_3^* > 0$ half-planes respectively, with parameterizations that trace both of them clockwise and such that a full loop along them requires $2\pi\rho$ and $2\pi\varrho$ units of time, respectively. Note that a jump from $u^* = -\delta$ to $u^* = +1$, and vice versa, occurs only if E_B intersects C_A along the axis $p_3^* = 0$. If this intersection does occur, we denote as C and D the points of intersection. Let r and r_δ denote the distance of either C or D from A and B respectively. Then E_B and C_A intersect only if $r \geq \rho$ and $r_\delta \geq \varrho$, and furthermore $r_\delta = \sqrt{r^2 + \varrho^2 - \rho^2}$ as shown in Fig. 4.

From Fig. 4 it follows that β corresponds to the travel time of the point $(p_3^*, \rho \dot{p}_3^*)$ from D to C along the circle C_{A}. The times α and γ are upper bounded by the travel time from C to D along the ellipse E_{B}. We observe that $\pi\rho$ is a strict lower bound for β since $\rho > 0$ (note that β tends to $\pi\rho$ as A gets closer to O but can never reach as far as $\rho > 0$). Furthermore, $2\pi\rho$ and $2\pi\varrho$ are strict uppers bound for β and both α and γ, respectively. To see why the previous remark is true, it suffices to observe that the bang arcs $\mathsf{b}^+_{2\pi\varrho}$ and $\mathsf{b}^-_{2\pi\rho}$ correspond to two full circles driving the system (1) to the same state, and thus both $\mathsf{b}^+_{2\pi\varrho}$ and $\mathsf{b}^-_{2\pi\rho}$ cannot be part of an optimal solution.

Next, we improve the upper bound on α, γ. In particular, we observe in Fig. 4 that given β, where $\beta = 2(\pi - \widehat{\mathsf{CAO}})\rho$, then α or γ is maximized if the point $(p_3^*, \rho \dot{p}_3^*)$ coincides with C at $t = 0$ or D at $t = T_{\mathrm{f}}$, respectively. Thus, $\max\{\alpha, \gamma\} \leq 2(\pi - \widehat{\mathsf{DBO}})\varrho$. By using simple geometric arguments, along with the fact that $\delta \in (0, 1]$, it follows that $\widehat{\mathsf{DBO}} = \operatorname{atan}\left(\delta \tan \widehat{\mathsf{CAO}}\right)$. Thus, $\max\{\alpha, \gamma\} \leq 2\left(\pi - \operatorname{atan}\left(\delta \tan \widehat{\mathsf{CAO}}\right)\right)\varrho$, and $\beta = 2(\pi - \widehat{\mathsf{CAO}})\rho$. Equation (16) follows immediately.

Finally, the third condition of the Proposition is proved by means of simple geometric arguments as in Lemma 3 of [46]. □

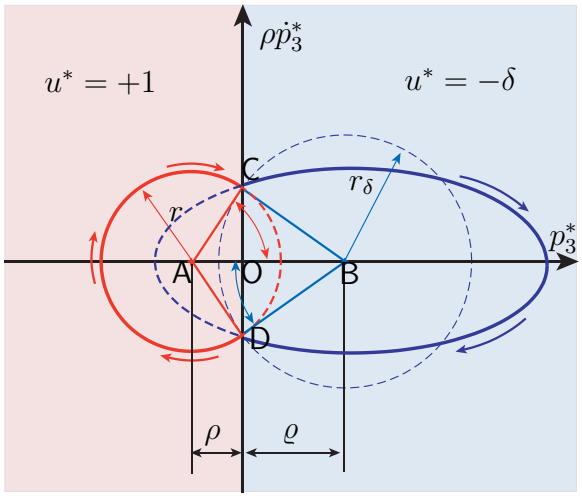

Figure 4: Phase portrait $(p_3^*, \rho \dot{p}_3^*)$.

Proposition 4. *An* $\mathsf{b}^-_\alpha \mathsf{s}_\beta \mathsf{b}^-_\gamma$ *path corresponds to a time-optimal trajectory of Problem 1 only if* $\alpha + \gamma \leq 2\pi\varrho$.

Proof. See the proof of Lemma 5 of Ref. [46]. □

Remark 1 Notice that Lemma 5 of [46] does not apply for $\mathsf{b}^+\mathsf{s}\mathsf{b}^+$ paths of the ASDMD problem. In particular, as is illustrated in Fig. 5, the ASDID car emanating from O reaches the terminal configuration $\mathsf{x}_\mathrm{f} = (x_\mathrm{f}, y_\mathrm{f}, \theta_\mathrm{f})$ by traversing an $\mathsf{b}^+_\alpha \mathsf{s}_\beta \mathsf{b}^+_\gamma$ path with $\alpha + \gamma > 2\pi\rho$. The total elapsed time is the same as if the ASDID car had traversed an $\mathsf{b}^-_\alpha \mathsf{s}_\beta \mathsf{b}^-_\gamma$ with $\alpha + \gamma \leq 2\pi$. Therefore, if the path $\mathsf{b}^-\mathsf{s}\mathsf{b}^-$ is time-optimal, then the $\mathsf{b}^+_\alpha \mathsf{s}_\beta \mathsf{b}^+_\gamma$ path is necessarily time-optimal as well. Thus, we conjecture that there exist $\mathsf{b}^+_\alpha \mathsf{s}_\beta \mathsf{b}^+_\gamma$ paths with $\alpha + \gamma > 2\pi\rho$, which are optimal paths of the ASDMD problem. As it is demonstrated in Section 3.4, our conjecture is indeed correct. Next we provide a conservative bound on the sum of α and γ along $\mathsf{b}^+_\alpha \mathsf{s}_\beta \mathsf{b}^+_\gamma$ paths.

Proposition 5. *An* $\mathsf{b}^+_\alpha \mathsf{s}_\beta \mathsf{b}^+_\gamma$ *path corresponds to a time-optimal trajectory of Problem 1 only if* $\alpha + \gamma \leq (4\pi - \theta_\mathrm{f})\rho$.

Finally, for $\mathsf{b}^-\mathsf{s}\mathsf{b}^+$ and $\mathsf{b}^+\mathsf{s}\mathsf{b}^-$ paths, as in the standard MD problem, we simply take the most conservative bounds. In particular, we have the following proposition.

Proposition 6. *An* $\mathsf{b}^+_\alpha \mathsf{s}_\beta \mathsf{b}^-_\gamma$ *and an* $\mathsf{b}^-_\alpha \mathsf{s}_\beta \mathsf{b}^+_\gamma$ *path corresponds to a time-optimal trajectory of Problem 1 only if* $\max\{\alpha, \delta\gamma\} < 2\pi\rho$ *and* $\max\{\delta\alpha, \gamma\} < 2\pi\rho$, *respectively.*

3.4 Time-Optimal Synthesis

In this section, we address the time-optimal synthesis problem for the ASDMD problem, and thus provide a complete characterization of the optimal control that solves Problem 1 with boundary conditions (3), for all $(x_\mathrm{f}, y_\mathrm{f}, \theta_\mathrm{f}) \in \mathbb{R}^2 \times \mathbb{S}^1$.

First, we show by means of an example, that the synthesis of optimal paths for the ASDMD problem may be quite different than for the MD problem. In particular,

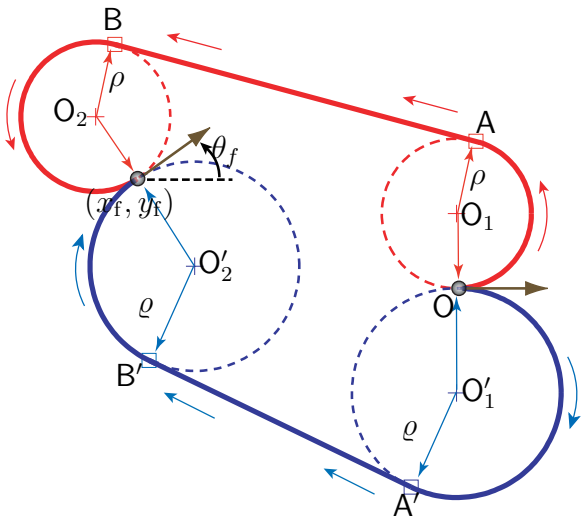

Figure 5: A $\mathsf{b}^+_\alpha \mathsf{s}_\beta \mathsf{b}^+_\gamma$ path with $\alpha+\gamma > 2\pi\rho$ can be an optimal solution of the ASDMD problem, in contrast to the solution of the standard MD problem.

let us consider the problem of characterizing the minimum-time path from $(0, 0, 0)$ to $(0, 0, \pi)$ for the ID and the ASDID cars. On the one hand, the optimal solution of the standard MD problem is either a $\mathsf{b}^+_\alpha \mathsf{b}^-_\beta \mathsf{b}^+_\gamma$ path or a $\mathsf{b}^-_\alpha \mathsf{b}^+_\beta \mathsf{b}^-_\gamma$ path, where $\alpha = \gamma = \pi\rho/3$ and $\beta = 5\pi\rho/3$, as shown in Fig. 6(a) (these two paths have exactly the same length). On the other hand, as is illustrated in Fig. 6(b), the optimal path for the ASDMD problem is either an $\mathsf{b}^-_\alpha \mathsf{b}^+_\beta \mathsf{b}^-_\gamma$ path, where $\alpha = \gamma = \varrho \operatorname{acos}(1/(1+\delta))$ and $\beta = \pi\rho + 2\delta\alpha$ or an $\mathsf{b}^+_\alpha \mathsf{s}_\beta \mathsf{b}^+_\gamma$ path, where $\alpha = \gamma = 3\pi\rho/2$ and $\beta = 2\rho$. The $\mathsf{b}^-_\alpha \mathsf{b}^+_\beta \mathsf{b}^-_\gamma$ and the $\mathsf{b}^+_\alpha \mathsf{s}_\beta \mathsf{b}^+_\gamma$ paths have exactly the same length when $\delta = \tilde{\delta}$, where $\tilde{\delta}$ is the solution of the equation: $1/(1+\delta) + \cos((\pi-\delta)/(1+\delta)) = 0$. Note that for this specific problem, the $\mathsf{b}^+_\alpha \mathsf{s}_\beta \mathsf{b}^+_\gamma$ path can never be an optimal path of the standard MD problem, in light of Lemma 5 of [46].

To simplify the presentation and without loss in generality, we henceforth consider the minimum trajectories of the ASDID car from $(0, 0, 0)$ to $(x_\mathrm{f}, y_\mathrm{f}, \theta_\mathrm{f}) \in P_{\theta_\mathrm{f}}$, where $P_{\theta_\mathrm{f}} := \{(x, y, \theta) \in \mathbb{R}^2 \times \mathbb{S}^1 \ : \ \theta = \theta_\mathrm{f}\}$ as suggested in [45, 46]. Let $\mathfrak{R}_{\theta_\mathrm{f}}(u)$ denote the reachable set that corresponds to the control sequence $u \in \mathsf{U}^*$. The coordinates of all points in P_{θ_f} that can be reached by means of a $\mathsf{b}^+\mathsf{s}\mathsf{b}^+$ control sequence can be expressed as functions of the times of motion along the three arcs of the path, namely

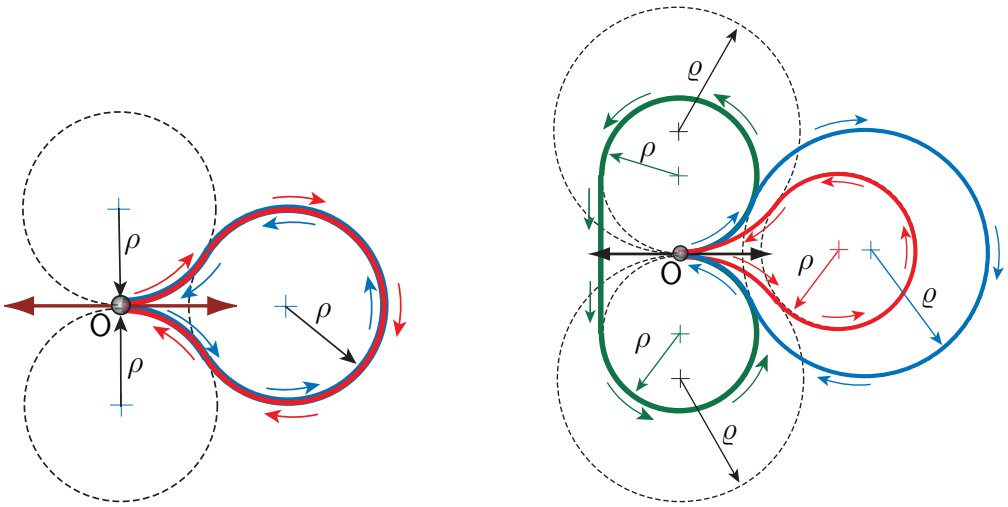

(a) Standard MD problem.

(b) Asymmetric sinistral/dextral Markov-Dubins problem.

Figure 6: The minimum-time paths for the steering problem from $(0,0,0)$ to $(0,0,\pi)$ for the ID and the ASDID cars.

α, β, and γ, by simply integrating the equations (1), from $t=0$ to $t=\alpha$ for $u=+1$, and subsequently, from $t=\alpha$ to $t=\alpha+\beta$ for $u=0$, and finally, from $t=\alpha+\beta$ to the final time $T_{\mathrm{f}}(\mathsf{b}^+\mathsf{sb}^+)=\alpha+\beta+\gamma$. Note that γ can always be expressed in terms of the parameters α and β (actually for a $\mathsf{b}^+\mathsf{sb}^+$ path γ depends only on α as we shall see shortly later). In particular, since the total change of the velocity direction θ (initially $\theta=0$) along the path $\mod 2\pi$ must equal θ_{f}, it follows readily that $\alpha/\rho+\gamma/\rho \mod 2\pi=\theta_{\mathrm{f}}$, which furthermore implies that

$$\gamma(\alpha)=\begin{cases}\rho\theta_{\mathrm{f}}-\alpha, & \text{if } \theta_{\mathrm{f}}\geq\dfrac{\alpha}{\rho},\\[2ex] \rho(2\pi+\theta_{\mathrm{f}})-\alpha, & \text{if } \theta_{\mathrm{f}}<\dfrac{\alpha}{\rho}.\end{cases} \tag{17}$$

It follows after routine calculations that

$$x_{\mathrm{f}}(\alpha,\beta)=\rho\sin\theta_{\mathrm{f}}+\beta\cos\frac{\alpha}{\rho},\qquad y_{\mathrm{f}}(\alpha,\beta)=\rho+\beta\sin\frac{\alpha}{\rho}-\rho\cos\theta_{\mathrm{f}}. \tag{18}$$

Furthermore, Proposition 5 determines the intervals of admissible values of α and β for a $\mathsf{b}^+\mathsf{sb}^+$ control sequence, denoted by $\mathcal{I}_\alpha(\mathsf{b}^+\mathsf{sb}^+)$ and $\mathcal{I}_\beta(\mathsf{b}^+\mathsf{sb}^+)$, respectively. Thus, the reachable set of the control sequence $\mathsf{b}^+\mathsf{sb}^+$ are constructed by determining all points $(x_{\mathrm{f}},y_{\mathrm{f}},\theta_{\mathrm{f}})\in P_{\theta_{\mathrm{f}}}$ for every pairs of $(\alpha,\beta)\in\mathcal{I}_\alpha(\mathsf{b}^+\mathsf{sb}^+)\times\mathcal{I}_\beta(\mathsf{b}^+\mathsf{sb}^+)$.

Conversely, given a point $(x_\mathrm{f}, y_\mathrm{f}, \theta_\mathrm{f}) \in \mathfrak{R}_{\theta_\mathrm{f}}(\mathsf{b}^+\mathsf{sb}^+)$ one can determine the parameters α and β such that x_f and y_f satisfy (18). In particular, after some algebra, it follows from (18) that

$$\alpha(x_\mathrm{f}, y_\mathrm{f}) = \rho\,\mathrm{atan2}(B(y_\mathrm{f}), A(x_\mathrm{f})), \qquad \beta(x_\mathrm{f}, y_\mathrm{f}) = \sqrt{A^2(x_\mathrm{f}) + B^2(y_\mathrm{f})}, \tag{19}$$

where $A(x_\mathrm{f}) = x_\mathrm{f} - \rho\sin\theta_\mathrm{f}$, $B(y_\mathrm{f}) = y_\mathrm{f} + \rho\cos\theta_\mathrm{f} - \rho$, and $\mathrm{atan2} : \mathbb{R}^2 \mapsto [0, 2\pi[$ is the two-argument arctangent function.

Figure 7(a) illustrates the reachable set $\mathfrak{R}_{\theta_\mathrm{f}}(\mathsf{b}^+\mathsf{sb}^+)$ of the ASDID car (note that for this path family the value of δ does not affect the geometry of the reachable set), whereas the same reachable set for the standard ID car is illustrated in 7(b). We observe that the former set is a superset of the latter. This is because for the ASDMD problem α satisfies $\alpha + \gamma(\alpha) \leq (4\pi - \theta_\mathrm{f})\rho$ (Proposition 5), whereas for the standard MD problem it satisfies the stricter condition $\alpha + \gamma(\alpha) \leq 2\pi\rho$ (Lemma 5 of [46]).

Finally, after having established the connection between (α, β) and $(x_\mathrm{f}, y_\mathrm{f})$ the total time $T_\mathrm{f}(\mathsf{b}^+\mathsf{sb}^+)$ is given, via (17), by

$$T_\mathrm{f}(\mathsf{b}^+\mathsf{sb}^+) = \begin{cases} \beta + \rho\theta_\mathrm{f}, & \text{if } \theta_\mathrm{f} \geq \alpha/\rho, \\ \beta + \rho(2\pi + \theta_\mathrm{f}), & \text{if } \theta_\mathrm{f} < \alpha/\rho. \end{cases} \tag{20}$$

The previous procedure can be applied mutatis mutandis for the rest of the control sequences from U^* (although the algebra, especially in the case of $\mathsf{b}^+\mathsf{b}^-\mathsf{b}^+$ or $\mathsf{b}^-\mathsf{b}^+\mathsf{b}^-$ paths, is significantly more evolved). In the Appendix A, we provide the equations that give α and β as functions of x_f and y_f, and vice versa, as well as the minimum-time T_f for all the control sequences $u \in \mathsf{U}^*$.

The next step involves the partitioning of P_{θ_f} into at most six domains, denoted as $\mathfrak{R}^*_{\theta_\mathrm{f}}(u)$, where $u \in \mathsf{U}^*$, such that if $(x_\mathrm{f}, y_\mathrm{f}, \theta_\mathrm{f}) \in \mathrm{int}\left(\mathfrak{R}^*_{\theta_\mathrm{f}}(u)\right)$, then $(x_\mathrm{f}, y_\mathrm{f}, \theta_\mathrm{f})$ cannot be reached faster with the application of $v \in \mathsf{U}^*$, where $v \neq u$. We shall refer to this partition of P_{θ_f} as the optimal control partition of the ASDMD problem. The

number of these domains can be strictly less than six in case the domain associated with a particular control sequence has an empty interior. As we shall see shortly after, such "pathological" cases arise in the time-optimal synthesis of the ASDMD problem in contrast to the optimal synthesis of the standard MD problem. The procedure required for the characterization of the domain over which the control sequence, say $\mathsf{b}^+\mathsf{sb}^+$, is optimal, is summarized below. We denote this domain by $\mathfrak{R}^*_{\theta_\mathrm{f}}(\mathsf{b}^+\mathsf{sb}^+)$. In particular, let $(x_\mathrm{f}, y_\mathrm{f}, \theta_\mathrm{f}) \in \mathfrak{R}_{\theta_\mathrm{f}}(\mathsf{b}^+\mathsf{sb}^+)$, and let $\mathsf{U}^c(\mathsf{b}^+\mathsf{sb}^+) \subset \mathsf{U}^*$ denote the set of control sequences u that are different from $\mathsf{b}^+\mathsf{sb}^+$ and such that $(x_\mathrm{f}, y_\mathrm{f}, \theta_\mathrm{f}) \in \mathfrak{R}_{\theta_\mathrm{f}}(u)$. Then $(x_\mathrm{f}, y_\mathrm{f}, \theta_\mathrm{f}) \in \mathfrak{R}^*_{\theta_\mathrm{f}}(\mathsf{b}^+\mathsf{sb}^+)$ if and only if $T_\mathrm{f}(\mathsf{b}^+\mathsf{sb}^+) \leq \min_{u \in \mathsf{U}^c(\mathsf{b}^+\mathsf{sb}^+)} T_\mathrm{f}(u)$.

Figure 8 illustrates the optimal control partition of $P_{\pi/3}$ as well as the level sets of the minimum-time T_f, for different values of the ratio $\delta^{-1} = \varrho/\rho$. In particular, each domain of the partition $P_{\pi/3}$ is illustrated by a colored set, whereas the level sets of the minimum time are denoted by solid black lines. We observe that as the ratio ϱ/ρ increases, the domains $\mathfrak{R}^*_{\pi/3}(\mathsf{b}^+\mathsf{sb}^+)$, $\mathfrak{R}^*_{\pi/3}(\mathsf{b}^-\mathsf{sb}^+)$ and $\mathfrak{R}^*_{\pi/3}(\mathsf{b}^+\mathsf{sb}^-)$, primarily, and the domain $\mathfrak{R}^*_{\pi/3}(\mathsf{b}^-\mathsf{b}^+\mathsf{b}^-)$, secondary, expand against the domain $\mathfrak{R}^*_{\pi/3}(\mathsf{b}^-\mathsf{sb}^-)$ as well as the disconnected components of $\mathfrak{R}^*_{\pi/3}(\mathsf{b}^+\mathsf{sb}^-)$ and $\mathfrak{R}^*_{\pi/3}(\mathsf{b}^-\mathsf{sb}^+)$ that are close to the origin of P_{θ_f}. We observe, in particular, that for $\varrho/\rho = 1.8$ (Fig 8(e)) the partition of $P_{\pi/3}$ consists of five domains since the domain $\mathfrak{R}^*_{\pi/3}(\mathsf{b}^+\mathsf{b}^-\mathsf{b}^+)$ is reduced to the empty set. Similarly, for $\varrho/\rho = 2$ (Fig 8(f)) only four domains are non-empty since $\mathfrak{R}^*_{\pi/3}(\mathsf{b}^-\mathsf{sb}^-) = \mathfrak{R}^*_{\pi/3}(\mathsf{b}^+\mathsf{b}^-\mathsf{b}^+) = \varnothing$. In addition, we observe in Fig 8(a)-8(f) that the boundaries of each domain change significantly as the ratio ϱ/ρ varies.

3.5 Time Optimal Synthesis and Reachable Sets of the ASDMD when the Final Tangent of the Path is Free

In this section, we consider the optimal synthesis of Problem 1, when θ_f is assumed to be free. The solution of this variation of Problem 1 will allow us to characterize analytically the set of points in the plane that can be reached by curves with asymmetric curvature constraints. These reachable sets along with the level sets of the

minimum time of the ASDMD problem, when θ_{f} is free, exhibit a few notable features related to the existence/abscence of symmetry planes that are not present neither in the reachable sets nor the syntheses of the standard MD and the ASDMD problems, when θ_{f} is fixed. Favoring the economy of presentation, we shall not discuss in details the analysis of this problem, which is similar to the discussion presented in Sections 4.3-4.4, and we will instead present the solution of the time-optimal synthesis problem directly.

First, we discuss briefly the structure of the family of extremal controls, which is sufficient for optimality for Problem 1, when θ_{f} is free. In particular, the new transversality condition for θ is given by $p_3^*(T_{\mathrm{f}}) = 0$. Following the same line of arguments as in [201], where the standard MD, when θ_{f} is free, is addressed in detail, we conclude that a composite path whose final arc is either an b^- or an b^+ arc, that is preceded by an s arc, cannot be part of an optimal path. The following proposition gives us the family of candidate optimal controls for Problem 1, when θ_{f} is free (it follows similarly to [201]).

Proposition 7. *The optimal control u^* of Problem 1, when θ_{f} is free, belongs necessarily to U^*, where*

$$\mathsf{U}^* := \{\{\mathsf{u}^{\pm}, 0\}, \{\mathsf{u}^{\pm}, \mathsf{u}^{\mp}\}\}, \qquad \mathsf{u}^+ := 1, \qquad \mathsf{u}^- := -\delta. \tag{21}$$

Proposition 7 implies that the set of candidate optimal controls of Problem 1, when θ_{f} is free, consists of only four control sequences with at most one switching. It follows that the minimum-time paths of Problem 1, when θ_{f} is free, necessarily admit one of the following structures: *i)* $\mathsf{b}_\alpha^+\mathsf{b}_\beta^-, \mathsf{b}_\alpha^-\mathsf{b}_\beta^+$, *ii)* $\mathsf{b}_\alpha^+\mathsf{s}_\beta, \mathsf{b}_\alpha^-\mathsf{s}_\beta$.

By repeating the analysis carried out in Sections 3.3 and 3.4, we can refine the family of candidate optimal controls (this analysis will lead to a number of propositions similar to Props. 3-6), and subsequently solve the synthesis problem for Problem 1, when θ_{f} is free. Favoring the economy of presentation, we directly show the solution

of the synthesis problem. In particular, Figure 9 illustrates the optimal control partition of the plane as well as the level sets of the minimum-time $T_{\rm f}$, when $\theta_{\rm f}$ is free (assuming that the ID/ASDID car starts from the origin with $\theta = 0$) for both the standard ID car (Fig. 9(a)) and the ASDID car (Figs. 9(b)-9(d)). Figs. 9(b)- 9(d) illustrate that as the agility of the ASDID to perform right turns, which is measured by the ratio ϱ/ρ, is reduced, the sets $\mathfrak{R}^*(\mathsf{b}^-\mathsf{s})$ and $\mathfrak{R}^*(\mathsf{b}^+\mathsf{b}^-)$ "shrink" in favor of the set $\mathfrak{R}^*(\mathsf{b}^+\mathsf{s})$, whereas the set $\mathfrak{R}^*(\mathsf{b}^-\mathsf{b}^+)$ remains invariant under the variations of the ratio ϱ/ρ.

It is worth noting that contrary to the synthesis of the ASDMD problem, when $\theta_{\rm f}$ is fixed, where both the level sets of the minimum-time and the domains of the optimal control partition are symmetric with respect to some plane of symmetry (also a characteristic of the optimal synthesis of the standard MD problem), both the level sets and the domains of the optimal control partition of the ASDMD problem, when $\theta_{\rm f}$ is free, do not enjoy similar symmetry properties. It appears that the term "asymmetric" used in the title of this chapter is more obviously justified in the case when $\theta_{\rm f}$ is free rather than when $\theta_{\rm f}$ is fixed.

Let $\tau > 0$ and let $\mathfrak{R}^{\rm s}_{t\leq\tau}$ and $\mathfrak{R}^{\rm asym}_{t\leq\tau}$ denote the set of points in the plane that can be reached by the ID and ASDID car in time $t \in [0, \tau]$, respectively (assuming again that the ID/ASDID car starts from the origin with $\theta = 0$). The reachable sets $\mathfrak{R}^{\rm asym}_{t\leq\tau}$ for different values of τ are illustrated in Fig. 10. In Figs.10(a)-10(d), we observe that the reachable sets $\mathfrak{R}^{\rm asym}_{t\leq\tau}$ are not symmetric with respect to the x-axis by contrast to the sets $\mathfrak{R}^{\rm s}_{t\leq\tau}$ (see, for example, [37, 190]). This comes at no surprise, since both $\mathfrak{R}^{\rm s}_{t\leq\tau}$ and $\mathfrak{R}^{\rm asym}_{t\leq\tau}$ can be interpreted as the union of all the level sets $\{(x, y) : \ T_{\rm f} = t\}$, for $t \in [0, \tau]$, which, as we have already mentioned, are symmetric with respect to x-axis for the standard MD problem but not for the ASDMD problem, when $\theta_{\rm f}$ is free.

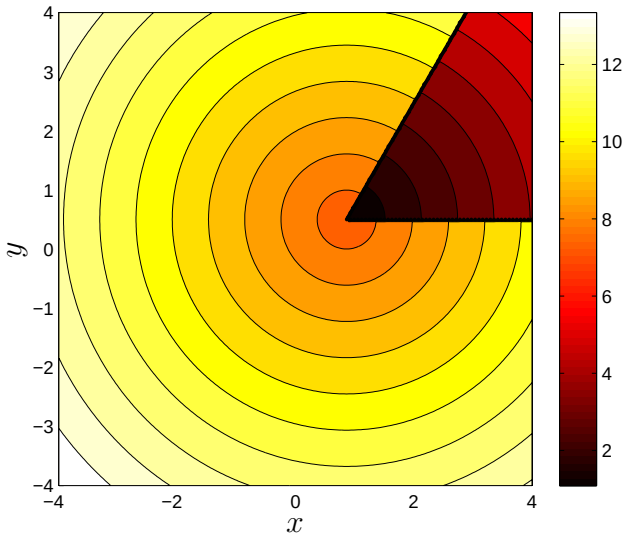

(a) $0 < \delta < 1$

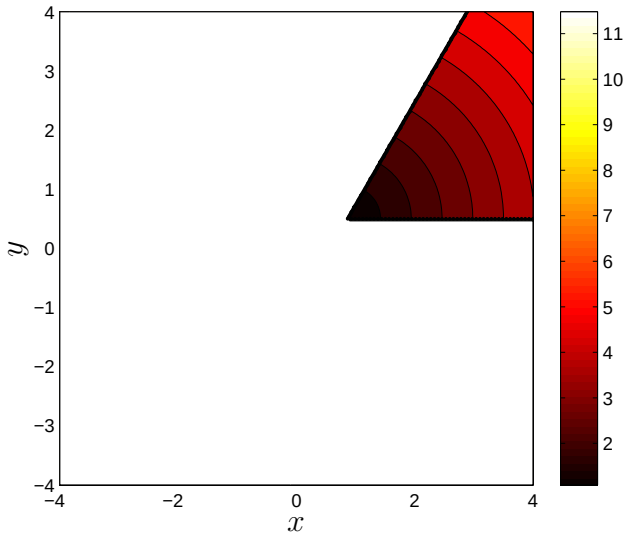

(b) $\delta = 1$ (standard MD)

Figure 7: Reachable set $\mathfrak{R}_{\theta_f}(\mathsf{b}^+\mathsf{sb}^+)$ for $\delta \in (0, 1)$ (ASDMD problem) and $\delta = 1$ (standard MD problem). The white colored region corresponds to terminal configurations that cannot be reached in minimum-time by means of a $\mathsf{b}^+\mathsf{sb}^+$ control sequence for the standard MD problem.

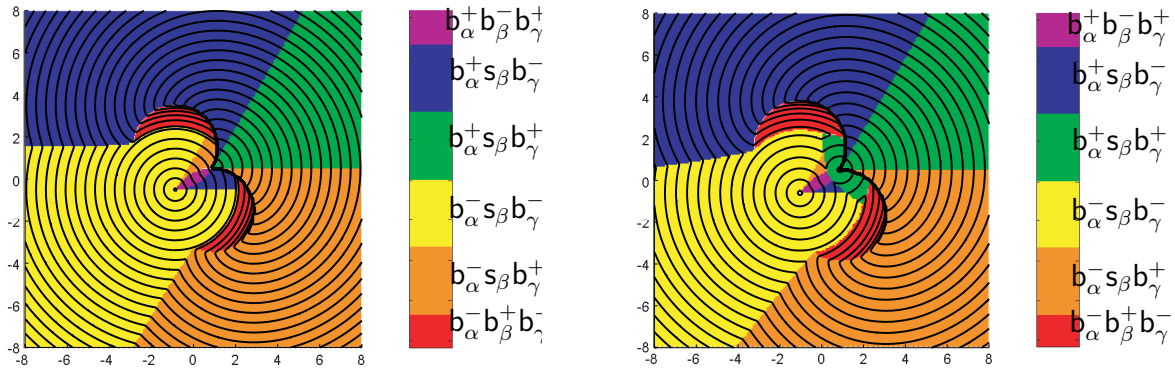

(a) $\varrho/\rho = 1.0$ (b) $\varrho/\rho = 1.2$

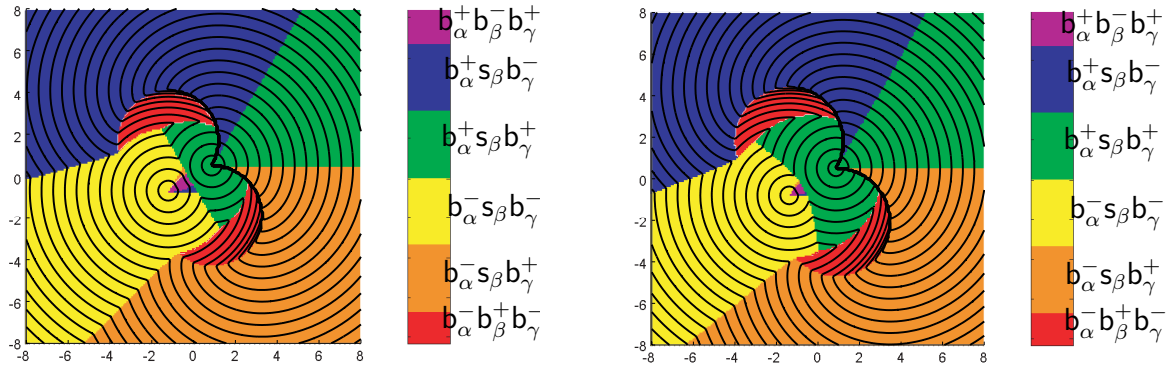

(c) $\varrho/\rho = 1.4$ (d) $\varrho/\rho = 1.6$

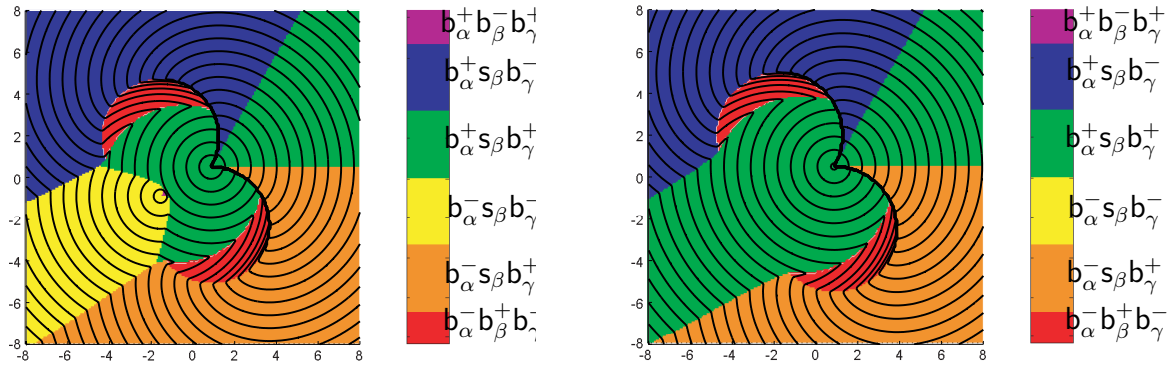

(e) $\varrho/\rho = 1.8$ (f) $\varrho/\rho = 2.0$

Figure 8: Partition of $P_{\pi/3}$ and level sets of $T_{\mathrm{f}} = T_{\mathrm{f}}(x, y)$ for different values of the ratio $\delta^{-1} = \varrho/\rho$.

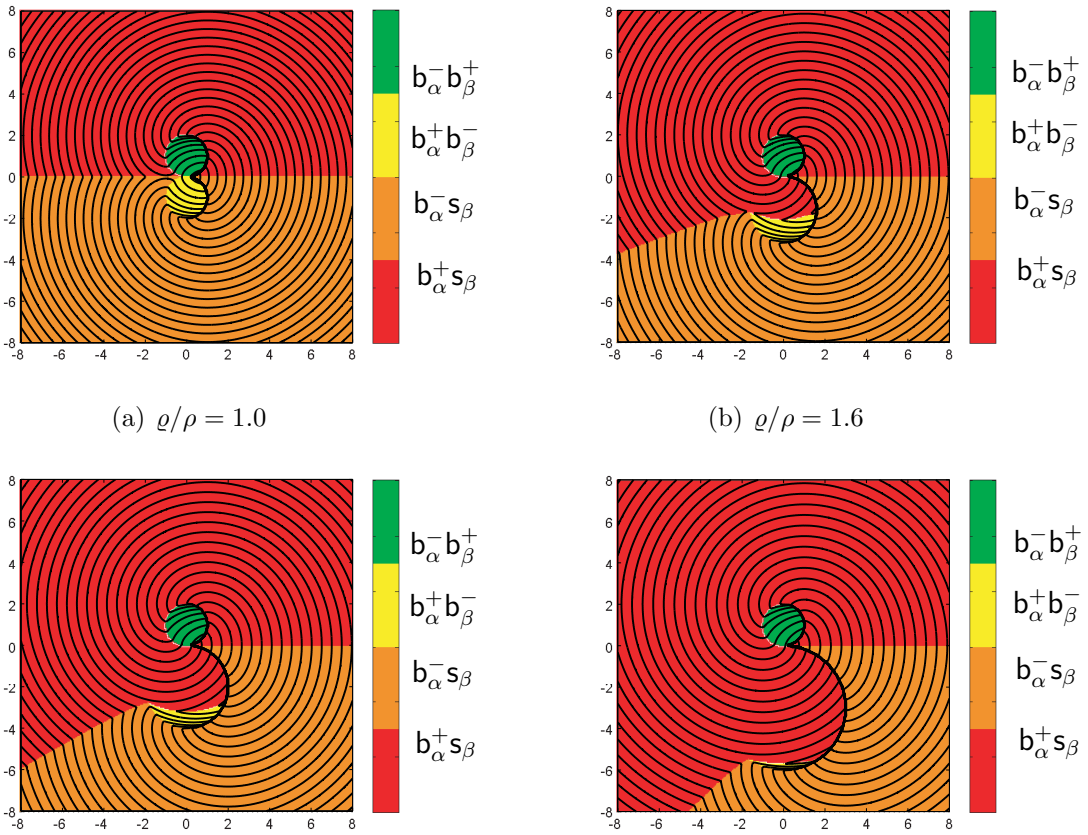

(a) $\varrho/\rho = 1.0$

(b) $\varrho/\rho = 1.6$

(c) $\varrho/\rho = 2.0$

(d) $\varrho/\rho = 3.0$

Figure 9: Partition of P and level sets of $T_\mathrm{f} = T_\mathrm{f}(x, y)$ for different values of the ratio ϱ/ρ.

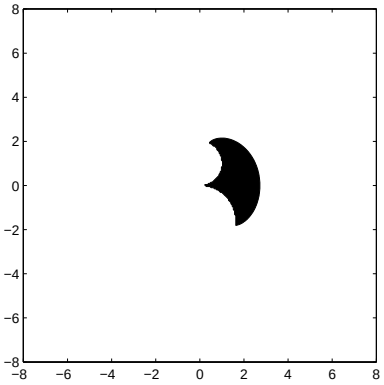

(a) $\mathfrak{R}^{\mathrm{asym}}_{t\leq\tau}$, $\tau = (\rho+\varrho)\pi/3$.

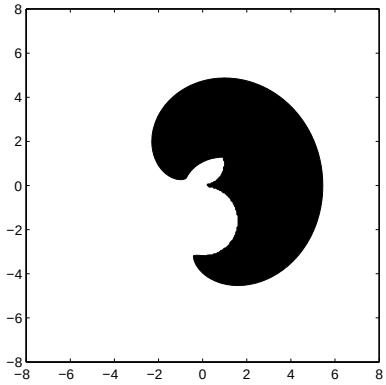

(b) $\mathfrak{R}^{\mathrm{asym}}_{t\leq\tau}$, $\tau = (\rho+\varrho)2\pi/3$.

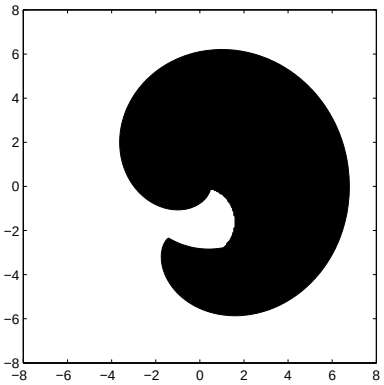

(c) $\mathfrak{R}^{\mathrm{asym}}_{t\leq\tau}$, $\tau = (\rho+\varrho)(3\pi+1)/4$.

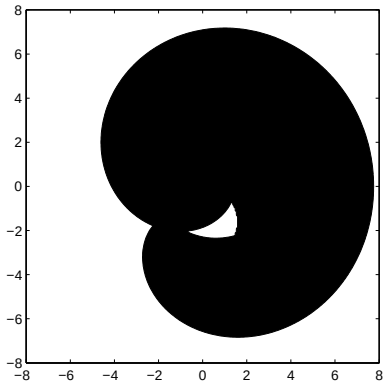

(d) $\mathfrak{R}^{\mathrm{asym}}_{t\leq\tau}$, $\tau = (\rho+\varrho)(3\pi+2.5)/4$.

Figure 10: Reachable sets $\mathfrak{R}^{\mathrm{asym}}_{t\leq\tau}$ for different values of τ and for $\varrho/\rho = 1.6$.

CHAPTER IV

OPTIMAL SYNTHESIS OF THE ZERMELO-MARKOV-DUBINS PROBLEM IN A CONSTANT DRIFT FIELD

The material in this chapter builds upon the results presented in [15].

4.1 Introduction

In this chapter, we consider the problem of guiding an aerial or marine vehicle with turning constraints to a prescribed terminal configuration in the presence of a constant drift field in minimum time. In particular, we assume that the vehicle travels in the plane with constant forward speed and such that the direction of its forward velocity cannot be changed faster than a prescribed upper bound. First, we revisit the ZMD problem for the special case of a constant drift field and, by using standard optimal control tools and geometric techniques, we rigorously characterize the structure of its extremals. Moreover, we highlight the existence of extremals of the ZMD problem that do not appear in the solution of the standard MD problem. The end result of our analysis is a family of extremals for the ZMD problem that is sufficient for complete controllability and necessary for optimality. Furthermore, we establish a direct correspondence between the reachable sets and the optimal syntheses of the MD and the ZMD problems by means of a discontinuous mapping. This mapping allows for a more analytical treatment of the optimal synthesis of the ZMD, and thus lifts the computational burden of numerically solving the system of transcendental equations for each terminal configuration.

4.2 Kinematic Model and Problem Formulation

In this section, we introduce the kinematic model of the vehicle and examine its controllability. Subsequently, we formulate the minimum-time problem and examine its feasibility.

4.2.1 Kinematic Model and Controllability Analysis

We consider an aerial/marine vehicle whose motion is described by the following set of equations

$$\dot{x} = \cos\theta + w_x, \quad \dot{y} = \sin\theta + w_y, \quad \dot{\theta} = \frac{u}{\rho}, \quad t \geq 0, \tag{22}$$

and initial conditions

$$x(0) = 0, \quad y(0) = 0, \quad \theta(0) = 0, \tag{23}$$

where $(x, y) \in \mathbb{R}^2$ are the Cartesian coordinates of a reference point of the vehicle, $\theta \in \mathbb{S}^1$ is the direction of the vehicle's forward velocity $v := (\cos\theta, \sin\theta)$, u is the control input, $w := (w_x, w_y)$ is the constant drift field induced by local winds/currents, and ρ is a positive constant. We write $w := \nu(\cos\phi, \sin\phi)$, where $\nu = |w|$ and $\phi \in \mathbb{S}^1$ is the direction of the drift. We assume that the set of admissible control inputs, denoted by $\mathcal{U}$, consists of all measurable functions defined on $[0, T]$, where $T \geq 0$, taking values in $U := [-1, 1]$.

Next, we interpret the problem of steering the system described by Eq. (22) to a prescribed terminal configuration as the intercept problem of a non-maneuvering target with a prescribed intercept angle. In particular, the equations of motion of the interceptor are given by

$$\dot{x}_{\mathcal{P}} = \cos\theta, \quad \dot{y}_{\mathcal{P}} = \sin\theta, \quad \dot{\theta}_{\mathcal{P}} = \frac{u}{\rho}, \quad t \geq 0, \tag{24}$$

with initial conditions

$$x_{\mathcal{P}}(0) = 0, \quad y_{\mathcal{P}}(0) = 0, \quad \theta_{\mathcal{P}}(0) = 0, \tag{25}$$

where $(x_{\mathcal{P}}, y_{\mathcal{P}}) \in \mathbb{R}^2$ are the Cartesian coordinates of the interceptor with respect to an inertial frame attached to its initial position, and $\theta_{\mathcal{P}} \in \mathbb{S}^1$ is the direction of the interceptor's velocity vector. Note that the kinematics of the interceptor coincide with those of the ID car. Furthermore, the target motion is described by the following set of equations

$$\dot{x}_{\mathcal{T}} = -w_x, \quad \dot{y}_{\mathcal{T}} = -w_y, \quad t \geq 0, \tag{26}$$

with initial conditions

$$x_{\mathcal{T}}(0) = x_{\mathrm{f}}, \quad y_{\mathcal{T}}(0) = y_{\mathrm{f}}, \tag{27}$$

where $(x_{\mathcal{T}}, y_{\mathcal{T}}) \in \mathbb{R}^2$ are the Cartesian coordinates of the non-maneuvering target measured with respect to an inertial frame attached to the initial position of the interceptor.

In the absence of drift, that is, for $w = 0$, the system described by Eq. (22) is completely controllable [199]. In the presence of a nonzero drift field w, however, controllability is not ensured. For example, if $\nu > 1$, then the set of unreachable configurations will be non-empty.

4.2.2 Controllability in the Case of a Constant Drift Field

Before proceeding to the formulation of the minimum-time steering problem, we examine its feasibility by studying the controllability of the system described by Eq. (22). The following proposition provides necessary and sufficient conditions for the complete controllability of the system described by Eq. (22).

Proposition 8. *Let $w = \nu(\cos\phi, \sin\phi)$ be a constant drift field. Then the system described by Eq.* (22) *is completely controllable if and only if $\nu < 1$.*

Proof. We show that for every $(x_{\mathrm{f}}, y_{\mathrm{f}}, \theta_{\mathrm{f}}) \in \mathbb{R}^2 \times \mathbb{S}^1$, there exists an admissible control $u \in \mathcal{U}$ that will drive the system described by Eq. (22) from $(0, 0, 0)$, at time $t = 0$, to

$(x_\mathrm{f}, y_\mathrm{f}, \theta_\mathrm{f})$, at time $t = t_\mathrm{f} < \infty$. First, we show sufficiency by using the interpretation of the ZMD problem as the minimum-time intercept Problem 3, as is illustrated in Fig. 11. In particular, let σ be the ray emanating from the initial position $(x_\mathrm{f}, y_\mathrm{f})$ of the target that is parallel to $\mathsf{e} := -(\cos\phi, \sin\phi)$, that is, $\mathsf{e} = -w/|w|$. Note that the target travels along σ with constant speed $v < 1$. Since the interceptor is a completely controllable system, there exists an admissible intercept strategy u that steers the interceptor to the initial position of the target $(x_\mathcal{T}(0), y_\mathcal{T}(0)) = (x_\mathrm{f}, y_\mathrm{f})$ on σ with $\theta_\mathcal{P} = \theta_\sigma$, where $\theta_\sigma = \pi + \phi \mod 2\pi$, at time $t = t_1 > 0$. Subsequently, the interceptor follows the target along σ. Since the interceptor is faster than the target, given that $\nu < 1$, then at some time $t = t_2 > t_1$, it will reach a point $(x'_\mathrm{f}, y'_\mathrm{f})$ on σ, sufficiently ahead of the target, say, at a distance $d \geq 0$. Given that the interceptor is a completely controllable system, there exists an admissible control $u_d \in \mathcal{U}$ to drive the interceptor from (x, y, θ_σ) to $(x, y, \theta_\mathrm{f})$, for any $(x, y) \in \mathbb{R}^2$, after $t_d = t_d(\phi, \theta_\mathrm{f})$ units of time. In particular,

$$(x_\mathcal{P}(t_\mathrm{f}), y_\mathcal{P}(t_\mathrm{f})) = (x_\mathcal{P}(t_2), y_\mathcal{P}(t_2)) = (x_\mathcal{T}(t_\mathrm{f}), y_\mathcal{T}(t_\mathrm{f})), \qquad \theta_\mathcal{P}(t_\mathrm{f}) = \theta_\mathrm{f}, \tag{28}$$

provided $d = \nu t_d$. The situation is illustrated in Fig. 11.

To show necessity, it suffices to observe that if $\nu \geq 1$, the target will travel faster than the interceptor. Thus, there exist boundary configurations for which no intercept will take place. □

4.2.3 Minimum-Time Problem Formulation

Next, we formulate the ZMD problem as a minimum-time problem with prescribed initial and terminal conditions.

Problem 2 (ZMD Minimum-Time Problem)**.** *Given the system described by Eq.* (22) *and a configuration* $(x_\mathrm{f}, y_\mathrm{f}, \theta_\mathrm{f}) \in \mathbb{R}^2 \times \mathbb{S}^1$*, determine a control input* $u^* \in \mathcal{U}$ *such that*

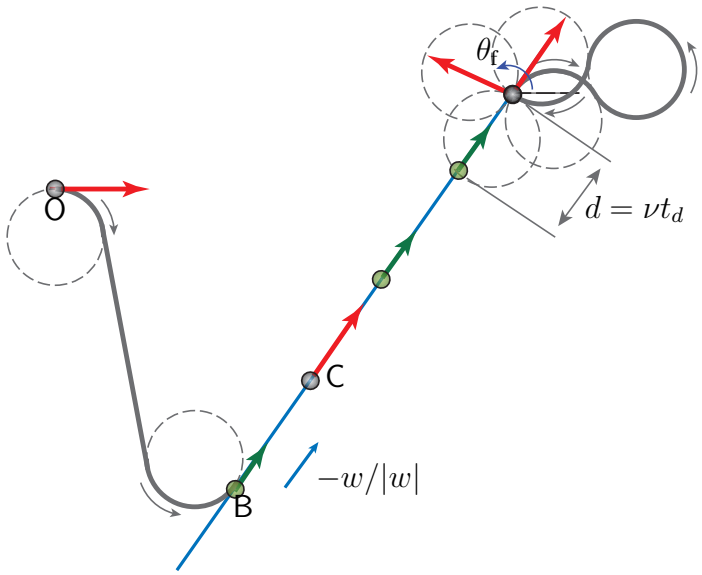

Figure 11: The system described by Eq. (22) is completely controllable if and only if $\nu < 1$.

(i) *The trajectory* $\mathsf{x}^* : [0, T_{\mathrm{f}}] \mapsto \mathbb{R}^2 \times \mathbb{S}^1$ *generated by the control* u^* *satisfies the boundary conditions*

$$\mathsf{x}^*(0) = (0, 0, 0), \qquad \mathsf{x}^*(T_{\mathrm{f}}) = (x_{\mathrm{f}}, y_{\mathrm{f}}, \theta_{\mathrm{f}}). \tag{29}$$

(ii) *The control* u^* *minimizes along the trajectory* x^* *the cost functional* $J(u) := T_{\mathrm{f}}$, *where* T_{f} *is the free final time.*

Note that if we assume, in addition, that the input value set is unbounded, that is, the input u can contain impulses and that both $\theta(0)$ and $\theta(T_{\mathrm{f}})$ are free, in which case, θ acts as a control input, then Problem 2 reduces to the Zermelo's navigation problem.

Next, we provide another alternative formulation of the ZMD problem as a minimum-time intercept problem of a non-maneuvering target from an interceptor with the kinematics of the ID car.

Problem 3. *Consider an interceptor and a non-maneuvering target, whose kinematics are described by Eq.* (24), *and Eq.* (26), *respectively, and let* $(x_{\mathrm{f}}, y_{\mathrm{f}}, \theta_{\mathrm{f}}) \in \mathbb{R}^2 \times \mathbb{S}^1$ *be given. Determine an intercept strategy* $u^* \in \mathcal{U}$ *such that*

(i) *The trajectory of the interceptor* $\mathsf{x}^*_{\mathcal{P}} : [0, T_{\mathrm{f}}] \mapsto \mathbb{R}^2 \times \mathbb{S}^1$, *where* $\mathsf{x}^*_{\mathcal{P}} := (x^*_{\mathcal{P}}, y^*_{\mathcal{P}}, \theta^*_{\mathcal{P}})$, *generated by the control* u^* *and the trajectory of the non-maneuvering target* $\mathsf{x}^*_{\mathcal{T}} := (x^*_{\mathcal{T}}, y^*_{\mathcal{T}})$ *satisfy the boundary conditions*

$$\mathsf{x}^*_{\mathcal{P}}(0) = (0, 0, 0), \qquad \mathsf{x}_{\mathcal{T}}(0) = (x_{\mathrm{f}}, y_{\mathrm{f}}), \tag{30}$$

$$x^*_{\mathcal{P}}(T_{\mathrm{f}}) = x^*_{\mathcal{T}}(T_{\mathrm{f}}), \qquad y^*_{\mathcal{P}}(T_{\mathrm{f}}) = y^*_{\mathcal{T}}(T_{\mathrm{f}}), \qquad \theta^*_{\mathcal{P}}(T_{\mathrm{f}}) = \theta_{\mathrm{f}}. \tag{31}$$

(ii) *The intercept strategy* u^* *minimizes along* $\mathsf{x}^*_{\mathcal{P}}$ *and* $\mathsf{x}^*_{\mathcal{T}}$ *the cost functional* $J(u) = T_{\mathrm{f}}$, *where* T_{f} *is the free intercept time.*

Note that Problems 2 and 3 are equivalent in the sense that a control $u^* \in \mathcal{U}$ is a solution of Problem 2 if and only if is a solution of Problem 3, and vice versa. At this point, it is worth mentioning that the ZMD problem was indirectly examined in [123], where the authors have analyzed the equivalent formulation of the ZMD problem as a minimum-time intercept problem of a non-maneuvering target (Problem 3). Furthermore, a variation of the min-time intercept Problem 3 was addressed in [89, 90]. In particular, the author of [89, 90] characterized a (suboptimal) solution of Problem 3 by considering a variation of the min-time intercept problem, where the hard constraint $u(t) \in U$, for all $t \geq 0$, was relaxed by considering the following cost function

$$J_{\mathrm{soft}}(u) = T_{\mathrm{f}} + \beta \int_0^{T_{\mathrm{f}}} u^2 \mathrm{d}t, \tag{32}$$

where β is a positive parameter to be chosen such that the input satisfies, if possible, the hard constraint $u(t) \in U$, for all $t \geq 0$, a posteriori. In this chapter, we will address the original formulation of the ZMD problem (Problem 2) directly, although in the subsequent analysis, we shall also employ the equivalent formulation of the ZMD problem as an intercept problem of a non-maneuvering target (Problem 3).

4.2.4 Existence of Optimal Solutions

To show existence of an optimal solution to Problem 2, we apply Filippov's Theorem for minimum-time problems with prescribed initial and terminal states [53]. In particular, we observe that the right hand side of Eq. (22) defines a vector field $f : \mathbb{R}^3 \times U \mapsto \mathbb{R}^2 \times \mathbb{S}^1 \subset \mathbb{R}^3$, where $f(\theta, u) := (\cos\theta + w_x, \sin\theta + w_y, u/\rho)$, which is continuous in u and continuously differentiable in θ. Furthermore, given that the vector field is affine in the control, and the input value set $U = [-1, 1]$ is convex and compact, it follows that for a given $\theta \in \mathbb{S}^1$, the set $f(\theta, U)$ is convex. To prove the existence of optimal solutions for the ZMD problem it suffices, in light of Filippov's Theorem, to show that there exists a constant $c > 0$ such that

$$|\langle \mathsf{x}, f(\mathsf{x}, u)\rangle| \leq c(1 + |\mathsf{x}|^2), \quad \text{for all} \quad (\mathsf{x}, u) \in \mathbb{R}^2 \times \mathbb{S}^1 \times U, \tag{33}$$

where $\mathsf{x} := (x, y, \theta)$, and the inner product and the norm that appear in Eq. (33) are the standard scalar product and the Euclidean norm in $\mathbb{R}^3$, respectively. Furthermore, in light of the triangle inequality, the Cauchy-Schwartz inequality, and the inequalities $\sqrt{x^2 + y^2} + |\theta| \leq \sqrt{2}|\mathsf{x}|$ and $2|\mathsf{x}| \leq 1 + |\mathsf{x}|^2$, it follows that

$$\begin{aligned}
|\langle \mathsf{x}, f(\mathsf{x}, u)\rangle| &\leq |x(\cos\theta + w_x) + y(\sin\theta + w_y)| + \frac{|u\theta|}{\rho} \\
&\leq \sqrt{x^2 + y^2}\sqrt{(w_x + \cos\theta)^2 + (w_y + \sin\theta)^2} + \frac{|\theta|}{\rho} \\
&\leq \sqrt{x^2 + y^2}(1 + \nu) + \frac{|\theta|}{\rho} \\
&\leq \frac{\sqrt{2}}{2}\max\left\{1 + \nu, \frac{1}{\rho}\right\}\left(1 + |\mathsf{x}|^2\right).
\end{aligned} \tag{34}$$

Thus, all conditions of Filippov's Theorem are satisfied, leading us to the following two propositions.

Proposition 9. *If there exists a control $u \in \mathcal{U}$ that drives the system described by Eq. (22) from $(0, 0, 0)$ to any $(x_\mathrm{f}, y_\mathrm{f}, \theta_\mathrm{f}) \in \mathbb{R}^2 \times \mathbb{S}^1$, then the minimum-time Problem 2 always has a solution.*

Proposition 10. *Let the drift field $w = \nu(\cos\phi, \sin\phi)$. If $\nu < 1$, then the minimum-time Problem 2 has a solution, for all $(x_\mathrm{f}, y_\mathrm{f}, \theta_\mathrm{f}) \in \mathbb{R}^2 \times \mathbb{S}^1$.*

Proof. If $\nu < 1$, then it follows from Proposition 8 that the system (22) is completely controllable. Thus, there always exists a feasible path from $(0, 0, 0)$ to any $(x_\mathrm{f}, y_\mathrm{f}, \theta_\mathrm{f}) \in \mathbb{R}^2 \times \mathbb{S}^1$, which furthermore implies, in light of Proposition 9, that a minimum-time path between these two configurations always exists. □

4.3 Optimal Control Analysis and Structure of Optimal Paths

In this Section, we revisit the ZMD problem posed in [123] and provide an in-depth examination of the structure of the extremals of the problem. Our analysis confirms or disproves prior conjectures about the existence of new extremals of the minimum-time problem and their optimality, which have appeared in the recent literature [123, 200, 15]

4.3.1 Variational Analysis

In order to characterize the extremals of Problem 2, we carry out a standard optimal control analysis based on Pontryagin's Maximum Principle (PMP) arguments [5]. To this aim, we consider the Hamiltonian $\mathcal{H} : \mathbb{R}^2 \times \mathbb{S}^1 \times \mathbb{R}^3 \times U \mapsto \mathbb{R}$ of Problem 2, which is defined as follows

$$\mathcal{H}(\mathsf{x}, \mathsf{p}, u) := p_0 + p_1 \cos\theta + p_2 \sin\theta + \frac{p_3 u}{\rho}, \tag{35}$$

where $\mathsf{p} := (p_1, p_2, p_3)$ and $p_0 \in \{0, 1\}$. By virtue of PMP, if $\mathsf{x}^* := (x^*, y^*, \theta^*)$ is a minimum-time trajectory of the ZMD problem generated by the control $u^* \in \mathcal{U}$, then there exists a scalar $p_0^* \in \{0, 1\}$ and an absolutely continuous function $\mathsf{p}^* : [0, T_\mathrm{f}] \mapsto \mathbb{R}^3$, where $\mathsf{p}^* := (p_1^*, p_2^*, p_3^*)$, known as the costate, such that

(i) $\|\mathsf{p}^*(t)\| + |p_0^*| \neq 0$, for all $t \in [0, T_\mathrm{f}]$,

(ii) $\mathsf{p}^*(t)$ satisfies, for almost all $t \in [0, T_\mathrm{f}]$, the canonical equation

$$\dot{\mathsf{p}}^* = -\frac{\partial \mathcal{H}(\mathsf{x}^*, \mathsf{p}^*, u^*)}{\partial \mathsf{x}}, \tag{36}$$

or, equivalently,

$$\dot{p}_1^* = 0, \quad \dot{p}_2^* = 0, \quad \dot{p}_3^* = p_1^* \sin\theta^* - p_2^* \cos\theta^*, \tag{37}$$

(iii) $\mathsf{p}^*(T_\mathrm{f})$ satisfies the transversality condition

$$\mathcal{H}(\mathsf{x}^*(T_\mathrm{f}), \mathsf{p}^*(T_\mathrm{f}), u^*(T_\mathrm{f})) = 0. \tag{38}$$

Because the Hamiltonian does not depend explicitly on time, it follows from (38) that

$$\mathcal{H}(\mathsf{x}^*(t), \mathsf{p}^*(t), u^*(t)) = 0, \quad \text{a.e.} \quad t \in [0, T_\mathrm{f}]. \tag{39}$$

It follows, by virtue of (37), that $p_1^* = p_1^*(0)$ and $p_2^* = p_2^*(0)$, for all $t \geq 0$, which furthermore implies, in light of (39), that

$$-p_0^* = p_1^*(0)(w_x + \cos\theta^*(t)) + p_2^*(0)(w_y + \sin\theta^*(t)) + \frac{p_3^*(t)u^*(t)}{\rho}, \quad \text{a.e.} \quad t \in [0, T_\mathrm{f}]. \tag{40}$$

Furthermore, the optimal control u^* necessarily minimizes the Hamiltonian evaluated along the optimal trajectory x^* and the corresponding costate vector p^*. Thus,

$$\mathcal{H}(\mathsf{x}^*, \mathsf{p}^*, u^*) = \min_{v \in [-1,1]} \mathcal{H}(\mathsf{x}^*, \mathsf{p}^*, v), \quad \text{a.e.} \quad t \in [0, T_\mathrm{f}]. \tag{41}$$

It follows from (41) that

$$u^*(t) = \begin{cases} +1, & \text{if} \quad p_3^*(t) < 0, \\ \bar{u} \in [-1, 1], & \text{if} \quad p_3^*(t) = 0, \\ -1, & \text{if} \quad p_3^*(t) > 0. \end{cases} \tag{42}$$

The following proposition follows similarly to [199].

Proposition 11. *The only singular control of Problem 2 is* $u = 0$.

Thus, a minimum-time trajectory of Problem 2 corresponds necessarily to concatenations of singular arcs, when $u = 0$, and bang arcs, when $u = \pm 1$. Henceforth, we denote a bang and a singular arc by b and s, respectively; furthermore, we write b_α and s_α to denote, respectively, a bang and a singular arc traversed in α units of time. In addition, we write b_α^+ (b_α^-) to denote the fact that the bang arc is generated with the application of the control input $u = +1$ ($u = -1$) for α units of time. We denote by $\mathsf{b}_\alpha^\pm \mathsf{b}_\beta^\mp$ the concatenation of either a b_α^+ arc followed by a b_β^- arc or a b_α^- arc followed by a b_β^+ arc. Finally, we denote by Σ_α^n a chain of n bang arcs, that is, a concatenation of n consecutive bang arcs, which is traversed in α units of time. We shall refer to the first and the last arc of a chain Σ_α^n as boundary arcs, and to the rest of them as intermediate.

4.3.2 Structure of Candidate Optimal Paths

Next, we investigate the behavior of the switching function p_3^*, and subsequently, we further examine the structure of the extremals of the ZMD problem. To this aim, let us consider an open interval $\mathcal{I} \subset [0, T_\mathrm{f}]$ such that $p_3^*(t) \neq 0$, for all $t \in \mathcal{I}$. The restriction of the optimal control u^* on $\mathcal{I}$ is a piecewise constant function, which may undergo a number of discontinuous jumps, and furthermore, $u^*(t) \in \{-1, +1\}$, for all $t \in \mathcal{I}$. By virtue of Eqs. (37) and (40), for any subinterval $\mathcal{I}_\mathsf{b}$ of $\mathcal{I}$, where $u^*(t)$ is constant, p_3^* satisfies the following differential equation

$$\ddot{p}_3^*(t) = -\frac{p_3^*(t)}{\rho^2} - \left(\frac{u^*(t) p_0^*}{\rho} + p_1^*(0) w_x + p_2^*(0) w_y \right), \quad \text{for a.e.} \quad t \in \mathcal{I}_\mathsf{b}. \tag{43}$$

The general solution of Eq. (43) restricted to the internal $\mathcal{I}_\mathsf{b}$ and its time derivative are given by

$$p_3^*(t) = C_1 \cos \frac{t u^*(t)}{\rho} + C_2 \sin \frac{t u^*(t)}{\rho} - \rho^2 \left(p_1^*(0) w_x + p_2^*(0) w_y + \frac{u^*(t) p_0^*}{\rho} \right), \tag{44}$$

$$\dot{p}_3^*(t) = \frac{u^*(t) C_2}{\rho} \cos \frac{t u^*(t)}{\rho} - \frac{u^*(t) C_1}{\rho} \sin \frac{t u^*(t)}{\rho}, \tag{45}$$

where C_1, C_2 are real constants and $u^*(t) \equiv \pm 1$. It follows readily that

$$(\rho \dot{p}_3^*(t))^2 + (p_3^*(t) + u^*(t) p_0^* \rho + \varrho)^2 = C_1^2 + C_2^2, \quad \text{for a.e.} \quad t \in \mathcal{I}_{\mathsf{b}}, \tag{46}$$

where $\varrho = \rho^2 (p_1^*(0) w_x + p_2^*(0) w_y)$.

Figures 12-13 illustrate the phase portrait of $(p_3^*, \rho \dot{p}_3^*)$ for a chain of abnormal ($p_0 = 0$) and normal ($p_0 = 1$) bang arcs, respectively. In particular, as we observe in Figs. 12(a)-12(b), the phase portrait of $(p_3^*, \rho \dot{p}_3^*)$ in the case of a chain of abnormal bang arcs consists of a family of circles centered at a point K with coordinates $(\pm \varrho, 0)$ and radius r, where $r = \sqrt{C_1^2 + C_2^2}$, with parameterizations that trace them out clockwise at constant angular velocity $1/\rho$. Note that the control switches from $u^* = +1$ to $u^* = -1$ only if $|\varrho| \leq r$. Furthermore, as is illustrated in Figs 12(a)-12(b), the time of motion along an abnormal bang arc of the ZMD problem is upper bounded by either $\pi\rho$ or $2\pi\rho$. This is in contrast to the standard MD problem, where the time of motion along an abnormal bang arc is always upper bounded by $\pi\rho$ [199]. On the other hand, the phase portrait of $(p_3^*, \rho \dot{p}_3^*)$ of a chain of normal bang arcs consists of two families of circles centered at points A and B, with coordinates $(\varrho - \rho, 0)$ and $(\rho + \varrho, 0)$, and radii r_+ (for $u^* = +1$) and r_- (for $u^* = -1$), respectively, with parameterizations that trace them out clockwise at constant angular velocity $1/\rho$; we denote these circles by $C(\mathsf{A}; r_+)$ and $C(\mathsf{B}; r_-)$, respectively. Note that a jump from $u^* = -1$ to $u^* = +1$, and vice versa, occurs only if $C(\mathsf{B}, r_-)$ intersects $C(\mathsf{A}, r_+)$ along the axis $p_3^* = 0$, that is, when $r_+ \geq |\varrho - \rho|$, $r_- \geq |\varrho + \rho|$, and $r_-^2 = r_+^2 + 4\varrho\rho$, as is illustrated in Fig. 13. It is interesting to note that the phase portrait of $(p_3^*, \rho \dot{p}_3^*)$ is asymmetric with respect to the axis $p_3^* = 0$, in contrast to the symmetric phase portrait of the standard MD problem [201]. It is worth mentioning that the phase portrait $(p_3^*, \rho \dot{p}_3^*)$ of the asymmetric sinistal/dextral MD problem, which was studied in [18], is also asymmetric with respect to the axis $p_3^* = 0$.

Next, we consider the optimality properties of a chain of bang arcs.

Proposition 12. *Let Σ_α^n be a chain of n bang arcs that is part of an optimal path of the ZMD problem from $(0,0,0)$ to some $(x_\mathrm{f}, y_\mathrm{f}, \theta_\mathrm{f}) \in \mathbb{R}^2 \times \mathbb{S}^1$. If $n \geq 4$, then the total time along two consecutive, intermediate bang arcs $\mathsf{b}_{\alpha_i}^{\pm}\mathsf{b}_{\alpha_{i+1}}^{\mp}$ of Σ_α^n satisfies the lower bound*

$$\alpha_i + \alpha_{i+1} \geq 2\pi\rho, \quad \text{for all} \quad i \in \{2, \ldots, n-2\}. \tag{47}$$

Proof. Let us consider the case of two consecutive, intermediate bang arcs $\mathsf{b}_{\alpha_i}^{+}\mathsf{b}_{\alpha_{i+1}}^{-}$, where $i \in \{2, \ldots, n-2\}$. The case of a sub-path $\mathsf{b}_{\alpha_i}^{-}\mathsf{b}_{\alpha_{i+1}}^{+}$ can be treated similarly. In the case of a chain of abnormal bang arcs, $\alpha_i + \alpha_{i+1}$ equals the time required for a particle with coordinates $(p_3^*, \rho p_3^*)$ to travel from point D to C, and subsequently, from C to D along the circle of radius r centered at K, as is illustrated in Fig. 12. We immediately conclude that $\alpha_i + \alpha_{i+1} = 2\pi\rho$, for all $i \in \{2, \ldots, n-2\}$. In the case of a chain of normal bang arcs, $\alpha_i + \alpha_{i+1}$ equals the time required for a particle with coordinates $(p_3^*, \rho p_3^*)$ to travel from point D to C along $C(\mathsf{A}, r_+)$, and subsequently, from C to D along $C(\mathsf{B}, r_-)$ with angular velocity $1/\rho$, as is illustrated in Fig. 13. There are two cases to consider. First, if $\alpha_i \geq \pi\rho$, for all $i \in \{2, \ldots, n-2\}$, then it follows that $\alpha_i + \alpha_{i+1} \geq 2\pi\rho$ (Fig. 13(a)). Second, if $0 < \alpha_i \leq \pi\rho$, for some $i \in \{2, \ldots, n-2\}$, then we observe that the time of motion from D to C along the circle $C(\mathsf{A}, r_+)$ is greater than the time of motion from D to C along the circle $C(\mathsf{B}, r_-)$ given that $\widehat{\mathsf{DAC}} > \widehat{\mathsf{DBC}}$ (Fig. 13(b)). Thus, it follows readily that $\alpha_i + \alpha_{i+1} \geq 2\pi\rho$, for all $i \in \{2, \ldots, n-2\}$. Therefore, in all cases, $\alpha_i + \alpha_{i+1} \geq 2\pi\rho$, for all $i \in \{2, \ldots, n-2\}$. □

Next, we shall employ Proposition 12 to establish a basic property enjoyed by the min-time paths of the ZMD problem, namely, that any chain of bang arcs that is part of an optimal path is necessarily finite, that is, no infinite chattering between bang arcs (Füller phenomenon) can occur.

Proposition 13. *Let the constant drift filed $w = \nu(\cos\phi, \sin\phi)$, where $\nu < 1$. A chain of bang arcs Σ_α^n can be part of an optimal path from $(0,0,0)$ to $(x_\mathrm{f}, y_\mathrm{f}, \theta_\mathrm{f}) \in \mathbb{R}^2 \times \mathbb{S}^1$*

only if it is finite.

Proof. In light of Proposition 10, there exists a minimum-time path of the ZMD problem from $(0,0,0)$ to $(x_\mathrm{f}, y_\mathrm{f}, \theta_\mathrm{f}) \in \mathbb{R}^2 \times \mathbb{S}^1$, and thus $T_\mathrm{f} < \infty$. Let assume, on the contrary, that a chain Σ_α^n, where $n \to \infty$, is part of a min-time path. By virtue of Proposition 12, the time of motion along the first $i+2$ bang arcs of Σ_α^n, where $i \in \{2, \ldots, n-2\}$, is lower bounded by $2i\pi\rho$. Then by taking $i \to \infty$, it follows that the time α is necessarily unbounded. Consequently, $T_\mathrm{f} = \infty$, which is absurd. □

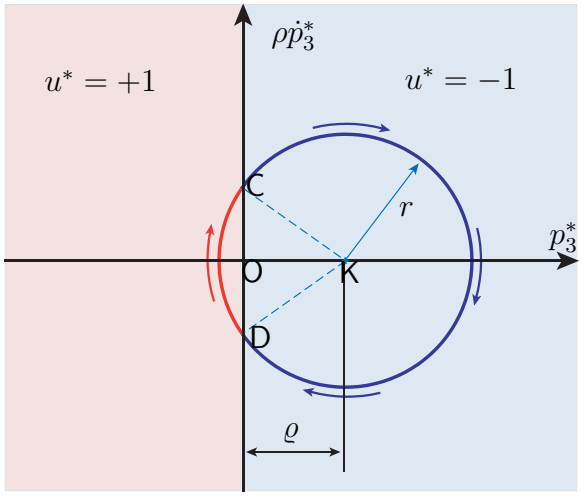

(a) $\varrho > 0$.

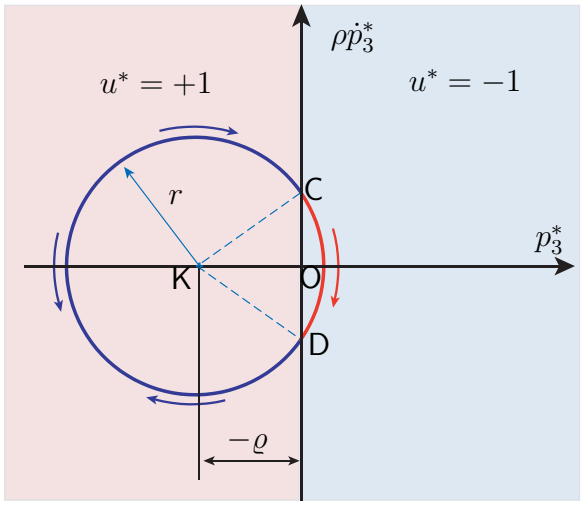

(b) $\varrho < 0$.

Figure 12: Phase portrait $(p_3^*, \rho\dot{p}_3^*)$ of a chain of bang arcs composed of abnormal extremals $(p_0^* = 0)$.

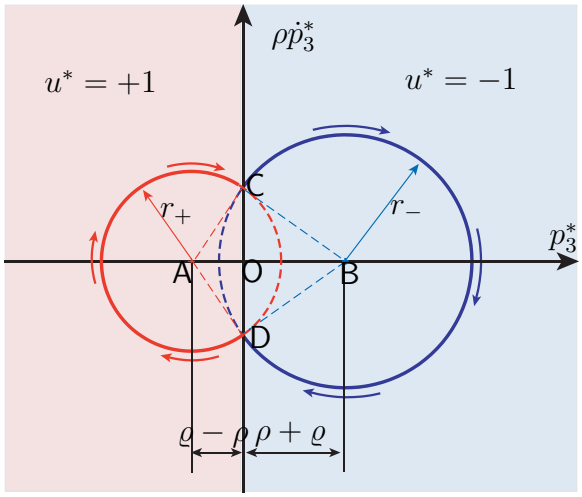

(a) $\alpha_i \geq \pi\rho$, for all i.

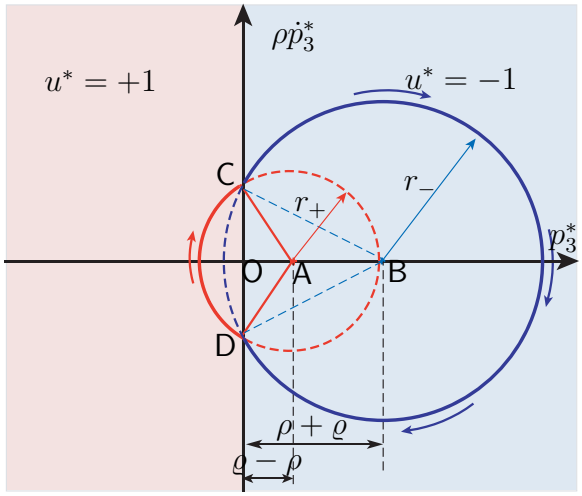

(b) $\alpha_i \geq \pi\rho$, for some i.

Figure 13: Phase portrait $(p_3^*, \rho\dot{p}_3^*)$ of a chain of bang arcs composed of normal extremals $(p_0^* = 1)$.

The following proposition highlights the existence of an extremal of the ZMD that does not belong to the optimal synthesis of the standard MD problem.

Proposition 14. *A* b_α *arc, where* $\alpha = 2\pi\rho$*, may be part of a minimum-time path of Problem 2.*

Proof. Let us consider the equivalent formulation of the ZMD problem as an intercept problem of a non-maneuvering target (Problem 3), as illustrated in Fig. 15. Let assume, without loss of generality, that $w = (\nu, 0)$ and let us consider the intercept

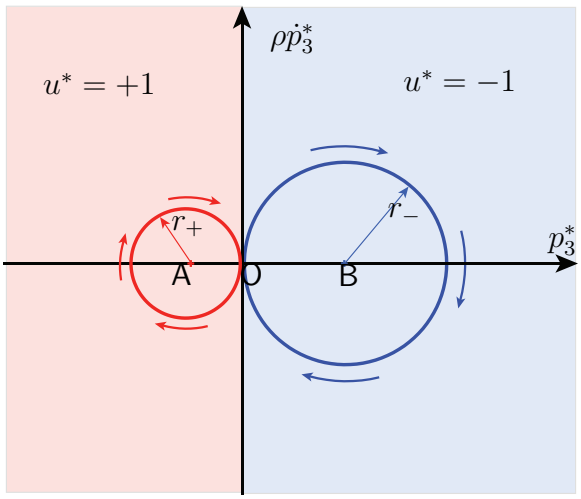

Figure 14: Phase portrait $(p_3^*, \rho\dot{p}_3^*)$, when a singular arc is part of a minimum-time path of the ZMD problem.

problem with $\theta_{\mathrm{f}} = 0$, when the non-maneuvering target is located, at time $t = 0$, at a point T with coordinates $(-2\pi\rho\nu, 0)$. Note that by driving the interceptor with the control input $u = +1$ or $u = -1$, for all $0 \leq t \leq 2\pi\rho$, intercept will take place at O with $\theta_{\mathcal{P}} = 0$. We claim that the moving target cannot be intercepted faster than $2\pi\rho$ units of time. Let assume on the contrary that the target can be intercepted with $\theta_{\mathcal{P}} = \theta_{\mathrm{f}}$, at time $t = t_1$, where $t_1 < 2\pi\rho$; something that requires that the intercept takes place at a point in the interior of TO. Since the point O is aft the point T, it follows that the direction of the interceptor's velocity necessarily changes from $\theta = 0$ to $\theta_{\mathrm{f}} = 0$, within the time interval $[0, t_1]$, while the interceptor is traversing a full loop. Since the interceptor can trace out a full loop at exactly $2\pi\rho$ units of time, it follows that $t_1 \geq 2\pi\rho$, which is absurd. □

Remark 2 Note that a b_α arc, where $\alpha = 2\pi\rho$, cannot be part of an optimal path of the standard MD problem [199]. As we shall see later, the fact that a b_α arc, where $\alpha = 2\pi\rho$, can be part of an optimal path of the ZMD problem will permit the existence of new extremals of the ZMD problem that do not belong to the sufficient for optimality family of extremals of the standard MD problem.

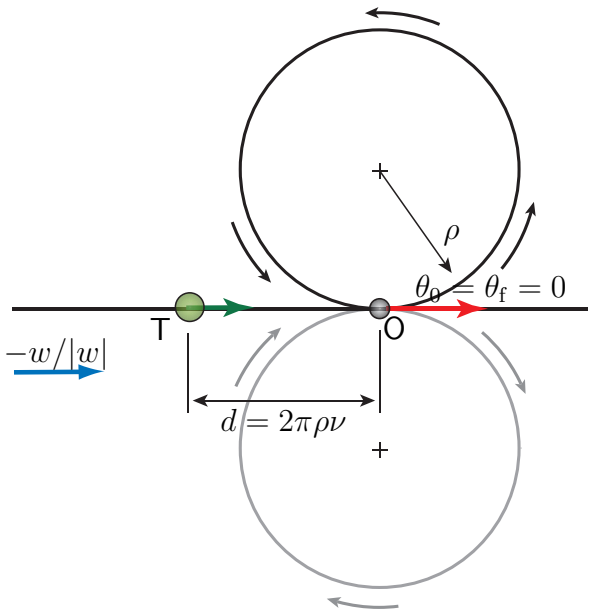

Figure 15: In contrast to the MD problem, a b_α arc, where $\alpha = 2\pi\rho$, may be part of an optimal solution of the ZMD problem.

Proposition 15. *Let $w = \nu(\cos\phi, \sin\phi)$, where $\nu < 1$. If a b_α arc, where $2\pi\rho < \alpha$, is part of an optimal path of the ZMD problem, then this arc can always be replaced by a finite chain of bang arcs Σ_α^n.*

Proof. We consider a b_α^+ arc, where $\alpha > 2\pi\rho$. The case of a b_α^- arc, where $\alpha > 2\pi\rho$, can be treated similarly. In [200], it was shown that a b_α^+ arc, where $\alpha = 4\pi\rho$, cannot be part of an optimal trajectory. Thus, we can restrict our attention to the case when $\alpha \geq (2\pi + \epsilon)\rho$, where $\epsilon \in (0, 2\pi)$. Using the moving target formulation of the ZMD problem (Problem 3), which is illustrated in Fig. 16, it follows that a b_α arc, where $\alpha = (2\pi + \epsilon)\rho$, can be part of an optimal path of the ZMD problem only if the interceptor, which is located, at time $t = 0$, at the origin O, can intercept the moving target at a point A with $\theta_{\mathcal{P}} = \epsilon$, at time $t = (2\pi + \epsilon)\rho$. Note that by driving the interceptor with the application of $u = -1$, from $t = 0$ to $t = 2\pi\rho$, and subsequently, $u = +1$, from $t = 2\pi\rho$ to $t = (2\pi + \epsilon)\rho$, intercept will occur at a point A, at time $t = (2\pi + \epsilon)\rho$. Therefore, a b_α^+ arc, where $\alpha = (2\pi + \epsilon)\rho$, can always be replaced by the chain $\mathsf{b}_{\alpha_1}^+ \mathsf{b}_{\alpha_2}^-$, where $\alpha_1 = 2\pi\rho$ and $\alpha_2 = \epsilon\rho$. □

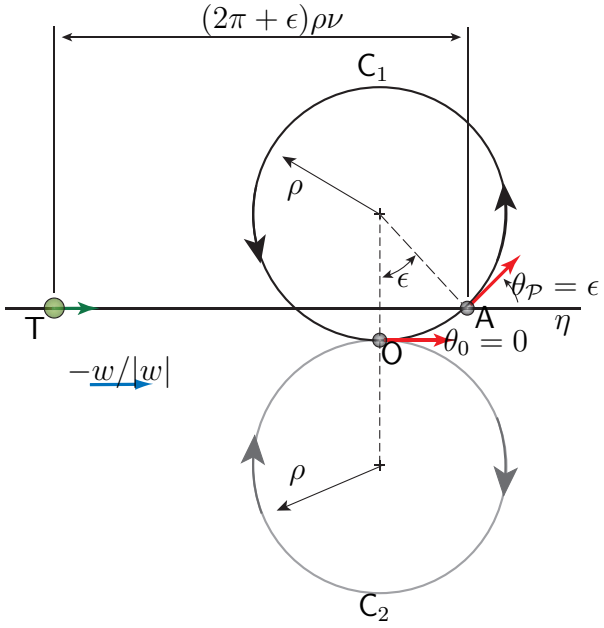

Figure 16: A b_α arc, where $\alpha > 2\pi\rho$, can always be replaced by a $\mathsf{b}^{\pm}_{\alpha_i}\mathsf{b}^{\mp}_{\alpha_{i+1}}$ sub-path, where $\alpha_i + \alpha_{i+1} = \alpha$.

The next proposition provides lower and upper bounds over the time of motion along a bang arc of a chain of bang arcs.

Proposition 16. *Let the constant drift $w = \nu(\cos\phi, \sin\phi)$, where $\nu < 1$ and let assume that a chain of n bang arcs Σ^n_α is part of a minimum-time path of the ZMD problem. If b_{α_i}, where $i \in \{1, \ldots, n\}$, is part of Σ^n_α, then*

(i) $\alpha_i \in [0, \pi\rho]$ or $\alpha_i \in [\pi\rho, 2\pi\rho]$, for all $i \in \{1, \ldots n\}$,

(ii) $\alpha_i + \alpha_{i+1} \geq 2\pi\rho$, for all $i \in \{2, \ldots n-2\}$.

Proof. It suffices to observe that, in the case of a chain of abnormal extremals, α_i corresponds to the travel time of a point with coordinates $(p^*_3, \rho\dot{p}^*_3)$ along a circle centered at K, as is illustrated in Fig. 12. In the case of a chain of normal bang arcs α_i corresponds to the travel time of a particle with coordinates $(p^*_3, \rho\dot{p}^*_3)$ from point D (C) to C (D) along the circle $C(\mathsf{A}; r_+)$ ($C(\mathsf{B}; r_-)$) with constant angular velocity $\pm 1/\rho$. The situation is illustrated in Figs. 13(a)-13(b). In particular, if $\varrho > 0$ and $\varrho < \rho$, then, as is illustrated in Fig. 13(a), $\alpha_i \in [\pi\rho, 2\pi\rho]$. In Fig. 13(b), we observe that,

given two consecutive bang arcs $\mathsf{b}^{\pm}_{\alpha_i}\mathsf{b}^{\mp}_{\alpha_{i+1}}$, for $i \in \{1, \ldots, n-2\}$, if $\varrho > 0$ and $\varrho > \rho$ (the case when $\varrho \leq 0$ and $\varrho \leq \rho$ can be treated similarly), then either $\alpha_i \in [0, \pi\rho]$ and $\alpha_{i+1} \in [\pi\rho, 2\pi\rho]$ or $\alpha_i, \alpha_{i+1} \in [\pi\rho, 2\pi\rho]$. The rest of the proof follows readily from Proposition 12. □

Remark 3 Note that the time of motion along an intermediate b_{α_i} arc of a chain of bang arcs Σ^n_α, where $n \leq 3$ necessarily, which is part of a minimum-time path of the standard MD problem, satisfies $\alpha_i \in (\pi\rho, 2\pi\rho)$ (see for example [199]). Therefore, Proposition 12 identifies the existence of extremals of the ZMD problem that do not belong to the sufficient for optimality family of extremals of the MD problem. In order to highlight the previous observation, we denote, henceforth, a b_{α_i} arc, where $\alpha_i \in [0\,\pi\rho]$, by $\tilde{\mathsf{b}}_{\alpha_i}$.

Next, we investigate the structure of paths that consist of both singular and bang arcs. Because along a singular arc $p_3^* = 0$, which furthermore implies that $\dot{p}_3^* = 0$, it follows that any s arc corresponds to the origin of the phase portrait $(p_3^*, \rho\dot{p}_3^*)$. First, we show that optimal paths that consist of both singular and bang arcs are necessarily finite.

Proposition 17. *Let the constant drift filed $w = \nu(\cos\phi, \sin\phi)$, where $\nu < 1$. An optimal path of the ZMD is necessarily a concatenation of a finite number of bang and singular arcs.*

Proof. In Proposition 13, we have shown that any chain of bang arcs that is part of an optimal trajectory of the ZMD problem consists necessarily of a finite number of bang arcs. Next, we show that both the total number of singular and bang arcs of an optimal path of the ZMD problem is necessarily finite, as well. In particular, we observe in Fig. 14, that a transition from a s_α arc to a different singular arc, say s_γ may occur after via a finite chain of bang arcs Σ^n_β, where $\mathsf{b}_{\beta_i} \in \Sigma^n_\beta$, $\beta_i = 2\pi\rho$ starting from and ending at the origin of the $(p_3^*, \rho\dot{p}_3^*)$ plane. Thus, the time of motion along

an optimal path that contains two s arcs interconnected by a chain of bang arcs Σ_β^n is necessarily lower bounded by $2n\pi\rho$. Consequently, if an optimal path consists of an infinite number of s arcs, then the minimum-time to traverse this path is necessarily unbounded, which is absurd. Using similar arguments, we can show that the time of motion along a trajectory that consists of an infinite number of finite chains of bang arcs, which are necessarily interconnected by singular arcs, is also unbounded. This completes the proof. □

The next proposition highlights the structure of extremals of the ZMD problem that are concatenations of both b and s arcs.

Proposition 18. *Let* $w = \nu(\cos\phi, \sin\phi)$*, where* $\nu < 1$*. Paths of type* (i) $\mathsf{b}^{\pm}\mathsf{s}\mathsf{b}^{\pm}$*,* (ii) $\mathsf{b}^{\pm}\mathsf{s}\mathsf{b}^{\mp}$*,* (iii) $\mathsf{b}^{\mp}\mathsf{s}\mathsf{b}^{\mp}$*,* (iv) $\mathsf{s}\mathsf{b}^{\mp}\mathsf{s}$*,* (v) $\mathsf{b}^{\pm}\mathsf{b}^{\mp}\mathsf{s}$*, and* (vi) $\mathsf{s}\mathsf{b}^{\pm}\mathsf{b}^{\mp}$*, may be part of a minimum-time path of the ZMD problem.*

Proof. In light of Proposition 17, it is straightforward to show that the path types (i)-(iii), which belong to the family of the extremals of the standard MD, may be part of a minimum-time path of the ZMD problem. In addition, as is illustrated in Fig. 14, for every $\mathsf{s}_\alpha\mathsf{b}_\beta^{\pm}\mathsf{s}_\gamma$, $\mathsf{b}_\alpha^{\pm}\mathsf{b}_\beta^{\mp}\mathsf{s}_\gamma$ and $\mathsf{s}_\alpha\mathsf{b}_\beta^{\pm}\mathsf{b}_\gamma^{\mp}$ path, $\beta = 2\pi\rho$. Given that, in light of Proposition 14, a b_β, where $\beta = 2\pi\rho$, may be part of a minimum-time path of the ZMD problem, the result follows readily. □

4.3.3 Sufficient for Controllability and Necessary for Optimality Family of Extremals of the ZMD

Next, we propose a family of extremal paths, which we henceforth denote by $\mathcal{P}^*_{\text{ZMD}}$, which consists of all admissible concatenations of singular and bang arcs that steer the system described by Eq. (22) to an arbitrary terminal configuration in a near time-optimal way. Since the trajectory of the system described by Eq. (22) uniquely determines the control that generates it, and vice versa, we can associate each of the extremal paths from $\mathcal{P}^*_{\text{ZMD}}$ with the corresponding control sequence. For example,

a path $\mathsf{b}_{\alpha}^{\pm}\mathsf{s}_{\beta}\mathsf{b}_{\gamma}^{\pm}$ corresponds to the control sequence $\{\pm 1, 0, \pm 1\}$. We denote this family of control sequences by $\mathsf{U}_{\mathrm{ZMD}}^{*}$. First, we present a family of extremals that are sufficient for the complete controllability of the system described by Eq. (22).

Proposition 19. *For any $(x_{\mathrm{f}}, y_{\mathrm{f}}, \theta_{\mathrm{f}}) \in \mathbb{R}^2 \times \mathbb{S}^1$, there exists a feasible path of the ZMD problem that belongs to the following family of extremal paths:*

(i) $\mathsf{b}_{\alpha}^{\pm}\mathsf{s}_{\beta}\mathsf{b}_{\gamma}^{\pm}$, $\mathsf{b}_{\alpha}^{\pm}\mathsf{s}_{\beta}\mathsf{b}_{\gamma}^{\mp}$, *where* $\alpha, \gamma \in [0, 2\pi\rho]$, $\beta \in [0, \infty[$,

(ii) $\mathsf{b}_{\alpha}^{\pm}\mathsf{b}_{\beta}^{\mp}\mathsf{b}_{\gamma}^{\pm}$, *where* $\alpha, \gamma \in [0, 2\pi\rho]$, $\beta \in [\pi, 2\pi\rho]$,

(iii) $\mathsf{b}_{\alpha}^{\pm}\tilde{\mathsf{b}}_{\beta}^{\mp}\mathsf{b}_{\gamma}^{\pm}$, *where* $\alpha, \gamma \in [0, 2\pi\rho]$, $\beta \in [0, \pi\rho]$.

Proof. The reader can refer to [123]. □

Remark 4 In [123], it is claimed that the family of paths of the ZMD problem given in Proposition 19 is sufficient for optimality. However, this claim was not rigorously proved. As we shall see shortly after, in most cases, the family of paths given in Proposition 19, after some mild modifications, will be sufficiently rich to provide feasible and nearly optimal solutions to the ZMD problem.

Theorem 1. *Any minimum-time path of the ZMD problem contains at least one of the following extremal paths*

(i) $\mathsf{b}_{\alpha}^{\pm}\mathsf{s}_{\beta}\mathsf{b}_{\gamma}^{\pm}$, $\mathsf{b}_{\alpha}^{\pm}\mathsf{s}_{\beta}\mathsf{b}_{\gamma}^{\mp}$, *where* $\alpha \in [0, 2\pi\rho]$, $\beta \in [0, \infty[$, *and* $(\pm\alpha/\rho \pm \gamma/\rho) \bmod 2\pi = \theta_{\mathrm{f}}$, $(\pm\alpha/\rho \mp \gamma/\rho) \bmod 2\pi = \theta_{\mathrm{f}}$, *respectively,*

(ii) $\mathsf{b}_{\alpha}^{\pm}\mathsf{b}_{\beta}^{\mp}\mathsf{b}_{\gamma}^{\pm}$, *where* $\alpha \in [0, 2\pi\rho]$, $\beta \in [\pi, 2\pi\rho]$, *and* $(\pm\alpha/\rho \mp \beta/\rho \pm \gamma/\rho) \bmod 2\pi = \theta_{\mathrm{f}}$,

(iii) $\mathsf{b}_{\alpha}^{\pm}\tilde{\mathsf{b}}_{\beta}^{\mp}\mathsf{b}_{\gamma}^{\pm}$, *where* $\alpha \in [0, 2\pi\rho]$, $\beta \in [0, \pi\rho]$, *and* $(\pm\alpha/\rho \mp \beta/\rho \pm \gamma/\rho) \bmod 2\pi = \theta_{\mathrm{f}}$,

(iv) $\mathsf{s}_{\alpha}\mathsf{b}_{\beta}^{\pm}\mathsf{s}_{\gamma}$, *where* $\beta = 2\pi\rho$, $\alpha, \gamma \in [0, \infty[$,

(v) $\mathsf{b}_{\alpha}^{\mp}\mathsf{b}_{\beta}^{\pm}\mathsf{s}_{\gamma}$, *where* $\mp\alpha \bmod 2\pi = \theta_{\mathrm{f}}$, *and* $\beta = 2\pi\rho$, *and* $\gamma \in [0, \infty[$,

(vi) $\mathsf{s}_\alpha \mathsf{b}^{\pm}_{\beta} \mathsf{b}^{\mp}_{\gamma}$, *where* $\alpha \in [0, \infty[$, *and* $\beta = 2\pi\rho$, *and* $\mp\gamma \bmod 2\pi = \theta_{\mathrm{f}}$.

We denote this family of paths by $\mathcal{P}^*_{\mathrm{ZMD}}$. *Let, furthermore,* $\mathsf{U}^*_{\mathrm{ZMD}}$ *be the corresponding family of control sequences that generate the paths of* $\mathcal{P}^*_{\mathrm{ZMD}}$. *Then* $\mathsf{U}^*_{\mathrm{ZMD}}$ *is sufficient for the complete controllability of the system described by Eq.* (22).

Proof. To show complete controllability of the system described by Eq. (22), when the control input is constrained to belong to $\mathsf{U}^*_{\mathrm{ZMD}}$, it suffices to note that any configuration that can be reached by some element of the family of extremal paths given in Proposition 19 can also be reached by some of the extremal paths (i)-(iii) of $\mathcal{P}^*_{\mathrm{ZMD}}$, and vice versa. The proof of the latter statement is based on the observation that the total change of θ along the ensuing trajectory of the agent from $(0, 0, 0)$ to $(x_{\mathrm{f}}, y_{\mathrm{f}}, \theta_{\mathrm{f}})$ mod 2π must be equal to θ_{f}. To better illustrate this point, let us consider the set of configurations that can be reached by means of a $\mathsf{b}^{\pm}_{\alpha} \mathsf{s}_\beta \mathsf{b}^{\pm}_{\gamma}$ path. We observe that θ changes from $\theta = 0$ to $\theta = \pm\alpha/\rho \mod 2\pi$ along the b_α arc. Subsequently, θ remains constant along the s_β arc, and finally, changes from $\theta = \pm\alpha/\rho \mod 2\pi$ to $\theta = (\pm\alpha/\rho \pm \gamma/\rho) \mod 2\pi$ along the b_γ arc. The proof for the rest of the extremal paths can be carried out similarly.

□

Remark 5 Note that the extremal paths (iii)-(vi) of Theorem 1 do not correspond to minimum-time paths of the standard MD problem. We should mention here, that the new path types (iv)-(vi) play a trivial role in the optimal synthesis of the ZMD problem, since, as we shall explain in more detail later, they correspond to candidate paths that may be optimal only for a set of boundary conditions in $\mathbb{R}^2 \times \mathbb{S}^1$ with either small or zero volume. For example, a path of type $\mathsf{s}_\alpha \mathsf{b}^{\pm}_{\beta} \mathsf{s}_\gamma$ (path type (iv) of $\mathcal{P}^*_{\mathrm{ZMD}}$), can be a candidate minimum-time of the ZMD problem only when $\theta(0) = \theta(T_{\mathrm{f}}) = 0$ owing to the fact that $\beta = 2\pi\rho$, which implies, in turn, that the total change of θ_{f} along the ensuing path should be equal to $\pm 2\pi$.

Remark 6 It is worth mentioning that the family of extremals proposed in Theorem 1 consists of paths that are concatenations of at most three arcs; a pattern that is also observed in the extremals of the standard MD problem. In contrast to the solution of the MD problem, one can also conjecture that there may exist boundary conditions such that a minimum-time path of the ZMD problem consists of more than three arcs. However, in light of Propositions 12 and 18, the motion along a chain of bang arcs and singular arcs is lower bounded by a strictly positive quantity that is proportional to the number of the consecutive bang or singular arcs. Thus, it is conjectured that they correspond to a rather trivial set of boundary conditions.

4.4 Time-Optimal Synthesis

In this section, we present a nearly time-optimal synthesis of the ZMD problem, and thus provide a complete characterization of a nearly optimal control scheme that solves Problem 2, for all $(x_{\mathrm{f}}, y_{\mathrm{f}}, \theta_{\mathrm{f}}) \in \mathbb{R}^2 \times \mathbb{S}^1$.

4.4.1 Reachability Analysis

First, we carry out the reachability analysis for the system described by Eq. (22), when the admissible control is constrained to be an element in $\mathsf{U}^*_{\mathrm{ZMD}}$. To simplify the presentation, and with no loss in generality, we henceforth consider the minimum-time trajectories of (22) from $(0,0,0)$ to $(x_{\mathrm{f}}, y_{\mathrm{f}}, \theta_{\mathrm{f}}) \in P_{\theta_{\mathrm{f}}}$, where $P_{\theta_{\mathrm{f}}} := \{(x,y,\theta) \in \mathbb{R}^2 \times \mathbb{S}^1 : \ \theta = \theta_{\mathrm{f}}\}$, as suggested in [45, 46]. Furthermore, we denote the reachable set that corresponds to the control sequence $u \in \mathsf{U}^*_{\mathrm{ZMD}}$ as $\mathfrak{R}_{\theta_{\mathrm{f}}}(u)$.

Next, we demonstrate how to characterize the reachable set $\mathfrak{R}_{\theta_{\mathrm{f}}}(u)$, for $u \in \mathsf{U}^*_{\mathrm{ZMD}}$, by briefly presenting the main steps for the construction of $\mathfrak{R}_{\theta_{\mathrm{f}}}(\mathsf{b}^+\mathsf{s}\mathsf{b}^+)$. In particular, we observe that the coordinates of any configuration in $P_{\theta_{\mathrm{f}}}$ that can be reached by means of the control sequence $\{+1, 0, +1\}$, or equivalently, a $\mathsf{b}^+_\alpha \mathsf{s}_\beta \mathsf{b}^+_\gamma$ path, can be expressed in terms of the time of motion along each of the three arcs of the path, namely α, β, and γ. In particular, by simply integrating (22) for $u = +1$, from $t = 0$

to $t = \alpha$, and subsequently, for $u = 0$, from $t = \alpha$ to $t = \alpha+\beta$, and finally, for $u = +1$, from $t = \alpha + \beta$ to the final time $T_{\mathrm{f}}(\mathsf{b}^+\mathsf{sb}^+) := \alpha + \beta + \gamma$, we obtain expressions of x_{f} and y_{f} as functions of α, β, and γ. Note that, in general, γ can always be expressed in terms of the parameters α, β, and θ_{f}. In the case of a $\mathsf{b}^+_\alpha\mathsf{s}_\beta\mathsf{b}^+_\gamma$ path, γ depends only on α, as we shall see shortly later. In particular, since along a $\mathsf{b}^+_\alpha\mathsf{s}_\beta\mathsf{b}^+_\gamma$ path the direction of the forward velocity of the vehicle changes from $\theta = 0$ to $\theta = \theta_{\mathrm{f}}$, it follows readily that $(\alpha/\rho + \gamma/\rho) \mod 2\pi = \theta_{\mathrm{f}}$, which furthermore implies that

$$\gamma(\alpha;\theta_{\mathrm{f}}) = \begin{cases} \rho\theta_{\mathrm{f}} - \alpha, & \text{if } \theta_{\mathrm{f}} \geq \dfrac{\alpha}{\rho}, \\ \rho(2\pi + \theta_{\mathrm{f}}) - \alpha, & \text{if } \theta_{\mathrm{f}} < \dfrac{\alpha}{\rho}. \end{cases} \tag{48}$$

In addition, it follows after routine calculations that

$$x_{\mathrm{f}}(\alpha,\beta) = \rho\sin\theta_{\mathrm{f}} + \beta\cos\frac{\alpha}{\rho} + w_x T_{\mathrm{f}}(\mathsf{b}^+\mathsf{sb}^+), \tag{49}$$

$$y_{\mathrm{f}}(\alpha,\beta) = \rho(1-\cos\theta_{\mathrm{f}}) + \beta\sin\frac{\alpha}{\rho} + w_y T_{\mathrm{f}}(\mathsf{b}^+\mathsf{sb}^+). \tag{50}$$

Conversely, given a point $(x_{\mathrm{f}}, y_{\mathrm{f}}, \theta_{\mathrm{f}}) \in \mathfrak{R}_{\theta_{\mathrm{f}}}(\mathsf{b}^+\mathsf{sb}^+)$, we can determine the corresponding pairs $(\alpha,\beta) \in [0, 2\pi\rho] \times [0,\infty[$. In particular, after some algebraic manipulation, it follows that β satisfies the following quadratic equation (decoupled from α)

$$(1-\nu^2)\beta^2 + 2(A(x_{\mathrm{f}},\theta_{\mathrm{f}})w_x + B(y_{\mathrm{f}},\theta_{\mathrm{f}})w_y)\beta - (A(x_{\mathrm{f}},\theta_{\mathrm{f}})^2 + B(y_{\mathrm{f}},\theta_{\mathrm{f}})^2) = 0, \tag{51}$$

where $A(x_{\mathrm{f}},\theta_{\mathrm{f}}) = x_{\mathrm{f}} - \rho\sin\theta_{\mathrm{f}} - w_x\rho\hat{\theta}_{\mathrm{f}}$, $B(y_{\mathrm{f}},\theta_{\mathrm{f}}) = y_{\mathrm{f}} + \rho(\cos\theta_{\mathrm{f}} - 1) - w_y\rho\hat{\theta}_{\mathrm{f}}$, and

$$\hat{\theta}_{\mathrm{f}} = \begin{cases} \theta_{\mathrm{f}}, & \text{if } \alpha \leq \rho\theta_{\mathrm{f}}, \\ (2\pi + \theta_{\mathrm{f}})\rho, & \text{if } \alpha > \rho\theta_{\mathrm{f}}. \end{cases} \tag{52}$$

Note that if $(x_{\mathrm{f}}, y_{\mathrm{f}}, \theta_{\mathrm{f}}) \in P_{\theta_{\mathrm{f}}}$, then Eq. (51) admits at most two solutions. Given a solution β of (51), then α is determined with back substitution in Eqs. (49)-(50). In particular, after some algebraic manipulation, it follows that $\alpha(x_{\mathrm{f}}, y_{\mathrm{f}}, \theta_{\mathrm{f}}) =$

$\hat{\alpha}(x_{\rm f}, y_{\rm f}, \theta_{\rm f})\rho$, where $\hat{\alpha} \in [0, 2\pi]$ satisfies

$$\cos\hat{\alpha}(x_{\rm f}, y_{\rm f}, \theta_{\rm f}) = \frac{\rho A(x_{\rm f}, \theta_{\rm f})}{\beta} - w_x, \qquad \sin\hat{\alpha}(x_{\rm f}, y_{\rm f}, \theta_{\rm f}) = \frac{\rho B(y_{\rm f}, \theta_{\rm f})}{\beta} + w_y, \tag{53}$$

when $\beta \neq 0$, whereas $\alpha(x_{\rm f}, y_{\rm f}, \theta_{\rm f}) = \rho\theta_{\rm f}$, otherwise. In this way, for a given $(x_{\rm f}, y_{\rm f}, \theta_{\rm f}) \in P_{\theta_{\rm f}}$, we obtain two pairs (α, β) and the corresponding final time $T_{\rm f}(\mathsf{b}^+\mathsf{s}\mathsf{b}^+) = \alpha + \beta + \gamma(\alpha; \theta_{\rm f})$. Subsequently, we associate the configuration $(x_{\rm f}, y_{\rm f}, \theta_{\rm f}) \in P_{\theta_{\rm f}}$ with the pair (α^*, β^*) that yields the minimum of the time $T_{\rm f}(\mathsf{b}^+\mathsf{s}\mathsf{b}^+)$, denoted by $T_{\rm f}^*(\mathsf{b}^+\mathsf{s}\mathsf{b}^+)$, where $T_{\rm f}^*(\mathsf{b}^+\mathsf{s}\mathsf{b}^+) := \alpha^* + \beta^* + \gamma(\alpha^*; \theta_{\rm f})$.

The previous procedure can be applied mutatis mutandis for the rest of the control sequences of $\mathsf{U}_{\rm ZMD}^*$ and obtain the equations which furnish α and β as functions of $x_{\rm f}$ and $y_{\rm f}$, and vice versa, for all the control sequences $u \in \mathsf{U}_{\rm ZMD}^*$. These equations form, in general, a system of coupled transcendental equations [200]. In the Appendix B, we have achieved to decouple the original system of transcendental equations for each extremal path of $\mathsf{U}_{\rm ZMD}^*$. This decoupled system of equations admit straightforward numerical or, in some cases, analytical solutions.

Next, we proceed with the characterization of the reachable set $\mathfrak{R}_{\theta_{\rm f}}(\mathsf{b}^+\mathsf{s}\mathsf{b}^+)$ along with the level sets of the minimum-time $T_{\rm f}^*(\mathsf{b}^+\mathsf{s}\mathsf{b}^+)$. In particular, the reachable set $\mathfrak{R}_{\theta_{\rm f}}(\mathsf{b}^+\mathsf{s}\mathsf{b}^+)$ consists of all points $(x_{\rm f}, y_{\rm f}, \theta_{\rm f}) \in P_{\theta_{\rm f}}$, where $x_{\rm f}$ and $y_{\rm f}$ are computed from Eqs. (49)-(50), by taking $\alpha \in [0, 2\pi\rho]$ and $\gamma \in [0, 2\pi\rho]$ such that $(\alpha/\rho + \gamma/\rho) \bmod 2\pi = \theta_{\rm f}$, which implies, in turn, that $0 \leq \alpha + \gamma(\alpha) \leq (4\pi - \theta_{\rm f})\rho$. On the other hand, the minimum time $T_{\rm f}^*(\mathsf{b}^+\mathsf{s}\mathsf{b}^+)$ is easily determined from Eqs. (51)-(53). The reachable sets $\mathfrak{R}_{\theta_{\rm f}}(\mathsf{b}^+\mathsf{s}\mathsf{b}^+)$, along with the contours of the minimum time $T_{\rm f}^*(\mathsf{b}^+\mathsf{s}\mathsf{b}^+)$, when $0 \leq \alpha + \gamma(\alpha) \leq (4\pi - \theta_{\rm f})\rho$, for the standard MD and the ZMD problems are illustrated, respectively, in Figs. 17(a)-17(b). We observe that $\mathfrak{R}_{\theta_{\rm f}}^{\rm MD}(\mathsf{b}^+\mathsf{s}\mathsf{b}^+) = P_{\theta_{\rm f}}$, whereas $\mathfrak{R}_{\theta_{\rm f}}^{\rm ZMD}(\mathsf{b}^+\mathsf{s}\mathsf{b}^+) \subset P_{\theta_{\rm f}}$, where the superscripts MD and ZMD are used to distinguish between the reachable set of the MD and the ZMD problems, respectively. In particular, the white region in Fig. 17(b) corresponds to the set of configurations $(x_{\rm f}, y_{\rm f}, \theta_{\rm f}) \in P_{\theta_{\rm f}}$ that cannot be reached by means of a $\mathsf{b}_\alpha^+\mathsf{s}_\beta\mathsf{b}_\gamma^+$ path, when $0 \leq$

$\alpha + \gamma(\alpha) \leq (4\pi - \theta_{\mathrm{f}})\rho$.

It is worth-mentioning that although $\mathfrak{R}^{\mathrm{MD}}_{\theta_{\mathrm{f}}}(\mathsf{b}^{+}\mathsf{s}\mathsf{b}^{+}) = P_{\theta_{\mathrm{f}}}$, when $0 \leq \alpha + \gamma(\alpha) \leq (4\pi - \theta_{\mathrm{f}})\rho$, the same does not hold, if we consider instead the stricter condition $0 \leq \alpha + \gamma(\alpha) \leq 2\pi\rho$, as is illustrated in Fig. 18(a). It should be highlighted that the last condition on α and γ is actually the optimality condition that $\mathsf{b}^{+}_{\alpha}\mathsf{s}_{\beta}\mathsf{b}^{+}_{\gamma}$ paths of the MD problem should satisfy (Lemma 5 of [46]). The reachable set $\mathfrak{R}^{\mathrm{ZMD}}_{\theta_{\mathrm{f}}}(\mathsf{b}^{+}\mathsf{s}\mathsf{b}^{+})$, when $\alpha + \gamma(\alpha) \leq 2\pi\rho$, is illustrated in Fig. 18(b). The important nuance is that the fact that either the reachable set $\mathfrak{R}^{\mathrm{MD}}_{\theta_{\mathrm{f}}}(u')$ or $\mathfrak{R}^{\mathrm{ZMD}}_{\theta_{\mathrm{f}}}(u')$, for a particular $u' \in \mathsf{U}^{*}_{\mathrm{MD}}$ or $\mathsf{U}^{*}_{\mathrm{ZMD}}$, is a proper subset of $P_{\theta_{\mathrm{f}}}$ is insignificant in so far the union of the reachable sets $\mathfrak{R}_{\theta_{\mathrm{f}}}(u)$, for all $u \in \mathsf{U}^{*}_{\mathrm{MD}}$ or $\mathsf{U}^{*}_{\mathrm{ZMD}}$, cover $P_{\theta_{\mathrm{f}}}$.

The reachability analysis for the remaining control sequences of $\mathsf{U}^{*}_{\mathrm{ZMD}}$ can be carried out mutatis mutandis. Due to space limitations, the details are left to the reader. Figure 19 illustrates the reachable sets $\mathfrak{R}^{\mathrm{MD}}_{\theta_{\mathrm{f}}}(\mathsf{b}^{+}\mathsf{s}\mathsf{b}^{-})$ (19(a)) and $\mathfrak{R}^{\mathrm{ZMD}}_{\theta_{\mathrm{f}}}(\mathsf{b}^{+}\mathsf{s}\mathsf{b}^{-})$ (Fig. 19(b)), respectively, when $\alpha \in [0, 2\pi\rho]$, $\beta \in [0, \infty)$ and $(\pm\alpha/\rho \mp \gamma/\rho) \bmod 2\pi = \theta_{\mathrm{f}}$. In addition, Figure 20 illustrates the reachable sets $\mathfrak{R}^{\mathrm{MD}}_{\theta_{\mathrm{f}}}(\mathsf{b}^{+}\mathsf{b}^{-}\mathsf{b}^{+})$ (Fig. 19(a)) and $\mathfrak{R}^{\mathrm{ZMD}}_{\theta_{\mathrm{f}}}(\mathsf{b}^{+}\mathsf{b}^{-}\mathsf{b}^{+})$ (Fig. 19(b)), respectively, when $\alpha \in [0, 2\pi\rho]$, $\beta \in [\pi\rho, 2\pi\rho]$ and $(\pm\alpha/\rho \mp \beta/\rho \pm \gamma/\rho) \bmod 2\pi = \theta_{\mathrm{f}}$.

One important remark here is that one can limit the reachability analysis to the extremal paths (i) $-$ (iii) of $\mathcal{P}^{*}$ZMD. To see why the last statement is true, let us consider the set of configurations $(x_{\mathrm{f}}, y_{\mathrm{f}}, \theta_{\mathrm{f}}) \in P_{\theta_{\mathrm{f}}}$ that can be reached by means of the following extremal paths (i) $\mathsf{s}_{\alpha}\mathsf{b}_{\beta}\mathsf{s}_{\gamma}$, where $\beta = 2\pi\rho$, (ii) $\mathsf{b}^{\pm}_{\alpha}\mathsf{b}^{\mp}_{\beta}\mathsf{s}_{\gamma}$, where $\alpha \in [0, 2\pi\rho]$, and $\beta = 2\pi\rho$, and (iii) $\mathsf{s}_{\alpha}\mathsf{b}^{\pm}_{\beta}\mathsf{b}^{\mp}_{\gamma}$, where $\alpha \in [0, \infty[$, and $\beta = 2\pi\rho$. Given that the coordinates $(x_{\mathrm{f}}, y_{\mathrm{f}}, \theta_{\mathrm{f}})$ of a configuration that can be reached by means of each of these path types depend only on the parameter α, whereas the parameter β is fixed. Therefore, the configurations that can be reached by means of extremal paths $\mathsf{s}_{\alpha}\mathsf{b}_{\beta}\mathsf{s}_{\gamma}$, $\mathsf{b}^{\pm}_{\alpha}\mathsf{b}^{\mp}_{\beta}\mathsf{s}_{\gamma}$ and $\mathsf{s}_{\alpha}\mathsf{b}^{\pm}_{\beta}\mathsf{b}^{\mp}_{\gamma}$ correspond necessarily to one-dimensional manifolds on $P_{\theta_{\mathrm{f}}}$. Consequently, the reachable sets of these extremal paths cover a trivial volume

in $\mathbb{R}^2 \times \mathbb{S}^1$. Therefore, one can restrict the nearly optimal control partition of the ZMD problem to consist of the domains that correspond, in turn, to the extremal paths (i)-(iii) of $\mathcal{P}^*_{\text{ZMD}}$ given in Theorem 1.

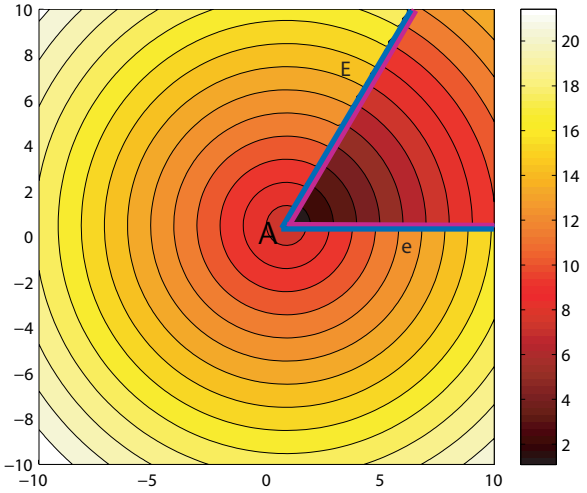

(a) Reachable set $\mathfrak{R}^{\text{MD}}_{\theta_{\text{f}}}(\mathsf{b}^+\mathsf{sb}^+)$.

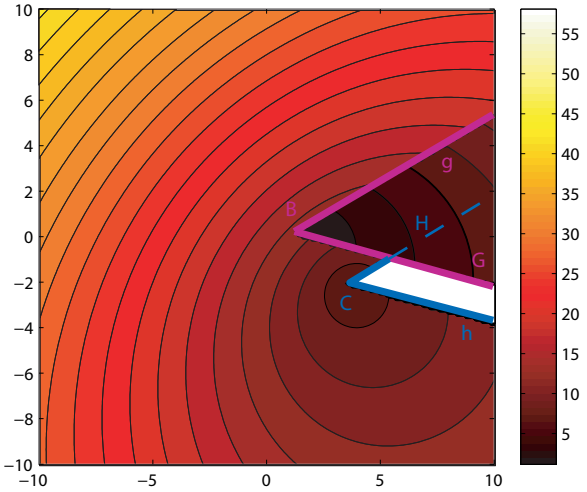

(b) Reachable set $\mathfrak{R}^{\text{ZMD}}_{\theta_{\text{f}}}(\mathsf{b}^+\mathsf{sb}^+)$.

Figure 17: Reachable sets $\mathfrak{R}_{\theta_{\text{f}}}(\mathsf{b}^+\mathsf{sb}^+)$ of the standard MD and the ZMD problems, when $\alpha + \gamma(\alpha) \leq (4\pi - \theta_{\text{f}})\rho$, and $\theta_{\text{f}} = \pi/3$.

4.4.2 The Direct Correspondence Between the Reachable Sets of the MD and the ZMD Problems

In this section, we introduce a set-valued discontinuous mapping that will allow us, by establishing a direct correspondence between the reachable sets of the MD and

the ZMD problems, to better explain the existence of unreachable configurations in $P_{\theta_\mathrm{f}} \backslash \mathfrak{R}^{\mathrm{ZMD}}_{\theta_\mathrm{f}}(\mathsf{b}^+\mathsf{sb}^+) \neq \varnothing$. To this aim, let us consider the following mapping

$$\mathrm{H}_T : (x_\mathrm{f}, y_\mathrm{f}, \theta_\mathrm{f}) \in \mathfrak{R}^{\mathrm{MD}}_{\theta_\mathrm{f}}(\mathsf{b}^+\mathsf{sb}^+) \mapsto \mathfrak{R}^{\mathrm{ZMD}}_{\theta_\mathrm{f}}(\mathsf{b}^+\mathsf{sb}^+), \quad T \geq 0 \tag{54}$$

where $(X_\mathrm{f}, Y_\mathrm{f}, \Theta_\mathrm{f}) = \mathrm{H}_T(x_\mathrm{f}, y_\mathrm{f}, \theta_\mathrm{f})$, and where

$$X_\mathrm{f} = x_\mathrm{f} + w_x T, \quad Y_\mathrm{f} = y_\mathrm{f} + w_x T, \quad \Theta_\mathrm{f} = \theta_\mathrm{f}. \tag{55}$$

The transformation H_T, where $T \geq 0$, given in Eqs. (54)-(55) can be interpreted as follows: Let a vehicle whose kinematics are described by Eq. (24) be steered with the application of some control input u from $(0, 0, 0)$ to $(x_\mathrm{f}, y_\mathrm{f}, \theta_\mathrm{f})$ after T units of time. Then, in the presence of a constant drift field (w_x, w_y), the vehicle, whose kinematics in this case are described by Eq. (22), will be steered by the same control input u to the point $(X_\mathrm{f}, Y_\mathrm{f}, \Theta_\mathrm{f})$ after T units of time. By taking $T = T^*_\mathrm{f}(\mathsf{b}^+\mathsf{sb}^+)$, it follows that each configuration $(x_\mathrm{f}, y_\mathrm{f}, \theta_\mathrm{f}) \in \mathfrak{R}^{\mathrm{MD}}_{\theta_\mathrm{f}}(\mathsf{b}^+\mathsf{sb}^+)$ is mapped via the composite mapping $\mathrm{H}_{T^*_\mathrm{f}(\mathsf{b}^+\mathsf{sb}^+)}$ to a configuration $(X_\mathrm{f}, Y_\mathrm{f}, \Theta_\mathrm{f}) \in \mathfrak{R}^{\mathrm{ZMD}}_{\theta_\mathrm{f}}(\mathsf{b}^+\mathsf{sb}^+)$. An important observation is that the time $T^*_\mathrm{f}(\mathsf{b}^+\mathsf{sb}^+)$ of the MD problem undergoes discontinuous jumps along the rays ϵ_1 and ϵ_2 emanating from the point A with coordinates $(x_\mathsf{A}, y_\mathsf{A}) = \rho(\sin\theta_\mathrm{f}, 1 - \cos\theta_\mathrm{f})$, where

$$\epsilon_1 := \{(x, y, \theta) \in P_{\theta_\mathrm{f}} : \ y = y_\mathsf{A}, \ x \geq x_\mathsf{A}, \ \theta = \theta_\mathrm{f}\},$$
$$\epsilon_2 := \{(x, y, \theta) \in P_{\theta_\mathrm{f}} : \ y = y_\mathsf{A} + s\sin\theta_\mathrm{f}, \ x = x_\mathsf{A} + s\cos\theta_\mathrm{f}, \ s \geq 0, \ \theta = \theta_\mathrm{f}\}.$$

The situation is illustrated in Fig. 17(a).

Let now $\mathcal{K}_{\theta_\mathrm{f}} \subset P_{\theta_\mathrm{f}}$ denote the cone with apex A defined by the rays ϵ_1 and ϵ_2, as is illustrated in Fig. 21. It can be shown [18] that every configuration $(x_\mathrm{f}, y_\mathrm{f}, \theta_\mathrm{f})$ in $\mathcal{K}_{\theta_\mathrm{f}} \subset \mathfrak{R}^{\mathrm{MD}}_{\theta_\mathrm{f}}(\mathsf{b}^+\mathsf{sb}^+) = P_{\theta_\mathrm{f}}$ can be reached in time $T^-(\mathsf{b}^+\mathsf{sb}^+) = T^*_\mathrm{f}(\mathsf{b}^+\mathsf{sb}^+)$, where

$$T^*_\mathrm{f}(\mathsf{b}^+\mathsf{sb}^+) = \rho\theta_\mathrm{f} + \sqrt{(x_\mathrm{f} - \rho\sin\theta_\mathrm{f})^2 + (y_\mathrm{f} + \rho\cos\theta_\mathrm{f} - \rho)^2}, \quad \text{for } (x_\mathrm{f}, y_\mathrm{f}, \theta_\mathrm{f}) \in \mathcal{K}_{\theta_\mathrm{f}}.$$

The remaining configurations in $\mathfrak{R}^{\mathrm{MD}}_{\theta_{\mathrm{f}}}(\mathsf{b}^+\mathsf{s}\mathsf{b}^+)\backslash\mathcal{K}_{\theta_{\mathrm{f}}} = P_{\theta_{\mathrm{f}}}\backslash\mathcal{K}_{\theta_{\mathrm{f}}}$ can be reached instead in minimum time $T^+(\mathsf{b}^+\mathsf{s}\mathsf{b}^+) = T^*_{\mathrm{f}}(\mathsf{b}^+\mathsf{s}\mathsf{b}^+)$, where

$$T^*_{\mathrm{f}}(\mathsf{b}^+\mathsf{s}\mathsf{b}^+) = \rho(2\pi + \theta_{\mathrm{f}}) + \sqrt{(x_{\mathrm{f}} - \rho\sin\theta_{\mathrm{f}})^2 + (y_{\mathrm{f}} + \rho\cos\theta_{\mathrm{f}} - \rho)^2},$$

for $(x_{\mathrm{f}}, y_{\mathrm{f}}, \theta_{\mathrm{f}}) \in P_{\theta_{\mathrm{f}}}\backslash\mathcal{K}_{\theta_{\mathrm{f}}}$. Thus along the rays ϵ_1 and ϵ_2 the minimum time $T^*_{\mathrm{f}}(\mathsf{b}^+\mathsf{s}\mathsf{b}^+)$ of the MD problem undergoes a discontinuous jump from $T^-(\mathsf{b}^+\mathsf{s}\mathsf{b}^+)$ to $T^+(\mathsf{b}^+\mathsf{s}\mathsf{b}^+) = T^-(\mathsf{b}^+\mathsf{s}\mathsf{b}^+) + 2\pi\rho$. In Fig. 21, we observe that the rays ϵ_1 and ϵ_2 are mapped via $\mathrm{H}_{T^-(\mathsf{b}^+\mathsf{s}\mathsf{b}^+)}$ to a new pair of rays, namely, ϵ'_1 and ϵ'_2, emanating from a point A' with coordinates $(x_{\mathsf{A}'}, y_{\mathsf{A}'}) = \mathrm{H}_{T^-(\mathsf{b}^+\mathsf{s}\mathsf{b}^+)}(x_{\mathsf{A}}, y_{\mathsf{A}})$. In addition, the rays ϵ_1 and ϵ_2 are mapped via $\mathrm{H}_{T^+(\mathsf{b}^+\mathsf{s}\mathsf{b}^+)}$ to another pair of rays, namely, ϵ''_1 and ϵ''_2, emanating from a point A'' with coordinates $(x_{\mathsf{A}''}, y_{\mathsf{A}''}) = \mathrm{H}_{T^+(\mathsf{b}^+\mathsf{s}\mathsf{b}^+)}(x_{\mathsf{A}}, y_{\mathsf{A}})$. We henceforth denote by $\mathcal{K}'_{\theta_{\mathrm{f}}}$ and $\mathcal{K}''_{\theta_{\mathrm{f}}}$ the cones defined by the apexes A' and A'' and the pairs of rays ϵ'_1, ϵ'_2 and ϵ''_1, ϵ''_2, respectively. The situation is illustrated in Fig. 21. Owing to the discontinuity of $T^*_{\mathrm{f}}(\mathsf{b}^+\mathsf{s}\mathsf{b}^+)$ of the MD problem along the rays ϵ_1 and ϵ_2, the composite mapping $\mathrm{H}_{T^*_{\mathrm{f}}(\mathsf{b}^+\mathsf{s}\mathsf{b}^+)}$ is also discontinuous along the rays ϵ_1 and ϵ_2. The fact that $\mathfrak{R}^{\mathrm{ZMD}}_{\theta_{\mathrm{f}}}(\mathsf{b}^+\mathsf{s}\mathsf{b}^+) \subset \mathfrak{R}^{\mathrm{MD}}_{\theta_{\mathrm{f}}}(\mathsf{b}^+\mathsf{s}\mathsf{b}^+) = P_{\theta_{\mathrm{f}}}$, when $0 \leq \alpha + \gamma(\alpha) \leq (4\pi - \theta_{\mathrm{f}})\rho$, can be now interpreted as a result of the discontinuity of the mapping H_T, which turns out to be a non-surjective mapping of $\mathfrak{R}^{\mathrm{MD}}_{\theta_{\mathrm{f}}}(\mathsf{b}^+\mathsf{s}\mathsf{b}^+)$ to $\mathfrak{R}^{\mathrm{ZMD}}_{\theta_{\mathrm{f}}}(\mathsf{b}^+\mathsf{s}\mathsf{b}^+)$. Another important remark, is that the time $T^*_{\mathrm{f}}(\mathsf{b}^+\mathsf{s}\mathsf{b}^+)$ of the ZMD problem undergoes discontinuous jumps along the ray ϵ'_2, the line segments $\mathsf{A}'\mathsf{B}$ and $\mathsf{B}\mathsf{A}''$, where B is the intersection point of ϵ'_1 and ϵ''_2, and the ray ϵ''_1. Furthermore, the set of configurations in $P_{\theta_{\mathrm{f}}}$ that cannot be reached by means of a $\mathsf{b}^+_\alpha\mathsf{s}_\beta\mathsf{b}^+_\gamma$ path, when $0 \leq \alpha + \gamma(\alpha) \leq (4\pi - \theta_{\mathrm{f}})\rho$, corresponds to the set $\mathcal{K}''_{\theta_{\mathrm{f}}}\backslash(\mathcal{K}'_{\theta_{\mathrm{f}}} \cap \mathcal{K}''_{\theta_{\mathrm{f}}})$. The situation is illustrated in Figs. 21 and 17(b).

4.4.3 Optimal Control Partition

The next step involves the partitioning of $P_{\theta_{\mathrm{f}}}$ into a finite number of domains denoted by $\mathfrak{R}^*_{\theta_{\mathrm{f}}}(u)$, where $u \in \mathsf{U}^*_{\mathrm{ZMD}}$, such that if $(x_{\mathrm{f}}, y_{\mathrm{f}}, \theta_{\mathrm{f}}) \in \mathrm{int}\left(\mathfrak{R}^*_{\theta_{\mathrm{f}}}(u)\right)$, then $(x_{\mathrm{f}}, y_{\mathrm{f}}, \theta_{\mathrm{f}})$

cannot be reached faster with the application of any other control sequence of $\mathsf{U}^*_{\mathrm{ZMD}}$ different than u. In particular, consider a configuration $(x_\mathrm{f}, y_\mathrm{f}, \theta_\mathrm{f}) \in \mathfrak{R}_{\theta_\mathrm{f}}(\mathsf{b}^+\mathsf{s}\mathsf{b}^+)$, and let $\mathsf{U}^c(\mathsf{b}^+\mathsf{s}\mathsf{b}^+) \subset \mathsf{U}^*_{\mathrm{ZMD}}$ denote the set of control sequences u different from $\mathsf{b}^+\mathsf{s}\mathsf{b}^+$ for which $(x_\mathrm{f}, y_\mathrm{f}, \theta_\mathrm{f}) \in \mathfrak{R}_{\theta_\mathrm{f}}(u)$. Then the configuration $(x_\mathrm{f}, y_\mathrm{f}, \theta_\mathrm{f})$ belongs to $\mathfrak{R}^*_{\theta_\mathrm{f}}(\mathsf{b}^+\mathsf{s}\mathsf{b}^+)$ if and only if $T^*_\mathrm{f}(\mathsf{b}^+\mathsf{s}\mathsf{b}^+) \leq \min_{u \in \mathsf{U}^c(\mathsf{b}^+\mathsf{s}\mathsf{b}^+)} T^*_\mathrm{f}(u)$. We shall refer to this partition of P_{θ_f} as the *optimal control partition*.

Figure 22 illustrates the optimal control partitions of P_{θ_f}, for $\theta_\mathrm{f} = \pi/3$, $\phi = -\pi/4$, and different values of the magnitude of the drift field $\nu \in]0, 1[$. In particular, we observe in Fig. 22(a) that, for $\nu = 0.2$, the structure of the optimal control partition of P_{θ_f} as well as the level sets of the minimum time $T^*_\mathrm{f} = \min T^*_\mathrm{f}(u)$, where $u \in \mathsf{U}^*_{\mathsf{ZMD}}$, do not significantly differ from those of the standard MD problem presented in [46]. The optimal control partition, as well as the level sets of the minimum time of the ZMD and MD problems, for higher values of ν, become, however, significantly different (Fig. 22(b)-22(d)). Furthermore, we observe that, as ν increases, the set $\mathfrak{R}^*_{\theta_\mathrm{f}}(\mathsf{b}^-\tilde{\mathsf{b}}^+\mathsf{b}^-)$ corresponds to a non-trivial portion of the optimal control partition (Figs. 22(c)-22(d)).

Figure 23 illustrates the optimal control partition of P_{θ_f}, for $\theta_\mathrm{f} = \pi/3$, $\nu = 0.5$ and different values of the drift direction ϕ. Figures 23(a)-23(d) illustrate how sensitive is the optimal control partition of P_{θ_f} for the ZMD problem to variations of the drift direction. It is interesting to note that, for $\phi = -3\pi/4$, the set $\mathfrak{R}^*_{\theta_\mathrm{f}}(\mathsf{b}^-\tilde{\mathsf{b}}^+\mathsf{b}^-)$ corresponds to a significant portion of the optimal control partition of P_{θ_f} (Fig. 23(a)). Furthermore, we observe that, as we change the value of ϕ, some extremal paths of $\mathcal{P}_{\mathrm{ZMD}}$ become more favorable than others, in terms of minimizing the travel time. For example, when $\phi = -3\pi/4$ (Fig. 23(a)) and $\phi = 3\pi/4$ (Fig. 23(d)), then respectively, the sets $\mathfrak{R}^*_{\theta_\mathrm{f}}(\mathsf{b}^-\mathsf{b}^+\mathsf{b}^-)$ and $\mathfrak{R}^*_{\theta_\mathrm{f}}(\mathsf{b}^-\mathsf{s}\mathsf{b}^+)$ correspond to significantly larger portions of the optimal control partition of P_{θ_f}, when compared with the standard MD problem.

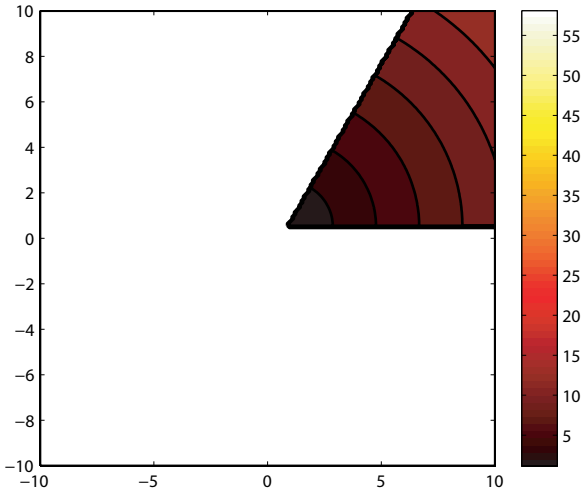

(a) Reachable set $\mathfrak{R}^{\mathrm{MD}}_{\theta_{\mathrm{f}}}(\mathsf{b}^{+}\mathsf{s}\mathsf{b}^{+})$ for the standard MD problem.

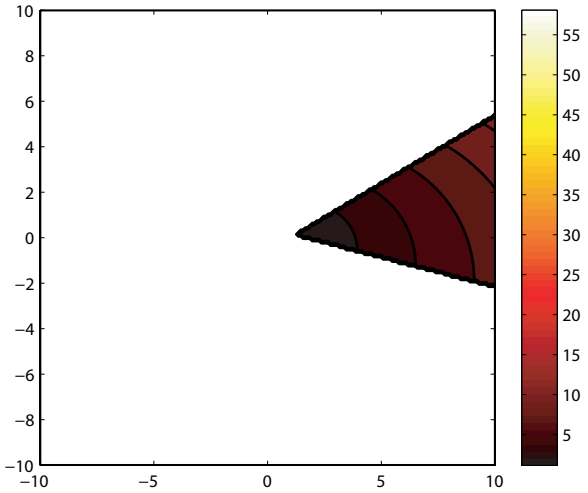

(b) Reachable set $\mathfrak{R}^{\mathrm{ZMD}}_{\theta_{\mathrm{f}}}(\mathsf{b}^{+}\mathsf{s}\mathsf{b}^{+})$.

Figure 18: Reachable sets $\mathfrak{R}_{\theta_{\mathrm{f}}}(\mathsf{b}^{+}\mathsf{s}\mathsf{b}^{+})$ of the standard MD and the ZMD problems, when $0 \leq \alpha + \gamma(\alpha) \leq 2\pi\rho$, and $\theta_{\mathrm{f}} = \pi/3$.

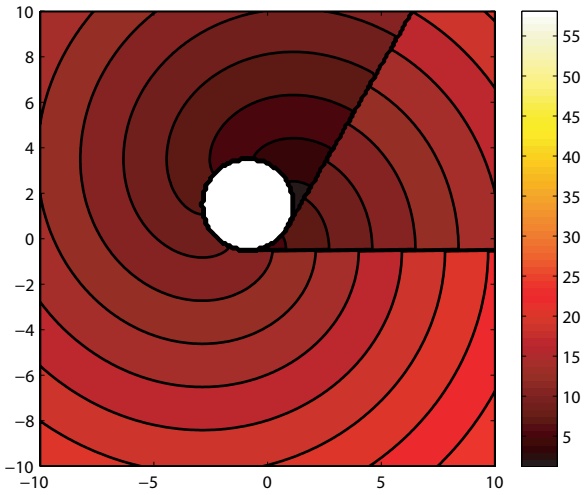

(a) Reachable set $\mathfrak{R}^{\mathrm{MD}}_{\theta_{\mathrm{f}}}(\mathsf{b}^{+}\mathsf{sb}^{-})$.

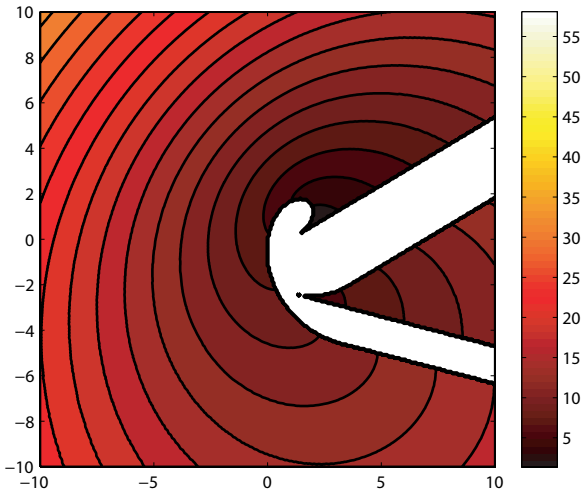

(b) Reachable set $\mathfrak{R}^{\mathrm{ZMD}}_{\theta_{\mathrm{f}}}(\mathsf{b}^{+}\mathsf{sb}^{+})$.

Figure 19: Reachable sets $\mathfrak{R}_{\theta_{\mathrm{f}}}(\mathsf{b}^{+}\mathsf{sb}^{+})$ of the standard MD and the ZMD problems, when $\alpha + \gamma(\alpha) \leq (4\pi - \theta_{\mathrm{f}})\rho$, and $\theta_{\mathrm{f}} = \pi/3$.

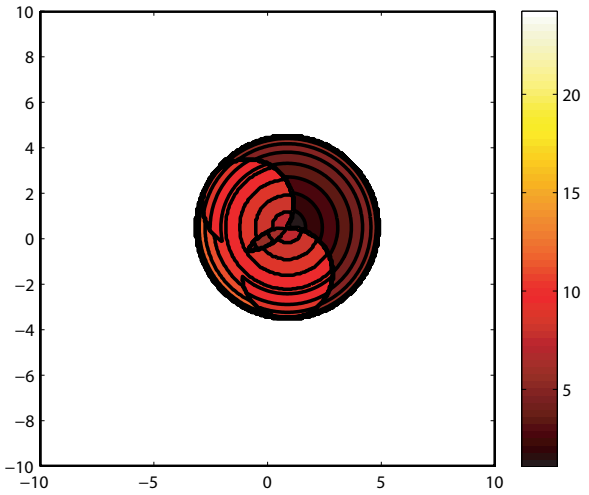

(a) Reachable set $\mathfrak{R}^{\mathrm{MD}}_{\theta_{\mathrm{f}}}(\mathsf{b}^{+}\mathsf{b}^{-}\mathsf{b}^{+})$.

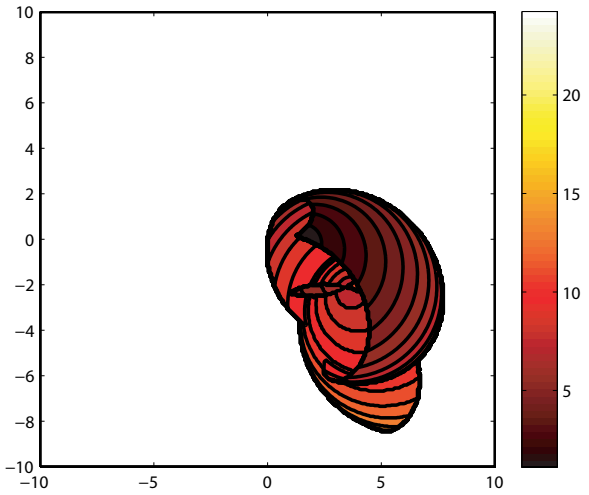

(b) Reachable set $\mathfrak{R}^{\mathrm{ZMD}}_{\theta_{\mathrm{f}}}(\mathsf{b}^{+}\mathsf{b}^{-}\mathsf{b}^{+})$.

Figure 20: Reachable sets $\mathfrak{R}_{\theta_{\mathrm{f}}}(\mathsf{b}^{+}\mathsf{b}^{-}\mathsf{b}^{+})$ of the standard MD and the ZMD problems, when $\alpha + \gamma(\alpha) \leq (4\pi - \theta_{\mathrm{f}})\rho$, and $\theta_{\mathrm{f}} = \pi/3$.

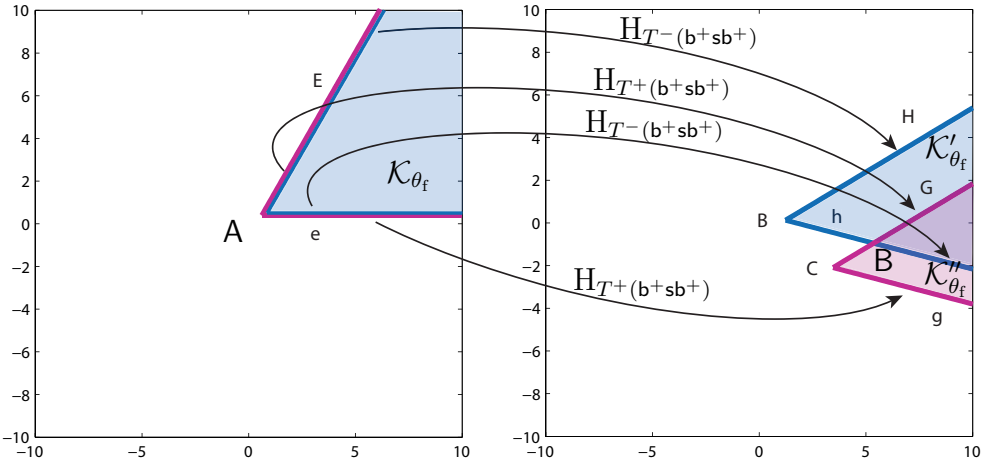

Figure 21: Owing to the discontinuity of the time-to-go, the rays ϵ_1 and ϵ_2 in $\in \mathfrak{R}^{\mathrm{MD}}_{\theta_f}(\mathsf{b}^+\mathsf{sb}^+)$ are mapped to two pairs of rays in $\in \mathfrak{R}^{\mathrm{ZMD}}_{\theta_f}(\mathsf{b}^+\mathsf{sb}^+)$.

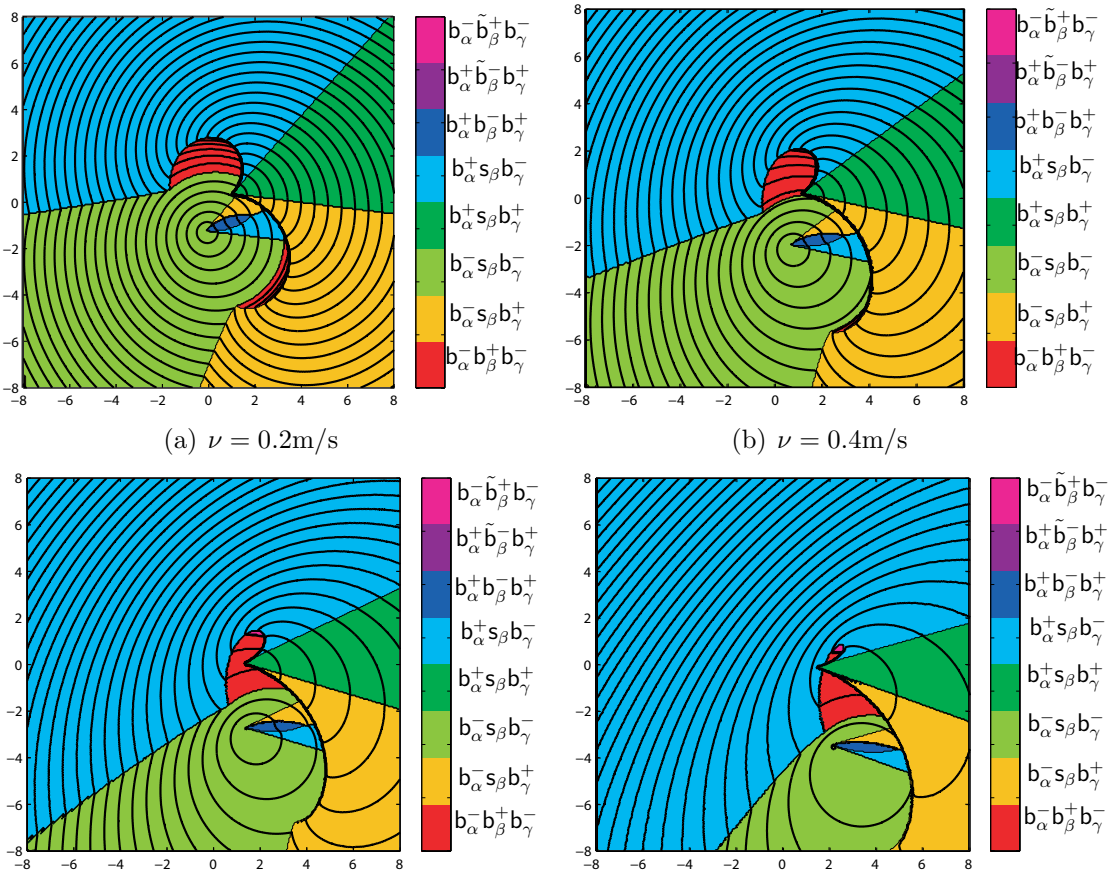

(a) $\nu = 0.2$m/s

(b) $\nu = 0.4$m/s

(c) $\nu = 0.6$m/s

(d) $\nu = 0.8$m/s

Figure 22: Optimal control partition of P_{θ_f}, for $\theta_f = \pi/3$, and contours of T^*_f for $\phi = -\pi/4$ and different values of ν.

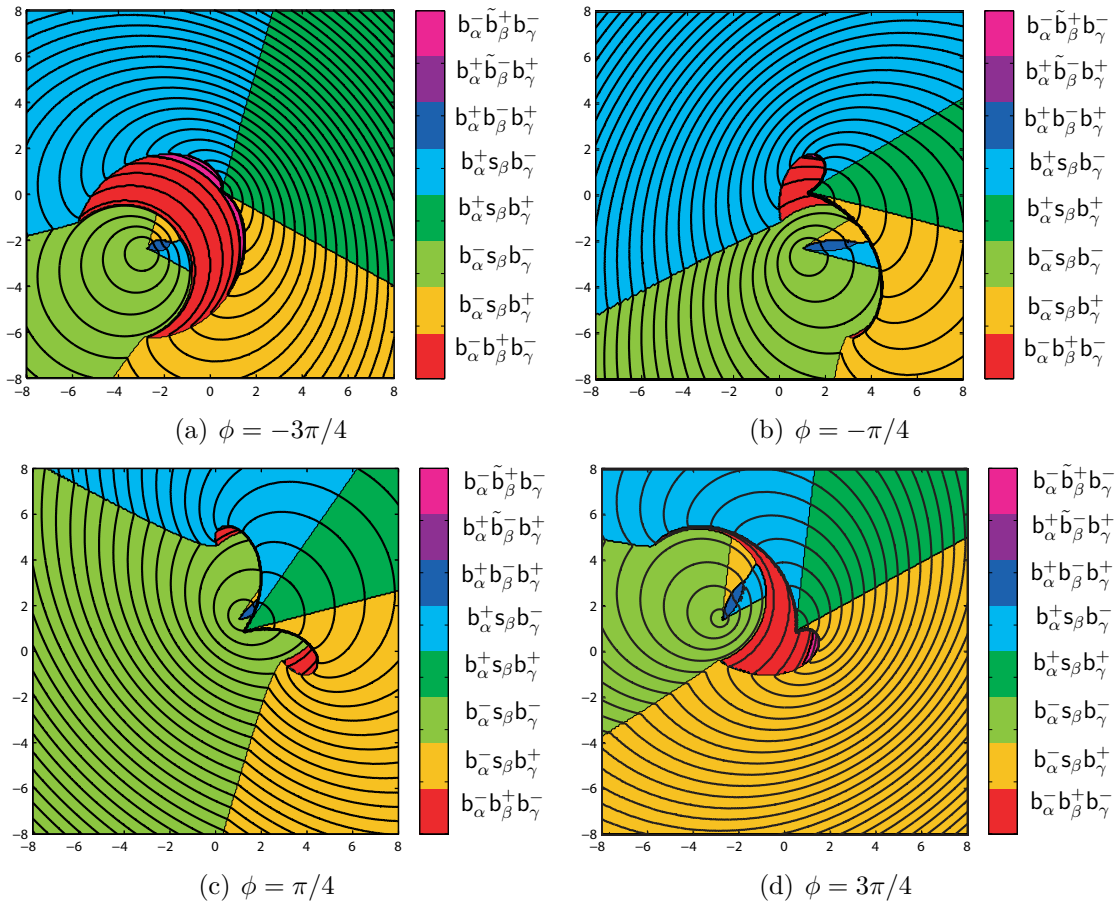

(a) $\phi = -3\pi/4$ (b) $\phi = -\pi/4$

(c) $\phi = \pi/4$ (d) $\phi = 3\pi/4$

Figure 23: Optimal control partition of P_{θ_f}, for $\theta_\mathrm{f} = \pi/3$, and contours of T_f^* for $\nu = 0.5$ and different values of ϕ.

CHAPTER V

ON THE GENERATION OF NEARLY OPTIMAL, PLANAR PATHS OF BOUNDED CURVATURE AND BOUNDED CURVATURE GRADIENT

The material presented in this chapter builds upon the results presented in [11].

5.1 Introduction

In this Chapter, we consider an extension of the MD problem dealing with the characterization of nearly length-minimal paths with bounded curvature and bounded derivative of the curvature. We devise a finite number of *path primitives* in order to construct nearly optimal paths. In particular, we design composite paths that are suitable concatenations of circular arcs, pieces of clothoids and line segments. The concatenation of these path primitives (*path maneuvers*) is based on the specific geometric transformations that uniquely relates the solution of the path planning problem treated in this chapter with the solution of the Markov-Dubins (MD) problem. We extensively employ ideas and results from the field of computational geometry, and in particular, from the work on clothoids by Meek and Walton [127]. While other approaches dealing with similar problems, such as [75, 153], use primarily numerical algorithms for the construction of the clothoid segments we use, instead, a more analytic and geometric approach. As a result, the computational cost associated with the curve generation problem is significantly reduced. In addition, we investigate how does the constraint over the derivative of the curvature of the path affect the set of configuration that can be reached by the Isaacs-Dubins (ID) car when driven by an angular acceleration input. The results of this analysis reveal the intrinsic difficulties

that arise as a result of imposing constraints both on the curvature and its derivative.

5.2 Kinematic Model and Problem Formulation

We consider the planar, shortest-path problem with prescribed positions and tangents when both curvature and curvature derivative are bounded by explicit bounds known a priori. In order to address the problem, we employ the kinematical model introduced by Boissonnat et al [41] (continuous curvature extension of the ID car), which is described by the following set of equations

$$\dot{x} = \cos\theta, \tag{56}$$

$$\dot{y} = \sin\theta, \tag{57}$$

$$\dot{\theta} = \kappa, \tag{58}$$

$$\dot{\kappa} = \gamma, \tag{59}$$

where $(x, y) \in \mathbb{R}^2$ are the cartesian coordinates of a reference point of the vehicle, $\theta \in \mathbb{S}^1$ is the vehicle's heading (always tangent to the ensuing path), $\kappa \in \mathbb{R}$ is the curvature of the ensuing path, and γ (steering acceleration) is the control input. We assume that the set of admissible control inputs is given by

$$\mathcal{U} := \{\gamma \in \mathfrak{U} : \ \gamma(t) \in U, \ t \in [0, T_{\mathrm{f}}]\}, \tag{60}$$

where $\mathfrak{U}$ is the set of measurable functions defined over the interval $[0, T_{\mathrm{f}}]$, for some $T_{\mathrm{f}} > 0$, $U := [-\gamma_{\max}, \gamma_{\max}]$, and $\gamma_{\max}$ is the maximum curvature gradient. The assumption that the vehicle travels only forward is reflected upon the requirement that the speed of the vehicle is constant and positive. We furthermore assume that the state κ satisfies the following constraint

$$|\kappa| \leq \kappa_{\max}. \tag{61}$$

Next, we formulate the shortest path problem with bounded curvature and curvature gradient as a minimum-time problem.

Problem 4. *Given the system described by equations (56)-(59) and the cost functional*

$$J(\gamma) = \int_0^{T_\mathrm{f}} 1 \mathrm{d}t = S_\mathrm{f}, \tag{62}$$

where T_f is the free final time and S_f is the total length of the path, determine a control input $\gamma^* \in \mathcal{U}$, with $\gamma^* : [0, T_\mathrm{f}] \mapsto U$ such that

i. The trajectory $\mathsf{x}^*(t) = (x^*(t), y^*(t), \theta^*(t), \kappa^*(t))$ generated by the control γ^* satisfies

(a) The boundary conditions

$$\mathsf{x}^*(0) = (x_0, y_0, \theta_0, \kappa_0), \tag{63}$$

$$\mathsf{x}^*(T_\mathrm{f}) = (x_\mathrm{f}, y_\mathrm{f}, \theta_\mathrm{f}, \kappa_\mathrm{f}). \tag{64}$$

(b) The global point-wise state constraint (61).

ii. The control γ^* minimizes the cost functional $J(\gamma)$ given in (62) evaluated along x^*.

The requirement of unit constant speed excludes curves that contain cusps from the set of feasible solutions of Problem 4.

5.3 Generation of G^2 Continuous Paths using Path Primitives

Boissonnat et al [41] and Sussmann [198] have examined Problem 4 when the state constraint (61) is not taken into account. In this special case, as shown in [41], [198], the problem is always feasible; however, when a line segment is part of the optimal path, then the corresponding optimal control γ may switch infinitely fast (chattering). Therefore, the solution of Problem 4 is likely to be irregular as well. Chattering optimal controllers cannot be implemented easily in practice, only their approximations are possible [81]. If the bound over the curvature gradient is not necessarily finite,

then as $\gamma_{\max}$ goes to ∞, Problem 4 reduces to the MD problem, whose solution, which consists of the so-called Dubins paths, is characterized in [77]. For many applications, however, Dubins paths are not suited for path tracking applications owing to the fact that their discontinuous curvature profiles induce an offset tracking error [75]. On the other hand, clothoids are curves, whose curvature varies linearly with the arc length s, that is,

$$\kappa(s) = \kappa_0 + \kappa_1 s, \tag{65}$$

where κ_0, $\kappa_1 \in \mathbb{R}$. Note that any circle of radius ρ as well as any straight line can be considered as degenerate clothoids with $\kappa_0 = \pm 1/\rho$, $\kappa_1 = 0$ and $\kappa_0 = 0$, $\kappa_1 = 0$ respectively.

In this section, we demonstrate an analytic/geometric approach to deal with Problem 4. In particular, we present a simple way to generate nearly length-optimal, G^2 continuous planar paths composed of line segments, circular arcs and pieces of clothoids, which form the set of *path primitives* of our scheme. By appropriate concatenations of path primitives, we obtain composite paths that characterize the family of *admissible paths* of Problem 4. The term G^2 continuity describes the family of curves with continuous tangent and curvature. By interconnecting line segments (zero curvature) and circles (constant nonzero curvature) or circles of different curvature via pieces of clothoids, we can construct composite curves which satisfy the G^2 continuity requirement everywhere. The key idea of our approach is to associate the G^2 path generation problem with a MD problem via a family of geometric transformations. This approach allows us to characterize in closed mathematical forms the paths that are nearly optimal solutions of Problem 4.

Next, we present some of the basic properties of clothoids which we will use later on.

5.3.1 Clothoid Curves

The standard clothoid with scaling factor σ is expressed naturally in terms of the angle of its tangent ϑ. In particular, the coordinates of the standard clothoid curve are given by [127]

$$x(\vartheta) = \sigma \int_0^{\vartheta} \frac{\cos(u)}{\sqrt{u}} \mathrm{d}u, \quad y(\vartheta) = \sigma \int_0^{\vartheta} \frac{\sin(u)}{\sqrt{u}} \mathrm{d}u, \quad \vartheta > 0. \tag{66}$$

The curvature and the arc length of the clothoid as a function of the angle ϑ are given by

$$|\kappa(\vartheta)| = \frac{\sqrt{\vartheta}}{\sigma}, \quad \mathrm{d}s = \frac{\sigma}{\sqrt{\vartheta}} \mathrm{d}\vartheta, \quad \vartheta > 0. \tag{67}$$

It follows from (67) that

$$|\gamma| = \left| \frac{\mathrm{d}\kappa}{\mathrm{d}s} \right| = \frac{1}{2\sigma^2}. \tag{68}$$

5.3.2 Family of Admissible Paths

In this section, we examine the admissible paths of our scheme. First, we consider the problem of driving a vehicle whose kinematics are described by equations (56)-(59) from the initial configuration $\mathsf{x}_0 = (x_0, y_0, 0, 0)$ to the terminal configuration $\mathsf{x}_\mathrm{f} = (x_\mathrm{f}, y_\mathrm{f}, \theta_\mathrm{f}, 1/\rho_1)$ as is illustrated in Fig. 24. This problem is equivalent to the problem of driving the vehicle initially located at $(x_0, y_0) \in \epsilon_2$ with heading $\theta_0 = 0$ to $(x_\mathrm{f}, y_\mathrm{f}) \in \mathcal{C}_1(\rho_1)$ with heading θ_f in finite time. The line segment ϵ_2 is assumed to be parallel to a line segment ϵ_1 that is tangent to $\mathcal{C}$ at some point $\mathsf{A} \in \mathcal{C}_1(\rho_1)$. In addition, let $\delta_s > 0$ denote the distance between ϵ_1 and ϵ_2.

Given the radius of the circle $\rho_1 > 0$, the angle ϑ_1^* of the tangent at the intersection point of $\mathcal{K}_1$ with $\mathcal{C}_1$ and the scaling factor σ_1 of the clothoid satisfy the following equations [127]

$$\sigma_1 - \rho_1 \sqrt{\vartheta_1^*} = 0 \tag{69}$$

$$\sqrt{\vartheta_1^*} \int_0^{\vartheta_1^*} \frac{\sin(u)}{\sqrt{u}} \mathrm{d}u + \cos\vartheta_1^* - 1 - \frac{\delta_s}{\rho_1} = 0 \tag{70}$$

In the subsequent analysis, we confine our selves in the case when the angle $\vartheta_1^* \in (0, \pi/2)$ for reasons that will become clear later on. Furthermore, we take δ_s to be a design parameter, whereas σ_1 and ϑ_1^* are derived uniquely from (69) and (70), as shown in the following proposition.

Proposition 20. *Given $\rho_1 > 0$, the system of equations (69)-(70) has a unique solution $(\sigma, \vartheta_1^*) \in (0, \rho_1\sqrt{2\pi}/2] \times (0, \pi/2)$ provided that*

$$0 < \delta_s < \rho_1 \left(\frac{\sqrt{2\pi}}{2} \int_0^{\pi/2} \frac{\sin u \mathrm{d}u}{\sqrt{u}} - 1 \right).$$

Proof. Consider the function $f : (0, \pi/2) \mapsto \mathbb{R}$ defined by

$$f(\vartheta) = \rho_1 \left(\sqrt{\vartheta} \int_0^{\vartheta} \frac{\sin u}{\sqrt{u}} \mathrm{d}u + \cos\vartheta - 1 \right). \tag{71}$$

It follows by Bolzano's intermediate value theorem [26], that for $\vartheta \in (0, \pi/2)$ the function $f(\vartheta)$ takes all the values between $f(0) = 0$ and $f(\pi/2) = \rho_1 \left(\frac{\sqrt{2\pi}}{2} \int_0^{\pi/2} \frac{\sin u \mathrm{d}u}{\sqrt{u}} - 1 \right)$. Thus, for $\delta_s \in \left(0, \rho_1 \left(\frac{\sqrt{2\pi}}{2} \int_0^{\pi/2} \frac{\sin u \mathrm{d}u}{\sqrt{u}} - 1 \right)\right)$, the equation (70) has at least one solution in $(0, \pi/2)$. Furthermore, the function f is monotonically increasing since $f'(\vartheta) > 0$ for all $\vartheta \in (0, \pi/2)$. Thus, f is injective and the solution of the system of equations (69)-(70) is unique. □

We write

$$\mathsf{SC}^+(\rho_1, \vartheta_1^*) := \epsilon_1 \circ \mathcal{K}_1 \circ \mathcal{C}_1, \tag{72}$$

where $\circ$ denotes concatenations of curves, to denote the G^2 continuous path and $\mathsf{SC}^+(\rho_1) := \epsilon_1 \circ \mathcal{C}_1$ to denote the corresponding Dubins path. This path constitutes a G^2 continuous *half turn* that plays the role of the archetype that we use to devise the rest of the maneuvers of our scheme. The letter C denotes a circular arc, where the superscript is $+$ when the parametrization of the arc traces it out counterclockwise and $-$ otherwise. Finally the letter S denotes a line segment.

Let us consider the path planning problem from the initial configuration $\mathsf{x}_0 = (x_0, y_0, \theta_0, -1/\rho_1)$ to the terminal configuration $\mathsf{x}_\mathrm{f} = (x_\mathrm{f}, y_\mathrm{f}, \theta_\mathrm{f}, 1/\rho_2)$ as illustrated in

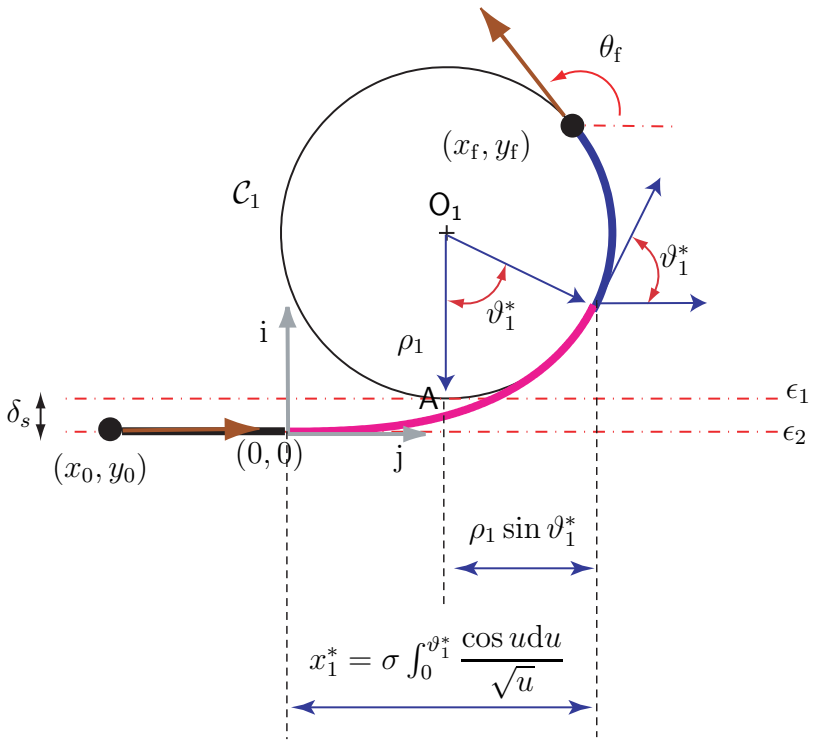

Figure 24: Interconnecting a piece of clothoid with a line segment ($\mathsf{SC}^+(\rho_1, \vartheta_1^*)$ path). The path that corresponds to the nearly optimal solution to the steering Problem 4 is composed of a line segment, a piece of clothoid and a circular arc denoted by a black, magenta and blue color, respectively.

Fig. 25. The ensuing path of the vehicle is assumed to be the concatenation of two circles $\mathcal{C}_1(\rho_1)$ and $\mathcal{C}_2(\rho_2)$ and the interconnecting composite curve, which is composed, in turn, of a piece of a clothoid curve $\mathcal{K}_1$, a line segment and a piece of a second clothoid curve $\mathcal{K}_2$. Let $\epsilon_1 = \{(x, y)|\ A_1x + B_1y + C = 0\}$ denote the common tangent line of $\mathcal{C}_(\rho_1)$ and $\mathcal{C}_(\rho_2)$. Let $\epsilon_2 = \{(x, y)|\ A_2x + B_2y + C = 0\}$ denote the line obtained after the rotation around P at an angle δ_r, where the pivot point P, is specified as the intersection point of the line ϵ_1 and the line segment $\mathsf{O_1O_2}$. The minimum distances $\delta_{s,1}$ and $\delta_{s,2}$ of the line ϵ_1 from the circles $\mathcal{C}_1(\rho_1)$ and $\mathcal{C}(\rho_2)$ are given by

$$\delta_{s,i} = \frac{|A_2X_i + B_2Y_i + C_2|}{\sqrt{A_2^2 + B_2^2}} - \rho_i, \quad i = 1, 2, \tag{73}$$

where (X_1, Y_1) and (X_2, Y_2) are the coordinates of the centers of $\mathcal{C}_1(\rho_1)$ and $\mathcal{C}_2(\rho_2)$ respectively. The composite curve that connects the two circles is the concatenation of a G^2 continuous SC^- with another G^2 continuous SC^+ path as is illustrated in Fig. 24 with δ_s replaced by $\delta_{s,1}$ and $\delta_{s,2}$, respectively, where $\delta_{s,1}/\delta_{s,2} = \rho_1/\rho_2$. The scaling factors σ_1 and σ_2 of the clothoid curves $\mathcal{K}_1$ and $\mathcal{K}_2$ are specified by algebraic equations similar to those given in (69) and (70). We write

$$\mathsf{C}^-\mathsf{SC}^+(\rho_1, \vartheta_1^*, \rho_2, \vartheta_2^*, \delta_r) := \mathcal{C}_1 \circ \mathcal{K}_1 \circ \epsilon_1 \circ \mathcal{K}_2 \circ \mathcal{C}_2, \tag{74}$$

to denote this G^2 continuous path, and $\mathsf{C}^-\mathsf{SC}^+(\rho_1, \rho_2)$ to denote the corresponding Dubins path.

Let us now consider the path planning problem from the initial configuration $\mathsf{x}_0 = (x_0, y_0, \theta_0, -1/\rho_1)$ to the terminal configuration $\mathsf{x}_\mathrm{f} = (x_\mathrm{f}, y_\mathrm{f}, \theta_\mathrm{f}, -1/\rho_2)$ as illustrated in Fig. 24. We consider the line $\epsilon_1 = \{(x, y)|\ A_1x + B_1y + C_1 = 0\}$ that is tangent to both $\mathcal{C}_1(\rho_1)$ and $\mathcal{C}_2(\rho_2)$ and the line $\epsilon_2 = \{(x, y)|\ A_2x + B_2y + C_2 = 0\}$ that is parallel to ϵ_1. Furthermore, δ_s is the distance between the two lines, i.e.,

$$\delta_s = \frac{|C_1 - C_2|}{\sqrt{A_1^2 + B_1^2}}. \tag{75}$$

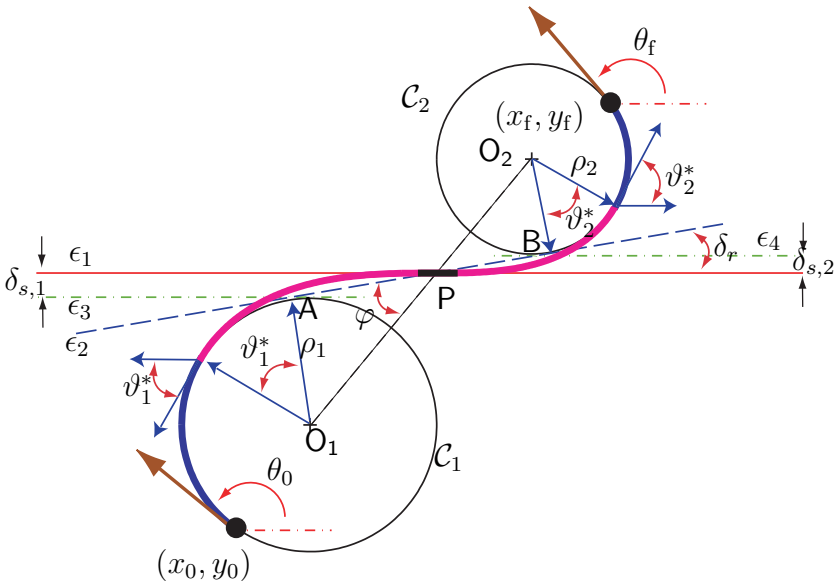

(a) Interconnecting two circles via a $\mathsf{C}^-\mathsf{SC}^+(\rho_1, \vartheta_1^*, \rho_2, \vartheta_2^*, \delta_r)$ path.

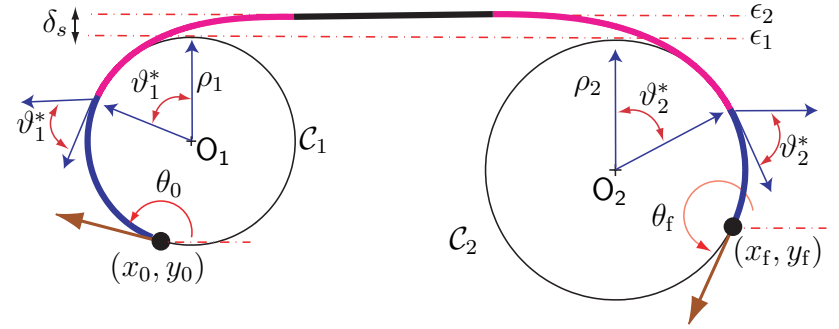

(b) Interconnecting two circles via a $\mathsf{C}^-\mathsf{SC}^-(\rho_1, \vartheta_1^*, \rho_2, \vartheta_2^*, \delta_s)$ path.

Figure 25: The path that corresponds to the near optimal solution to the steering Problem 4 when the two boundary conditions x_0 and x_f are associated with two different circles, is composed of a line segment, two pieces of clothoids and two circular arcs denoted by black, magenta and blue color, respectively.

The composite curve in this case is the concatenation of two G^2 continuous SC^- paths as shown in Fig. 24. We write

$$\mathsf{C}^-\mathsf{SC}^-(\rho_1, \vartheta_1^*, \rho_2, \vartheta_2^*, \delta_s) := \mathcal{C}_1 \circ \mathcal{K}_1 \circ \epsilon_1 \circ \mathcal{K}_2 \circ \mathcal{C}_2, \tag{76}$$

to denote the G^2 continuous path, and $\mathsf{C}^-\mathsf{SC}^-(\rho_1, \rho_2)$ to denote the corresponding Dubins path.

In Fig. 26 we observe three circles, namely $\mathcal{C}_1(\rho_1), \mathcal{C}_{12}(\rho_{12})$ and $\mathcal{C}_2(\rho_2)$ located at points $\mathsf{O}_1, \mathsf{O}_2$ and O_{12}, respectively, which are interconnected via a $\mathsf{C}^-\mathsf{SC}^+$ and a

$\mathsf{C}^+\mathsf{SC}^-$ path. The corresponding Dubins path is a concatenation of $\mathcal{C}_1(\rho_1)$ and $\mathcal{C}_2(\rho_2)$ with the common tangent circle $\mathcal{C}_{12}(\rho_{12})$ located at O'_{12}, where $\rho_{12} = \min\{\rho_1, \rho_2\}$. By construction, the straight line passing through O'_{12} and O_{12} bisects the line segment $\mathsf{O}_1\mathsf{O}_2$ at point A. Let δ_{C} denote the length of the segment $\mathsf{O}'_{12}\mathsf{O}_{12}$. For $\delta_{\mathsf{C}} > 0$ the circles $\mathcal{C}_1(\rho_1)$ and $\mathcal{C}_{12}(\rho_{12})$ can be interconnected by means of a $\mathsf{C}^-\mathsf{SC}^+$ path, whereas $\mathcal{C}_{12}(\rho_{12})$ and $\mathcal{C}_2(\rho_2)$ via a $\mathsf{C}^+\mathsf{SC}^-$ path. We write

$$\begin{aligned}\mathsf{C}^-\mathsf{C}^+\mathsf{C}^-(\rho_1, \rho_{12}, \rho_2, \delta_{\mathsf{C}}) = \mathsf{C}^-\mathsf{SC}^+(\rho_1, \vartheta^*_{d,1}, \rho_{12}, \vartheta^*_{a,12}, \delta_{r,12}) \\ \circ\, \mathsf{C}^+\mathsf{SC}^-(\rho_2, \vartheta^*_{d,12}, \rho_{12}, \vartheta^*_{a,2}, \delta_{r,23})\end{aligned} \tag{77}$$

where $\vartheta^*_{d,k}, \quad k \in \{1, 12\}$, and $\vartheta^*_{a,\ell}, \quad \ell \in \{12, 2\}$, correspond to the angle of tangent at the point of departure from $\mathcal{C}_k(\rho_k)$ and the point of arrival to $\mathcal{C}_\ell(\rho_\ell)$, respectively. Finally, we write $\mathsf{C}^-\mathsf{C}^+\mathsf{C}^-(\rho_1, \rho_{12}, \rho_2)$ to denote the corresponding Dubins path.

Remark 7 Of course only the Dubins paths that are associated with a change in the vehicle orientation along $\mathcal{C}_{12}(\rho_{12})$ that is greater than π and less than 2π can be paths of minimal length. The situation is illustrated in Fig. 26, where the shortest length solution to the steering problem with boundary conditions specified by the tangent angles $\theta_{0,a}$ and $\theta_{\mathrm{f},a}$ is achieved by the appropriate $\mathsf{C}^-\mathsf{C}^+\mathsf{C}^-(\rho_1, \rho_{12}, \rho_2)$ path, whereas the one specified by $\theta_{0,a}$ and $\theta_{\mathrm{f},a}$ is achieved by the appropriate $\mathsf{C}^-\mathsf{SC}^-(\rho_1, \rho_2)$ path rather than the $\mathsf{C}^+\mathsf{C}^-\mathsf{C}^+(\rho_1, \rho_{12}, \rho_2)$ path.

5.4 Path Admissibility and Length Minimality

The issue of admissibility of each element of the family of admissible paths introduced in Section 5.3 for different boundary configurations requires special attention. For simplicity, in this section we analyze in detail only the admissibility of $\mathsf{C}^-\mathsf{SC}^-$ paths. After the necessary modifications, similar results can be derived mutatis mutandis for the rest of the path primitives introduced in Section 5.3.

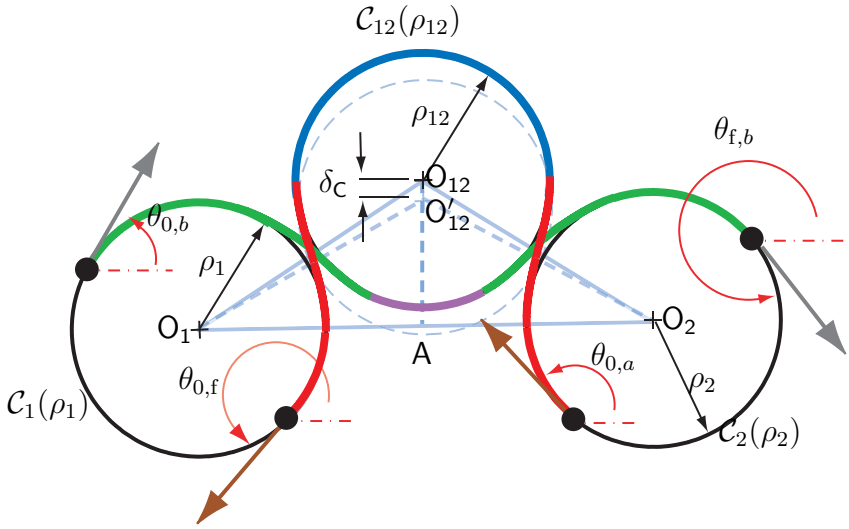

Figure 26: The G^2 continuous path obtained from the $\mathsf{C}^-\mathsf{C}^+\mathsf{C}^-$ path that solves the steering problem with initial and final headings $\theta_{0,a}$ and $\theta_{\mathrm{f},a}$, respectively, is the concatenation of the two red curves, which correspond to a $\mathsf{C}^-\mathsf{SC}^+$ and a $\mathsf{C}^+\mathsf{SC}^-$ path, and the blue circular arc along $\mathcal{C}_{12}(\rho_{12})$. The concatenation of the green curves ($\mathsf{C}^-\mathsf{SC}^+$ and $\mathsf{C}^+\mathsf{SC}^-$) and the purple circular arc along $\mathcal{C}_{12}(\rho_{12})$ solve the steering problem with initial and final headings $\theta_{0,b}$ and $\theta_{\mathrm{f},b}$, respectively.

The path admissibility is mainly related to the G^2 continuity requirement, which, in turn, reflects the smooth, forward only motion requirement for the vehicle (paths with cusps or corners fail to satisfy the G^2 continuity requirement). In particular, we characterize any steering problem in which the two pieces of clothoids of the $\mathsf{C}^-\mathsf{SC}^-$ path intersect as inadmissible. Note that if we allow an intersection between the two clothoid curves to take place, then the vehicle would have to track either a curve with a corner, something that would result to a violation of the kinematic equations (56)-(58), or a path with an arc of backward motion along the line ϵ_2 and between the endpoints D and E of the two clothoid curves, where D is now aft of E compared to the situation depicted in Fig. 25. Before analyzing the connection between the G^2 continuity condition and the admissibility of the $\mathsf{C}^-\mathsf{SC}^-$ path, we introduce the following lemma.

Lemma 1. *For $\vartheta \in (0, \pi/2)$, we have that*

$$\vartheta - \frac{\vartheta^3}{5} \leq \sqrt{\vartheta} \int_0^{\vartheta} \frac{\sin u}{u^{\frac{3}{2}}} \mathrm{d}u \leq \vartheta + \frac{\vartheta^3}{6}. \tag{78}$$

Proof. For $\vartheta \in (0, \pi/2)$, we have, by the Taylor expansion theorem for cos and sin functions, the following inequalities

$$1 - \frac{\vartheta^2}{2} \leq \cos\vartheta \leq 1, \tag{79}$$

$$\vartheta - \frac{\vartheta^3}{6} \leq \sin\vartheta \leq \vartheta. \tag{80}$$

It follows from (79) that

$$2\vartheta - \frac{\vartheta^3}{5} \leq \sqrt{\vartheta}\int_0^{\vartheta} \frac{\cos u}{\sqrt{u}}\mathrm{d}u \leq 2\vartheta. \tag{81}$$

Using integration by parts it follows that

$$\int_0^{\vartheta} \frac{\sin u}{u^{\frac{3}{2}}}\mathrm{d}u = 2\int_0^{\vartheta} \frac{\cos u}{\sqrt{u}}\mathrm{d}u - 2\frac{\sin\vartheta}{\sqrt{\vartheta}}. \tag{82}$$

The result follows by (79) and (81). □

Proposition 21. *The G^2 continuous $\mathsf{C}^-\mathsf{S}\mathsf{C}^-$ path is admissible only if the distance L between the centers of $\mathcal{C}_1$ and $\mathcal{C}_2$ satisfy the following condition*

$$L \geq \sqrt{(\rho_1 - \rho_2)^2 + \frac{1}{4}\left(\sum_{i=1}^{2}\rho_i\left(\vartheta_i^* - \frac{(\vartheta_i^*)^3}{5}\right)\right)^2} \tag{83}$$

Proof. With the aid of Fig. 27 we observe that the two pieces of clothoids do not intersect only if

$$\Delta x_1 + \Delta x_2 \leq \sqrt{L^2 - (\rho_1 - \rho_2)^2}, \tag{84}$$

where

$$\Delta x_i = \sigma_i \int_0^{\vartheta_i^*} \frac{\cos u}{\sqrt{u}}\mathrm{d}u - \rho_i \sin\vartheta_i^*, \quad i = 1, 2. \tag{85}$$

Applying equations (69)-(70) on (85) and integrating by parts the integral $\int_0^{\vartheta_i^*} \frac{\cos u \mathrm{d}u}{\sqrt{u}}$, we obtain

$$\Delta x_i = \frac{1}{2}\rho_i\sqrt{\vartheta_i^*}\int_0^{\vartheta_i^*} \frac{\sin u}{u^{\frac{3}{2}}}\mathrm{d}u, \quad i = 1, 2, \tag{86}$$

Thus, condition (84) is satisfied only if

$$L \geq \sqrt{(\rho_1 - \rho_2)^2 + \frac{1}{4}\left(\sum_{i=1}^{2}\rho_i\sqrt{\vartheta_i^*}\int_0^{\vartheta_i^*} \frac{\sin u}{u^{\frac{3}{2}}}\mathrm{d}u\right)^2}. \tag{87}$$

Using Lemma 1 the result follows. □

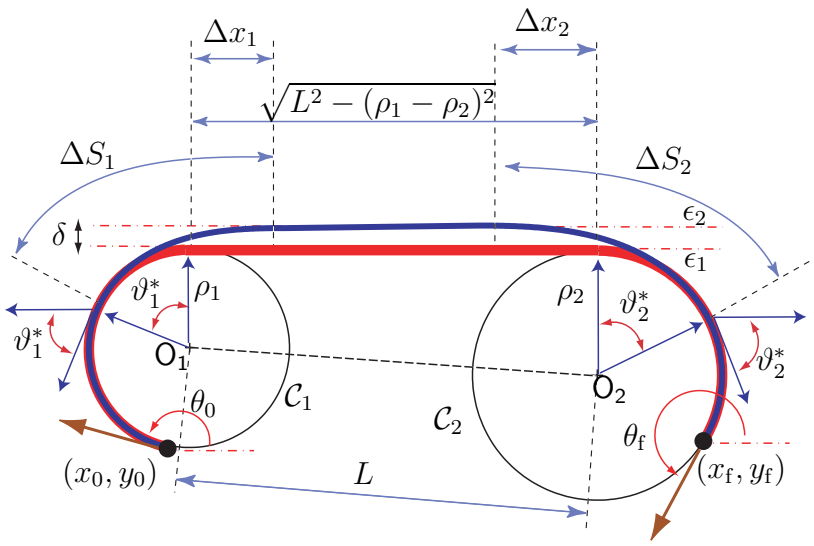

Figure 27: Total length of a composite curve that contains two pieces of clothoid.

It is important to examine how does the use of clothoids affect the length minimality of a G^2 continuous $\mathsf{C}^-\mathsf{SC}^-$ path compared with its corresponding Dubins path. In particular, equations (60) and (69) place a restriction on the minimum allowable value of the tangent angle ϑ^* as follows

$$\vartheta_i^* \geq \vartheta_{i,\min}^* = \frac{1}{2\gamma_{\max}\rho_i^2}, \quad i = 1, 2. \tag{88}$$

The constraint (18), in turn, restricts the set of initial configurations x_0 associated with $\mathcal{C}_1(\rho_1)$ and/or terminal configurations x_f associated with $\mathcal{C}_2(\rho_2)$ for which a nearly optimal, admissible $\mathsf{C}^-\mathsf{SC}^-$ path exists. Before we address this problem in more detail we need the following definition.

Definition 1. *A path from x_0 to x_f is defined as a weakly admissible $\mathsf{C}^-\mathsf{SC}^-$ path if and only if the difference between the total length of this path and the corresponding Dubins path is bounded from below by a strictly positive quantity that does not depend on neither $\vartheta_{1,\min}^*$ nor $\vartheta_{2,\min}^*$. It is defined as strongly admissible otherwise.*

Figure 28 illustrates the steering problem from $\mathsf{x}_0 = (x_0, y_0, \theta_0, -1/\rho_1)$ to $\mathsf{x}_\mathrm{f} = (x_\mathrm{f}, y_\mathrm{f}, \theta_\mathrm{f}, -1/\rho_2)$. We observe that if $\theta_0 \in [0, \vartheta_{1,\min}^*)$ and $\theta_\mathrm{f} \in [0, 2\pi)$, or $\theta_0 \in [0, 2\pi)$ and $\theta_\mathrm{f} \in (2\pi - \vartheta_{2,\min}^*, 2\pi)$, then x_0 and x_f can be connected by means of weakly

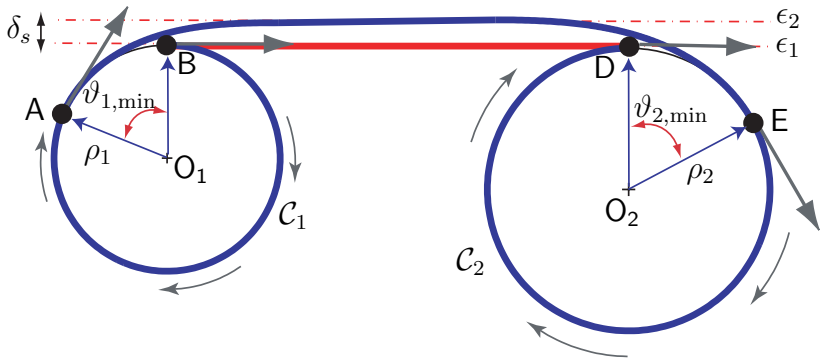

Figure 28: Boundary conditions for which the ID car satisfies the strong admissibility condition may correspond to configurations for which the strong admissibility condition is not satisfied, when the derivative of the curvature is also bounded.

admissible $\mathsf{C}^{-}\mathsf{SC}^{-}$ paths only. However, there always exists a strongly admissible $\mathsf{C}^{-}\mathsf{SC}^{-}$ path if $\theta_0 \in [\vartheta^*_{1,\min}, 2\pi)$ and $\theta_{\mathrm{f}} \in (0, 2\pi - \vartheta^*_{2,\min}]$. It is possible that a set of boundary conditions that cannot be connected by a strongly admissible $\mathsf{C}^{-}\mathsf{SC}^{-}$ path may admit, for example, a strongly admissible $\mathsf{C}^{-}\mathsf{C}^{+}\mathsf{C}^{-}$ path.

Remark 8 We observe that both the strong admissibility property would have been satisfied by all configurations associated with $\mathcal{C}_1$ and $\mathcal{C}_2$ respectively, if the vehicle was allowed to move backwards. Ref. [178] introduces a strong topological property known as topological admissibility, which is similar to the admissibility notion introduced earlier. In particular, a system satisfies the topological property presented in [178] if it can reach a final configuration within an arbitrarily small neighborhood of its initial configuration such that its ensuing path lies completely in the same neighborhood. In our case, we have seen that this topological admissibility property is not satisfied.

The previous observations reveal the intrinsic difficulties associated with the curvature-constrained, shortest path problem when one takes into account a constraint over the curvature derivative for a vehicle allowed to move only forward. Next, we compare the total length of a Dubins path and the corresponding G^2 continuous path in case the latter path is strongly admissible.

5.5 Comparison of Strongly Admissible G^2 Continuous Paths and the Corresponding Dubins Paths

A question that naturally rises from the previous analysis is how suboptimal, in terms of total length, is each of the G^2 continuous paths that we introduced in Section 5.3, compared to the corresponding minimum-length Dubins path, in case the G^2 continuous path is strongly admissible. For the $\mathsf{C}^-\mathsf{SC}^-$ paths, and with the aid of Fig. 27, we can easily show that

$$S = \rho_1\theta_0 + \rho_2(2\pi - \theta_\mathrm{f}) + \sqrt{L^2 - (\rho_1 - \rho_2)^2}, \tag{89}$$

$$S' = S + \rho_1\vartheta_1^* + \rho_2\vartheta_2^* - \frac{1}{2}\sum_{i=1}^{2}\rho_i\sqrt{\vartheta_i^*}\int_0^{\vartheta_i^*}\frac{\sin u}{u^{\frac{3}{2}}}\mathrm{d}u. \tag{90}$$

where S and S' denote the total length of the Dubins path and the corresponding composite G^2 continuous path, respectively.

Next we investigate whether a Dubins curve $c^* = \mathsf{C}^-\mathsf{SC}^-(\rho,\rho)$ can be approximated by a sequence of G^2 continuous maneuvers $\mathsf{C}^-\mathsf{SC}^-(\rho,\vartheta_1^*,\rho,\vartheta_2^*,\delta_s)$. We assume that the boundary conditions of the steering problem in hand satisfy the strong admissibility condition presented in Section 5.4. Note that for $\rho_1 = \rho_2 = \rho$ and for given δ_s, equations (69)-(70) imply that $\sigma_1 = \sigma_2 = \sigma$ and $\vartheta_1^* = \vartheta_2^* = \vartheta^*$. Thus, the two pieces of the clothoids $\mathcal{K}_1$ and $\mathcal{K}_2$ differ in terms of plane isometries.

Furthermore, Proposition 21 implies that given the distance L between $\mathcal{C}_1$ and $\mathcal{C}_2$ the *no cusp* condition places a restriction over the maximum allowable value of ϑ^*, i.e., $\vartheta^* \leq \vartheta^*_{\max}$ where $\vartheta^*_{\max} \in (0,\pi/2)$, which in conjunction with the constraint over the curvature derivative (inequality (88)) of the path characterize the set of admissible values of ϑ^*. This set uniquely characterizes, via equation (70), the set of admissible values for the geometric, design parameter δ_s of the $\mathsf{C}^-\mathsf{SC}^-$ path. In particular,

$$0 < \delta_{s,\min} < \delta_s < \delta_{s,\max} < \rho_1\left(\frac{\sqrt{2\pi}}{2}\int_0^{\pi/2}\frac{\sin u}{\sqrt{u}}\mathrm{d}u - 1\right),$$

where $\delta_{s,j} = f(\vartheta_j^*),\ j \in \{\min,\max\}$ and the function f is defined as in Proposition 2.

Consider the sequence

$$\left\{\delta_s^0, \delta_s^1, \dots\right\} \in (\delta_{\min}, \delta_{\max})$$

and the corresponding sequence

$$\{\vartheta_0^*, \vartheta_1^*, \dots\} \in (\vartheta_{\min}^*, \vartheta_{\max}^*)\,,$$

where, for each $n \in \{0, 1, \dots\}$, the terms ϑ_n^*, δ_s^n of the two sequences are uniquely related by equation (70).

Proposition 22. *The sequence $\{\delta_s^0, \delta_s^1, \dots\}$ is non-increasing if and only if the corresponding sequence $\{\vartheta_0^*, \vartheta_1^*, \dots\} \subset (0, \pi/2)$ is non-increasing.*

Proof. Let us consider the function $f : [0, \pi/2) \mapsto \mathbb{R}$ with

$$f(\vartheta^*) = \rho\left(\sqrt{\vartheta^*}\int_0^{\vartheta^*} \frac{\sin u}{\sqrt{u}}\mathrm{d}u + \cos\vartheta^* - 1\right). \tag{91}$$

The function f is monotonically increasing given that $f'(\vartheta^*) > 0$ for all $\vartheta^* \in [0, \pi/2)$. Because $f(0) = 0$ it follows that $f(\vartheta^*) > 0$ for all $\vartheta^* \in [0, \pi/2)$. Furthermore, the function f is injective. Thus, the inverse function $f^{-1} : (0, +\infty) \mapsto (0, \pi/2)$ is monotonically increasing as well.

Let us now assume that the sequence $\{\delta_s^0, \delta_s^1, \dots\}$ is non-increasing. Because f^{-1} is monotonically increasing, it follows that

$$\delta_s^{n-1} \geq \delta_s^n \Rightarrow f^{-1}(\delta_s^{n-1}) \geq f^{-1}(\delta_s^n) \tag{92}$$

or, equivalently, $\vartheta_{n-1}^* \geq \vartheta_n^*$. The converse is proved similarly. □

In order to investigate the relation between the G^2 continuous maneuvers with the corresponding Dubins paths, let us relax the constraint on the maximum allowable curvature gradient by letting $\delta_{s,\min} = \vartheta_{\min} = 0$.

Proposition 23. *Let the sequence $\{\delta_s^0, \delta_s^1, \dots\} \subset (0, \delta_{\max})$ be non-increasing and let the corresponding sequence $\{\vartheta_0^*, \vartheta_1^*, \dots\} \in (0, \theta_{\max})$. Then $\lim_{n\to\infty} \delta_s^n = 0$ if and only if $\lim_{n\to\infty} \vartheta_n^* = 0$.*

Proof. The sequences of real numbers $\{\delta_s^0, \delta_s^1, \dots\}$ and $\{\vartheta_0^*, \vartheta_1^*, \dots\}$ are both bounded from below by zero and furthermore, by virtue of Proposition 22, they are both non-increasing. Thus, in light of the monotone convergence theorem, it follows that $\{\delta_s^0, \delta_s^1, \dots\}$ and $\{\vartheta_0^*, \vartheta_1^*, \dots\}$ are convergent sequences in $[0, +\infty)$. Let us assume that $\lim_{n\to\infty} \vartheta_n^* = 0$. Then, by virtue of equation (70), we take that $\lim_{n\to\infty} \delta_s^n = 0$.

Vice versa, we assume that $\lim_{n\to\infty} \delta_s^n = 0$. We suppose on the contrary that $\lim_{n\to\infty} \vartheta_n^* = \vartheta^* > 0$. It follows by equation (70) that $\lim_{n\to\infty} \delta_s^n = f(\vartheta^*)$. However, as we have shown in Proposition 22 $\vartheta^* > 0$, which implies that $f(\theta^*) > 0$. Therefore, $0 < f(\vartheta^*) = \lim_{n\to\infty} \delta_s^n$. This is absurd since by hypothesis the sequence $\{\delta_s^0, \delta_s^1, \dots\}$ converges to zero. Thus, we conclude that $\lim_{n\to\infty} \vartheta_n^* = 0$. □

Given $\rho > 0$ the sequence $\{\delta_s^0, \delta_s^1, \dots\}$ induces through equations (69)-(70) a sequence of G^2 continuous curves $\{c_0, c_1, \dots\}$, where $c_n = \mathsf{C}^-\mathsf{SC}^-(\rho, \vartheta_n^*, \rho, \vartheta_n^*, \delta_s)$.

Proposition 24. *Let $\{\delta_s^0, \delta_s^1, \dots\}$ be a non-increasing sequence in $(0, \infty)$ with*

$$\lim_{n\to\infty} \delta_s^n = 0.$$

The sequence of G^2 continuous, strongly admissible curves $\{c_0, c_1, \dots\}$, converges uniformly to the Dubins curve $c^* = \mathsf{C}^-\mathsf{SC}^-(\rho_{\min}, \rho_{\min})$.

Proof. Let $d(z, y) = \sup_{\mathcal{I}} \big|||z(t)|| - ||y(t)|||\big|$ be the metric function of the space $G^2(\mathcal{I})$ that is induced by the uniform norm. We have that

$$\sup_{\mathcal{I}_x} \big|||c_n(x)|| - ||c^*(x)|||\big| = \delta_s^n, \tag{93}$$

where $\mathcal{I}_x$ is the subinterval of the real line that corresponds to the projection of the Dubins curve to the x-axis. It follows that $d(c_n, c^*) = \delta_s^n$. Therefore, $\lim_{n\to\infty} d(c_n, c^*) = 0$. □

Thus, by constructing a non-increasing sequence $\{\delta_s^0, \delta_s^1, \dots\}$, we can always approximate the Dubins curve $c^* = \mathsf{C}^-\mathsf{SC}^-(\rho, \rho)$ by a sequence of G^2 continuous curves

$\{c_0, c_1, \dots\}$. The rate of convergence of $\{c_0, c_1, \dots\}$ to the Dubins curve is exactly the rate of convergence of the sequence $\{\delta_s^0, \delta_s^1, \dots\}$ to zero. The situation is depicted Fig. 29.

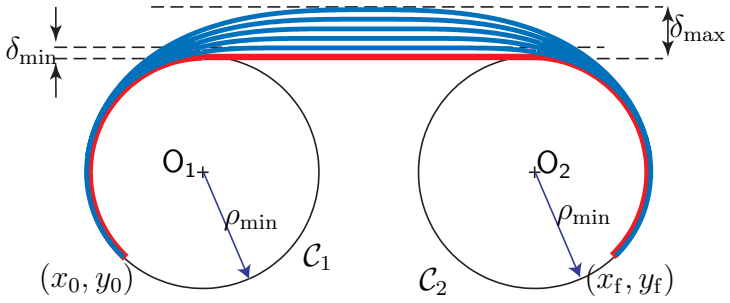

Figure 29: Approximating a Dubins path by a sequence of G^2 continuous curves.

Furthermore, owing to the fact the Dubins curve does not belong to the space of G^2 continuous curves we claim that the space of G^2 continuous curves is not complete.

Corollary 1. *The metric space $G^2(\mathcal{I})$ equipped with the uniform norm is not complete.*

Proof. The proof is a direct consequence of Proposition 24. □

Equation (90) gives the total length of each curve in $\{c_0, c_1, \dots\}$. In particular,

$$S'_n - S = 2\rho\vartheta_n^* + \rho\sqrt{\vartheta_n^*}\int_0^{\vartheta_n^*} \frac{\sin u}{u^{\frac{3}{2}}}\mathrm{d}u, \quad n = 0, 1, \dots \tag{94}$$

We claim that the sequence $\{S'_0, S'_1, \dots\}$ converges to L. Furthermore, we use trigonometric inequalities in order to obtain information on the rate of the convergence.

Proposition 25. *The sequence $\{S'_0, S'_1, \dots\}$ converges to L. Furthermore, $m(\vartheta_N^*) \leq S'_N - L \leq M(\vartheta_N^*)$, where*

$$m(\vartheta_N^*) = 4\rho\vartheta_N^* + \rho\left(\vartheta_N^* - \frac{(\vartheta_N^*)^3}{5}\right) \tag{95}$$

$$M(\vartheta_N^*) = 4\rho\vartheta_N^* + \rho\left(\vartheta_N^* + \frac{(\vartheta_N^*)^3}{6}\right). \tag{96}$$

Proof. For any $N \in \{0, 1, \dots\}$ it follows by (94) and Proposition 1 that

$$m(\vartheta_N^*) \leq S'_N - S^* \leq M(\vartheta_N^*). \tag{97}$$

Finally, as $N \to \infty$ both $m(\vartheta_N^*)$ and $M(\vartheta_N^*)$ go to zero. Thus,

$$\lim_{n \to \infty} S'_n = L. \tag{98}$$

□

Proposition 25 implies that for large values of ϑ_N^*, or equivalently, of δ_s^N, the relative error between the total length of c_N and the Dubins curve c^* increases rapidly. This observation is illustrated in Fig. 30(a). Furthermore, we observe in Fig. 30(a) that, on the one hand, the total length of c_N approaches to the optimal value when the ratio ρ/L is small. On the other hand, the constraint on the maximum allowable derivative of curvature becomes less stringent as the values of δ_s and the ratio ρ/L increase as is illustrated in Fig. 30(b).

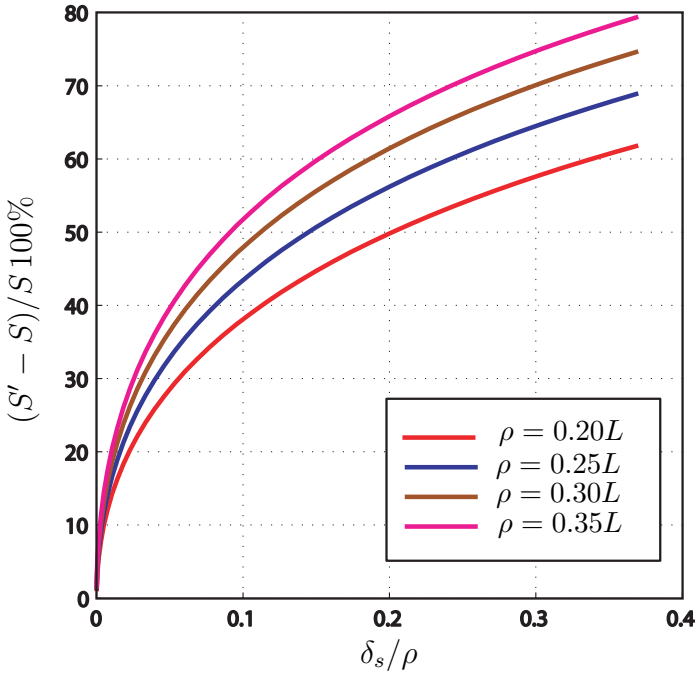

(a) Relative error of the total length between the G^2 continuous curve c_N and the corresponding Dubins path versus δ_s^N/ρ.

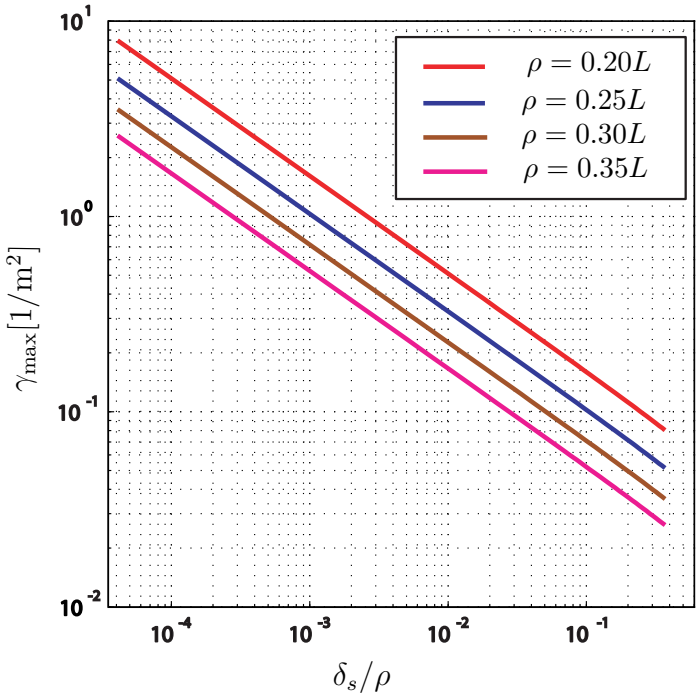

(b) Maximum allowable curvature gradient $\gamma_{\max}$ versus δ_s^N/ρ_j.

Figure 30: Plots of the total length error between the G^2 continuous curve c_N and the corresponding Dubins path and the maximum curvature derivative of c_N versus δ_s^N/ρ.

CHAPTER VI

FEEDBACK NAVIGATION IN AN UNCERTAIN FLOW FIELD

The material presented in this chapter builds upon the results presented in [16].

6.1 Introduction

In this chapter, we address a variation of the classical Zermelo's Navigation Problem [210] (ZNP for short), which seeks a navigation law to steer an aerial / marine vehicle, whose motion is described by single integrator kinematics, to a prescribed destination in the presence of drift in minimum time. In contrast to the solution of the classical ZNP, which yields non-causal/anticipative controllers that require, in general, global and perfect knowledge of the drift field, the objective of this chapter is to present instead causal/non-anticipative steering laws that require only partial and local knowledge of the drift field; consequently, these navigation laws are robust to uncertainties arising from incomplete information about the local drift field dynamics. In particular, three cases are considered: (a) the agent has perfect and reliable knowledge of the local drift; (b) the knowledge of the local drift field is imperfect; and (c) the local drift field is completely unknown. With the proposed navigation schemes, useful insights can be gleaned for a large spectrum of applications, ranging from path planning, vehicle routing, to motion coordination for, say, environmental monitoring or surveillance and reconnaissance missions in the presence of drift, thus extending the available results in the literature, which typically deal with cases when the drift is either a priori known or completely ignored [149, 52, 145, 47, 94, 131, 12, 191].

6.2 Formulation of the Navigation Problem

Consider an agent whose kinematics are described by

$$\dot{\mathsf{x}} = u + w(\mathsf{x}) + \Delta w(t, \mathsf{x}), \qquad \mathsf{x}(0) = \mathsf{x}_0, \tag{99}$$

where $\mathsf{x} := [x,\ y]^\mathsf{T} \in \mathbb{R}^2$ and $\mathsf{x}_0 := [x_0,\ y_0]^\mathsf{T} \in \mathbb{R}^2$ denote the position vector of the agent at time t and $t = 0$, respectively, and u is the control input (velocity vector) of the agent. It is assumed that $u \in \mathcal{U}$, where $\mathcal{U}$ consists of all piece-wise continuous functions taking values in the set $U = \{u \in \mathbb{R}^2 : |u| \leq \bar{u}\}$, where $\bar{u}$ is a positive constant (maximum allowable forward speed), and $|\cdot|$ denotes the standard Euclidean vector norm. Furthermore, $w(\mathsf{x}) + \Delta w(t, \mathsf{x})$ is the drift induced by the winds/currents in the vicinity of the agent. In particular, $w(\mathsf{x})$ denotes the component of the local drift that is perfectly known to the agent, and which is assumed to be at least C^1 in the domain of interest. The term $\Delta w(t, \mathsf{x})$ denotes the unknown component of the drift and is assumed to be a piece-wise continuous function of time t, and C^1 with respect to the agent's position x. Furthermore, it is assumed that there exist $\bar{w} > 0$ and $\Delta\bar{w} > 0$ such that

$$|w(\mathsf{x})| \leq \bar{w}, \qquad |\Delta w(t, \mathsf{x})| \leq \Delta\bar{w}, \qquad \text{for all } \ t \geq 0 \text{ and } \mathsf{x} \in \mathbb{R}^2. \tag{100}$$

6.2.1 Formulation of the Minimum-Time Navigation Problem

First, the classical Zermelo Navigation Problem (ZNP) [210] is revisited. The ZNP deals with the characterization of a navigation law to steer an agent, whose kinematics are described by Equation (99), to a prescribed destination in minimum time, in the special case when the drift is perfectly known, that is, when $\Delta w(t, \mathsf{x}) \equiv 0$ (deterministic minimum-time problem).

Problem 5 (ZNP)**.** *Let the system described by Equation* (99) *with* $\Delta w(t, \mathsf{x}) \equiv 0$*. Determine a control input* $u_* \in \mathcal{U}$ *such that*

i) The trajectory $\mathsf{x}_* : [0, \mathrm{T_f}] \mapsto \mathbb{R}^2$ *generated by the control* u_* *satisfies the boundary conditions*

$$\mathsf{x}_*(0) = \mathsf{x}_0, \qquad \mathsf{x}_*(\mathrm{T_f}) = 0. \tag{101}$$

ii) The control u_* *minimizes, along the trajectory* x_**, the cost functional* $J(u) := \mathrm{T_f}$*, where* $0 \leq \mathrm{T_f} < \infty$ *is the free final time.*

It can be shown that the control law that solves Problem 5 has necessarily the following structure:

$$u_* = \bar{u}[\cos\theta_*, \ \sin\theta_*]^\mathsf{T}, \tag{102}$$

where θ_* satisfies the following differential equation, known as the *navigation formula* (for more details, see, for example, [50])

$$\dot{\theta}_* = \nu_x(\mathsf{x}_*)\sin^2\theta_* - \mu_y(\mathsf{x}_*)\cos^2\theta_* + (\mu_x(\mathsf{x}_*) - \nu_y(\mathsf{x}_*))\cos\theta_*\sin\theta_*, \tag{103}$$

where $w := [\mu, \ \nu]^\mathsf{T}$ and $\mu_x := \partial\mu/\partial x$, $\mu_y := \partial\mu/\partial y$, $\nu_x := \partial\nu/\partial x$, and $\nu_y := \partial\nu/\partial y$. It follows that the candidate optimal control u_* is determined up to a single parameter, namely $\bar{\theta} = \theta_*(0) \in [0, 2\pi)$, from Equations (102)-(103). One immediately observes that a candidate optimal control of the ZNP depends explicitly on the current position vector x_*, as well as both the drift w and its Jacobian matrix $\partial w/\partial\mathsf{x}$, through the navigation formula (103). Therefore, the ZNP cannot be solved in practice, unless the agent has a priori perfect and global knowledge of the drift vector field $w(\mathsf{x})$, in which case the ZNP can be addressed as a standard, deterministic two-point boundary value minimum-time problem. The objective of this chapter is to present feedback navigation laws that require information about the drift field only in the vicinity of the agent, and which are completely independent of the Jacobian of the drift field (navigation with local information).

6.2.2 Formulation of the Navigation Problem with Local Information

Next, the problem of characterizing feedback navigation laws for different information patterns regarding the drift in the vicinity of the agent is considered. To this end, let the kinematics of the agent be described by Equation (99) as before, but with the distinctive difference that $u(\mathsf{x})$ is a state feedback control law. In particular, it is assumed that $u \in \mathcal{U}_f$, where $\mathcal{U}_f := \{f \in \mathrm{LC}(\mathbb{R}^2\backslash\{0\}) : \ f(\mathsf{x}) \in U, \text{ for all } \mathsf{x} \neq 0\}$, and where $\mathrm{LC}(\mathbb{R}^2\backslash\{0\})$ denotes the set of all locally Lipschitz continuous functions on $\mathbb{R}^2\backslash\{0\}$. Different information patterns regarding the drift in the vicinity of the agent are considered, namely,

i) the drift is perfectly known only in the vicinity of the agent, that is, $w(\mathsf{x}) \not\equiv 0$, and $\Delta w(t, \mathsf{x}) \equiv 0$,

ii) the drift is not known perfectly, that is, $w(\mathsf{x}) \not\equiv 0$, and $\Delta w(t, \mathsf{x}) \not\equiv 0$,

iii) the drift is completely unknown, that is, $w(\mathsf{x}) \equiv 0$, and $\Delta w(t, \mathsf{x}) \not\equiv 0$.

Next, the navigation problem, when the drift field is only locally known, is formulated.

Problem 6. *Let the system described by Equation* (99)*, where, at every instant of time t, only the local drift field $w(\mathsf{x})$ is known. Given $\varepsilon > 0$, determine a control input $u \in \mathcal{U}_f$ such that the trajectory $\mathsf{x} : [0, \mathrm{T_f}] \mapsto \mathbb{R}^2$ generated by the control u satisfies, for every $|\mathsf{x}_0| > \varepsilon$, the boundary conditions*

$$\mathsf{x}(0) = \mathsf{x}_0, \qquad |\mathsf{x}(\mathrm{T_f})| \leq \varepsilon, \tag{104}$$

for some $0 \leq \mathrm{T_f} < \infty$.

One of the differences between Problem 5 and Problem 6 is that in the formulation of the latter, the requirement that the agent should exactly reach its destination has been relaxed. Instead, in Problem 6, and in order to account for the possibility of imperfect knowledge of the local drift field, it is only required that the agent reaches a

ball of radius ε centered at $\mathsf{x} = 0$. Furthermore, the control law that solves Problem 6 has been restricted to the class of (time invariant) state feedback control laws.

6.2.3 The Navigation Problem as a Problem of Pursuit of a Maneuvering Target

Next, the interpretation of the navigation Problem 6 as a problem of pursuit of a maneuvering target is discussed. To this end, consider a pursuer and a moving target whose kinematics are described by the following set of equations

$$\dot{\mathsf{x}}_{\mathcal{P}} = u_{\mathcal{P}}(\mathsf{x}_{\mathcal{P}}, \mathsf{x}_{\mathcal{T}}), \qquad \mathsf{x}_{\mathcal{P}}(0) = \mathsf{x}_0, \tag{105}$$

$$\dot{\mathsf{x}}_{\mathcal{T}} = -w(\mathsf{x}_{\mathcal{P}}, \mathsf{x}_{\mathcal{T}}) - \Delta w(t, \mathsf{x}_{\mathcal{P}}, \mathsf{x}_{\mathcal{T}}), \qquad \mathsf{x}_{\mathcal{T}}(0) = 0, \tag{106}$$

where $\mathsf{x}_{\mathcal{P}} := [x_{\mathcal{P}},\ y_{\mathcal{P}}]^{\mathsf{T}} \in \mathbb{R}^2$, and $\mathsf{x}_{\mathcal{T}} := [x_{\mathcal{T}},\ y_{\mathcal{T}}]^{\mathsf{T}} \in \mathbb{R}^2$ are the position vectors of the pursuer and the moving target at time t, respectively. In addition, $u_{\mathcal{P}} \in \mathcal{U}_{\mathcal{P},f}$, where $\mathcal{U}_{\mathcal{P},f} := \{f \in \mathrm{LC}(\mathbb{R}^4 \backslash \mathcal{M}) :\ f(\mathsf{x}) \in U,\ \text{for all } \mathsf{x} \notin \mathcal{M}\}$, and $\mathcal{M} = \{(\mathsf{x}_{\mathcal{P}}, \mathsf{x}_{\mathcal{T}}) \in \mathbb{R}^4 :\ \mathsf{x}_{\mathcal{P}} = \mathsf{x}_{\mathcal{T}}\}$. Furthermore, $-w(\mathsf{x}_{\mathcal{P}}, \mathsf{x}_{\mathcal{T}}) - \Delta w(t, \mathsf{x}_{\mathcal{P}}, \mathsf{x}_{\mathcal{T}})$ is the target's velocity, where $w(\mathsf{x}_{\mathcal{P}}, \mathsf{x}_{\mathcal{T}})$ (the known component of the instantaneous target's velocity) and $\Delta w(t, \mathsf{x}_{\mathcal{P}}, \mathsf{x}_{\mathcal{T}})$ (the unknown component of the instantaneous target's velocity) satisfy the same regularity conditions as in the formulation of the ZNP. Next, a problem of pursuit of a maneuvering target, which, as it is shown later, turns out to be equivalent to Problem 6, is presented.

Problem 7. *Let the kinematics of a pursuer and a moving target be described by Equations* (105) *and* (106)*, respectively, and assume that, at each instant of time, the pursuer has only knowledge of* $-w(\mathsf{x})$*. Given* $\varepsilon > 0$*, find a control law* $u_{\mathcal{P}} \in \mathcal{U}_{\mathcal{P},f}$*, such that the trajectories* $\mathsf{x}_{\mathcal{P}}(\cdot; u_{\mathcal{P}})$ *and* $\mathsf{x}_{\mathcal{T}}(\cdot; -w - \Delta w)$ *generated by* $u_{\mathcal{P}}$ *and* $-w - \Delta w$*, respectively, satisfy, for all* $|\mathsf{x}_0| > \varepsilon$*, the boundary conditions*

$$\mathsf{x}_{\mathcal{P}}(0) = \mathsf{x}_0, \qquad \mathsf{x}_{\mathcal{T}}(0) = 0, \qquad |\mathsf{x}_{\mathcal{P}}(\mathrm{T_f}; u_{\mathcal{P}}) - \mathsf{x}_{\mathcal{T}}(\mathrm{T_f}; -w - \Delta w)| \leq \varepsilon, \tag{107}$$

for some $0 \leq \mathrm{T_f} < \infty$.

Let one consider the special case when $u_{\mathcal{P}}(\mathsf{x}_{\mathcal{P}}, \mathsf{x}_{\mathcal{T}}) = u_{\mathcal{P}}(\mathsf{x}_{\mathcal{P}} - \mathsf{x}_{\mathcal{T}})$, $w(\mathsf{x}_{\mathcal{P}}, \mathsf{x}_{\mathcal{T}}) = w(\mathsf{x}_{\mathcal{P}} - \mathsf{x}_{\mathcal{T}})$, $\Delta w(t, \mathsf{x}_{\mathcal{P}}, \mathsf{x}_{\mathcal{T}}) = \Delta w(t, \mathsf{x}_{\mathcal{P}} - \mathsf{x}_{\mathcal{T}})$. By taking $\mathsf{x} = \mathsf{x}_{\mathcal{P}} - \mathsf{x}_{\mathcal{T}}$ and $u = u_{\mathcal{P}}$, it is easy to see that

$$\begin{aligned} \dot{\mathsf{x}} &= u_{\mathcal{P}}(\mathsf{x}_{\mathcal{P}} - \mathsf{x}_{\mathcal{T}}) + w(\mathsf{x}_{\mathcal{P}} - \mathsf{x}_{\mathcal{T}}) + \Delta w(t, \mathsf{x}_{\mathcal{P}} - \mathsf{x}_{\mathcal{T}}) \\ &= u(\mathsf{x}) + w(\mathsf{x}) + \Delta w(t, \mathsf{x}). \end{aligned} \tag{108}$$

Furthermore, $\mathsf{x}(0) = \mathsf{x}_{\mathcal{P}}(0) - \mathsf{x}_{\mathcal{T}}(0) = \mathsf{x}_0$, and $|\mathsf{x}(\mathrm{T_f})| = |\mathsf{x}_{\mathcal{P}}(\mathrm{T_f}; u_{\mathcal{P}}) - \mathsf{x}_{\mathcal{T}}(\mathrm{T_f}; -w - \Delta w)| \leq \varepsilon$. Therefore, a navigation law u that solves Problem 6 is also a pursuit law $u_{\mathcal{P}}$ that solves Problem 7, and vice versa. This correspondence between Problem 6 and Problem 7 is an illustration of the duality between the ZNP and the problem of pursuit of a maneuvering target, in the special case when both the motions of the pursuer and the target are described by single integrator kinematics, and, in addition, their strategies are functions of their relative positions with respect to each other. By making use of this duality between the navigation and the pursuit problems, navigation laws that are dual to well-known pursuit strategies are proposed in the next section. Furthermore, the equivalence of some intuitive solutions to the navigation problem with standard pursuit strategies is established.

6.3 Navigation with Perfect Local Drift Information

First, a class of feedback laws solving Problem 6, when the agent has perfect knowledge of the local drift, that is, when $\Delta w(t, \mathsf{x}) \equiv 0$, is considered. Before proceeding with the presentation of this class of navigation laws, a few geometric concepts that shall be extensively used throughout this chapter are introduced. In particular, it is assumed that a moving frame $(\mathsf{e}^1_{\mathsf{x}}, \mathsf{e}^2_{\mathsf{x}})$ is attached to the current position of the agent x, where $\mathsf{e}^1_{\mathsf{x}} := -\mathsf{x}/|\mathsf{x}|$, and $\mathsf{e}^2_{\mathsf{x}} := \mathbf{S}\mathsf{e}^1_{\mathsf{x}}$, for all $\mathsf{x} \in \mathbb{R}^2 \backslash \{0\}$, and where $\mathbf{S} := \left[\begin{smallmatrix} 0 & -1 \\ 1 & 0 \end{smallmatrix}\right]$. Note that $\mathsf{e}^1_{\mathsf{x}}$ is the unit vector parallel to the direction towards its destination (origin) as observed by the agent, whereas $\mathsf{e}^2_{\mathsf{x}}$ is the unit vector perpendicular to $\mathsf{e}^1_{\mathsf{x}}$. The ray emanating from the agent's current position parallel to $\mathsf{e}^1_{\mathsf{x}}$ is henceforth referred to as the

line-of-sight (LoS), and it will be denoted by $\ell_{\mathrm{LS}}(\mathsf{x}) := \{\mathsf{z} \in \mathbb{R}^2 : \ \mathsf{z} = \rho\mathsf{x}, \ \rho \in [0,1]\}$. After some algebraic manipulations, one can show that

$$\dot{\mathsf{e}}_{\mathsf{x}}^1 = -\frac{\langle \dot{\mathsf{x}}, \mathsf{e}_{\mathsf{x}}^2 \rangle}{|\mathsf{x}|}\mathsf{e}_{\mathsf{x}}^2, \qquad \dot{\mathsf{e}}_{\mathsf{x}}^2 = \frac{\langle \dot{\mathsf{x}}, \mathsf{e}_{\mathsf{x}}^2 \rangle}{|\mathsf{x}|}\mathsf{e}_{\mathsf{x}}^1. \tag{109}$$

Furthermore, let λ denote the angle of the LoS measured with respect to some fixed reference direction, as illustrated in Fig. 31. It follows readily from (109) that the rate of change of λ is given by

$$\dot{\lambda}(\mathsf{x}) = -\frac{\langle \dot{\mathsf{x}}, \mathsf{e}_{\mathsf{x}}^2 \rangle}{|\mathsf{x}|}. \tag{110}$$

The following identity will be useful in the subsequent discussion,

$$2|\mathsf{x}|\frac{\mathrm{d}}{\mathrm{d}t}|\mathsf{x}| = \frac{\mathrm{d}}{\mathrm{d}t}|\mathsf{x}|^2 = \frac{\mathrm{d}}{\mathrm{d}t}\langle \mathsf{x}, \mathsf{x} \rangle = 2\langle \dot{\mathsf{x}}, \mathsf{x} \rangle, \tag{111}$$

which implies that

$$\frac{\mathrm{d}}{\mathrm{d}t}|\mathsf{x}| = \frac{\langle \dot{\mathsf{x}}, \mathsf{x} \rangle}{|\mathsf{x}|} = -\langle \dot{\mathsf{x}}, \mathsf{e}_{\mathsf{x}}^1 \rangle, \quad \text{for all} \ \ \mathsf{x} \in \mathbb{R}^2 \backslash \{0\}. \tag{112}$$

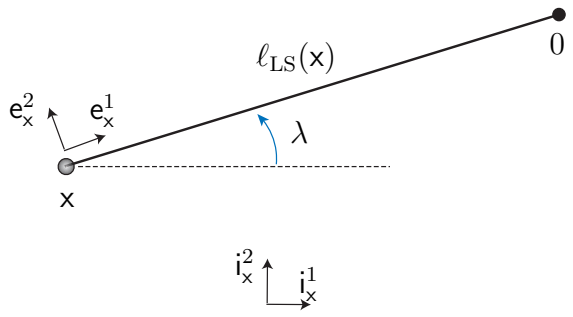

Figure 31: Global and local frames of reference.

6.3.1 Line-of-Sight Feedback Navigation Laws

In this section, a class of feedback navigation laws that steer the agent to its destination such that the agent remains at all times on $\ell_{\mathrm{LS}}(\mathsf{x}_0)$ is presented. In particular,

two different navigation laws, which constraint the agent to travel along the LoS by canceling the component of the drift perpendicular to $\mathsf{e}^1_{\mathsf{x}_0}$, are considered.

The first navigation law steers the agent towards its destination while the latter maintains, at all times, maximum forward speed $\bar{u}$ as the agent travels along $\ell_{\mathrm{LS}}(\mathsf{x}_0)$. The situation is illustrated in Fig. 32(a). This navigation law will be henceforth referred to as the optimal line-of-sight (OLoS) navigation, since among all navigation laws that steer the agent along the original LoS, it is the one that point-wise maximizes the speed along the ensuing path. The analytic expression of this feedback law is given by

$$\begin{aligned} u_{\mathrm{OLS}}(\mathsf{x}) &= u_{\mathrm{OLS},1}(\mathsf{x})\mathsf{e}^1_{\mathsf{x}_0} + u_{\mathrm{OLS},2}(\mathsf{x})\mathsf{e}^2_{\mathsf{x}_0}, \\ u_{\mathrm{OLS},1}(\mathsf{x}) &:= \sqrt{\bar{u}^2 - \langle w(\mathsf{x}), \mathsf{e}^2_{\mathsf{x}_0}\rangle^2}, \qquad u_{\mathrm{OLS},2}(\mathsf{x}) := -\langle w(\mathsf{x}), \mathsf{e}^2_{\mathsf{x}_0}\rangle. \end{aligned} \tag{113}$$

The following proposition provides sufficient conditions for the feasibility of the navigation law (113).

Proposition 26. *Let $\varepsilon > 0$ and $\Delta w(t, \mathsf{x}) \equiv 0$. Then, for all $|\mathsf{x}_0| > \varepsilon$, the navigation law* (113) *will drive the system* (99) *to the set $\{\mathsf{x} : \ |\mathsf{x}| \leq \varepsilon\}$ in finite time, provided there exist $\bar{w}_1 > 0$ and $\bar{w}_2 > 0$ such that*

$$|\langle w(\mathsf{x}), \mathsf{e}^1_{\mathsf{x}_0}\rangle| \leq \bar{w}_1 < \sqrt{\bar{u}^2 - \bar{w}_2^2}, \tag{114}$$

$$|\langle w(\mathsf{x}), \mathsf{e}^2_{\mathsf{x}_0}\rangle| \leq \bar{w}_2 < \bar{u}, \tag{115}$$

for all $\mathsf{x} \in \ell_{\mathrm{LS}}(\mathsf{x}_0)$. Finally, the time of travel satisfies the upper bound

$$\mathrm{T_f} \leq \frac{|\mathsf{x}_0| - \varepsilon}{\sqrt{\bar{u}^2 - \bar{w}_2^2} - \bar{w}_1} < \infty. \tag{116}$$

Proof. Note that (115) guarantees that $u_{\mathrm{OLS},1}(\mathsf{x})$ is well defined along $\ell_{\mathrm{LS}}(\mathsf{x}_0)$. Furthermore, in view of (115), it follows that

$$u_{\mathrm{OLS},1}(\mathsf{x}) = \sqrt{\bar{u}^2 - \langle w(\mathsf{x}), \mathsf{e}^2_{\mathsf{x}_0}\rangle} \geq \sqrt{\bar{u}^2 - \bar{w}_2^2}. \tag{117}$$

In addition, it follows readily, after plugging (113) in (99), and in light of (114) and (117), that

$$\begin{aligned}\frac{\mathrm{d}}{\mathrm{d}t}|\mathsf{x}| &= -\langle \dot{\mathsf{x}}, \mathsf{e}^1_{\mathsf{x}_0}\rangle = -\langle u_{\mathrm{OLS}}(\mathsf{x}) + w(\mathsf{x}), \mathsf{e}^1_{\mathsf{x}_0}\rangle \\ &= -u_{\mathrm{OLS},1}(\mathsf{x}) - \langle w(\mathsf{x}), \mathsf{e}^1_{\mathsf{x}_0}\rangle \\ &\leq -\sqrt{\bar{u}^2 - \bar{w}_2^2} + \bar{w}_1. \end{aligned} \tag{118}$$

Note that (114) implies that the right-hand-side of (118) is strictly negative, and thus, the navigation law (113) will drive the system (99) to the set $\{\mathsf{x} : \ |\mathsf{x}| \leq \varepsilon\}$ in finite time, for all $|\mathsf{x}_0| > \varepsilon$. Furthermore, (116) follows after integrating both sides of (118). □

Note that Proposition 26 implies that the navigation law (113) solves Problem 6, provided the drift component perpendicular to $\mathsf{e}^1_{\mathsf{x}_0}$ can be canceled by the agent's control actions, and furthermore, the projection of the drift on $-\mathsf{e}^1_{\mathsf{x}_0}$ (opposite of the LoS direction) never dominates the forward speed of the agent. The reader should notice here that conditions (114)-(115) may hold even if $|w(\mathsf{x})| > \bar{u}$, for some $\mathsf{x} \in \ell_{\mathrm{LS}}(\mathsf{x}_0)$. Thus, the standard assumption, which is typically made in problems of pursuit of a maneuvering target, where the pursuer is assumed to have a speed advantage over the target, has been relaxed. Note that if the target is faster than the pursuer, then the former can always escape capture by simply traveling along the original LoS direction with its maximum speed. In the problem of navigation, the assumptions for the feasibility of the navigation law (113) can be relaxed given that the notional maneuvering target, whose velocity is $-w(\mathsf{x})$, may not necessarily act as an adversarial, non-cooperative opponent, in contrast to the classical pursuit problem.

Next, a second navigation law that will enforce motion of the agent along $\ell_{\mathrm{LS}}(\mathsf{x}_0)$

is introduced. The expression of this control law is given by

$$
\begin{aligned}
u_{\mathrm{NLS}}(\mathsf{x}) &:= u_{\mathrm{NLS},1}(\mathsf{x})\mathsf{e}^1_{\mathsf{x}_0} + u_{\mathrm{NLS},2}(\mathsf{x})\mathsf{e}^2_{\mathsf{x}_0}, \\
u_{\mathrm{NLS},1}(\mathsf{x}) &:= \bar{u} - |w(\mathsf{x})| - \langle w(\mathsf{x}), \mathsf{e}^1_{\mathsf{x}_0}\rangle, \qquad u_{\mathrm{NLS},2}(\mathsf{x}) := -\langle w(\mathsf{x}), \mathsf{e}^2_{\mathsf{x}_0}\rangle.
\end{aligned} \tag{119}
$$

The interpretation of navigation law (119) is as follows: The agent first completely "cancels" the effect of the drift, and subsequently allocates the remaining control authority along the original LoS. Note that the navigation law (119) can also be written as follows

$$
u_{\mathrm{NLS}}(\mathsf{x}) = -w(\mathsf{x}) + (\bar{u} - |w(\mathsf{x})|)\mathsf{e}^1_{\mathsf{x}_0}. \tag{120}
$$

The situation is illustrated in Figure 32(b). One important observation here is that $|u_{\mathrm{NLS}}(\mathsf{x})| \not\equiv \bar{u}$, for all $\mathsf{x} \in \ell_{\mathrm{LS}}(\mathsf{x}_0)$, that is, the agent may not necessarily maintain maximum forward speed along its ensuing path. This may be useful when the agent is approaching a landing/docking point (rendezvous problem), where a "smooth" final approach is more important than a fast one. Note, furthermore, that $|u_{\mathrm{NLS}}(\mathsf{x})| = \bar{u}$ only if $w(\mathsf{x}) = -|w(\mathsf{x})|\mathsf{e}^1_{\mathsf{x}_0}$, in which case, the navigation laws (113) and (119) turn out to be exactly the same. The following proposition provides a sufficient condition for the feasibility of the navigation law (119).

Proposition 27. *Let $\varepsilon > 0$ and $\Delta w(t, \mathsf{x}) \equiv 0$. Then, for all $|\mathsf{x}_0| > \varepsilon$, the navigation law* (119) *will drive the system* (99) *to the set $\{\mathsf{x} : \ |\mathsf{x}| \leq \varepsilon\}$ in finite time, provided there exists $\bar{w} > 0$ such that*

$$
|w(\mathsf{x})| \leq \bar{w} < \bar{u}, \qquad \text{for all } \ \mathsf{x} \in \ell_{\mathrm{LS}}(\mathsf{x}_0). \tag{121}
$$

Finally, the time of travel satisfies the upper bound

$$
\mathrm{T_f} \leq \frac{|\mathsf{x}_0| - \varepsilon}{\bar{u} - \bar{w}} < \infty. \tag{122}
$$

Proof. Note that (121) implies that the component of the drift $w(\mathsf{x})$ can be canceled by the agent's forward velocity. In addition, by plugging (119) in (99), and by virtue

of (121), it follows readily that

$$\begin{aligned}\frac{\mathrm{d}}{\mathrm{d}t}|\mathsf{x}| &= -\langle \dot{\mathsf{x}}, \mathsf{e}^1_{\mathsf{x}_0}\rangle = -\langle u_{\mathrm{NLS}}(\mathsf{x}) + w(\mathsf{x}), \mathsf{e}^1_{\mathsf{x}_0}\rangle \\ &= -\langle (\bar{u} - |w(\mathsf{x})|)\mathsf{e}^1_{\mathsf{x}_0}, \mathsf{e}^1_{\mathsf{x}_0}\rangle \\ &\leq -(\bar{u} - \bar{w}). \end{aligned} \tag{123}$$

The rest of the proof is similar to the proof of Proposition 26, and it is omitted. □

One of the main drawbacks of the feedback law (119), compared to (113), is that for its application it is necessary that the control authority of the agent always dominates the drift as the agent moves along the original LoS. Note that (121) is more restrictive than conditions (114)-(115). Another restriction of the navigation law (119) has to do with the fact that, as it has already been mentioned, when the agent is driven by this law, it may not maintain constant forward speed along its ensuing path. This may be an undesirable situation for several applications, say, fixed-wing UAVs, where the forward speed of the aircraft must remain, at all times, above stall speed. On the other hand, as it has already been mentioned, the navigation law (119) may be more practical than (113), when, for example, a smooth final approach is more preferable than a quick one.

It is interesting to note that the control law (119) corresponds to a pursuit strategy known as "*pursuit with neutralization*" [93]. With this strategy, the pursuer first neutralizes the action of its opponent (maneuvering target) and, subsequently, uses the remaining control authority (provided the pursuer has a speed advantage over its opponent) to diminish their relative distance.

6.3.2 Three-Point Navigation and LoS Guidance

Next, a navigation scheme that, in contrast to the navigation laws (113) and (119), does not require the forward velocity of the agent to dominate the component of the drift perpendicular to the LoS direction is presented. The proposed navigation is

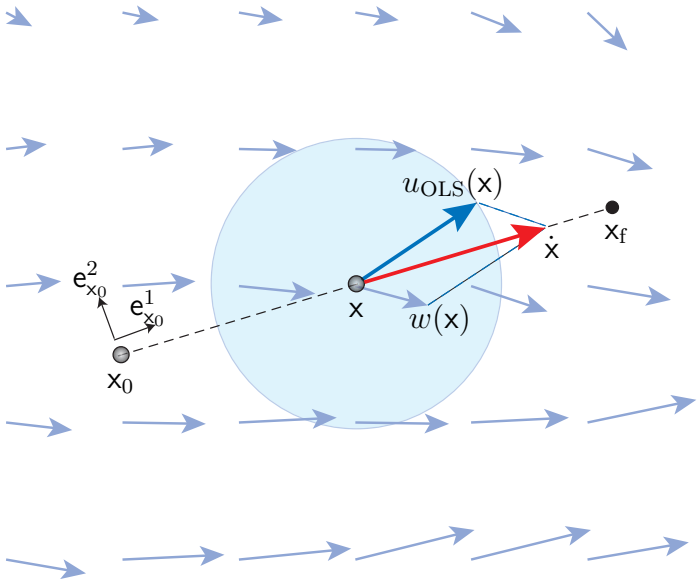

(a) Optimal LOS navigation.

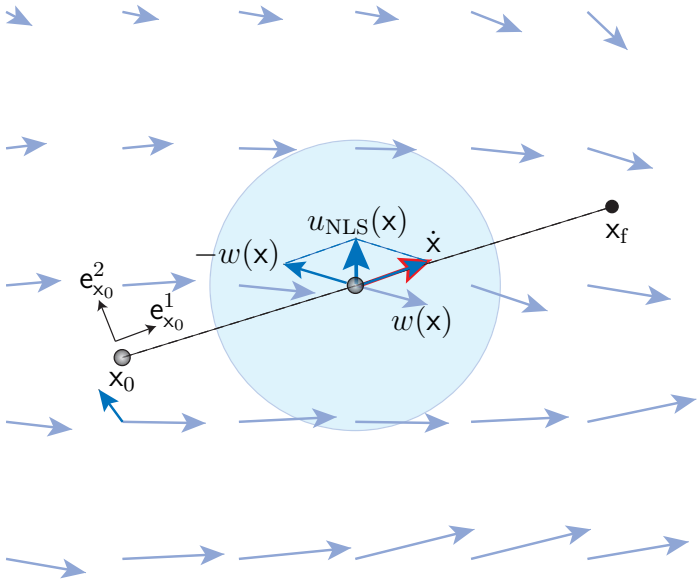

(b) LOS navigation with drift neutralization.

Figure 32: Motion along the LOS direction is achieved when the agent's forward velocity can cancel the drift component perpendicular to the LoS direction.

derived from a well-known pursuit strategy, namely the *LoS* or *three-point guidance law* [186]. It turns out that this pursuit strategy enforces the geometric constraint of motion camouflage with respect to a fixed point [192, 88], which stipulates, in turn, that the position vector of the pursuer with respect to the reference point

x_0 is, at all times, parallel to the position vector of the target with respect to the pursuer. Equivalently, the pursuer always lies on the line segment defined by the target's current position and the reference point x_0. It is worth-mentioning that the term "motion camouflage" was first coined by Srinivasan and Davey to describe an effective deception strategy adopted by various animal and insect species, where a pursuer (the *shadower*) conceals its apparent motion from an evader (the *shadowee*) by emulating the optical flow produced by a stationary point [192]. By eliminating any motion parallax, the pursuer's motion reduces the ability of the evader to accurately obtain depth information regarding its actual relative distance from the pursuer [192]. Depending on whether the distance of the fixed reference point from the pursuer is finite or infinite, one refers to "motion camouflage with respect to a fixed point" and to "motion camouflage with respect to a point at infinity," respectively. While in the former case the pursuer's strategy is to match the angular velocity of its motion with that of the target, in the latter, the pursuer's line-of-sight has a fixed direction in space.

Note that the LoS guidance law is a pursuit strategy that entails two LoS directions, namely, the direction from x_0 to $\mathsf{x}_\mathcal{P}$, and the direction from $\mathsf{x}_\mathcal{P}$ to $\mathsf{x}_\mathcal{T}$. Alternatively, the same pursuit strategy involves three points of interest, namely x_0, $\mathsf{x}_\mathcal{P}$ and $\mathsf{x}_\mathcal{T}$, which must remain collinear at all times. The situation is illustrated in Figure 33.

In this section, the applicability of the LoS guidance law to the navigation problem, when the drift field is only partially known, is examined. Let $\lambda_\mathcal{P}$ and $\lambda_\mathcal{T}$ denote, respectively, the angular positions of the pursuer and the target from x_0 with respect to some fixed reference direction, at time t. With the aid of Fig. 33, one can observe that the motion camouflage condition implies that $\dot{\lambda}_\mathcal{P} = \dot{\lambda}_\mathcal{T}$. Thus, the components of the velocity of both the target and the pursuer perpendicular to e^1_x (or $\mathsf{e}^1_{\mathsf{x}_\mathcal{P}}$) satisfy

$$\frac{\langle u_\mathcal{P}, \mathsf{e}^2_\mathsf{x}\rangle}{|\mathsf{x}_\mathcal{P} - \mathsf{x}_0|} = -\frac{\langle w(\mathsf{x}_\mathcal{P} - \mathsf{x}_\mathcal{T}), \mathsf{e}^2_\mathsf{x}\rangle}{|\mathsf{x}_\mathcal{T} - \mathsf{x}_0|} = -\frac{\langle w(\mathsf{x}), \mathsf{e}^2_\mathsf{x}\rangle}{|\mathsf{x}_\mathcal{T} - \mathsf{x}_0|} = -\frac{\langle w(\mathsf{x}), \mathsf{e}^2_\mathsf{x}\rangle}{|\mathsf{x}_\mathcal{P} - \mathsf{x}_0| + |\mathsf{x}|}, \tag{124}$$

in light of the identity

$$|\mathsf{x}_{\mathcal{T}} - \mathsf{x}_0| = |\mathsf{x}_{\mathcal{T}} - \mathsf{x}_{\mathcal{P}}| + |\mathsf{x}_{\mathcal{P}} - \mathsf{x}_0| = |\mathsf{x}| + |\mathsf{x}_{\mathcal{P}} - \mathsf{x}_0|, \tag{125}$$

which follows, in turn, from the collinearity of x_0, $\mathsf{x}_{\mathcal{P}}$ and $\mathsf{x}_{\mathcal{T}}$. Therefore,

$$\langle u_{\mathcal{P}}, \mathsf{e}^2_{\mathsf{x}} \rangle = -\frac{|\mathsf{x}_{\mathcal{P}} - \mathsf{x}_0|}{|\mathsf{x}_{\mathcal{P}} - \mathsf{x}_0| + |\mathsf{x}|} \langle w(\mathsf{x}), \mathsf{e}^2_{\mathsf{x}} \rangle, \tag{126}$$

and the expression of the pursuit strategy $u_{\mathcal{P}}$ for LoS guidance is given by

$$\begin{aligned} u_{\mathcal{P}}(\mathsf{x}, \mathsf{x}_{\mathcal{P}}) &:= u_{\mathcal{P},1}(\mathsf{x}, \mathsf{x}_{\mathcal{P}}) \mathsf{e}^1_{\mathsf{x}} + u_{\mathcal{P},2}(\mathsf{x}, \mathsf{x}_{\mathcal{P}}) \mathsf{e}^2_{\mathsf{x}}, \\ u_{\mathcal{P},1}(\mathsf{x}, \mathsf{x}_{\mathcal{P}}) &:= \sqrt{\bar{u}^2 - u^2_{\mathcal{P},2}(\mathsf{x}, \mathsf{x}_{\mathcal{P}})}, \qquad u_{\mathcal{P},2}(\mathsf{x}, \mathsf{x}_{\mathcal{P}}) := -\frac{|\mathsf{x}_{\mathcal{P}} - \mathsf{x}_0|}{|\mathsf{x}_{\mathcal{P}} - \mathsf{x}_0| + |\mathsf{x}|} \langle w(\mathsf{x}), \mathsf{e}^2_{\mathsf{x}} \rangle. \end{aligned} \tag{127}$$

Note that the pursuit strategy (127) depends explicitly on both x and $\mathsf{x}_{\mathcal{P}}$. Therefore, the control law (127) cannot be used directly as a navigation law for the system (99), since it depends on $\mathsf{x}_{\mathcal{P}}$, in addition to the current location of the agent x. Before applying the control law (127) to the navigation problem, the kinematic model described by Equation (99) needs to be dynamically extended to the following kinematic model

$$\dot{\mathsf{x}} = u_{\mathrm{TPN}}(\mathsf{x}, \mathsf{x}_{\mathcal{P}}) + w(\mathsf{x}), \qquad \mathsf{x}(0) = \mathsf{x}_0, \tag{128}$$

$$\dot{\mathsf{x}}_{\mathcal{P}} = u_{\mathrm{TPN}}(\mathsf{x}, \mathsf{x}_{\mathcal{P}}), \qquad \mathsf{x}_{\mathcal{P}}(0) = \mathsf{x}_0, \tag{129}$$

where $u_{\mathrm{TPN}}(\mathsf{x}, \mathsf{x}_{\mathcal{P}}) := u_{\mathcal{P}}(\mathsf{x}, \mathsf{x}_{\mathcal{P}})$. The control law u_{TPN} is henceforth referred to as the *three-point navigation law*.

One noteworthy observation for the three-point navigation law u_{TPN} is that the component of $u_{\mathcal{P}}$ perpendicular to the LoS direction never dominates the component of the drift along the same direction, as it follows readily from (127). Thus, in contrast to the navigation laws (113) and (119), the applicability of the control law (127) may not be limited to navigation problems where the control authority of the agent can cancel the term $\langle w(\mathsf{x}), \mathsf{e}^2_{\mathsf{x}} \rangle$.

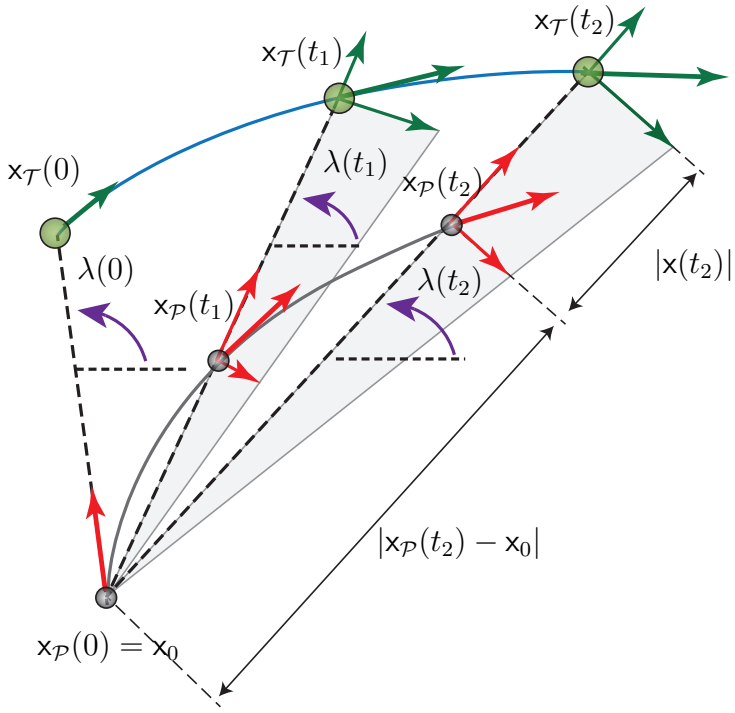

Figure 33: LoS or three-point guidance is synonymous to motion camouflage with respect to a fixed point. At all times, the rate of change of the angular positions of both the pursuer and the target from point x_0 and with respect to some fixed reference direction is exactly the same.

Proposition 28. *Let $\varepsilon > 0$ and $\Delta w(t, \mathsf{x}) \equiv 0$. Then, for all $|\mathsf{x}_0| > \varepsilon$, the navigation law (127) will drive the system (99) to the set $\{\mathsf{x} : \ |\mathsf{x}| \leq \varepsilon\}$ in finite time, provided there exist $\bar{w}_1 > 0$ and $\bar{w}_2 > 0$ such that*

$$|\langle w(\mathsf{x}), \mathsf{e}^1_{\mathsf{x}} \rangle| \leq \bar{w}_1 < \sqrt{\bar{u}^2 - \bar{w}_2^2}, \tag{130}$$

$$|\langle w(\mathsf{x}), \mathsf{e}^2_{\mathsf{x}} \rangle| \leq \bar{w}_2, \tag{131}$$

for all $\mathsf{x} \in \mathbb{R}^2 \backslash \{0\}$. Furthermore, the time of travel satisfies the upper bound

$$\mathrm{T_f} \leq \frac{|\mathsf{x}_0| - \varepsilon}{\sqrt{\bar{u}^2 - \bar{w}_2^2} - \bar{w}_1} < \infty. \tag{132}$$

Proof. It follows from (131) that

$$|u_{\mathcal{P},2}(\mathsf{x}, \mathsf{x}_{\mathcal{P}})| = \frac{|\mathsf{x}_{\mathcal{P}} - \mathsf{x}_0|}{|\mathsf{x}_{\mathcal{P}} - \mathsf{x}_0| + |\mathsf{x}|} |\langle w(\mathsf{x}), \mathsf{e}^2_{\mathsf{x}} \rangle| \leq |\langle w_{\mathcal{T}}(\mathsf{x}), \mathsf{e}^2_{\mathsf{x}} \rangle| \leq \bar{w}_2, \tag{133}$$

which implies, in turn, that $u_{\mathcal{P},1}(\mathsf{x},\mathsf{x}_{\mathcal{P}}) = \sqrt{\bar{u}^2 - u_{\mathcal{P},2}^2(\mathsf{x},\mathsf{x}_{\mathcal{P}})} \geq \sqrt{\bar{u}^2 - \bar{w}_2^2}$, for all $(\mathsf{x},\mathsf{x}_{\mathcal{P}}) \in \mathbb{R}^4 \backslash \{0\}$. Furthermore, it follows that

$$\begin{aligned}\frac{\mathrm{d}}{\mathrm{d}t}|\mathsf{x}| &= -\langle \dot{\mathsf{x}}, \mathsf{e}_{\mathsf{x}}^1 \rangle = -\langle u_{\mathrm{TPN}}(\mathsf{x}) + w(\mathsf{x}), \mathsf{e}_{\mathsf{x}}^1 \rangle \\ &= -u_{\mathcal{P},1}(\mathsf{x}_{\mathcal{P}},\mathsf{x}) - \langle w(\mathsf{x}), \mathsf{e}_{\mathsf{x}}^1 \rangle \\ &\leq -\sqrt{\bar{u}^2 - \bar{w}_2^2} + \bar{w}_1. \end{aligned} \tag{134}$$

The rest of the proof follows similarly to the proof of Proposition 26, and it is omitted.

□

6.3.3 Navigation with Local Drift Information and Pursuit with Motion Camouflage

A common theme in both the navigation laws (113) and (119) is that when the agent is driven by either of these two control laws, its direction of motion is constant and parallel to $\mathsf{e}_{\mathsf{x}_0}^1$ (the original LoS direction). The interpretation of the previous observation, within the context of the problem of pursuit of a maneuvering target, is that the relative position vector of the pursuer from the target remains, at all times, parallel to a constant vector, namely $\mathsf{e}_{\mathsf{x}_0}^1$. Equivalently, the relative angular position of the target from the pursuer, and vice versa, is constant. Therefore, both the pursuit strategies $u_{\mathcal{P}}(\mathsf{x}) = u_{\mathrm{OLS}}(\mathsf{x})$ and $u_{\mathcal{P}}(\mathsf{x}) = u_{\mathrm{NLS}}(\mathsf{x})$ satisfy the so-called requirement for *motion camouflage* with respect to a point *at infinity* [192], also known in the field of missile guidance as the condition for *parallel guidance/navigation* [186]. The situation is illustrated in Figure 34.

Another way to reach the same conclusion, is by showing that when the pursuer is driven by either the control law (113) or (119), the LoS angle λ remains constant during the course of the pursuit. In particular, in light of (110),

$$\dot{\lambda} = -\frac{\langle \dot{\mathsf{x}}_{\mathcal{P}} - \dot{\mathsf{x}}_{\mathcal{T}}, \mathsf{e}_{\mathsf{x}}^2 \rangle}{|\mathsf{x}_{\mathcal{P}} - \mathsf{x}_{\mathcal{T}}|} = -\frac{\langle \dot{\mathsf{x}}, \mathbf{S}\mathsf{e}_{\mathsf{x}}^1 \rangle}{|\mathsf{x}|}. \tag{135}$$

It is easy to show that when the pursuer is driven by either the control law (113) or (119), the vector $\dot{\mathsf{x}} = \dot{\mathsf{x}}_{\mathcal{P}} - \dot{\mathsf{x}}_{\mathcal{T}}$ remains parallel to $\mathsf{e}_{\mathsf{x}}^1 \equiv \mathsf{e}_{\mathsf{x}_0}^1$. Consequently, the inner

product in the numerator of (135) is zero, given that $\mathbf{S}$ is a skew symmetric matrix, and thus λ is constant at all times. Note that when the agent is steered by either the LoS navigation law (113) or (119), it will remain on the original LoS during its course to its destination, and thus the points x, x_0, and the origin $\mathsf{x} = 0$ will always be collinear. Thus, both of the navigation laws (113) and (119) satisfy the condition for motion camouflage with respect to a *fixed point*, namely x_0, rather than the condition for motion camouflage with respect to a *point at infinity*, which is satisfied, when (113) or (119) are used as pursuit strategies.

The three-point navigation law is derived directly from the pursuit strategy (127), which satisfies, by construction, the geometric condition for motion camouflage with respect to a fixed point, namely x_0. Note that the geometric condition for motion camouflage with respect to neither a fixed point (that is, collinearity of x_0, x and the origin) nor a point at infinity (that is, $\dot{\lambda} = 0$) are necessarily satisfied when the control (127) is used as a navigation law.

6.4 Navigation with Imperfect Information

In this section, feedback navigation laws for the case when the information about the local drift field available to the agent is imperfect are presented. The proposed navigation laws are derived from the control laws presented in Section 6.3, after the necessary modifications reflecting the lack of complete knowledge of the drift field have been carried out. Specifically, note that the control laws (113) and (119) depend on the initial LoS direction $\mathsf{e}^1_{\mathsf{x}_0}$ and its normal direction $\mathsf{e}^2_{\mathsf{x}_0}$, and both of them remain constant throughout. By updating the initial LoS direction with the most current LoS direction $\mathsf{e}^1_{\mathsf{x}}$ and its corresponding normal direction by $\mathsf{e}^2_{\mathsf{x}}$, the control law can use the most up-to-date information of its relative position to its destination. In other words, the drift components along the current LoS direction and its perpendicular entail enough information about the prevailing wind/current field so that the controller can

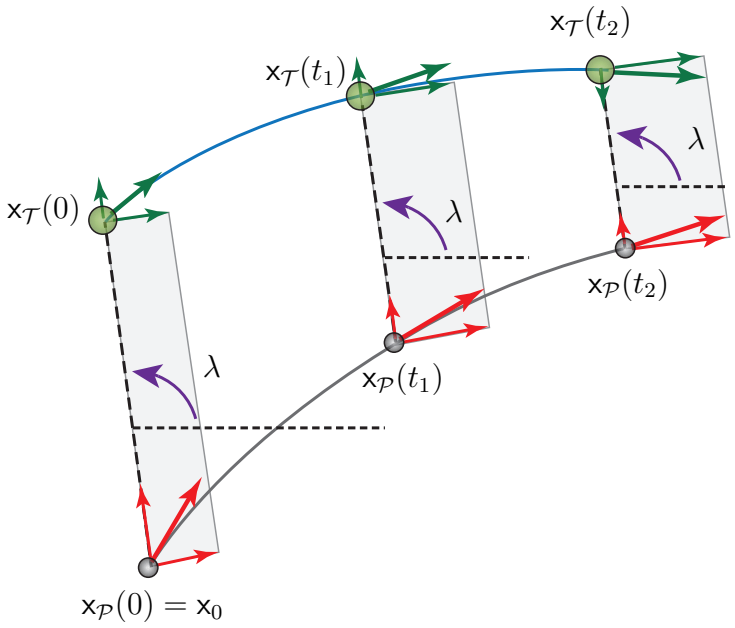

Figure 34: Motion camouflage with respect to a point at infinity is synonymous to parallel guidance/navigation, where the LoS angle between the pursuer and the target, when measured with respect to some fixed reference direction, remains constant at all times. Equivalently, the components of the velocities of the pursuer and the target perpendicular to the LoS direction remain the same at every instant of time.

compensate its effect on the ensuing path of the agent.

6.4.1 Robust LoS Navigation Laws with Imperfect Local Information of the Drift

One important remark from the discussion in Section 6.3 is that for the implementation of both the navigation laws (113) and (119), the agent must have perfect knowledge of the local drift at every instant of time. If, however, the local drift is not known perfectly, that is, $\Delta w(t, \mathsf{x}) \not\equiv 0$, then the navigation laws (113) and (119) will not successfully cancel the component of the drift perpendicular to the LoS direction. Consequently, the agent may fail to reach its destination. To alleviate this deficiency, two variations of the navigation laws (113) and (119), which are robust to model uncertainties induced by the incomplete knowledge of the local drift field, are introduced.

The adopted approach is based on the observation that, in contrast to the pursuit problem, where motion camouflage is often used to introduce the element of deception, the enforcement of the geometric condition for motion camouflage in the navigation problem has no apparent practical value. Therefore, one can relax the motion camouflage requirement and consider instead the following modification of the navigation law (113)

$$\begin{aligned} u^{\star}_{\mathrm{OLS}}(\mathsf{x}) &= u^{\star}_{\mathrm{OLS},1}(\mathsf{x})\mathsf{e}^1_{\mathsf{x}} + u^{\star}_{\mathrm{OLS},2}(\mathsf{x})\mathsf{e}^2_{\mathsf{x}}, \\ u^{\star}_{\mathrm{OLS},1}(\mathsf{x}) &= \sqrt{\bar{u}^2 - \langle w(\mathsf{x}), \mathsf{e}^2_{\mathsf{x}}\rangle^2}, \quad u^{\star}_{\mathrm{OLS},2}(\mathsf{x}) = -\langle w(\mathsf{x}), \mathsf{e}^2_{\mathsf{x}}\rangle. \end{aligned} \tag{136}$$

Note that the navigation laws (113) and (136) are almost identical modulo the replacement of $\mathsf{e}^1_{\mathsf{x}_0}$ and $\mathsf{e}^2_{\mathsf{x}_0}$ by $\mathsf{e}^1_{\mathsf{x}}$ and $\mathsf{e}^2_{\mathsf{x}}$, respectively, which is induced, in turn, by the relaxation of the geometric constraint of motion camouflage. The situation is illustrated in Fig. 35.

The following proposition furnishes sufficient conditions for the feasibility of the navigation law (136).

Proposition 29. *Let $\varepsilon > 0$. Then, for all $|\mathsf{x}_0| > \varepsilon$, the navigation law* (136) *will drive the system* (99) *to the set $\{\mathsf{x} \in \mathbb{R}^2 : \ |\mathsf{x}| \leq \varepsilon\}$ in finite time, provided there exist $\bar{w}_1 > 0$ and $\bar{w}_2 > 0$ such that*

$$|\langle w(\mathsf{x}) + \Delta w(t, \mathsf{x}), \mathsf{e}^1_{\mathsf{x}}\rangle| \leq \bar{w}_1 < \sqrt{\bar{u}^2 - \bar{w}_2^2}, \tag{137}$$

$$|\langle w(\mathsf{x}), \mathsf{e}^2_{\mathsf{x}}\rangle| \leq \bar{w}_2 < \bar{u}, \tag{138}$$

for all $\mathsf{x} \in \mathbb{R}^2 \backslash \{0\}$. Furthermore, the arrival time satisfies the upper bound

$$\mathrm{T_f} \leq \frac{|\mathsf{x}_0| - \varepsilon}{\sqrt{\bar{u}^2 - \bar{w}_2^2} - \bar{w}_1} < \infty. \tag{139}$$

Proof. The proof follows similarly to the proof of Proposition 26, and it is omitted. □

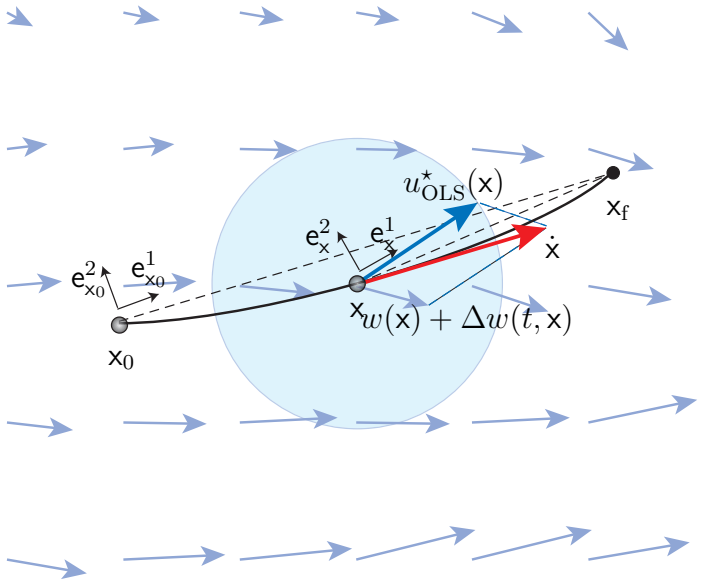

Figure 35: Robust LoS navigation. The direction of motion of the agent does not always align with the current LoS owing to the presence of the unknown drift component Δw.

Similarly, one can consider a variation of the navigation law (119), whose expression is given by

$$u^\star_{\mathrm{NLS}}(\mathsf{x}) := u^\star_{\mathrm{NLS},1}(\mathsf{x})\mathsf{e}^1_{\mathsf{x}} + u^\star_{\mathrm{NLS},2}(\mathsf{x})\mathsf{e}^2_{\mathsf{x}},$$
$$u^\star_{\mathrm{NLS},1}(\mathsf{x}) := \bar{u} - |w(\mathsf{x})| - \langle w(\mathsf{x}), \mathsf{e}^1_{\mathsf{x}}\rangle, \qquad u^\star_{\mathrm{NLS},2}(\mathsf{x}) := -\langle w(\mathsf{x}), \mathsf{e}^2_{\mathsf{x}}\rangle. \tag{140}$$

The following proposition presents sufficient conditions for the feasibility of the navigation law (140).

Proposition 30. *Let $\varepsilon > 0$. Then, for all $|\mathsf{x}_0| > \varepsilon$, the navigation law (140) will drive the system (99) to the set $\{\mathsf{x} \in \mathbb{R}^2 : |\mathsf{x}| \leq \varepsilon\}$ in finite time provided there exist $\bar{w} > 0$ and $\Delta\bar{w}_1 > 0$ such that*

$$|w(\mathsf{x})| \leq \bar{w} < \bar{u}, \tag{141}$$
$$|\langle \Delta w(t, \mathsf{x}), \mathsf{e}^1_{\mathsf{x}}\rangle| \leq \Delta\bar{w}_1 < \bar{u} - \bar{w}, \tag{142}$$

for all $t \geq 0$ and $\mathsf{x} \in \mathbb{R}^2\backslash\{0\}$. Furthermore, the time $\mathrm{T_f}$ satisfies the upper bound

$$\mathrm{T_f} \leq \frac{|\mathsf{x}_0| - \varepsilon}{\bar{u} - \bar{w} - \Delta\bar{w}_1} < \infty. \tag{143}$$

Proof. The proof follows similarly to the proof of Proposition 27, and it is omitted. □

If one uses the navigation laws (136) or (140) as pursuit strategies for Problem 7, then the condition for motion camouflage with respect to a point at infinity will not be satisfied. This comes as a consequence of the fact that any discrepancies between the actual and the known drift would result in a non-zero $\dot{\lambda}$, in general. In particular, it can easily be shown that

$$\dot{\lambda} = -\frac{\langle \Delta w(t, \mathsf{x}), \mathsf{e}_{\mathsf{x}}^2 \rangle}{|\mathsf{x}|}. \tag{144}$$

Since $\dot{\lambda}$ is not zero for $\Delta w(t, \mathsf{x}) \neq 0$, the constant LoS angle requirement (the condition for motion camouflage with respect to a point at infinity) is not satisfied. Another important observation from Equation (144) is that as $|\mathsf{x}| \to 0$, $\dot{\lambda}$ grows unbounded, which implies, in turn, that the normal acceleration of the agent along its ensuing path grows unbounded as well; this is an undesirable, from the application point of view, situation. The following proposition furnishes a sufficient condition for $\dot{\lambda}$ to remain bounded at all times.

Proposition 31. *Let $\varepsilon > 0$, and let all assumptions of Propositions 29 and 30 hold. Furthermore, assume that there exists $\Delta\bar{w} > 0$ such that*

$$|\Delta w(t, \mathsf{x})| \leq \Delta\bar{w}, \qquad \text{for all } \ t \geq 0 \text{ and } \mathsf{x} \in \mathbb{R}^2. \tag{145}$$

If $\Delta w(t, \mathsf{x}) = \mathcal{O}(|\mathsf{x}|)$, as $|\mathsf{x}| \to 0$, uniformly for all $t \geq 0$, then $\dot{\lambda}$ remains bounded for all $t \in [0, \mathrm{T_f}]$ and for all $|\mathsf{x}_0| > \varepsilon$.

Proof. By hypothesis, there exists $k(\varepsilon) > 0$ such that $|\Delta w(t, \mathsf{x})| \leq k(\varepsilon)|\mathsf{x}|$, for all $t \geq 0$ and $|\mathsf{x}| \leq \varepsilon$. Furthermore, by virtue of the Cauchy-Schwartz inequality, it follows that

$$\frac{|\langle \Delta w(t, \mathsf{x}), \mathsf{e}_{\mathsf{x}}^2 \rangle|}{|\mathsf{x}|} \leq \frac{|\Delta w(t, \mathsf{x})|}{|\mathsf{x}|} \leq \frac{\Delta\bar{w}}{\varepsilon}, \qquad \text{for all } t \geq 0 \text{ and } \mathsf{x} \in \{\mathsf{y} \in \mathbb{R}^2 : \ |\mathsf{y}| > \varepsilon\}. \tag{146}$$

In light of (144) and (146), it follows that

$$|\dot{\lambda}| = \frac{|\langle \Delta w(t,\mathsf{x}), \mathsf{e}_{\mathsf{x}}^2 \rangle|}{|\mathsf{x}|} \leq \max\{k(\varepsilon), \Delta\bar{w}/\varepsilon\} < \infty, \qquad \text{for all } t \geq 0 \text{ and } \mathsf{x} \in \mathbb{R}^2 \backslash \{0\}, \tag{147}$$

and thus completing the proof. □

6.4.2 Robust Three-Point Navigation

In case the local drift is not perfectly known, that is, when $\Delta w(t,\mathsf{x}) \not\equiv 0$, the pursuit strategy (127) will not satisfy the condition for motion camouflage with respect to a fixed point, that is, the points $\mathsf{x}_{\mathcal{P}}$, $\mathsf{x}_{\mathcal{T}}$ and x_0 may not be collinear at all times. Since the enforcement of the motion camouflage condition has no apparent practical value for the navigation problem, one can proceed with the design of a navigation law, at the geometric level, by relaxing the motion camouflage constraint. In particular, it is assumed that the condition for motion camouflage is satisfied with respect to a moving point, denoted henceforth by $\mathsf{x}_0^\star(t)$, rather than with respect to the fixed point x_0. This variation of the navigation law (127) is denoted by $u_{\text{TPN}}^\star$.

Let the moving reference point $\mathsf{x}_0^\star(t)$ be defined, for all $t \geq 0$, by the following set of equations

$$|\mathsf{x}_{\mathcal{P}}(t) - \mathsf{x}_0^\star(t)| = |\mathsf{x}_{\mathcal{P}}(t) - \mathsf{x}_0|, \tag{148}$$

$$\langle \mathsf{x}_{\mathcal{P}}(t) - \mathsf{x}_0^\star(t), \mathsf{e}_{\mathsf{x}}^1 \rangle = |\mathsf{x}_{\mathcal{P}}(t) - \mathsf{x}_0^\star(t)|. \tag{149}$$

It follows readily from (149) that $\mathsf{x}_{\mathcal{P}}(t)$, $\mathsf{x}_0^\star(t)$ and $\mathsf{x}_{\mathcal{T}}(t)$ are collinear for all $t \geq 0$, and, furthermore,

$$|\mathsf{x}_{\mathcal{T}}(t) - \mathsf{x}_0^\star(t)| = |\mathsf{x}_{\mathcal{P}}(t) - \mathsf{x}_0^\star(t)| + |\mathsf{x}_{\mathcal{T}}(t) - \mathsf{x}_{\mathcal{P}}(t)|. \tag{150}$$

The situation is illustrated in Fig. 36. It follows readily that, at each time $t \geq 0$, the moving reference point $\mathsf{x}_0^\star(t)$ belongs to the intersection of a circle centered at x_0 with radius $|\mathsf{x}_{\mathcal{P}}(t) - \mathsf{x}_0|$ with the line defined by $\mathsf{x}_{\mathcal{T}}(t)$ and $\mathsf{x}_{\mathcal{P}}(t)$. As it shall be

explained later, the exact location of $\mathsf{x}_0^\star(t)$ will not affect the analytic expression of the navigation law. Indeed, in light of (150), it follows that

$$\frac{\langle u^\star_{\mathrm{TPN}}(\mathsf{x},\mathsf{x}_\mathcal{P}),\mathsf{e}^2_\mathsf{x}\rangle}{|\mathsf{x}_\mathcal{P}-\mathsf{x}_0^\star|}=-\frac{\langle w(\mathsf{x}),\mathsf{e}^2_\mathsf{x}\rangle}{|\mathsf{x}_\mathcal{T}-\mathsf{x}_0^\star|}=-\frac{\langle w(\mathsf{x}),\mathsf{e}^2_\mathsf{x}\rangle}{|\mathsf{x}_\mathcal{P}-\mathsf{x}_0^\star|+|\mathsf{x}|}. \tag{151}$$

Finally, since by construction $|\mathsf{x}_\mathcal{P}(t)-\mathsf{x}_0^\star(t)|\equiv|\mathsf{x}_\mathcal{P}(t)-\mathsf{x}_0|$, for all $t\geq 0$, it follows that

$$\frac{\langle u^\star_{\mathrm{TPN}}(\mathsf{x},\mathsf{x}_\mathcal{P}),\mathsf{e}^2_\mathsf{x}\rangle}{|\mathsf{x}_\mathcal{P}-\mathsf{x}_0^\star|}=\frac{\langle u^\star_{\mathrm{TPN}}(\mathsf{x},\mathsf{x}_\mathcal{P}),\mathsf{e}^2_\mathsf{x}\rangle}{|\mathsf{x}_\mathcal{P}-\mathsf{x}_0|}=-\frac{\langle w(\mathsf{x}),\mathsf{e}^2_\mathsf{x}\rangle}{|\mathsf{x}_\mathcal{P}-\mathsf{x}_0|+|\mathsf{x}|}. \tag{152}$$

Therefore, one can easily conclude from (152) that $u^\star_\mathcal{P}=u_\mathcal{P}$, or, equivalently,

$$u^\star_{\mathrm{TPN}}(\mathsf{x},\mathsf{x}_\mathcal{P})=u_{\mathrm{TPN}}(\mathsf{x},\mathsf{x}_\mathcal{P}). \tag{153}$$

Thus, the analytic expressions of the three-point-navigation law derived after relaxing the motion camouflage constraint and the original three-point-navigation law (127) are exactly the same. On the grounds of the previous observation, one concludes that the navigation law (127) is robust to model uncertainties of the local drift. The following proposition follows readily from the previous discussion.

Proposition 32. *Let $\varepsilon>0$. Then, for all $|\mathsf{x}_0|>\varepsilon$, the navigation law* (127) *will drive the system* (99) *to the set $\{\mathsf{x}:\ |\mathsf{x}|\leq\varepsilon\}$ in finite time, provided there exist $\bar{w}_1>0$ and $\bar{w}_2>0$ such that*

$$|\langle w(\mathsf{x})+\Delta w(t,\mathsf{x}),\mathsf{e}^1_{\mathsf{x}_0}\rangle|\leq\bar{w}_1<\sqrt{\bar{u}^2-\bar{w}_2^2}, \tag{154}$$

$$|\langle w(\mathsf{x}),\mathsf{e}^2_\mathsf{x}\rangle|\leq\bar{w}_2, \tag{155}$$

for all $t\geq 0$ and $\mathsf{x}\in\mathbb{R}^2\backslash\{0\}$. Finally, the time of travel satisfies the upper bound

$$\mathrm{T_f}\leq\frac{|\mathsf{x}_0|-\varepsilon}{\sqrt{\bar{u}^2-\bar{w}_2^2}-\bar{w}_1}<\infty. \tag{156}$$

6.5 Navigation in Unknown Drift

In this section, the problem of steering the agent in the presence of a completely unknown drift field, that is, $w(\mathsf{x})\equiv 0$ and $\Delta w(t,\mathsf{x})\not\equiv 0$, is considered.

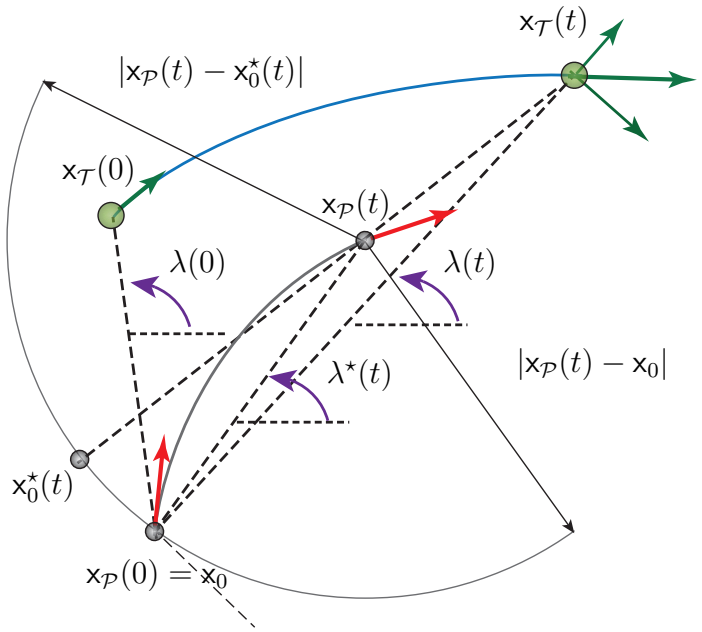

Figure 36: Three-point guidance or motion camouflage with respect to a moving point $\mathsf{x}_0^\star$ rather than x_0. The condition for motion camouflage with respect to the fixed point x_0 is violated when $\lambda(t) \neq \lambda^\star(t)$.

6.5.1 Direct-Bearing Navigation

The feedback navigation law

$$u_{\mathrm{PP}}(\mathsf{x}) = \bar{u}\mathsf{e}_{\mathsf{x}}^1 \tag{157}$$

steers the agent's forward velocity to always point towards its destination. It is worth-mentioning that due to the absence of any knowledge about the local drift at x, the navigation law (157) steers the inertial velocity of the agent so that it points towards a direction different than the LoS. This fact may incur some loss of performance, in terms of minimizing the arrival time, when compared with, for example, the navigation law (113) (see also the discussion on Section 6.6). The situation is illustrated in Figure 37. One of the main advantages of the navigation law (157) is that it is completely independent of the drift $\Delta w(t, \mathsf{x})$, and thus, it is robust to model uncertainties induced by the local drift. The navigation law (157) is the dual to the well-known *pure pursuit* or *hound-hare pursuit* strategy [186], where

the pursuer velocity vector always points towards the current position of the target. The following proposition provides a sufficient condition for the feasibility of the navigation law (157).

Proposition 33. *Let $\varepsilon > 0$ and $w(\mathsf{x}) \equiv 0$. Then, for all $|\mathsf{x}_0| > \varepsilon$, the navigation law* (157) *will drive the system* (99) *to the set $\{\mathsf{x} \in \mathbb{R}^2 : \ |\mathsf{x}| \leq \varepsilon\}$ in finite time, provided there exists $\Delta\bar{w}_1 > 0$ such that*

$$|\langle \Delta w(t, \mathsf{x}), \mathsf{e}^1_{\mathsf{x}} \rangle| \leq \Delta\bar{w}_1 < \bar{u}, \qquad \text{for all} \ \ t \geq 0 \text{ and } \mathsf{x} \in \mathbb{R}^2. \tag{158}$$

Furthermore, the arrival time satisfies the upper bound

$$\mathrm{T_f} \leq \frac{|\mathsf{x}_0| - \varepsilon}{\bar{u} - \Delta\bar{w}_1} < \infty. \tag{159}$$

Proof. It follows readily that

$$\begin{aligned} \frac{\mathrm{d}}{\mathrm{d}t}|\mathsf{x}| &= -\langle \dot{\mathsf{x}}, \mathsf{e}^1_{\mathsf{x}} \rangle = -\langle u_{\mathrm{PP}}(\mathsf{x}) + \Delta w(t, \mathsf{x}), \mathsf{e}^1_{\mathsf{x}} \rangle \\ &= -\bar{u} - \langle \Delta w(t, \mathsf{x}), \mathsf{e}^1_{\mathsf{x}} \rangle \\ &\leq -\bar{u} + \Delta\bar{w}_1. \end{aligned} \tag{160}$$

The rest of the proof follows similar to the proof of Proposition 26, and it is omitted. □

6.6 Gradient Descent Laws for Navigation in a Flow Field with Limited Information

In this section, the proposed navigation laws are reinterpreted as gradient descent laws in terms of different performance indices. To simplify the presentation, it is henceforth assumed that

$$|w(\mathsf{x}) + \Delta w(t, \mathsf{x})| < \bar{u}, \qquad \text{for all} \ \ t \geq 0 \text{ and } \mathsf{x} \in \mathbb{R}^2. \tag{161}$$

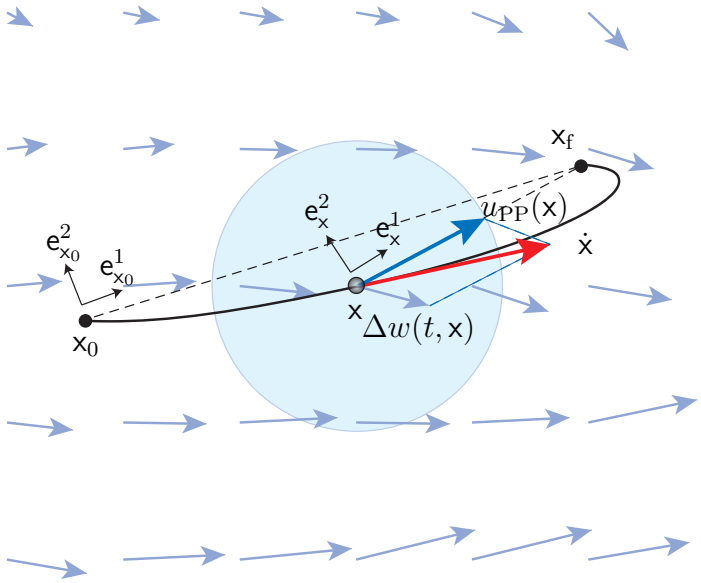

Figure 37: Direct-bearing navigation. The forward velocity of the agent is aligned with the LoS direction at every instant in time.

First, it is shown that the navigation law (136) is a (pseudo-)gradient descent law in terms of an estimate of the time required for the agent to reach its destination (time-to-come). In particular, a simple estimate of the time-to-come, which is henceforth denoted by $\widetilde{\mathrm{T}}(\mathsf{x})$, is given by

$$\widetilde{\mathrm{T}}(\mathsf{x}) := \frac{\sqrt{\langle \mathsf{x}, w(\mathsf{x})\rangle^2 + (\bar{u}^2 - |w(\mathsf{x})|^2)|\mathsf{x}|^2}}{\bar{u}^2 - |w(\mathsf{x})|^2} - \frac{\langle \mathsf{x}, w(\mathsf{x})\rangle}{\bar{u}^2 - |w(\mathsf{x})|^2}. \tag{162}$$

Note that $\widetilde{\mathrm{T}}(\mathsf{x})$ is the minimum time required for the agent located at x, at time $t = \tau$, to reach the origin, assuming that the drift will remain constant and equal to $w(\mathsf{x})$, for all $t \geq \tau$.

Let $\nabla\widetilde{\mathrm{T}}(\mathsf{x})$ denote the gradient of $\widetilde{\mathrm{T}}(\mathsf{x})$, which is, in general, a function of x, $w(\mathsf{x})$ and $\partial w/\partial \mathsf{x}$. Because, by hypothesis, the Jacobian $\partial w/\partial \mathsf{x}$ is unknown to the agent, a pseudo-gradient operator acting on $\widetilde{\mathrm{T}}(\mathsf{x})$, denoted by $\widetilde{\nabla}\widetilde{\mathrm{T}}(\mathsf{x})$, where $\widetilde{\nabla}\widetilde{\mathrm{T}}(\mathsf{x}) := \nabla\widetilde{\mathrm{T}}(\mathsf{x})\big|_{\frac{\partial w}{\partial \mathsf{x}}=0}$, is introduced instead. It is straightforward to show that the (pseudo-)gradient descent control law

$$u_{\mathrm{PGDN}}(\mathsf{x}) := -\bar{u}\frac{\widetilde{\nabla}\widetilde{\mathrm{T}}(\mathsf{x})}{|\widetilde{\nabla}\widetilde{\mathrm{T}}(\mathsf{x})|} \tag{163}$$

satisfies $u_{\text{PGDN}}(\mathsf{x}) = u^{\star}_{\text{OLS}}(\mathsf{x})$, for all $\mathsf{x} \in \mathbb{R}^2 \backslash \{0\}$.

Next, it is shown that the LoS navigation law (136) can also be interpreted as a quickest descent control law [204] in terms of the Euclidean distance of the agent from its destination. In other words, the time derivative of $\mathrm{V}(\mathsf{x}) = |\mathsf{x}|$ evaluated along the trajectories of the system (99), after closing the loop with $u(\mathsf{x}) = u^{\star}_{\text{OLS}}(\mathsf{x})$, is point-wise minimized.

Proposition 34. *The navigation law* $u^{\star}_{\text{OLS}}(\mathsf{x})$ *is the quickest descent law for the system* (99) *with respect to the descent function* $\mathrm{V}(\mathsf{x}) = |\mathsf{x}|$.

Proof. Let $u(\mathsf{x}) \in \mathcal{U}_f$. The time derivative of $\mathrm{V}(\mathsf{x})$ evaluated along the trajectories of system (99), after closing the loop, is given by

$$\frac{\mathrm{d}}{\mathrm{d}t}\mathrm{V}(\mathsf{x}) = \nabla \mathrm{V}(\mathsf{x})\dot{\mathsf{x}} = -\langle u(\mathsf{x}) + w(\mathsf{x}) + \Delta w(t, \mathsf{x}), \mathsf{e}^1_{\mathsf{x}} \rangle, \tag{164}$$

where the identity $\nabla \mathrm{V}(\mathsf{x}) = \mathsf{x}/|\mathsf{x}| = -\mathsf{e}^1_{\mathsf{x}}$ has been used. It follows readily that the quickest descent control $u(\mathsf{x})$ satisfies

$$u(\mathsf{x}) + w(\mathsf{x}) = \max_{|u| \leq \bar{u}} \langle u(\mathsf{x}) + w(\mathsf{x}), \mathsf{e}^1_{\mathsf{x}} \rangle \, \mathsf{e}^1_{\mathsf{x}}. \tag{165}$$

Equation (165) implies that $\langle u(\mathsf{x}) + w(\mathsf{x}), \mathsf{e}^2_{\mathsf{x}} \rangle = 0$ and $|u(\mathsf{x})| = \bar{u}$. Therefore, $\langle u(\mathsf{x}), \mathsf{e}^2_{\mathsf{x}} \rangle = -\langle w(\mathsf{x}), \mathsf{e}^2_{\mathsf{x}} \rangle$, which implies, in turn, that $\langle u(\mathsf{x}), \mathsf{e}^1_{\mathsf{x}} \rangle = \sqrt{\bar{u}^2 - \langle w(\mathsf{x}), \mathsf{e}^2_{\mathsf{x}} \rangle^2}$. Therefore, it follows that $u(\mathsf{x}) = u^{\star}_{\text{OLS}}(\mathsf{x})$, for all $\mathsf{x} \in \mathbb{R}^2 \backslash \{0\}$, thus completing the proof. □

Finally, the direct-bearing navigation law (157) can also be viewed as a gradient descent control law. It is easy to show that

$$u_{\text{PP}}(\mathsf{x}) \equiv -\bar{u}\frac{\nabla \mathrm{V}(\mathsf{x})}{|\nabla \mathrm{V}(\mathsf{x})|}, \tag{166}$$

where $\mathrm{V}(\mathsf{x}) := |\mathsf{x}|$. Note that $\mathrm{V}(\mathsf{x})$ is a reasonable heuristic function in terms of the time-to-come for the navigation problem in a completely unknown drift field (this follows readily by setting $w(\mathsf{x}) \equiv 0$ in Equation (162)). An interesting question

is when, and under which conditions, the direct bearing navigation law (157) is a minimum-time control law for Problem 6. The following proposition addresses the previous questions.

Proposition 35. *Let $\varepsilon > 0$. The navigation law* (157) *is a minimum-time control law of the ZNP provided there exists a Lipschitz continuous function $f : [\varepsilon, \infty) \mapsto \mathbb{R}$ such that $\langle w(\mathsf{x}), \mathsf{e}^1_{\mathsf{x}} \rangle = f(|\mathsf{x}|)$. Furthermore, the system* (99) *will converge to the set $\{\mathsf{x} : \ |\mathsf{x}| \leq \varepsilon\}$ in finite time, for all $|\mathsf{x}_0| > \varepsilon$, if and only if $f(z) < \bar{u}z$, for all $\varepsilon \leq z \leq |\mathsf{x}_0|$. In addition, the final arrival time is given by*

$$\mathrm{T_f} = \int_{\varepsilon}^{|\mathsf{x}_0|} \frac{z \, \mathrm{d}z}{\bar{u}z - f(z)}. \tag{167}$$

Proof. The reader can refer to [17]. □

Proposition 35 highlights a rather surprising result, namely, that although the measurement of the local drift $w(\mathsf{x})$ does not appear at all in the expression of the navigation law (157), in contrast to all the other navigation laws presented in this chapter, which explicitly account for the local drift, the direct bearing navigation law (157) can be the minimum-time navigation law for some drift fields.

6.7 Simulation Results

In this section, simulation results that illustrate the previous developments are presented. The drift field is assumed to be expressed as the vector sum of a uniform flow component and the local flow induced by a finite number of distinct, nonlinear flow singularities [60]. In particular, it is assumed that the known part of the drift $w(\mathsf{x})$ can be modeled as follows

$$w(\mathsf{x}) = w^0 + \sum_{i=1}^{n_s} \alpha_i^{-1}(|\mathsf{x} - \mathsf{x}_{s_i}|)\mathbf{A}_i(\mathsf{x} - \mathsf{x}_{s_i}), \tag{168}$$

where n_s is the number of flow singularities, x_{s_i} is the location of the i^{th} flow singularity, $\alpha_i : [0, \infty) \mapsto \mathbb{R}$ is a continuous function, which may vanish only at $\mathsf{x} = \mathsf{x}_{s_i}$,

and $\mathbf{A}_i$ is a 2×2 matrix, whose structure captures the local characteristics of the i^{th} flow singularity [150]. Note that the flow model given in Equation (168) extends the model adopted in [150] to account for multiple flow singularities located at distinct positions.

Figure 38 illustrates the trajectories of the agent, when the latter is steered by the minimum-time control law of the ZNP (Fig. 38(a)), the robust optimal LoS navigation law (136) (Fig. 38(b)), the three-point navigation law (127) (Fig. 38(c)), and the direct-bearing navigation law (157) (Fig. 38(d)). For the computation of the minimum-time paths, we have used GPOPS [161], which is an open source software for numerical optimal control. The following problem data are used: $\bar{u} = 1$, $n_s = 2$, $\mathbf{A}_1 = \mathbf{S}$, $\mathbf{A}_2 = \left[\begin{smallmatrix} 2 & -1 \\ 1 & 0 \end{smallmatrix}\right]$, $\mathsf{x}_{s_1} = [5,\ 0]^\mathsf{T}$, $\mathsf{x}_{s_2} = [-6,\ -4]^\mathsf{T}$, $w^0 = [0,\ 0]^\mathsf{T}$, $\alpha_1(|\mathsf{x} - \mathsf{x}_{s_1}|) = |\mathbf{A}_1(\mathsf{x} - \mathsf{x}_{s_1})|/0.3$, and $\alpha_2(|\mathsf{x} - \mathsf{x}_{s_2}|) = |\mathbf{A}_2(\mathsf{x} - \mathsf{x}_{s_2})|/0.4$. Furthermore, it is assumed that the unknown part of the drift field is given by $\Delta w(t, \mathsf{x}) = \sqrt{3}|\mathsf{x}|/6[0.3(1 - \cos(t/\pi)),\ -0.25]^\mathsf{T}$. One can observe from Figs. 38(b)-38(d) that, despite the presence of the unknown part $\Delta w(t, \mathsf{x})$ of the local drift field, the agent driven by the robust optimal LoS, the three-point and the direct-bearing navigation laws successfully reaches its destination. Furthermore, it is observed that the geometry of the ensuing paths of the agent, when the agent is far away from its destination and it is driven by the navigation laws (127) and (157), exhibit notable similarities, as is illustrated in Figs. 38(c)-38(d). The ensuing paths of the agent are also similar when the agent is close to its destination and is driven by the navigation laws (136) and (127), as is illustrated in Figs. 38(b)-38(c). The last two observations are justified by the fact that the navigation law (127) becomes approximately equal to (157), for large $|\mathsf{x}|$ (in light of (126), the component of (127) along e_x^2 becomes approximately equal to zero as $|\mathsf{x}| \to \infty$), whereas it approximates (136), for $|\mathsf{x}|$ sufficiently small (in light of (126), the component of (127) along e_x^2 becomes approximately equal to $-\langle w(\mathsf{x}), \mathsf{e}_\mathsf{x}^2 \rangle$ as $|\mathsf{x}| \to 0$).

Figure 39 illustrates the level sets of the minimum time-to-come of the ZNP as well as the level sets of the time-to-come for the robust LoS navigation law (136) (Fig. 39(b)), the three-point navigation law (127) (Fig. 39(c)), and the direct-bearing navigation law (157) (Fig. 39(d)), in the special case of a completely known drift field, that is, when $\Delta w(t, \mathsf{x}) \equiv 0$. One immediately concludes that the anticipative minimum-time controller that solves the ZNP is not significantly superior, in terms of minimizing the arrival time, to the causal controllers presented in this chapter.

Figure 40 illustrates the level sets of the time-to-come for the robust LoS navigation law (136) (Fig. 39(b)), the three-point navigation law (127) (Fig. 40(b)), and the direct-bearing navigation law (157) (Fig. 40(c)), in the presence of the unknown drift $\Delta w(t, \mathsf{x})$. One can observe that when the agent is driven by the robust LoS navigation law (136), it reaches its destination faster than when it is driven by the three-point navigation law (127), which is, in turn, significantly faster than the direct-bearing navigation law (157).

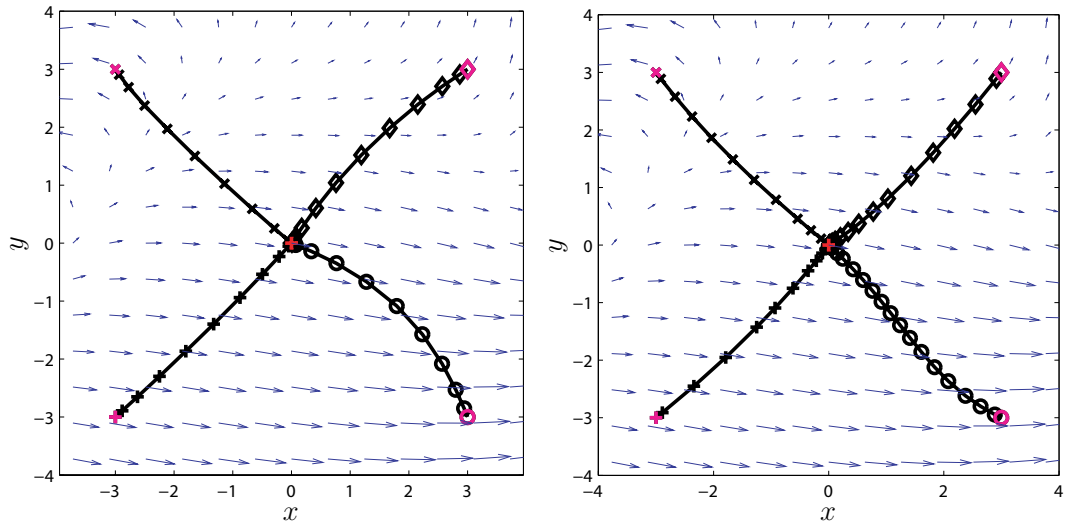

(a) Minimum-time navigation in a perfectly known drift field.

(b) Robust, optimal LOS navigation with imperfect knowledge of the local drift.

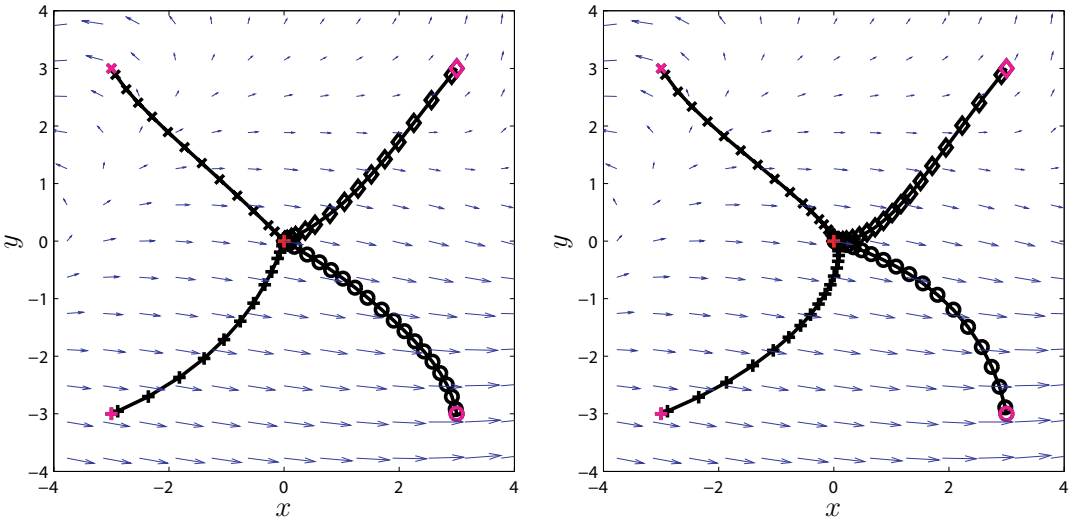

(c) Three-point navigation with imperfect knowledge of the local drift.

(d) Direct-bearing navigation in an unknown drift field.

Figure 38: Trajectories of an agent towards the origin driven by the robust optimal LoS, the three-point and the direct-bearing navigation laws.

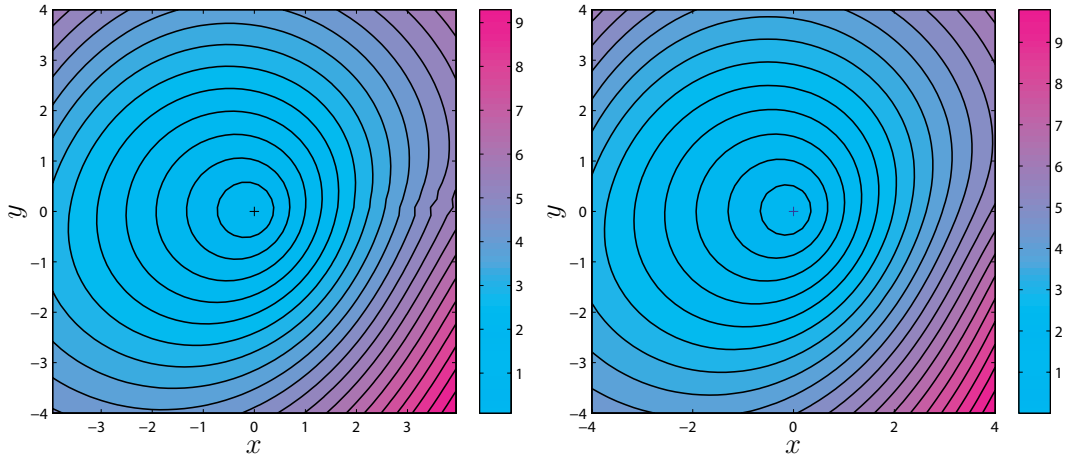

(a) Level sets of the minimum time-to-come (to the origin) of the ZNP.

(b) Level sets of the time-to-come (to the origin) using the robust, optimal LOS navigation law.

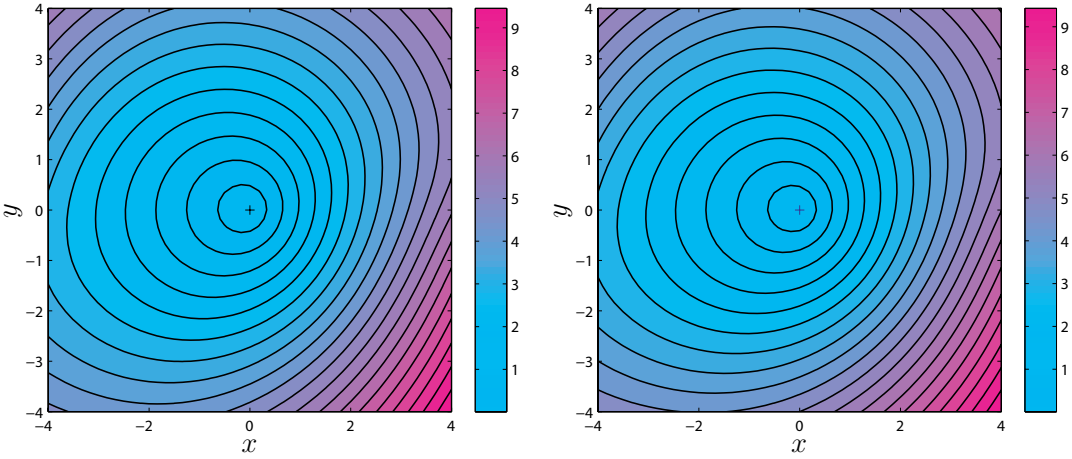

(c) Level sets of the time-to-come (to the origin) using the three-point navigation law.

(d) Level sets of the time-to-come (to the origin) using the direct-bearing navigation law.

Figure 39: Level sets of the minimum time-to-come and time-to-come (to the origin) when the agent is driven by the robust optimal LoS, the three-point and the direct-bearing navigation laws in the presence of a perfectly known drift field.

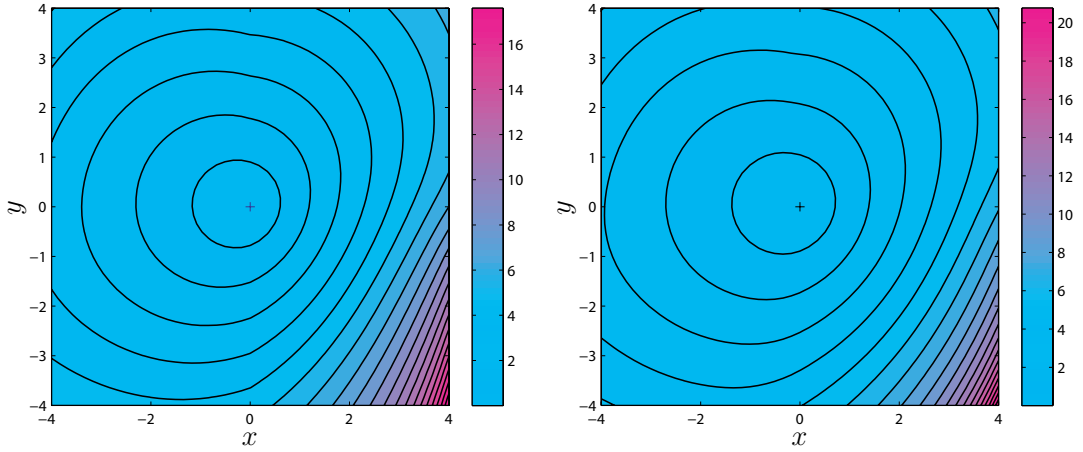

(a) Level sets of the time-to-come (to the origin) using the robust, optimal LOS navigation law.

(b) Level sets of the time-to-come (to the origin) using the three-point navigation law.

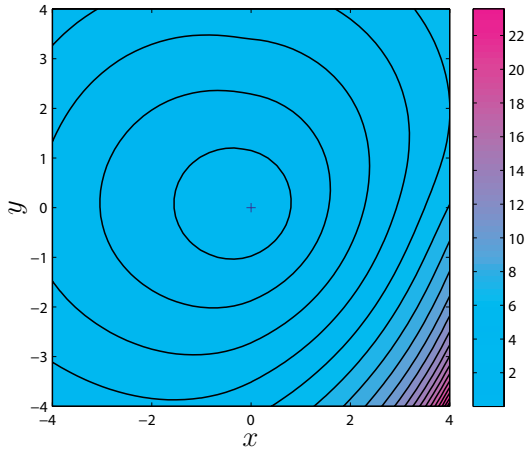

(c) Level sets of the time-to-come (to the origin) using the direct-bearing navigation law.

Figure 40: Level sets of the time-to-come (to the origin) when the agent is driven by the robust optimal LoS, the three-point and the direct-bearing navigation laws, in the presence of unknown drift.

CHAPTER VII

THE ZERMELO-VORONOI DIAGRAM: A DYNAMIC PARTITION PROBLEM

The material presented in this chapter builds on the results in [14].

7.1 Introduction

In this chapter, we deal with a Voronoi-like partition in the plane for a given (finite) set of generators, such that each element in this partition is uniquely associated with a particular generator in the following sense: An aerial / marine vehicle that resides in a particular set of the partition at a given instant of time can arrive at the generator associated with this set faster than any other agent that may be located anywhere outside this set at the same instant of time. It is assumed that the vehicle's motion is affected by the presence of temporally-varying drift. Since the generalized distance of this Voronoi-like partition problem is the minimum time of the Zermelo's navigation problem [210], we shall henceforth refer to this partition of the state space of the agent as the Zermelo-Voronoi Diagram (ZVD).

The Zermelo-Voronoi Diagram problem therefore deals with a special partition of the Euclidean plane with respect to a generalized distance function, which is the minimum time of the Zermelo's navigation problem [210]. The characterization of this Voronoi-like partition will allow us to address questions dealing with the proximity relations between an aerial / vehicle that travels in the presence of winds/currents and the set of Voronoi generators. For example, the question of determining the generator from a given set which is the "closest," in terms of arrival time, to the agent at a particular instant of time, reduces to the problem of determining the set of the

Zermelo-Voronoi partition that the agent resides at the given instant of time (the latter question is known in the computational geometry parlance as the *point location* problem). Furthermore, by assuming that the generators of the partition correspond to the initial positions of the vehicles from a team of spatially distributed autonomous vehicles, we introduce the Dual Zermelo-Voronoi Diagram (DZVD) problem. The DZVD is a partition similar to the ZVD, with the difference that the generalized distance that determines the proximity relations in the DZVD is the minimum time of the Zermelo navigation problem *from* a Voronoi generator *to* a point in the plane. Since the minimum time of the Zermelo navigation problem is not a symmetric function with respect to the initial and final configurations, the ZVD and the DZVD are not, in general, identical.

7.2 Problem Formulation

We will be dealing with the movement of autonomous mobile vehicles (agents) in the plane. It is assumed that the agent's motion is described by the following equation

$$\dot{\mathsf{x}} = u + w(t), \tag{169}$$

where $\mathsf{x} := (x, y)^\intercal \in \mathbb{R}^2$ is the position vector of the agent, $u \in \mathbb{R}^2$ is the control input and $w := (\mu, \nu)^\intercal \in \mathbb{R}^2$ is the drift, which is assumed to vary uniformly with time[1]. Note that w is to be interpreted as a time-varying velocity field induced by the winds/currents in the vicinity of the agent, which is assumed to be known a priori. In addition, it is assumed that $|w(t)| < 1$ for all $t \geq 0$, which implies, in turn, that the system (169) is completely controllable (see for example [50, p. 242]). Furthermore, the set of admissible control inputs is given by $\mathcal{U} := \big\{u \in \mathfrak{U}_{[0,T]} : u(t) \in U, \text{ for all } t \in [0, T],\ T > 0\big\}$, where $\mathfrak{U}_{[0,T]}$ is the set of all measurable functions on $[0, T]$, and $U = \{(u_1, u_2) \in \mathbb{R}^2 : u_1^2 + u_2^2 \leq 1\}$ (closed unit

[1]In the original formulation of the Zermelo's navigation problem, the drift is assumed to be both spatially and temporally-varying. In this chapter, we deal with the case of a temporally-varying drift only.

ball) is the corresponding input value set. The Zermelo's navigation problem (ZNP) can then be formulated as follows.

Problem 8 (ZNP)**.** *Given the system described by equation* (169)*, determine the control input* $u^* \in \mathcal{U}$ *such that*

i) The control u^* *minimizes the cost functional* $J(u) := T_\mathrm{f}$*, where* T_f *is the free final time.*

ii) The trajectory $\mathsf{x}^* : [0, T_\mathrm{f}] \mapsto \mathbb{R}^2$ *generated by the control* u^* *satisfies the boundary conditions*

$$\mathsf{x}^*(0) = \mathsf{x}_0, \quad \mathsf{x}^*(T_\mathrm{f}) = \mathsf{x}_\mathrm{f}. \tag{170}$$

The following proposition follows by virtue of Filippov's theorem on the existence of solutions for minimum-time problems [53, p. 311-317] and the complete controllability of the system (169) when $|w(t)| < 1$ for all $t \geq 0$ (see for example [50, p. 242]).

Proposition 36. *Let* x_0 *and* x_f *be two points in* $\mathbb{R}^2$*. If* $|w(t)| < 1$ *for all* $t \geq 0$*, then the system described by equation* (169) *admits a minimum-time path from* x_0 *to* x_f*.*

It can be shown [50, p. 370-373] that the solution of Problem 8 when $w = w(t)$ is the control $u^*(\theta^*) = (\cos\theta^*, \sin\theta^*)^\intercal$, where θ^* is a constant angle. It is worth noting that in the special case $w \equiv 0$, equation (169) becomes $\dot{\mathsf{x}} = u$, and subsequently the Zermelo's navigation problem is reduced to the shortest path problem in the plane.

Next, we formulate the Zermelo-Voronoi Diagram problem (ZVDP).

Problem 9 (ZVDP)**.** *Given the system described by equation* (169)*, a collection of goal destinations* $P := \{\mathsf{p}_i \in \mathbb{R}^2 : \ i \in \mathcal{I}_n\}$*, where* $\mathcal{I}_n := \{1, \ldots, n\}$ *is a finite index set, and a transition cost*

$$c(\mathsf{x}_0, \mathsf{p}_i) := T_\mathrm{f}(\mathsf{x}_0, \mathsf{p}_i), \tag{171}$$

determine a partition $\mathfrak{V} = \{\mathfrak{V}_i : \ i \in \mathcal{I}_n\}$ *of* $\mathbb{R}^2$ *such that*

i) $\mathbb{R}^2 = \bigcup_{i \in \mathcal{I}_n} \mathfrak{V}_i$.

ii) $\overline{\mathfrak{V}_i} = \mathfrak{V}_i$, for each $i \in \mathcal{I}_n$.

iii) for each $\mathsf{x} \in \text{int}(\mathfrak{V}_i)$, $c(\mathsf{x}, \mathsf{p}_i) < c(\mathsf{x}, \mathsf{p}_j)$ for $j \neq i$.

Henceforth, we shall refer to P, $\mathfrak{V}_i$, and $\mathfrak{V}$ as the set of *Voronoi generators* or *sites*, the *Dirichlet domain*, and the *Zermelo-Voronoi Diagram* of $\mathbb{R}^2$, respectively. In addition, two Dirichlet domains $\mathfrak{V}_i$ and $\mathfrak{V}_j$ are characterized as neighboring if they have a non-empty and non-trivial (i.e., single point) intersection.

Note that for the case $w \equiv 0$ Problem 9 reduces to the standard Voronoi Diagram problem. Next, we show that it is possible to associate the ZVDP with a standard Dynamic Voronoi Diagram, that is, a partitioning problem in the plane with respect to the Euclidean distance in the case of moving Voronoi generators, by means of a time-varying transformation.

Remark 9 In the problem formulation of the ZNP, it is assumed that the drift $w(t)$ in equation (169), which is induced by the winds/currents, is known in advance over a sufficiently long (but finite) time horizon. This is a realistic assumption if adequate weather forecast data over the area of interest are available.

7.3 The Zermelo-Voronoi Diagram Interpreted as a Dynamic Voronoi Diagram

An important observation is that the minimum time of the ZNP does not provide, in general, a generalized distance function that would allow one to reduce the ZVDP to a generalized Voronoi Diagram, for the construction of which efficient numerical techniques are available [40, 141]. Therefore, one needs to adopt an alternative approach. Our strategy will be to associate Problem 9 with a standard Voronoi Diagram generated by the same point-set, which can be interpreted, in turn, as the solution of Problem 9, when $w \equiv 0$.

First, we observe that Problem 1 can be formulated alternatively as a moving target problem as follows.

Problem 10 (ZNMTP)**.** *Given the system described by the equation*

$$\dot{\mathsf{X}} := \dot{\mathsf{x}} - w(t) = u(t), \quad \mathsf{X}(0) = \mathsf{x}_0 \tag{172}$$

determine the control input $u^* \in \mathcal{U}$ *such that*

i) The control u^* *minimizes the cost functional* $J(u) := T_\mathrm{f}$*, where* T_f *is the free final time.*

ii) The trajectory $\mathsf{X}^* : [0, T_\mathrm{f}] \mapsto \mathbb{R}^2$ *generated by the control* u^* *satisfies the boundary conditions*

$$\mathsf{X}^*(0) = \mathsf{x}_0, \qquad \mathsf{X}^*(T_\mathrm{f}) = \mathsf{x}_\mathrm{f} - \int_0^{T_\mathrm{f}} w(\tau)\,\mathrm{d}\tau. \tag{173}$$

It is clear that Problems 8 and 10 are equivalent, in the sense that a solution of Problem 8 is also a solution of Problem 10, and vice versa. Furthermore, an optimal trajectory X^* of Problem 10 is related to an optimal trajectory x^* of Problem 8 by means of the time-varying transformation

$$\mathsf{X}^*(t) = \mathsf{x}^*(t) - \int_0^t w(\tau)\mathrm{d}\tau. \tag{174}$$

The ZNMTP can be interpreted, in turn, as an optimal pursuit problem as follows: Given a pursuer and a moving target obeying the following kinematic equations

$$\dot{\mathsf{x}}_\mathcal{P} = \dot{\mathsf{X}} = u, \qquad \mathsf{x}_\mathcal{P}(0) = \mathsf{X}_0 = \mathsf{x}_0, \tag{175}$$

$$\dot{\mathsf{x}}_\mathcal{T} = -w(t), \qquad \mathsf{x}_\mathcal{T}(0) = \mathsf{x}_\mathrm{f}, \tag{176}$$

where $\mathsf{x}_\mathcal{P} = \mathsf{X}$, and $\mathsf{x}_\mathcal{T}$ are the coordinates of the pursuer and the moving target, respectively, find the optimal pursuit control law u such that the pursuer intercepts the moving target in minimum time T_f, that is,

$$\mathsf{x}_\mathcal{P}(T_\mathrm{f}) = \mathsf{X}(T_\mathrm{f}) = \mathsf{x}_\mathcal{T}(T_\mathrm{f}) = \mathsf{x}_\mathrm{f} - \int_0^{T_\mathrm{f}} w(\tau)\mathrm{d}\tau. \tag{177}$$

We have previously shown that the optimal control of Problem 8 is given by $u^* = (\cos\theta^*, \sin\theta^*)^\intercal$ (x coordinates), where θ^* is a constant. Furthermore, equation (172) implies that the same control u^* is also the optimal control for the moving target Problem 3 (X coordinates). Figure 41 illustrates the optimal control strategy for the ZNMTP based on its interpretation as an optimal pursuit problem, where the pursuer and the moving target are denoted by a black and a green dot, respectively. Note that because the angle θ^* is necessarily constant, the pursuer is constrained to travel along a ray emanating from x_0 with constant unit speed, whereas the target moves along the time-parameterized curve $\mathsf{x}_\mathcal{T} : [0, \infty) \mapsto \mathbb{R}^2$, where $\mathsf{x}_\mathcal{T}(t) = \mathsf{x}_\mathrm{f} - \int_0^t w(\tau)\,\mathrm{d}\tau$. From Proposition 36 it follows that there exists a time $T > 0$ such that $\mathsf{x}_\mathcal{P}(T) = \mathsf{X}(T) = \mathsf{x}_\mathcal{T}(T)$. The optimal value of θ^* corresponds to the least T, denoted by T_f, such that $\mathsf{x}_\mathcal{P}(T_\mathrm{f}) = \mathsf{X}(T_\mathrm{f}) = \mathsf{x}_\mathcal{T}(T_\mathrm{f})$. It is easy to show that the minimum time T_f is the least positive root of the following integral-algebraic equation

$$T = |\mathsf{x}_\mathrm{f} - \mathsf{x}_0 - \int_0^T w(\tau)\,\mathrm{d}\tau|, \tag{178}$$

whereas θ^* is given by

$$\theta^* = \mathrm{Arg}\left(\mathsf{x}_\mathrm{f} - \mathsf{x}_0 - \int_0^{T_\mathrm{f}} w(\tau)\,\mathrm{d}\tau\right). \tag{179}$$

It is worth mentioning here that the minimum time T_f is a directionally weighted (anisotropic) "distance" function, that is, the time to go from x_0 to x_f, and vice versa, not only depends on the Euclidean distance between these two points, but also on the direction of motion from x_0 and x_f. Therefore T_f is not a "true" distance function in the strict mathematical sense (the time to go from x_0 to x_f is, in general, different than the time to go from x_0 to x_f and therefore the symmetry axiom is not satisfied).

The idea of reducing the ZNP to a moving target problem in the Euclidean plane with no winds (ZNMTP), can also be applied to the ZVDP. In particular, the ZVDP can be formulated as a Dynamic Voronoi Diagram Problem (DVDP).

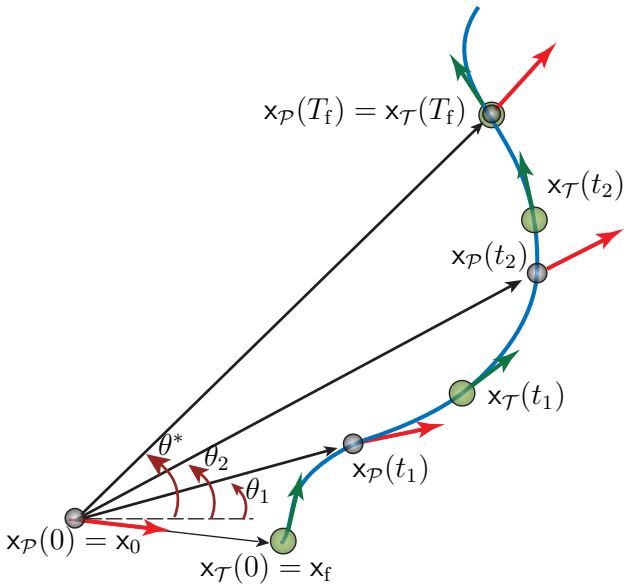

Figure 41: Time-optimal control strategy for the ZNMTP interpreted as an optimal pursuit problem.

Problem 11 (DVDP)**.** *Given the system described by equation* (172)*, a collection of moving targets* $P^d := \{\mathsf{P}_i : \mathsf{P}_i(t) = \mathsf{p}_i - \int_0^t w(\tau)\,\mathrm{d}\tau,\ i \in \mathcal{I}_n\}$*, where* $\mathcal{I}_n$ *and* p_i *as in Problem 9, and a transition cost*

$$c^d(\mathsf{X}_0, \mathsf{P}_i) := |\mathsf{X}_0 - \mathsf{P}_i(T_{\mathrm{f}}(\mathsf{X}_0, \mathsf{p}_i))|, \tag{180}$$

determine a partition $V^d = \{V_i^d :\ i \in \mathcal{I}_n\}$ *of* $\mathbb{R}^2$ *such that*

i) $\mathbb{R}^2 = \bigcup_{i\in\mathcal{I}_n} V_i^d$.

ii) $\overline{V_i^d} = V_i^d$, for each $i \in \mathcal{I}_n$.

iii) $c^d(\mathsf{X}, \mathsf{P}_i) < c^d(\mathsf{x}, \mathsf{P}_j)$, for $j \neq i$ and for all $\mathsf{X} \in \mathrm{int}(V_i^d)$, .

Note that in the formulation of the DVDP the generalized distance function does not depend explicitly on time. The generalized distance function is the Euclidean distance between the initial configuration of the agent and the location of the moving target P_i at a specific instant of time, namely, $T_{\mathrm{f}}(\mathsf{x}_0, \mathsf{p}_i)$, that is, at the time when the pursuer, whose kinematics are described by equation (177), intercepts the moving

target P_i (minimum intercept time). Figure 42 illustrates the interpretation of the ZVDP as a Dynamic Voronoi Diagram Problem. In particular, the target set, which is at time $t = 0$ the set of Voronoi generators $P = \{\mathsf{p}_i,\ i \in \mathcal{I}_n\}$ of the ZVDP, moves uniformly with time along the integral curves of the velocity field $-w$.

As it has been shown previously, the system (172) emanating from $\mathsf{X}(0) = \mathsf{X}_0$ reaches a point X_f in minimum time $T_\mathrm{f} = |\mathsf{X}_0 - \mathsf{X}_\mathrm{f}|$. Thus, by reversing time in (174), the system (169) starting from point x'_0 at $t = 0$ reaches the point $\mathsf{x}_\mathrm{f} = \mathsf{X}_\mathrm{f}$ in minimum time $T_\mathrm{f} = |\mathsf{X}_0 - \mathsf{X}_\mathrm{f}|$, provided that

$$\mathsf{x}'_0 = \mathsf{X}_0 - \int_0^{d(\mathsf{X}_0,\mathsf{X}_\mathrm{f})} w(\tau)\,\mathrm{d}\tau, \tag{181}$$

where $d(\mathsf{X}_0, \mathsf{X}_\mathrm{f}) := |\mathsf{X}_0 - \mathsf{X}_\mathrm{f}|$.

For each p, equation (181) induces a state transformation $f_\mathsf{p} : \mathbb{R}^2 \mapsto \mathbb{R}^2$ where

$$f_\mathsf{p}(\mathsf{X}) := \mathsf{X} - \int_0^{d(\mathsf{X},\mathsf{p})} w(\tau)\,\mathrm{d}\tau. \tag{182}$$

The following proposition will prove useful for the following discussion.

Proposition 37. *Let $\mathsf{p} \in \mathbb{R}^2$ be given. The state transformation in (182) defines a bijective mapping with non-singular Jacobian for all $\mathsf{X} \in \mathbb{R}^2$, provided that $|w(t)| < 1$ for all $t \geq 0$.*

Proof. First, it is shown that f_p is an injective mapping. Let X_1 and X_2 be such that $f_\mathsf{p}(\mathsf{X}_1) = f_\mathsf{p}(\mathsf{X}_2)$, equivalently,

$$\mathsf{X}_2 - \mathsf{X}_1 = \int_{d(\mathsf{X}_2,\mathsf{p})}^{d(\mathsf{X}_1,\mathsf{p})} w(\tau)\,\mathrm{d}\tau. \tag{183}$$

Thus,

$$|\mathsf{X}_2 - \mathsf{X}_1| \leq \int_{d(\mathsf{X}_2,\mathsf{p})}^{d(\mathsf{X}_1,\mathsf{p})} |w(\tau)|\,\mathrm{d}\tau. \tag{184}$$

Since $|w(t)| < 1$ for all $t \geq 0$, it follows that

$$|\mathsf{X}_2 - \mathsf{X}_1| \leq |d(\mathsf{X}_1, \mathsf{p}) - d(\mathsf{X}_2, \mathsf{p})| \leq |\mathsf{X}_2 - \mathsf{X}_1|, \tag{185}$$

and thus $\mathsf{X}_2 = \mathsf{X}_1$. Furthermore, the Jacobian of f_{p} at X is equal to

$$Df_{\mathsf{p}}(\mathsf{X}) = I_2 - w(d(\mathsf{X},\mathsf{p}))(\mathsf{X}-\mathsf{p})^{\mathsf{T}}/d(\mathsf{X},\mathsf{p}). \tag{186}$$

It can be shown easily that the nonzero eigenvalue of the rank one matrix $w(d(\mathsf{X},\mathsf{p}))(\mathsf{X}-\mathsf{p})^{\mathsf{T}}/d(\mathsf{X},\mathsf{p})$ is given by

$$\lambda_2(\mathsf{X}) = w^{\mathsf{T}}(d(\mathsf{X},\mathsf{p}))(\mathsf{X}-\mathsf{p})/d(\mathsf{X},\mathsf{p}) \leq |w(d(\mathsf{X},\mathsf{p}))| < 1. \tag{187}$$

Thus $0 \notin \mathrm{spec}(Df_{\mathsf{p}}(\mathsf{X}))$ and the Jacobian $Df_{\mathsf{p}}(\mathsf{X})$ is non-singular for all $\mathsf{X} \in \mathbb{R}^2$. Finally, because the Jacobian of F is nonsingular everywhere, it follows, in light of the surjective mapping theorem [26, p. 378], that F is surjective. □

The following two propositions follow readily from the previous discussion.

Proposition 38. *The coordinates of every element of the set P are invariant under the state transformation* (182)*, that is, $f_{\mathsf{p}}(\mathsf{p}) = \mathsf{p}$, for all $\mathsf{p} \in P$.*

Proposition 39. *Let $\mathsf{p} \in \mathbb{R}^2$ be given. Then $c(\mathsf{x},\mathsf{p}) = |\mathsf{X}-\mathsf{p}|$, provided that $\mathsf{x} = f_{\mathsf{p}}(\mathsf{X})$.*

In the next section, the interpretation of the ZNP as an optimal pursuit problem will allow us to associate the ZVD with the standard Voronoi diagram of the same set of generators by means of a homeomorphism which derives, in turn, from the state transformation (181).

Remark 10 Notice that although in this interpretation of the ZNP as a pursuer/moving target problem both the targets and (virtual) pursuers are moving, the Zermelo-Voronoi partition $\mathfrak{V}$ is independent of their motion after time $t = 0$. This is because it is assumed that each agent/pursuer follows the optimal min-time intercept strategy to each target. The final partition therefore already encodes the effect of the future motion of each agent and there is no need to re-compute the standard Voronoi partitions as the targets move along the integral curves of the (negative) velocity field.

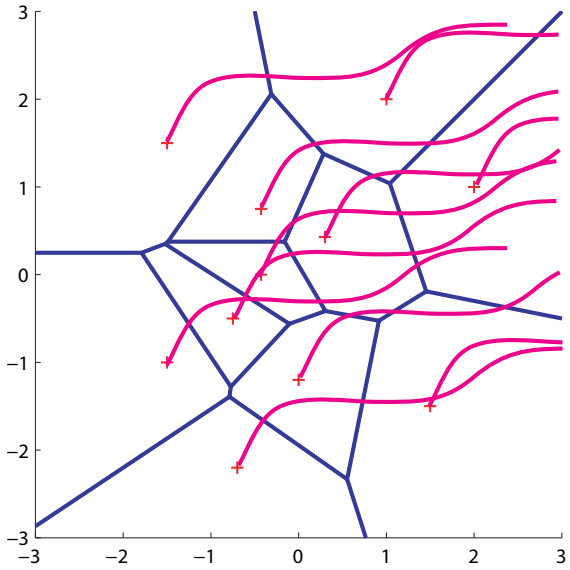

Figure 42: The Zermelo-Voronoi Diagram can be interpreted as a Dynamic Voronoi Diagram.

7.4 Construction of the Zermelo-Voronoi Diagram

In this section, we present the steps required for the construction of the ZVD. In particular, we show that, for the case of two Voronoi generators, the state transformation (182) directly associates the ZVD with the standard Voronoi Diagram generated by the same pair of generators. Subsequently, the previous result are generalized to the case of arbitrary finite sets of Voronoi generators.

Let us first consider two distinct points, p_1 and p_2, in the Euclidean plane. The bisector of p_1 and p_2 is the straight line $\chi(\mathsf{p}_1, \mathsf{p}_2)$ defined by

$$\begin{aligned}\chi(\mathsf{p}_1, \mathsf{p}_2) &:= \left\{\mathsf{X} \in \mathbb{R}^2 : |\mathsf{X} - \mathsf{p}_1| = |\mathsf{X} - \mathsf{p}_2|\right\} \\ &= \left\{\mathsf{X} \in \mathbb{R}^2 : (\mathsf{p}_2 - \mathsf{p}_1)^\intercal \mathsf{X} = (|\mathsf{p}_2|^2 - |\mathsf{p}_1|^2)/2\right\}.\end{aligned}$$

Correspondingly, the bisector of p_1 and p_2 with respect to the cost (171) is the curve $\gamma(\mathsf{p}_1, \mathsf{p}_2)$ defined by

$$\gamma(\mathsf{p}_1, \mathsf{p}_2) := \{\mathsf{x} \in \mathbb{R}^2 : c(\mathsf{x}, \mathsf{p}_1) = c(\mathsf{x}, \mathsf{p}_2)\}. \tag{188}$$

The bisector $\chi(\mathsf{p}_1, \mathsf{p}_2)$ divides $\mathbb{R}^2$ into two closed half-planes, namely $H_1(\mathsf{p}_1, \mathsf{p}_2) = \{\mathsf{X} \in \mathbb{R}^2 : |\mathsf{X} - \mathsf{p}_1| \leq |\mathsf{X} - \mathsf{p}_2|\}$ and $H_2(\mathsf{p}_1, \mathsf{p}_2) = \{\mathsf{X} \in \mathbb{R}^2 : |\mathsf{X} - \mathsf{p}_1| \geq |\mathsf{X} - \mathsf{p}_2|\}$.

The following proposition will allow us to associate the sets of points that are closer, in terms of the cost (171), to p_1 and p_2 with the half planes $H_1(\mathsf{p}_1, \mathsf{p}_2)$ and $H_2(\mathsf{p}_1, \mathsf{p}_2)$, respectively, by means of a homeomorphism.

Proposition 40. *Given $\mathsf{p}_1, \mathsf{p}_2 \in \mathbb{R}^2$, and a time-varying drift w, with $|w(t)| < 1$ for all $t \geq 0$, and let the function $F : \mathbb{R}^2 \mapsto \mathbb{R}^2$ be defined by*

$$F(\mathsf{X}) := \begin{cases} f_{\mathsf{p}_1}(\mathsf{X}), & \mathsf{X} \in H_1(\mathsf{p}_1, \mathsf{p}_2), \\ f_{\mathsf{p}_2}(\mathsf{X}), & \mathsf{X} \in H_2(\mathsf{p}_1, \mathsf{p}_2). \end{cases} \tag{189}$$

Then the following statements are true.

i) The map F is continuous for all $\mathsf{X} \in \mathbb{R}^2$ and continuously differentiable for all $\mathsf{X} \notin \chi(\mathsf{p}_1, \mathsf{p}_2)$.

ii) The sets $F(H_1(\mathsf{p}_1, \mathsf{p}_2))$ and $F(H_2(\mathsf{p}_1, \mathsf{p}_2))$ are connected.

iii) The sets $F(H_1(\mathsf{p}_1, \mathsf{p}_2))$ and $F(H_2(\mathsf{p}_1, \mathsf{p}_2))$ are closed, and $\partial F(H_1(\mathsf{p}_1, \mathsf{p}_2)) = \partial F(H_2(\mathsf{p}_1, \mathsf{p}_2)) = F(\chi(\mathsf{p}_1, \mathsf{p}_2))$.

iv) $\mathrm{int}(F(H_1(\mathsf{p}_1, \mathsf{p}_2))) \cap \mathrm{int}(F(H_2(\mathsf{p}_1, \mathsf{p}_2))) = \varnothing$ and $F(H_1(\mathsf{p}_1, \mathsf{p}_2)) \cap F(H_2(\mathsf{p}_1, \mathsf{p}_2)) = F(\chi(\mathsf{p}_1, \mathsf{p}_2))$.

v) The map F is a homeomorphism.

vi) $\mathsf{p}_1 \in \mathrm{int}(F(H_1(\mathsf{p}_1, \mathsf{p}_2)))$ and $\mathsf{p}_2 \in \mathrm{int}(F(H_2(\mathsf{p}_1, \mathsf{p}_2)))$.

vii) For all $\mathsf{x} \in \mathrm{int}(F(H_1(\mathsf{p}_1, \mathsf{p}_2)))$, we have that $c(\mathsf{x}, \mathsf{p}_1) < c(\mathsf{x}, \mathsf{p}_2)$. Similarly, for all $\mathsf{x} \in \mathrm{int}(F(H_2(\mathsf{p}_1, \mathsf{p}_2)))$, we have that $c(\mathsf{x}, \mathsf{p}_2) < c(\mathsf{x}, \mathsf{p}_1)$.

viii) The bisector of p_1 and p_2 with respect to the cost c satisfies

$$\gamma(\mathsf{p}_1, \mathsf{p}_2) = \{\mathsf{x} \in \mathbb{R}^2 : \mathsf{x} = F(\mathsf{X}),\ \mathsf{X} \in \chi(\mathsf{p}_1, \mathsf{p}_2)\}.$$

Proof. *i*) First, we show that F is well defined for $\mathsf{X} \in H_1(\mathsf{p}_1, \mathsf{p}_2) \cap H_2(\mathsf{p}_1, \mathsf{p}_2) = \chi(\mathsf{p}_1, \mathsf{p}_2)$. In particular, for $\mathsf{X} \in \chi(\mathsf{p}_1, \mathsf{p}_2)$, we have that $d(\mathsf{X}, \mathsf{p}_1) = d(\mathsf{X}, \mathsf{p}_2)$, which implies that $f_{\mathsf{p}_1}(\mathsf{X}) = f_{\mathsf{p}_2}(\mathsf{X})$. The continuity of F follows readily. Furthermore, the Jacobian of F is well defined and invertible (see Proposition 37) for all $\mathsf{X} \in \mathbb{R}^2 \backslash \chi(\mathsf{p}_1, \mathsf{p}_2)$, and it is given by (186) for X in $H_1(\mathsf{p}_1, \mathsf{p}_2)$ and $H_2(\mathsf{p}_1, \mathsf{p}_2)$, respectively.

ii) It follows immediately from the continuity of F.

iii) First, notice that the restriction of F on $H_1(\mathsf{p}_1, \mathsf{p}_2)$ is f_{p_1} which is an injective, continuously differentiable map with non-singular Jacobian (Proposition 37). It follows that f_{p_1} is a diffeomorphism from $H_1(\mathsf{p}_1, \mathsf{p}_2)$ to $F(H_1(\mathsf{p}_1, \mathsf{p}_2)) = f_{\mathsf{p}_1}(H_1(\mathsf{p}_1, \mathsf{p}_2))$ and therefore $F(H_1(\mathsf{p}_1, \mathsf{p}_2))$ is closed since $H_1(\mathsf{p}_1, \mathsf{p}_2))$ is closed. Furthermore, $\partial F(H_1(\mathsf{p}_1, \mathsf{p}_2)) = F(\partial H_1(\mathsf{p}_1, \mathsf{p}_2)) = F(\chi(\mathsf{p}_1, \mathsf{p}_2))$. The proof for $F(H_2(\mathsf{p}_1, \mathsf{p}_2))$ is similar.

iv) Assume, on the contrary, that there exists $\mathsf{y} \in \text{int}(F(H_1(\mathsf{p}_1, \mathsf{p}_2))) \cap \text{int}(F(H_2(\mathsf{p}_1, \mathsf{p}_2)))$. It follows from iii) that there are points $\mathsf{X}_1 \in \text{int}(H_1(\mathsf{p}_1, \mathsf{p}_2))$ and $\mathsf{X}_2 \in \text{int}(H_2(\mathsf{p}_1, \mathsf{p}_2))$ with $F(\mathsf{X}_1) = F(\mathsf{X}_2) = \mathsf{y}$. Thus $c(F(\mathsf{X}_1), \mathsf{p}_1) = c(F(\mathsf{X}_2), \mathsf{p}_1)$ and $c(F(\mathsf{X}_1), \mathsf{p}_2) = c(F(\mathsf{X}_2), \mathsf{p}_2)$, which imply, using Proposition 39, that $|\mathsf{X}_1 - \mathsf{p}_1| = |\mathsf{X}_2 - \mathsf{p}_1| = \delta_1$ and $|\mathsf{X}_1 - \mathsf{p}_2| = |\mathsf{X}_2 - \mathsf{p}_2| = \delta_2$ respectively, for some positive constants δ_1 and δ_2. Thus X_1 and X_2 lie necessarily at the intersection of two circles centered at p_i with radii δ_i, $i \in \{1, 2\}$, respectively. This intersection is non-empty if one of the following conditions hold true: a) $\delta_1 < \delta_2$ with $|\mathsf{p}_1 - \mathsf{p}_2| \leq \delta_1 + \delta_2$, which implies that both X_1 and X_2 are in $H_1(\mathsf{p}_1, \mathsf{p}_2)$, b) $\delta_1 > \delta_2$ with $|\mathsf{p}_1 - \mathsf{p}_2| \leq \delta_1 + \delta_2$, which implies that both X_1 and X_2 are in $H_2(\mathsf{p}_1, \mathsf{p}_2)$ and finally, c) $\delta_1 = \delta_2$ with $|\mathsf{p}_1 - \mathsf{p}_2| \leq \delta_1 + \delta_2$, which implies that both X_1 and X_2 are in $\chi(\mathsf{p}_1, \mathsf{p}_2)$. All previous cases contradict the assumption that $\mathsf{X}_1 \in \text{int}(H_1(\mathsf{p}_1, \mathsf{p}_2))$ and $\mathsf{X}_2 \in \text{int}(H_2(\mathsf{p}_1, \mathsf{p}_2))$. The second part of the statement follows readily.

v) First, we show that F is injective. First, notice that, by definition, F is injective on $H_1(\mathsf{p}_1, \mathsf{p}_2)$ and $H_2(\mathsf{p}_1, \mathsf{p}_2)$. Let now $\mathsf{X}_1 \in \text{int}(H_1(\mathsf{p}_1, \mathsf{p}_2))$ and $\mathsf{X}_2 \in \text{int}(H_2(\mathsf{p}_1, \mathsf{p}_2))$ and assume, on the contrary, that $F(\mathsf{X}_1) = F(\mathsf{X}_2)$. But $F(\mathsf{X}_1) \in F(\text{int}(H_1(\mathsf{p}_1, \mathsf{p}_2))) \subseteq \text{int}(F(H_1(\mathsf{p}_1, \mathsf{p}_2)))$ since the restriction of F on $H_1(\mathsf{p}_1, \mathsf{p}_2)$ is an open map. Similarly, $F(\mathsf{X}_2) \in F(\text{int}(H_2(\mathsf{p}_1, \mathsf{p}_2))) \subseteq \text{int}(F(H_2(\mathsf{p}_1, \mathsf{p}_2)))$. Hence $F(\mathsf{X}_1) = F(\mathsf{X}_2)$ implies that $\text{int}(F(H_1(\mathsf{p}_1, \mathsf{p}_2))) \cap \text{int}(F(H_2(\mathsf{p}_1, \mathsf{p}_2))) \neq \varnothing$, which contradicts iv). Since F is injective it follows readily that its inverse F^{-1} exists and is defined by

$$F^{-1}(\mathsf{x}) := \begin{cases} f_{\mathsf{p}_1}^{-1}(\mathsf{x}), & \mathsf{x} \in F(H_1(\mathsf{p}_1, \mathsf{p}_2)), \\ f_{\mathsf{p}_2}^{-1}(\mathsf{x}), & \mathsf{x} \in F(H_2(\mathsf{p}_1, \mathsf{p}_2)), \end{cases}$$

with $f_{\mathsf{p}_1}^{-1}$ and $f_{\mathsf{p}_2}^{-1}$ continuous on $H_1(\mathsf{p}_1, \mathsf{p}_2)$ and $H_2(\mathsf{p}_1, \mathsf{p}_2)$, respectively. Next we show that F^{-1} is a continuous function for all $\mathsf{x} \in \mathbb{R}^2$. It suffices to show that F^{-1} is well defined for $\mathsf{x} \in F(H_1(\mathsf{p}_1, \mathsf{p}_2)) \cap F(H_2(\mathsf{p}_1, \mathsf{p}_2)) = F(\chi(\mathsf{p}_1, \mathsf{p}_2))$. To this end, notice that the statement $\mathsf{x} \in F(\chi(\mathsf{p}_1, \mathsf{p}_2))$ implies that there exists $\mathsf{X} \in \chi(\mathsf{p}_1, \mathsf{p}_2)$ such that $\mathsf{x} = F(\mathsf{X})$. But $\mathsf{X} \in \chi(\mathsf{p}_1, \mathsf{p}_2)$ implies that $|\mathsf{X} - \mathsf{p}_1| = |\mathsf{X} - \mathsf{p}_2|$ and hence $\mathsf{x} = f_{\mathsf{p}_1}(\mathsf{X}) = f_{\mathsf{p}_2}(\mathsf{X})$. It follows that $f_{\mathsf{p}_1}^{-1}(\mathsf{x}) = f_{\mathsf{p}_2}^{-1}(\mathsf{x})$ for all $\mathsf{x} \in F(\chi(\mathsf{p}_1, \mathsf{p}_2))$.

vi) Since $\mathsf{p}_1 \in \text{int}(H_1(\mathsf{p}_1, \mathsf{p}_2))$ [$\mathsf{p}_2 \in \text{int}(H_2(\mathsf{p}_1, \mathsf{p}_2))$] and the restriction of F on $\text{int}(H_1(\mathsf{p}_1, \mathsf{p}_2))$ [$\text{int}(H_2(\mathsf{p}_1, \mathsf{p}_2))$] yields an open map, it follows that $\mathsf{p}_1 = F(\mathsf{p}_1) \in F(\text{int}(H_1(\mathsf{p}_1, \mathsf{p}_2))) \subset \text{int}(F(H_1(\mathsf{p}_1, \mathsf{p}_2)))$ [$\mathsf{p}_2 \in \text{int}(F(H_2(\mathsf{p}_1, \mathsf{p}_2))$].

vii) Let us assume, on the contrary, that there exists $\mathsf{x} \in \text{int}(F(H_1(\mathsf{p}_1, \mathsf{p}_2)))$ such that $c(\mathsf{x}, \mathsf{p}_1) \geq c(\mathsf{x}, \mathsf{p}_2)$. Let $\mathsf{X} \in H_1(\mathsf{p}_1, \mathsf{p}_2)$ such $\mathsf{x} = F(\mathsf{X})$. Note that iii) implies that $\mathsf{X} \in \text{int}(H_1(\mathsf{p}_1, \mathsf{p}_2))$. It follows from Proposition 39 that $|\mathsf{X} - \mathsf{p}_1| \geq |\mathsf{X} - \mathsf{p}_2|$, contradicting the fact that $\mathsf{X} \in \text{int}(H_1(\mathsf{p}_1, \mathsf{p}_2))$.

viii) The proof follows from iii), vii) and Proposition 39.

□

Figure 43(b) illustrate how the half-planes $H_1(\mathsf{p}_1, \mathsf{p}_2)$ and $H_2(\mathsf{p}_1, \mathsf{p}_2)$ and the bisector curve $\chi(\mathsf{p}_1, \mathsf{p}_2)$ are transformed under the mapping F. Note that every point in $\chi(\mathsf{p}_1, \mathsf{p}_2)$ is equidistant, with respect to the Euclidean distance, to p_1 and p_2, and the same is true for the curve $\gamma(\mathsf{p}_1, \mathsf{p}_2)$, which is the image of $\chi(\mathsf{p}_1, \mathsf{p}_2)$ under F, with respect, however, to the generalized distance function (171). Furthermore, if $\mathsf{A} \in \chi(\mathsf{p}_1, \mathsf{p}_2)$ with $|\mathsf{p}_1 - \overrightarrow{\mathsf{OA}}| = |\mathsf{p}_2 - \overrightarrow{\mathsf{OA}}| = \delta$, then it also holds that $T_{\mathrm{f}}(\mathsf{C}, \mathsf{p}_1) = T_{\mathrm{f}}(\mathsf{C}, \mathsf{p}_2) = \delta$, where the point C lies on the curve $\gamma(\mathsf{p}_1, \mathsf{p}_2)$ and satisfies $\overrightarrow{\mathsf{OC}} = F(\overrightarrow{\mathsf{OA}})$.

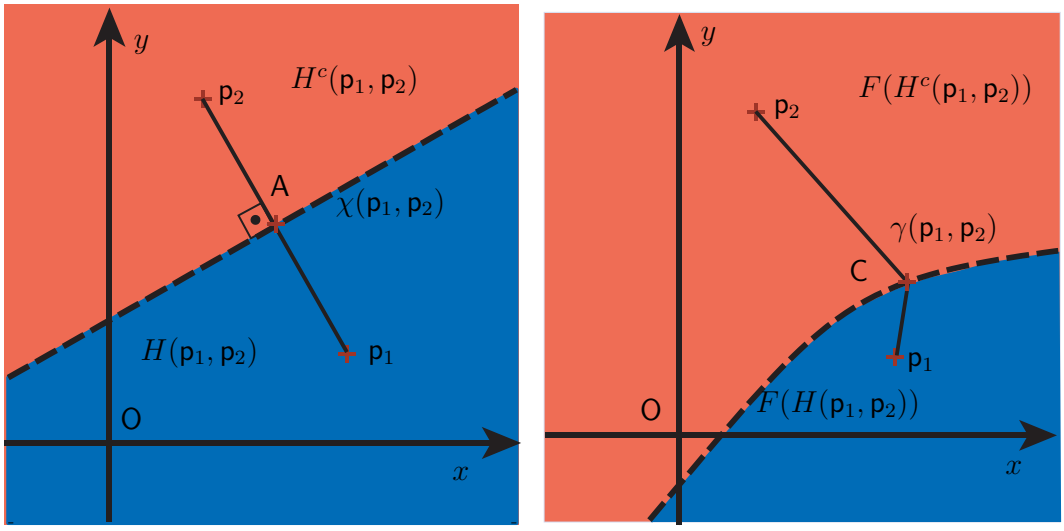

(a) The bisector χ and two half planes $H(\mathsf{p}_1, \mathsf{p}_2)$ and $H^c(\mathsf{p}_1, \mathsf{p}_2)$.

(b) The images of χ, $H(\mathsf{p}_1, \mathsf{p}_2)$ and $H^c(\mathsf{p}_1, \mathsf{p}_2)$ under the mapping F.

Figure 43: The image of the bisector $\chi(\mathsf{p}_1, \mathsf{p}_2)$ under the mapping F, denoted as $\gamma(\mathsf{p}_1, \mathsf{p}_2)$, is the bisector of p_1 and p_2 with respect to the generalized distance function of Problem 10.

Proposition 40 deals with the construction of the ZVD in the special case $P = \{\mathsf{p}_1, \mathsf{p}_2\}$. In particular, it implies that $\mathfrak{V} = \{\mathfrak{V}_1, \mathfrak{V}_2\}$, where $\mathfrak{V}_1 = F(H_1(\mathsf{p}_1, \mathsf{p}_2))$ and $\mathfrak{V}_2 = F(H_2(\mathsf{p}_1, \mathsf{p}_2))$. Furthermore, the standard Voronoi Diagram of $P = \{\mathsf{p}_1, \mathsf{p}_2\}$ is given by $V = \{V_1, V_2\}$, where $V_1 = H_1(\mathsf{p}_1, \mathsf{p}_2)$ and $V_2 = H_2(\mathsf{p}_1, \mathsf{p}_2)$. Therefore, $\mathfrak{V} = \{F(V_1), F(V_2)\}$. We are now ready to state the main theorem of this chapter.

Theorem 2. *Let $V := \{V_i, i \in \mathcal{I}_n\}$ be the standard Voronoi partition generated by the point-set $P := \{\mathsf{p}_i, i \in \mathcal{I}_n\}$. Assume that $|w(t)| < 1$, for all $t \geq 0$ and let the function $F : \mathbb{R}^2 \mapsto \mathbb{R}^2$ be defined by*

$$F(\mathsf{X}) = f_{\mathsf{p}_i}(\mathsf{X}), \qquad \mathsf{X} \in V_i,\ i \in \mathcal{I}_n, \tag{190}$$

where

$$f_{\mathsf{p}_i}(\mathsf{X}) = \mathsf{X} - \int_0^{d(\mathsf{X},\mathsf{p}_i)} w(\tau)\,\mathrm{d}\tau, \quad i \in \mathcal{I}_n. \tag{191}$$

The solution of the ZVDP is the partition defined by the image of V under the mapping F, that is,

$$\mathfrak{V} := \{\mathfrak{V}_i :\ i \in \mathcal{I}_n\} = F(V) := \{f_{\mathsf{p}_i}(V_i) :\ \ i \in \mathcal{I}_n\}, \tag{192}$$

or equivalently, $\mathfrak{V}_i = f_{\mathsf{p}_i}(V_i)$, for all $i \in \mathcal{I}_n$.

Proof. The Dirichlet domain V_i of the standard Voronoi partition V is determined by [84]

$$V_i = \bigcap_{j \neq i} H_i(\mathsf{p}_i, \mathsf{p}_j). \tag{193}$$

Thus

$$F(V_i) = F(\bigcap_{j \neq i} H_i(\mathsf{p}_i, \mathsf{p}_j)), \tag{194}$$

which implies, by virtue of F being injective (Proposition 40(v)), that $F(V_i) = \bigcap_{j \neq i} F(H_i(\mathsf{p}_i, \mathsf{p}_j))$. The proof can be carried out similarly to Proposition 40 using induction. □

Corollary 2. *Let $\mathfrak{V} := \{F(V_i) :\ \ i \in \mathcal{I}_n\}$ be the Voronoi partition for the set of Voronoi generators $P := \{\mathsf{p}_i, i \in \mathcal{I}_n\}$ of Problem 9. Then*

i) The sets $F(V_i)$ are closed and connected.

ii) $\mathsf{p}_i \in \mathrm{int}(F(V_i))$.

iii) If $\mathsf{p}_i \in \partial\text{co}(P)$*, where* $\text{co}(P)$ *denotes the convex hull of the set* P*, then* $F(V_i)$ *is an unbounded set, and it is a compact set otherwise.*

Proof. The proofs of (i) and (ii) follow similarly as the proofs of (i), (ii) and (vi) of Proposition 40. To prove (iii), first note that a Dirichlet domain V_i of the standard Voronoi Diagram of P is an unbounded set if and only if $\mathsf{p}_i \in \partial\text{co}(P)$ [84] and it is a compact set otherwise. Thus, by virtue of (v) of Proposition 40, the Dirichlet domain $F(V_i) = \mathfrak{V}_i$ that corresponds to $\mathsf{p}_i \in \partial\text{co}(P)$ is an unbounded set. Finally, if $\mathsf{p}_i \notin \partial\text{co}(P)$, then the Dirichlet domain V_i and its image under the continuous mapping F are both compact sets.

□

7.5 The Dual Zermelo-Voronoi Diagram

So far, we have presented a methodology for constructing a generalized Voronoi Diagram with respect to the minimum time from a point in plane to the set of generators (obtained from the solution of Zermelo's navigation problem). In many autonomous agent applications, however, it may be more appropriate to consider the Voronoi generators to be the agents' locations at a particular instant of time rather than being the destinations. For instance, consider the following scenario: Given a group of agents/guards distributed over a certain area, divide this area into guard/patrol zones (one for each agent) such that each point in a zone can be reached/intercepted by the corresponding agent faster than any other agent. Such a decomposition essentially provides a "first response" partition of the area for which the agents are responsible.

In this context, given the positions of a finite set of agents at time $t = 0$, we want to characterize, for every $i \in \mathcal{I}_n$, where $\mathcal{I}_n$ denotes the index set of the set of agents, the collections of all positions, denoted as $\tilde{\mathfrak{V}}_i$, that can be reached by the agent i faster than any other agent j, with $j \neq i$. We call the problem of characterizing the partition $\tilde{\mathfrak{V}} := \{\tilde{\mathfrak{V}}_i : \ i \in \mathcal{I}_n\}$ the Dual Zermelo-Voronoi Diagram Problem (DZVDP).

Note that, as already mentioned, the minimum time of the ZNP is, in general, non-symmetric, that is, the minimum time to drive the system (169) from a point A to B, and vice versa, are not necessarily equal. Therefore the solutions of the DZVDP and the ZVDP are not expected to be the same, in general.

The DZVDP can be formulated similarly to the ZVDP. In particular, the distance function for the DZVDP is defined by

$$\tilde{c}(\mathsf{p}_i, \mathsf{x}_\mathrm{f}) := T_\mathrm{f}(\mathsf{p}_i, \mathsf{x}_\mathrm{f}), \tag{195}$$

that is, the minimum time for the Zermelo navigation problem from a Voronoi generator p_i to the agent's terminal configuration x_f. The generalized distance function for the DZVDP can be reduced to the distance function for the ZVDP by reversing the order of the function arguments. The construction of the DZVDP is thus similar to the solution of the ZVDP.

Corollary 3. *Let $V := \{V_i : \quad i \in \mathcal{I}_n\}$ be the standard Voronoi partition for the set of Voronoi generators $P := \{\mathsf{p}_i : \ i \in \mathcal{I}_n\}$. Assume that $|w(t)| < 1$ for all $t \geq 0$ and let the function $\tilde{F} : \mathbb{R}^2 \mapsto \mathbb{R}^2$ be defined by*

$$\tilde{F}(\mathsf{X}) := \tilde{f}_{\mathsf{p}_i}(\mathsf{X}), \qquad \mathsf{X} \in V_i, \quad i \in \mathcal{I}_n, \tag{196}$$

where

$$\tilde{f}_{\mathsf{p}_i}(\mathsf{X}) := \mathsf{X} + \int_0^{d(\mathsf{X},\mathsf{p}_i)} w(\tau)\,\mathrm{d}\tau, \quad i \in \mathcal{I}_n. \tag{197}$$

Then the solution of the DZVDP is the partition be defined by the image of the set V under the mapping $\tilde{F}$, that is,

$$\tilde{\mathfrak{V}} := \{\tilde{\mathfrak{V}}_i : \quad i \in \mathcal{I}_n\} = \tilde{F}(V) = \{\tilde{f}_{\mathsf{p}_i}(V_i) : \quad i \in \mathcal{I}_n\}, \tag{198}$$

or equivalently, $\tilde{\mathfrak{V}}_i := \tilde{f}_{\mathsf{p}_i}(V_i)$, for all $i \in \mathcal{I}_n$.

Note that the transformation (197) of the DZVDP differs from the transformation (191) of the ZVDP by a sign change.

7.6 Simulation Results

In this section, we provide numerical simulations to better illustrate the previous developments. Let us assume that the wind velocity field is defined by

$$w(t) = \begin{cases} \bar{w} + \rho t, \ 0 \leq t \leq \bar{t}, \\ \bar{w} + \rho \bar{t}, \quad t > \bar{t}, \end{cases} \tag{199}$$

where $\bar{w} = (\mu, \nu)^\intercal \in \mathbb{R}^2$ with $|\bar{w}| < 1$, $\rho \in \mathbb{R}^2$ constants, and $\bar{t} < (1 - |\bar{w}|)/|\rho|$.

We first construct the Zermelo-Voronoi Diagram by gridding the entire space and propagating the isocost fronts of the respective min-time problems emanating from each generator and we compare the results with the proposed approach of this chapter in terms of computational efficiency. In particular, given a set of Voronoi generators $P := \{\mathsf{p}_i : \ i \in \mathcal{I}_n\}$, the minimum cost-to-go from x to some $\mathsf{p}_i \in P$ is defined as the function

$$K_{\mathsf{p}_i}(\mathsf{x}) := c(\mathsf{x}, \mathsf{p}_i). \tag{200}$$

Note that, for the particular wind field in (199), it readily follows that $c(\mathsf{x}, \mathsf{p}_i)$ is the smallest positive root of either the polynomial equation

$$\begin{aligned} \frac{|\rho|^2}{4} T_{\mathrm{f}}^4 + \bar{w}^\intercal \rho T_{\mathrm{f}}^3 + (|\bar{w}|^2 - 1 - (\mathsf{p}_i - \mathsf{x})^\intercal \rho) T_{\mathrm{f}}^2 \\ - 2(\mathsf{p}_i - \mathsf{x})^\intercal \bar{w} T_{\mathrm{f}} + |\mathsf{p}_i - \mathsf{x}|^2 = 0, \end{aligned} \tag{201}$$

if $T_{\mathrm{f}} < \bar{t}$, or the quadratic equation

$$\begin{aligned} (|\bar{w} + \rho \bar{t}| - 1) T_{\mathrm{f}}^2 - (2(\mathsf{p}_i - \mathsf{x}) + \bar{t}^2 \rho)^\intercal (\bar{w} + \rho \bar{t}) T_{\mathrm{f}} \\ + |\mathsf{p}_i - \mathsf{x}|^2 + \bar{t}^2 (\mathsf{p}_i - \mathsf{x})^\intercal \rho + \bar{t}^2 |\rho|^2 / 4 = 0, \end{aligned} \tag{202}$$

if $T_{\mathrm{f}} \geq \bar{t}$. Furthermore, the minimum cost-to-go to the set P is defined as the function

$$K_P(\mathsf{x}) = \min_{\mathsf{p}_i \in P} c(\mathsf{x}, \mathsf{p}_i). \tag{203}$$

Each Dirichlet domain of the ZVD can be determined by projecting the intersection of the surfaces K_P and K_{p_i} onto $\mathbb{R}^2$. Figure 44 illustrates a fine approximation

of the ZVD, which is constructed by the previous exhaustive numerical method for $\bar{w} = (-0.3, 0.2)$, $\rho = (0.05, -0.1)$, and a set of eleven Voronoi generators.

A more computationally tractable approach, compared to solving directly the polynomial equations in (201)-(202) for each node of a fine grid that discretizes the space, is to expand the iso-cost fronts of each K_{p} by means of a fast marching algorithm. The fast marching implementation will give an approximation of the ZVD with time complexity $O(NM^2 \log M)$, where N is the number of elements of P, and M^2 is the number of nodes of a grid that discretizes $\mathbb{R}^2$ [183, 139]. Note that the boundaries of each Dirichlet domain of the ZVD are not line segments, in general, and thus for their specification a fine grid is required, that is, the size of the grid should be at least of order $O(N^{\eta})$, where $\eta > 2$.

Next, the approach introduced in this chapter is applied. In particular, the standard Voronoi Diagram of the set P is first constructed, and subsequently, the Zermelo-Voronoi Diagram is obtained with the application of Theorem 1. Note that the construction of the standard Voronoi Diagram requires $O(N \log N)$ time, where N is the number of elements of P, by using, for example, Fortune's algorithm [80, 144]. The mapping of the standard Voronoi Diagram, which consists of $O(N)$ edges, to the ZVD requires $O(N)$ time, giving a total time complexity for the construction of the ZVD which is of order $O(N \log N)$. Note, additionally, that the approach of this chapter is completely grid-free, and it does not also require the solution of a PDE by contrast to the fast marching approach. These remarks elucidate the significance of the results presented in Section 7.4 from a computational perspective. Figure 45 illustrates the ZVD obtained after the application of the state-transformation to the standard Voronoi Diagram.

Figure 46 illustrates the ZVD and the DZVD partitions for the wind velocity fields $w_1(t) = (0.5 + 0.1\sin(t/\pi), -0.35 - 0.1\cos(t/\pi))$ (Fig. 46(a)) and $w_2(t) = (0.15, 0.65 - 0.2\exp(-t/\pi))$ (Fig. 46(b)). It is interesting to note that, as the wind

becomes stronger, the Voronoi generators move closer to the boundaries of their corresponding Dirichlet domains, a pattern similar to the one observed in [194]. In all cases, however, the generators remain interior to their corresponding domains, in light of Proposition 40 (vi), provided that $|w(t)| < 1$ for all $t \geq 0$.

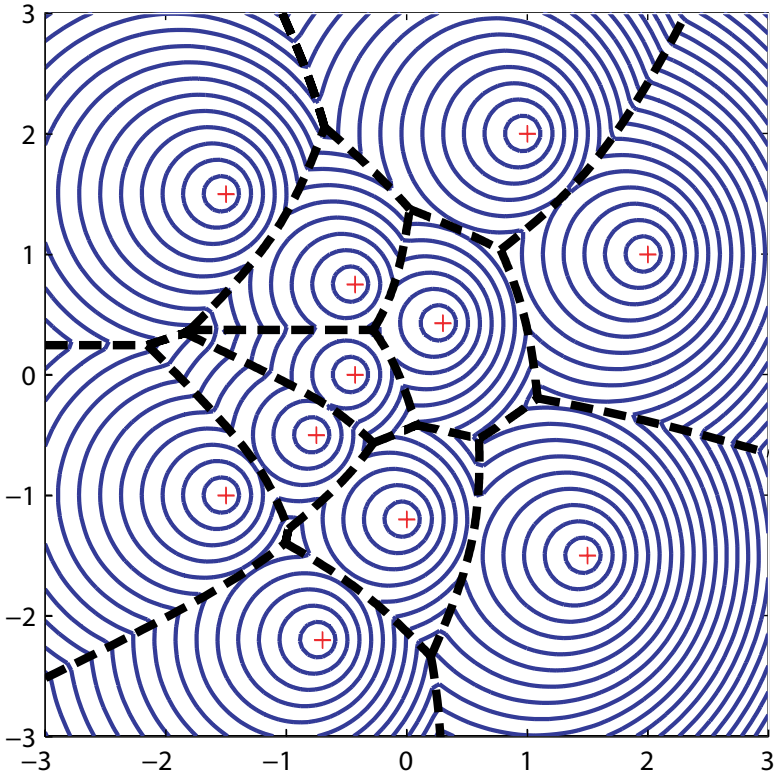

Figure 44: The ZVD and the minimum cost-to-go interpretation. Computation using exhaustive numerical calculations of the min-time wavefronts.

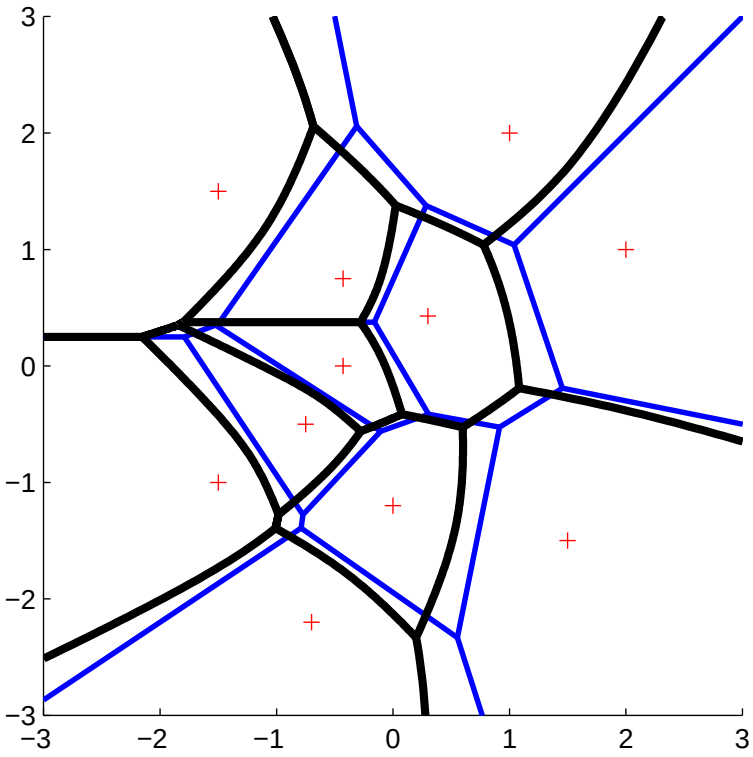

Figure 45: The ZVD (black) and its corresponding standard Voronoi Diagram (blue). Computation using the computational scheme proposed in this chapter.

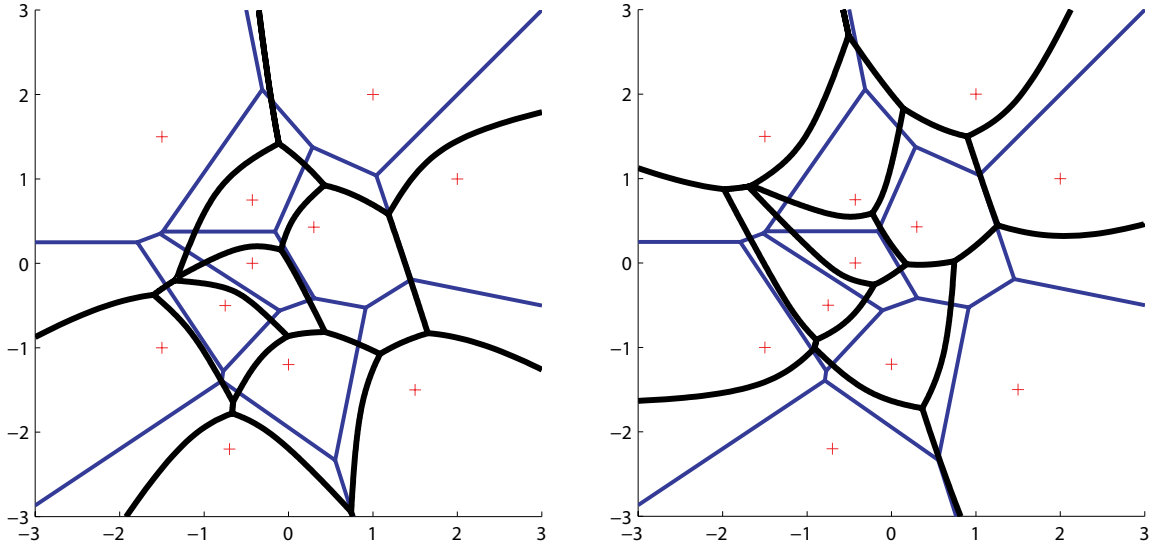

(a) The ZVD (left) and DZVD (right) for the wind field w_1.

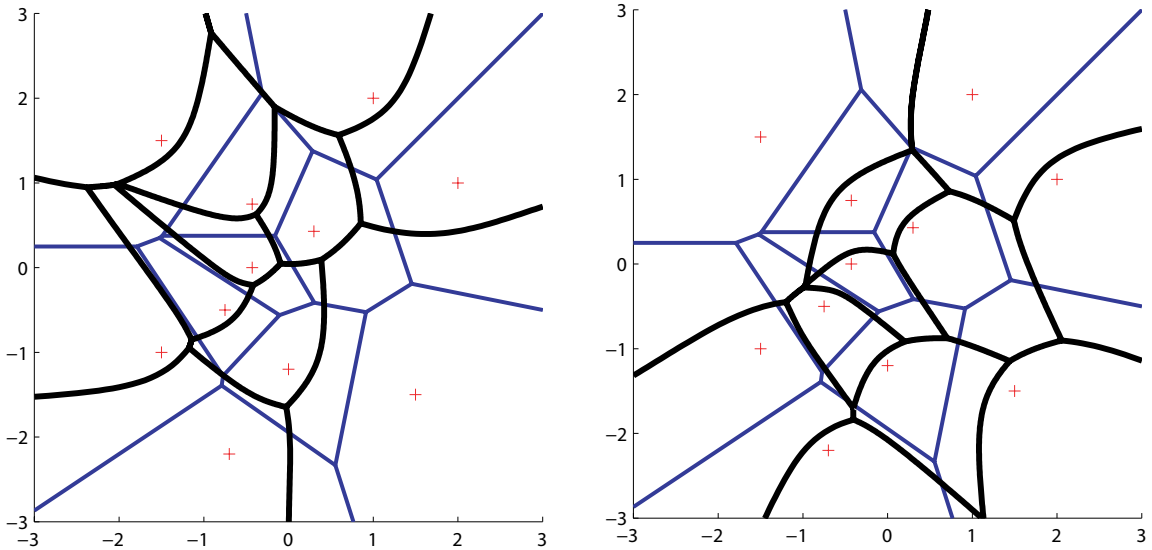

(b) The ZVD (left) and DZVD (right) for the wind field w_2.

Figure 46: The Zermelo-Voronoi Diagram for two different time-varying wind velocity fields.

CHAPTER VIII

THE ZERMELO-VORONOI DIAGRAM FOR A TIME-VARYING INHOMOGENEOUS LINEAR DRIFT FIELD

In this chapter, we address the Zermelo-Voronoi diagram problem introduced in Chapter 7 when the drift field not only varies with time but it has a spatial distribution as well. To simplify the analysis and in order to avoid some computational pathogenies that arise in the case of an arbitrary nonlinear drift field, we consider instead a time-varying inhomogeneous linear field. The construction of the Zermelo-Voronoi diagram is based on an efficient scheme that propagates the level sets of the minimum time-to-go function. The proposed approach utilizes the structure of the solution of the Zermelo's navigation problem without resorting to exhaustive numerical techniques.

8.1 Problem Formulation

Consider a set consisting of distinct points $\mathcal{P} := \{\mathsf{p}^i,\ i \in \mathcal{I}_n\}$, where $\mathcal{I}_n := \{1, \ldots, n\}$. It is assumed that at each point $\mathsf{p}^i \in \mathcal{P}$ resides, at time $t = 0$, an aerial / marine vehicle, which we henceforth refer to as the i–th vehicle. The motion of the i–th vehicle is described by the following equation

$$\dot{\mathsf{x}}^i = u^i(t) + w(t, \mathsf{x}^i), \qquad \mathsf{x}^i(0) = \mathsf{p}^i, \qquad i \in \mathcal{I}_n, \tag{204}$$

where $\mathsf{x}^i := [x^i,\ y^i]^\mathsf{T} \in \mathbb{R}^2$ and u^i is, respectively, the position vector and the control input of the i–th vehicle, and $w(t, \mathsf{x}^i)$ is the drift field induced by the local winds / currents. It is assumed that the set of admissible control inputs, denoted by $\mathcal{U}$, consists of all piecewise continuous functions of time taking values in the closed unit ball. In general, $w(t, \mathsf{x}^i)$ is a piecewise continuous function of time t and a $\mathbf{C}^1$ function

of the state x^i. To simplify the analysis and streamline the presentation, it will be assumed that the drift field can be approximated by a time-varying inhomogeneous drift field. In particular, it is henceforth assumed that

$$w(t, \mathsf{x}^i) = \nu(t) + \mathsf{A}(t)\mathsf{x}^i, \tag{205}$$

where $\mathsf{A}(t) := \big(a_{[i,j]}(t)\big)$ and $\nu(t) := (v_i(t))$ is a 2×2 matrix and a two-dimensional column vector, respectively. In addition, it is assumed that $a_{[i,j]}$ and v_i, for all $i, j \in \{1, 2\}$ and $i \in \{1, 2\}$, respectively, are real, piecewise continuous functions of time t.

Given a point $\mathsf{x} \in \mathbb{R}^2$, the objective of the i–th vehicle is to go from a point $\mathsf{p}^i \in \mathcal{P}$, at time $t = 0$, to the point x in minimum-time. We shall refer to this problem as the i-th Navigation Problem (i–th NP).

Problem 12 (i–th Navigation Problem)**.** *Given the system described by Equation* (204)*, and* $\mathsf{x} \in \mathbb{R}^2$ *determine the control input* $u^i_* \in \mathcal{U}$*, such that*

i. The trajectory $\mathsf{x}^i_* : [0, T_\mathrm{f}] \mapsto \mathbb{R}^2$ *generated by the control* u^i_* *satisfies the boundary conditions*

$$\mathsf{x}^i_*(0) = \mathsf{p}^i, \qquad \mathsf{x}^i_*(T_\mathrm{f}) = \mathsf{x}. \tag{206}$$

ii. The control u^i_* *minimizes along* x^*_i *the cost functional* $J(u^i) := T_\mathrm{f}$*, where* T_f *is the free final time.*

Henceforth, we denote by $T_\mathrm{f}(\mathsf{x}; \mathsf{p}^i)$ *the cost functional evaluated at* $u = u^i_*$*.*

Next, we investigate the feasibility as well as the existence of optimal solutions of Problem 12. Let $\mathsf{x}^i(t; \mathsf{p}^i, u^i)$ denote the endpoint of the trajectory of the system described by (204) generated by some control input $u^i \in \mathcal{U}$ applied in the time interval $[0, t]$. By applying the variation of constants formula, it follows that

$$\mathsf{x}^i(t; \mathsf{p}^i, u^i) = \Phi(t, 0)\mathsf{p}^i + \int_0^t \Phi(t, \tau)(u^i(\tau) + \nu(\tau))\mathrm{d}\tau, \qquad \mathsf{x}^i(0) = \mathsf{p}^i, \qquad i \in \mathcal{I}_n, \tag{207}$$

where $\Phi(t,s) := \mathsf{X}(t)\mathsf{X}^{-1}(s)$ and X is the fundamental matrix solution of the homogeneous linear system $\dot{\mathsf{x}}^i = \mathsf{A}(t)\mathsf{x}^i$ with $\mathsf{X}(0) = \mathsf{I}_{2\times 2}$.

We define the *reachable set* or *set of attainability* [112] of (204) from p^i, at time $t = \tau \geq 0$, as follows

$$\mathfrak{R}_\tau(\mathsf{p}^i) := \bigcup_{u^i \in \mathcal{U}} \{\mathsf{x} \in \mathbb{R}^2 : \ \mathsf{x} = \mathsf{x}^i(\tau; \mathsf{p}^i, u^i)\}.$$

The following proposition provides a necessary and sufficient condition for the feasibility of the i–th NP.

Proposition 41. *Let $\mathsf{x} \in \mathbb{R}^2$ and $\mathsf{p}^i \in \mathcal{P}$. Then i–th NP has a feasible solution if and only if there exists $0 \leq \tau < \infty$ such that $\mathsf{x} \in \mathfrak{R}_\tau(\mathsf{p}^i)$.*

Proposition 41 implies that the feasibility of the i–th NP from $\mathsf{p}^i \in \mathcal{P}$ to a given terminal state x is equivalent to the finite-time controllability of system (204) from p^i to x. The controllability question for the system (204) requires a rather detailed and careful treatment due to the existence of the drift field $w(t, \mathsf{x}^i)$, and the fact that the control u^i is bounded [102].

In particular, as we demonstrate shortly afterwards, the system (204) will not be able to evolve along every possible direction if the norm of the local drift exceeds the vehicle's forward speed (normalized to unit). The situation is illustrated in Fig. 47. In particular, Fig. 47(a) illustrates that if the norm of the drift at time t, when the i–th vehicle is located at x, is less than or equal to one, then the vehicle can move to every direction except from the direction parallel to $-w$ in the case when $|w(t, \mathsf{x}^i)| = 1$. On the contrary, as is illustrated in Fig. 47(b), if $|w(t, \mathsf{x}^i)| > 1$, then, at time t, the vehicle's inertial velocity, which is denoted by V^i, where $\mathsf{V}^i := w + u^i$, is constrained to lie, for all $u^i \in \mathcal{U}$ and $t \geq 0$, within a pencil of directions. We shall refer to this pencil of directions, which will be denoted henceforth by $\mathcal{K}$, as the *cone of admissible directions of motion*. It follows readily from Fig. 47(b) that $\mathcal{K}$ is defined as follows

$$\mathcal{K}(w) := \{v \in \mathbb{R}^2 : |\angle(w, v)| \leq \arcsin(1/|w|)\}, \tag{208}$$

where $\angle(a,b) : \mathbb{R}^2 \times \mathbb{R}^2 \mapsto [-\pi, \pi)$ denotes the angle from a to b . Note that $\mathcal{K}(w)$ is a right (non-oblique) cone of angle $\vartheta_{\mathcal{K}} := 2\arcsin(1/|w|)$, whose apex is x^i (current position of the vehicle) and its axis is parallel to w.

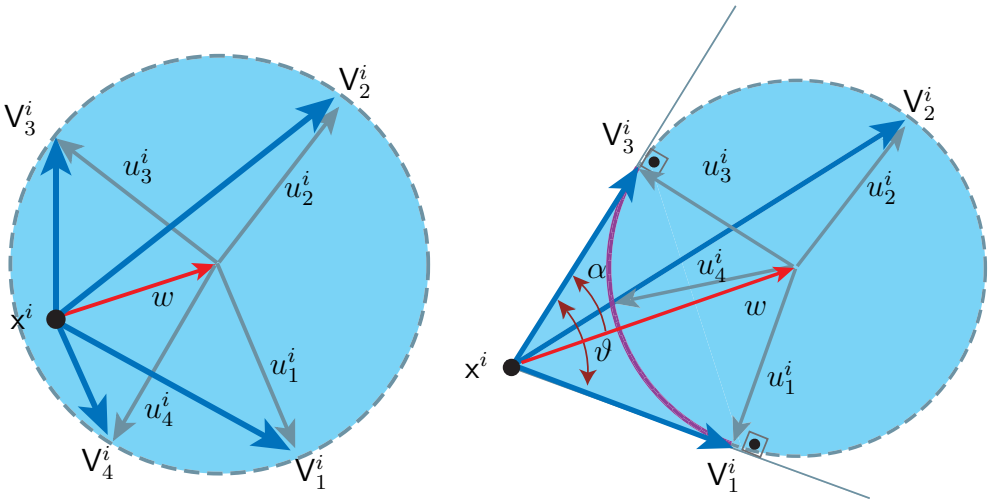

(a) Local controllability analysis for the Zermelo's navigation problem when $|w| \leq 1$. The vehicle can move to every direction except from $-w$ when $|w| = 1$.

(b) Local controllability analysis for the Zermelo's navigation problem when $|w| > 1$. The vehicle is constrained to move within a cone whose apex is its current position x, its axis is parallel to w and its angle ϑ equals $2\arcsin 1/|w|$.

Figure 47: Local controllability analysis for the Zermelo's navigation problem.

The following proposition provides a sufficient condition for the existence of a solution of Problem 12.

Proposition 42. *Let $\mathsf{x} \in \mathfrak{R}_\tau(\mathsf{p}^i)$, for some $0 \leq \tau < \infty$. If there exists α, $\beta > 0$ such that $|\mathsf{A}(t)| < \alpha$ and $|\nu(t)| < \beta$, for all $0 \leq t < \tau$, where $|\cdot|$ denote the induced 2-norm, then the i–th NP has an optimal solution.*

Proof. From Filippov's Theorem on the existence of solutions of minimum-time problems [53, pp.310-317], it suffices to prove that there exists $k > 0$ such that

$$\langle \dot{\mathsf{x}}^i, \mathsf{x}^i \rangle \leq k(1 + |\mathsf{x}^i|^2). \tag{209}$$

Indeed, by virtue of the triangle and Cauchy-Schwartz inequalities, and the fact that

$|u^i| \leq 1$ it follows

$$\begin{aligned}\langle \dot{\mathsf{x}}^i, \mathsf{x}^i \rangle &\leq (|\mathsf{A}(t)||\mathsf{x}^i| + |\nu(t)| + |u^i|)|\mathsf{x}^i| \\ &\leq \alpha |\mathsf{x}^i|^2 + (\beta + 1)|\mathsf{x}^i|. \end{aligned} \tag{210}$$

The result follows readily from the inequality $2|\mathsf{x}^i| \leq 1 + |\mathsf{x}^i|^2$. □

Let $\mathfrak{R}(\mathsf{p}^i)$ denote the reachable set of the system described by (204) from p^i, where

$$\mathfrak{R}(\mathsf{p}^i) := \lim_{t\to\infty} \bigcup_{0\leq t\leq \tau} \mathfrak{R}_\tau(\mathsf{p}^i) = \overline{\bigcup_{0\leq \tau<\infty} \mathfrak{R}_\tau(\mathsf{p}^i)}.$$

Note that $\mathfrak{R}(\mathsf{p}^i)$ and, in particular, its boundary, denoted by $\partial\mathfrak{R}(\mathsf{p}^i)$ may contain points that can be reached by the system described by (204) emanating from p^i only asymptotically, that is, as $t \to \infty$. Therefore, if the i–th NP may not be necessarily feasible for a point $\mathsf{x} \in \mathfrak{R}(\mathsf{p}^i)$, owing to the fact that it is not always true that the point x can be reached in finite time. For more practical reasons, it is more suitable to work with sets that consist of points that can be reached from each $\mathsf{p}^i \in \mathcal{P}$ only in finite time rather those that include points that can be reached asymptotically. Therefore, we consider finite-time reachable sets of the following form

$$\mathfrak{R}_{t\leq\tau}(\mathsf{p}^i) := \bigcup_{0\leq t\leq\tau} \mathfrak{R}_\tau(\mathsf{p}^i) = \bigcup_{0\leq t\leq\tau} \bigcup_{u\in\mathcal{U}} \{\mathsf{x} \in \mathbb{R}^2 : \ \mathsf{x} = \mathsf{x}^i(t; \mathsf{p}^i, u^i)\},$$

where $\tau > 0$ is given. Note that $\mathfrak{R}_{t\leq\tau}(\mathsf{p}^i) \subseteq \mathfrak{R}(\mathsf{p}^i)$.

Next, we formulate the problem of characterizing a generalized Voronoi diagram generated by the point-set $\mathcal{P}$. The proximity metric of the Voronoi-like partitioning problem is the minimum time-to-go function of the i–th NP. In addition, the space to be partitioned, denoted henceforth by $\mathfrak{R}_{t\leq\tau}(\mathcal{P})$, is defined as the union of the sets $\mathfrak{R}_{t\leq\tau}(\mathsf{p}^i)$, for all $i \in \mathcal{I}_n$, that is,

$$\mathfrak{R}_{t\leq\tau}(\mathcal{P}) := \bigcup_{\mathsf{p}^i\in\mathcal{P}} \mathfrak{R}_{t\leq\tau}(\mathsf{p}^i) = \bigcup_{i\in\mathcal{I}_n} \mathfrak{R}_{t\leq\tau}(\mathsf{p}^i), \tag{211}$$

where $\tau > 0$ is given. In addition, we define $\mathfrak{R}(\mathcal{P}) := \bigcup_{i\in\mathcal{I}_n} \mathfrak{R}(\mathsf{p}^i)$. It follows readily that $\mathfrak{R}(\mathcal{P}) \supseteq \mathfrak{R}_{t\leq\tau}(\mathcal{P})$, for all $0 \leq \tau < \infty$.

Problem 13. *Let $\tau > 0$ and a collection of points $\mathcal{P} := \{\mathsf{p}^i \in \mathbb{R}^2 : \ i \in \mathcal{I}_n\}$ be given. Let, furthermore, $T_{\mathrm{f}}(\mathsf{x}; \mathsf{p}^i)$ denote the minimum time required to drive the system described by Eq.* (204) *from $\mathsf{p}^i \in \mathcal{P}$ to $\mathsf{x} \in \mathfrak{R}_\tau(\mathsf{p}^i)$, then determine a partition $\mathfrak{V} = \{\mathfrak{V}^i : \ i \in \mathcal{I}_n\}$ of $\mathfrak{R}_{t \leq \tau}(\mathcal{P})$ such that*

i. $\mathfrak{R}_{\tau \leq t}(\mathcal{P}) = \bigcup_{i \in \mathcal{I}_n} \mathfrak{V}^i$;

ii. $\overline{\mathfrak{V}^i} = \mathfrak{V}^i$, *for each* $i \in \mathcal{I}_n$;

iii. for each $\mathsf{x} \in \mathfrak{V}^i$, $T_{\mathrm{f}}(\mathsf{x}; \mathsf{p}^i) \leq T_{\mathrm{f}}(\mathsf{x}; \mathsf{p}^j)$, *for* $j \neq i$.

Note that Problem 13 is an extension of the Zermelo Voronoi Diagram (ZVD) problem discussed before, with the distinctive difference that the drift field now varies both spatially and temporally. The sets $\mathcal{P}$ and $\mathfrak{V}^i$ constitute the set of the Voronoi generators and the Zermelo-Voronoi cells of the ZVD, respectively.

8.2 Construction of the Voronoi Partitions

At this point, it is not clear whether the minimum time-to-go function of the i–th NP enjoys properties such as isotropy and convexity, that would allow us to associate Problem 13 with generalized Voronoi-like partitioning problems, for which efficient computational methods exist in the literature. Therefore, we need to adopt an alternative approach.

To this aim, given $\tau \geq 0$, let us consider the lower envelope function $c_* : \mathfrak{R}_{t \leq \tau}(\mathcal{P}) \mapsto [0, \infty)$, where

$$c_*(\mathsf{x}) := \min_{i \in \mathcal{I}_n} T_{\mathrm{f}}(\mathsf{x}; \mathsf{p}^i). \tag{212}$$

In addition, let us define the sets

$$\mathcal{S}_i := \{(\mathsf{x}, z) : \ \mathsf{x} \in \mathfrak{R}_{t \leq \tau}(\mathsf{p}^i) \text{ and } z = T_{\mathrm{f}}(\mathsf{x}; \mathsf{p}^i), \text{ for } i \in \mathcal{I}_n\}, \tag{213}$$

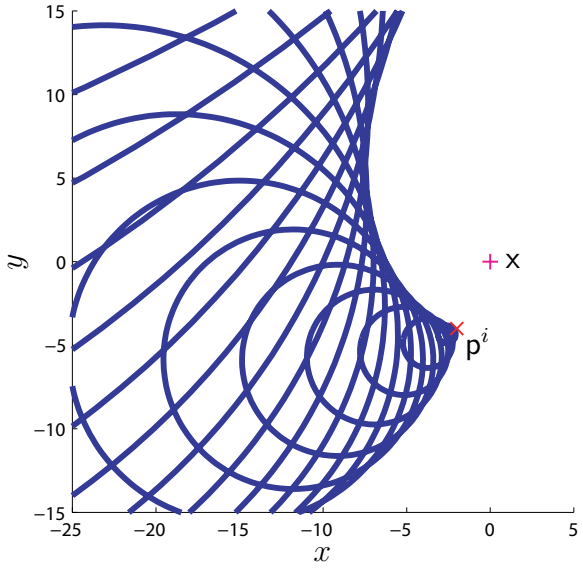

(a) Unfeasible case: x belongs to the complement of $\mathfrak{R}(\mathsf{p}^i)$

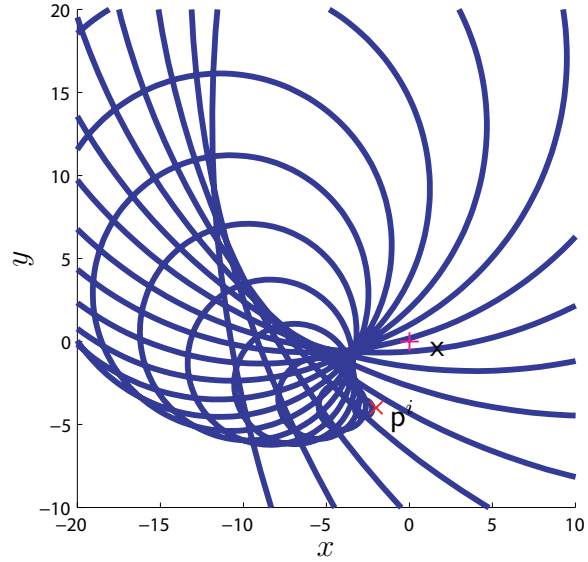

(b) Solvable case: $\mathsf{x} \in \mathfrak{R}_{t\leq\tau}(\mathsf{p}^i)$, for some $\tau > 0$

Figure 48: The i-th NP is solvable if and only if the destination point x (red x-cross), belongs to the reachable set $\mathfrak{R}_{t\leq\tau}(\mathsf{p}^i)$ of p^i (magenta cross) for some $\tau > 0$.

and let $\mathcal{S}_{\mathcal{P}}$ denote the most tight lower envelope of the union of these surfaces, which is defined as follows

$$\mathcal{S}_{\mathcal{P}} := \{(\mathsf{x}, z) : \ \mathsf{x} \in \mathfrak{R}_{t\leq\tau}(\mathcal{P}) \text{ and } z = c_*(\mathsf{x})\}. \tag{214}$$

Note that $\mathcal{S}_i$, for $i \in \mathcal{I}_n$, and $\mathcal{S}_{\mathcal{P}}$ are surfaces embedded in $\mathbb{R}^3$. Let us consider the

following projection operator

$$\mathbf{P} : \mathfrak{R}_{t\leq\tau}(\mathcal{P}) \times [0,\infty) \mapsto \mathfrak{R}_{t\leq\tau}(\mathcal{P}),$$

where $\mathbf{P}(\mathsf{x}, z) = \mathsf{x}$ and $\tau \in [0,\infty)$ is given. Then the solution of Problem 13 can be characterized by projecting the intersections of the lower envelope surface $\mathcal{S}_{\mathcal{P}}$ with each cost surface $\mathcal{S}_i$, for all $i \in \mathcal{I}_n$, onto $\mathfrak{R}_{t\leq\tau}(\mathcal{P})$. The projector operator $\mathbf{P}$ essentially attaches to each point $\mathsf{x} \in \mathfrak{R}_{t\leq\tau}(\mathcal{P})$ an index from $\mathcal{I}_n$. In particular, let us consider the set-valued function $\mathbf{I} : \mathfrak{R}_{t\leq\tau}(\mathcal{P}) \rightrightarrows \mathcal{I}_n$, where

$$\mathbf{I}(\mathsf{x}) = i, \quad \text{if} \;\; c_*(\mathsf{x}) = T_{\mathrm{f}}(\mathsf{x}; \mathsf{p}^i).$$

Note that the points in $\mathfrak{R}_{t\leq\tau}(\mathcal{P})$ where $\mathbf{I}$ attains multiple values belong to the common boundaries of neighboring cells of the partition $\mathfrak{V}$ generated by $\mathcal{P}$.

In particular, let $\mathfrak{V} = \{\mathfrak{V}^i : \; i \in \mathcal{I}_n\}$ denote the ZVD generated by $\mathcal{P}$. Then the cell $\mathfrak{V}^i$ can be computed as follows

$$\mathfrak{V}^i = \{\mathbf{P}(\mathsf{x}, z) : \; (\mathsf{x}, z) \in \mathcal{S}_{\mathcal{P}} \cap \mathcal{S}_i\}, \tag{215}$$

or, equivalently,

$$\mathfrak{V}^i = \{\mathsf{x} \in \mathfrak{R}_{t\leq\tau}(\mathcal{P}) : \; \mathbf{I}(\mathsf{x}) = i\}. \tag{216}$$

It readily follows from the previous discussion that for the characterization of the partition $\mathfrak{V} = \{\mathfrak{V}^i, \; i \in \mathcal{I}_n\}$, it suffices to construct the surfaces $\mathcal{S}_i$, for $i \in \mathcal{I}_n$, and subsequently construct the lower envelope $\mathcal{S}_{\mathcal{P}}$. Before we get into the details of the characterization of the surfaces $\mathcal{S}_i$, for $i \in \mathcal{I}_n$, we first need to introduce the concept of level set. In particular, given $\tau \geq 0$, we say that the set

$$\ell_\tau(\mathsf{p}^i) := \{\mathsf{x} \in \mathfrak{R}_{t\leq\tau}(\mathsf{p}^i) : \; T_{\mathrm{f}}(\mathsf{x}; \mathsf{p}^i) = \tau\} \tag{217}$$

is the level set of the minimum time-to-go function emanating from p^i. The following proposition highlights an important observation.

Proposition 43. *Given* $0 < \tau < \infty$ *and* $\mathsf{p}^i \in \mathcal{P}$*, it holds that*

$$\mathfrak{R}_{t\leq\tau}(\mathsf{p}^i) = \bigcup_{0\leq t\leq\tau} \ell_\tau(\mathsf{p}^i). \tag{218}$$

Proof. Let $\mathsf{x} \in \mathfrak{R}_{t\leq\tau}(\mathsf{p}^i)$. Then there exists $\tau_0 \in [0, \tau]$ such that the system (204) will reach the state x starting from p^i after τ_0 units of time. In light of Proposition 42, there exists a minimum-time control law that will steer (204) to x in minimum time $T_{\mathrm{f}}(\mathsf{x}; \mathsf{p}^i) \leq \tau_0$. Therefore, $\mathsf{x} \in \ell_{T_{\mathrm{f}}(\mathsf{x};\mathsf{p}^i)}$, which implies, in turn, that $\mathsf{x} \in \bigcup_{0\leq t\leq\tau} \ell_\tau(\mathsf{p}^i)$. Thus, we have shown that $\mathfrak{R}_{t\leq\tau}(\mathsf{p}^i) \subseteq \bigcup_{0\leq t\leq\tau} \ell_\tau(\mathsf{p}^i)$.

Conversely, if $\mathsf{x} \in \ell_\tau(\mathsf{p}^i)$, then it follows immediately that $\mathsf{x} \in \mathfrak{R}_{t\leq\tau}(\mathsf{p}^i)$. Therefore, $\bigcup_{0\leq t\leq\tau} \ell_\tau(\mathsf{p}^i) \subseteq \mathfrak{R}_{t\leq\tau}(\mathsf{p}^i)$. The result follows readily. □

Therefore, for a given $\tau \geq 0$, the implementation of the previously described method requires a computationally efficient scheme that propagates the level sets $\ell_\tau(\mathsf{p}^i)$, for $0 \leq t \leq \tau$. In particular, note that if $\mathsf{x} \in \ell_\tau(\mathsf{p}^i)$, for $0 \leq t \leq \tau$, then $(\mathsf{x}, \tau) \in \mathcal{S}_i$. The propagation of the level sets of the minimum time-to-go function emanating from each generator $\mathsf{p}^i \in \mathcal{P}$ can be done numerically by employing, for example, either a fast marching or a marker-particle algorithm, as in [139, 140]. The approaches presented in [139, 140], however, do not take advantage of the structure of the solution of the ZNP. More importantly, they deal for time-invariant drift fields only and do not guarantee, in general, that numerical pathogenies will not arise. In particular, as is stressed in [24], the system (204) is not necessarily small-time locally controllable [50], and consequently, the computation of the minimum time-to-go function of the i–th NP may suffer from numerical pathogenies, which cannot be handled effectively unless more sophisticated numerical techniques, than those presented in [139, 140], are employed (for example, approaches that find weak solutions of the HJB equation of the ZNP [24]). Instead of resorting to exhaustive computational methods, next we investigate whether there exists a more direct and efficient method to solve Problem 13 that takes advantage of the structure of the solution of the ZNP to significantly

simplify the process of expanding the level sets of $\mathcal{S}_i$ for each $i \in \mathcal{I}_n$.

8.2.1 Structure of Optimal Solutions and Reachable Sets of the i–th Navigation Problem

We first present some key results from the solution of the i–th NP, which are necessary for the subsequent discussion. The reader interested in a more detailed treatment of the ZNP may refer to [50, pp. 239-247, pp. 370-373]. In particular, if the i^{th} problem is feasible, then the control u^i_* that solves the i–th NP has necessarily the following structure: $u^i_* = [\cos\theta^i_*,\ \sin\theta^i_*]^{\mathsf{T}}$, where θ^i_* satisfies the following differential equation [50]

$$\dot{\theta}^i_* = (a_{[1,1]}(t) - a_{[2,2]}(t))\cos\theta^i_* \sin\theta^i_* + a_{[2,1]}(t)\sin^2\theta^i_* - a_{[1,2]}(t)\cos^2\theta^i_*, \quad \theta^i_*(0) = \bar{\theta}^i, \tag{219}$$

where $a_{[k,\ell]}(t)$, for $k, \ell \in \{1, 2\}$, are the elements of the matrix $\mathsf{A}(t)$. It follows that the (candidate) optimal control u^i_* is determined up to one parameter, namely $\bar{\theta}^i$. Henceforth, we write $u^i_*(\cdot; \bar{\theta}^i)$.

Let $\mathsf{x}^i_*(t; \mathsf{p}^i, \bar{\theta}^i)$ denote the solution of the differential equation (204) for $u^i = u^i_*(\cdot; \bar{\theta}^i)$, which we henceforth refer to as the extremal curve of the i–th NP. Note that $\mathsf{x}^i_*(t; \mathsf{p}^i, \bar{\theta}^i)$ is given by (207) modulo the replacement of u^i by u^i_*.

Proposition 44. *Let $\mathsf{p}^i \in \mathcal{P}$. Then, for all $0 \leq \tau < \infty$ and $\mathsf{p}^i \in \mathcal{P}$,*

$$\ell_\tau(\mathsf{p}^i) \subseteq \mathfrak{R}_\tau(\mathsf{p}^i). \tag{220}$$

Proof. It suffices to note that, in light of Proposition 42, if $\mathsf{x} \in \mathfrak{R}_\tau(\mathsf{p}^i)$, then there exists $\bar{\theta}^i \in [0, 2\pi)$ such that $\mathsf{x} = \mathsf{x}^i_*(t; \mathsf{p}^i, \bar{\theta}^i)$, for some $t \in [0, \tau]$. □

From Proposition 44, the interval $\mathbb{I} := [0, 2\pi)$ admits, at every time $t \geq 0$, the following decomposition

$$\mathbb{I} = \Theta^i_t \cup (\Theta^i_t)^c, \quad \Theta^i_t \cap (\Theta^i_t)^c = \varnothing,\ t \geq 0, \tag{221}$$

where Θ_t^i denotes the set of $\bar{\theta}^i$ such that $\mathsf{x}_*^i(t;\mathsf{p}^i,\bar{\theta}^i) \in \ell_t(\mathsf{p}^i)$. Note that a point $\mathsf{x} \in \ell_t^c(\mathsf{p}^i) \cap \mathfrak{R}_t(\mathsf{p}^i)$ can be reached after t units of time by means of extremal curves that are either regular minimizing or maximizing curves, or abnormal curves (that is, extremal curves that do not satisfy the strengthened Legendre condition [102]). Before, we proceed further we need to introduce the concept of weak and strong curve norms as well as weak and strong minimizing or maximizing curves. In particular, given a $\mathbf{C}^1$ curve $\mathsf{x}^i(\cdot;\mathsf{p}^i;\bar{\theta}^i) : [0,\tau] \mapsto \mathbb{R}^2$, we define, respectively, its weak and strong norm as follows

$$\|\mathsf{x}^i(\cdot;\mathsf{p}^i;\bar{\theta}^i)\|_w = \max_{t\in[0,\tau]} |\mathsf{x}^i(t;\mathsf{p}^i;\bar{\theta}^i)|,$$

$$\|\mathsf{x}^i(\cdot;\mathsf{p}^i;\bar{\theta}^i)\|_s = \max_{t\in[0,\tau]} |\mathsf{x}^i(t;\mathsf{p}^i;\bar{\theta}^i)| + \max_{t\in[0,\tau]} |\dot{\mathsf{x}}^i(t;\mathsf{p}^i;\bar{\theta}^i)|.$$

Next we define the concept of a weak and strong minimizing / maximizing curve [173].

Definition 2. *Given $\tau > 0$, $\mathsf{p}^i \in \mathcal{P}$, and $\mathsf{x} \in \mathbb{R}^2$, then an extremal curve $\mathsf{x}_*^i(t;\mathsf{p}^i;\bar{\theta}^i)$ with $\mathsf{x}_*^i(0;\mathsf{p}^i;\bar{\theta}^i) = \mathsf{p}^i$ and $\mathsf{x}_*^i(\tau;\mathsf{p}^i;\bar{\theta}^i) = \mathsf{x}$ is a strong minimizing (maximizing) curve of the i–th NP if*

$$\tau \leq \tau_{\mathsf{z}} \quad (\textit{respectively, } \tau \geq \tau_{\mathsf{z}}),$$

for all $\mathbf{C}^1$ curves $\mathsf{z} : [0,\tau_{\mathsf{z}}] \mapsto \mathbb{R}^2$, with $\mathsf{z}(0) = \mathsf{p}^i$ and $\mathsf{z}(\tau_{\mathsf{z}}) = \mathsf{x}$, such that

$$\|\mathsf{x}^i(\cdot;\mathsf{p}^i;\bar{\theta}^i) - \mathsf{z}(t)\|_w < \delta,$$

for some $\delta > 0$.

The definition of a weak minimizing / maximizing curve follows as in Definition 2 modulo the replacement of the weak norm by the strong norm.

The following proposition provides us with sufficient conditions that allow us to classify the extremals of Problem 12 [210, 50].

Proposition 45. *Let $\mathsf{x}_*^i(t;\mathsf{p}^i,\bar{\theta}^i)$ be the extremal curve generated by $u_*^i(t;\bar{\theta}^i)$, for $t \in [0,\tau]$, for a given $\tau \geq 0$, and let the functional*

$$E(t,\mathsf{x}_*^i,\bar{\theta}^i) := 1 + \langle w(t,\mathsf{x}_*^i,), u_*^i(t;\bar{\theta}^i)\rangle. \tag{222}$$

If $E(t, \mathsf{x}^i_*, \bar{\theta}^i) > 0$ $(E(t, \mathsf{x}^i_*, \bar{\theta}^i) < 0)$, *at* $t = 0$, *then* x^i_* *is a regular, strong minimizing (respectively, maximizing) curve, for all* $t \geq 0$. *Furthermore, if* $E(t, \mathsf{x}^i_*, u^i_*) = 0$, *for all* $t \in [0, \tau]$, *then* x^i_* *is an abnormal extremal curve of the* i*-th NP.*

Proof. As is shown in [50], $E(t, \mathsf{x}^i_*, u^i_*(\cdot; \bar{\theta}^i))$ has, for all $t \in [0, \tau]$, the same sign as the function $\omega : [0, \infty) \mapsto \mathbb{R}$, where $\omega(t)$ satisfies the following homogeneous linear differential equation

$$\dot{\omega} = \lambda_\omega(t)\omega, \tag{223}$$

$$\lambda_\omega(t) = -(a_{[1,1]}(t)\cos^2\theta^*(t) + (a_{[1,2]}(t) + a_{[1,2]}(t))\sin\theta^*(t)\cos\theta^*(t) + a_{[2,2]}(t)\sin^2\theta^*(t)). \tag{224}$$

In addition, as is shown in [50], ω has the same sign with the Weierstrass excess function $\mathcal{E}$ of the i–th NP, where

$$\mathcal{E}(t, \omega, \theta^i_*, \theta') = \omega(t)(1 - \cos(\theta^i_* - \theta')), \quad \text{for } \theta' \in [0, 2\pi),\ t \in [0, \tau].$$

Therefore, ω, E and $\mathcal{E}$ have the same sign for all $0 \leq t \leq \tau$. In addition, it follows from Eq. (223) that

$$\omega(t) = \omega(0)\mathrm{e}^{\int_0^t \lambda_\omega(t)\mathrm{d}t}. \tag{225}$$

It follows that $\omega(t)$ preserves the sign of $\omega(0)$, for all $t \geq 0$. Thus, if $\omega(0) > 0$ $(\omega(0) < 0)$, then $\mathcal{E}(t, \omega, \theta^i_*, \theta') > 0$ (respectively, $\mathcal{E}(t, \omega, \theta^i_*, \theta') < 0$), for all $0 \leq t \leq \tau$, which in light of the Weierstrass excess function theorem implies that $\mathsf{x}^i_*(t; \mathsf{p}^i, \bar{\theta}^i)$ is a strong, minimizing (respectively, maximizing) curve of the i–th NP.

Finally, if $E = 0$ it follows that $\mathcal{E}(t, \omega, \theta^i_*, \theta') = 0$, which implies, as shown in [50], that $\mathsf{x}^i_*(t; \mathsf{p}^i, \bar{\theta}^i)$ is an abnormal extremal curve of the i–th NP, for all $0 \leq t \leq \tau$. □

Remark 11 An important observation is that Proposition 45 does not allow us to distinguish between the abnormal extremals of the minimum and the corresponding maximum time problems. As it is argued by Carathéodory [50], our intuition tells us that an extremal curve can be an abnormal extremal curve of both the minimum and maximum time at the same time.

Another important observation is that (222) needs to be checked only once, namely at time $t = 0$, provided that the drift field has the structure given in (205). For more generic nonlinear drift fields, one should check condition (222), for all $t \in [0, \tau]$. In particular, for a nonlinear drift field, given $\tau > 0$, the Weierstrass excess function may not maintain its sign for all $t \in [0, \tau]$. Therefore, for more general nonlinear drift fields, one cannot check condition (222) point-wisely but should instead keep track of any possible changes of the sign of E along the extremal curves.

Note that Proposition 45 has a simple physical interpretation. In particular, an extremal curve x^i_* is a locally minimizing curve of the i–th NP problem, if the angle between the direction of motion of the vehicle, which is parallel to $\dot{\mathsf{x}}^i_*$, and the forward velocity u^i_* of the i–th vehicle is less than $\pi/2$ or, equivalently, $\langle \dot{\mathsf{x}}^i_*, u^i_* \rangle > 0$.

Corollary 4. *Let $\mathsf{x}^i_*(t; \mathsf{p}^i, \bar{\theta}^i)$ be the extremal curve generated by $u^i_*(t; \bar{\theta}^i)$, for $t \in [0, \tau]$. If*

$$\langle \dot{\mathsf{x}}^i_*(0), u^i_*(0) \rangle > 0 \quad (\langle \dot{\mathsf{x}}^i_*(0), u^i_*(0) \rangle < 0),$$

then x^i_* is a strong, locally or globally minimizing (respectively, maximizing) curve. Furthermore, if $E(\tau, \mathsf{x}^i_*, \bar{\theta}^i) = 0$ for some $t = \tau \geq 0$, then x^i_* is an abnormal extremal curve of the i–th NP, for all $t \geq \tau$.

Proof. We have that, for $t \geq 0$,

$$\langle \dot{\mathsf{x}}^i_*(t), u^i_*(t; \bar{\theta}^i) \rangle = \langle w(t, \mathsf{x}^i_*(t)) + u^i_*(t; \bar{\theta}^i), u^i_*(t; \bar{\theta}^i) \rangle \tag{226}$$

$$= \langle w(t, \mathsf{x}^i_*(t)), u^i_*(t; \bar{\theta}^i) \rangle + |u^i_*(t; \bar{\theta}^i)|^2 \tag{227}$$

$$= \langle w(t, \mathsf{x}^i_*(t)), u^i_*(t; \bar{\theta}^i) \rangle + 1. \tag{228}$$

Therefore, $\langle \dot{\mathsf{x}}^i_*, u^i_*(t; \bar{\theta}^i) \rangle = E(t, \mathsf{x}^i_*, \bar{\theta}^i)$, for all $t \geq 0$. The result follows readily from Proposition 45. □

Remark 12 The reader should not hastily jump to the conclusion that $\Theta^i_t \equiv \Theta^i_0$, when the drift field has the structure given in (205). This is because, as we shall see

in more detail later, a curve $\mathsf{x}^i_*(t;\mathsf{p}^i,\bar{\theta}^i)$ may only be globally minimizing until some time $t=\tau$, after which it degenerates to at most a locally minimizing curve.

Figure 49 illustrates the field of extremals of the system (204) associated with the i–th NP. In other words, Fig. 49 illustrates the integral curves that form the flow of the system (204) emanating from some $\mathsf{p}^i \in \mathcal{P}$, driven by the candidate optimal control $u^i_*(\cdot;\bar{\theta})$ when all maximizing curves have been removed. To streamline the presentation, which is mainly based on the analysis presented in [50] (more brief discussions than the one presented in [50] can be found alternatively in, for example, [102, 182]), let us assume that both A and ν are time-invariant. There are three cases of interest.

The first case we consider is when $\mathsf{p}^i \notin \Omega$, where $\Omega := \{\mathsf{x} \in \mathbb{R}^2 : \ |w(\mathsf{x})| \leq 1\}$. In this case, as is illustrated in Fig. 49(a), p^i may lie either in the interior of the set $\mathfrak{R}_\tau(\mathsf{p}^i)$, for all $\tau \geq 0$, or, in the boundary of $\mathfrak{R}_\tau(\mathsf{p}^i)$, for all $0 < \tau \leq \tau_1$, and in the interior of $\mathfrak{R}_\tau(\mathsf{p}^i)$, for all $\tau > \tau_1$, for some $\tau_1 > 0$. In this case, there exist two abnormal curves denoted by $\tilde{\mathsf{x}}^i_1$ and $\tilde{\mathsf{x}}^i_2$ as is illustrated in Fig. 49(a). Interestingly, there exist minimizing curves that, as time evolves, cross the boundary of the reachable set from p^i after intersecting one of the abnormal curves $\tilde{\mathsf{x}}^i_1$ and $\tilde{\mathsf{x}}^i_2$, and subsequently evolve towards the interior of the reachable set. It is obvious that after the time $t=\tau$ when a minimizing curve crosses the boundary of the reachable set $\mathfrak{R}_{t\leq\tau_0}$, where $\tau_0 < \tau$, this curve cannot be a candidate globally minimizing curve of the i–th NP, for all $t \geq \tau$. The last observation holds true in light of the fact that there exists another minimizing curve that reach the points in the interior of $\mathfrak{R}_{\tau\leq t_0}$ in less than t units of time.

The second case is when $\mathsf{p}^i \in \text{int}\Omega$. In this case, it is easy to show that $\mathsf{p}^i \in \text{int}\mathfrak{R}_\tau(\mathsf{p}^i)$, for all $\tau \geq 0$, or equivalently, the system (204) is small-time local controllable at p^i [7]. No abnormal curves are observed in this case.

The third case that can be observed is when the extremal curves emanate from a

point in $\mathrm{bd}\Omega$. In this case, there will exist $\bar{\theta}_\star \in \mathbb{I}$ such that $\langle \dot{\mathsf{x}}(0), u_*^i(0;\bar{\theta}_\star^i)\rangle = 0$, and thus, the corresponding extremal will be abnormal, for all $t \geq 0$. Now let $\{\bar{\theta}_n^i\}_{n=0}^\infty$ be a sequence in $\mathbb{I}$ with $\lim_{n\to\infty} \bar{\theta}_n^i = \bar{\theta}_\star$. As it was first shown in [50], the abnormal curve $\tilde{\mathsf{x}}^i = \mathsf{x}_*^i(t;\mathsf{p}^i,\bar{\theta}_\star)$ is the limit curve that the sequence of regular minimizing curves $\mathsf{x}_*^i(t;\mathsf{p}^i,\bar{\theta}_n^i)$ converges to uniformly as $\bar{\theta}_n^i \to \bar{\theta}_\star$. The situation is illustrated in Fig. 49(c).

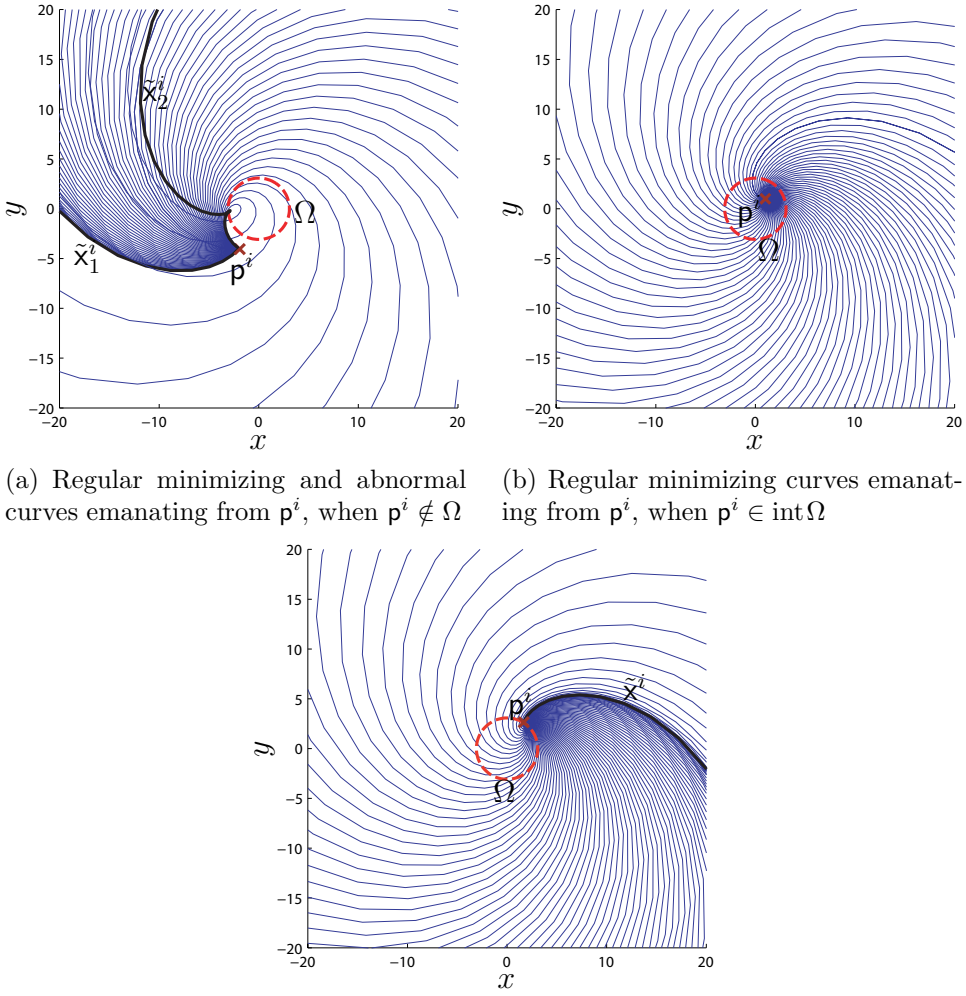

(a) Regular minimizing and abnormal curves emanating from p^i, when $\mathsf{p}^i \notin \Omega$

(b) Regular minimizing curves emanating from p^i, when $\mathsf{p}^i \in \mathrm{int}\Omega$

(c) Regular minimizing and abnormal curves emanating from p^i, when $\mathsf{p}^i \in \mathrm{bd}\Omega$

Figure 49: Integral curves forming the flow of the system (204) driven by the candidate optimal control $u_*(\cdot;\bar{\theta})$.

8.2.2 Characterization of the Level Sets of the Minimum Time-to-go Function

Using Proposition 45, one can readily determine all $\bar{\theta}^i \in \mathbb{I} \backslash \Theta_t^i$ that correspond to either locally or globally maximizing curves of the ZNP. We next define the set $\mathfrak{K}_\tau^*(\mathsf{p}^i)$ as follows

$$\mathfrak{K}_\tau^*(\mathsf{p}^i) := \bigcup_{\bar{\theta}^i \in \mathbb{I}} \{\mathsf{x}_*^i(\tau; \mathsf{p}^i, \bar{\theta}^i) \text{ and } E(t, \mathsf{x}_*^i, u_*^i) \geq 0, \text{ for all } 0 \leq t \leq \tau\}, \tag{229}$$

where $\tau \geq 0$ is given. Note that, for a given $\tau \geq 0$, the set $\mathfrak{K}_\tau^*(\mathsf{p}^i)$ is obtained from $\mathfrak{R}_\tau(\mathsf{p}^i)$ after applying Proposition 45 and removing the points that belong to maximizing curves. In the special case of a time-varying inhomogeneous drift field, the set $\mathfrak{K}_\tau^*(\mathsf{p}^i)$ is alternatively defined, in light of Corollary 4, as follows

$$\mathfrak{K}_\tau^*(\mathsf{p}^i) := \bigcup_{\bar{\theta}^i \in \mathbb{I}} \{\mathsf{x}_*^i(\tau; \mathsf{p}^i, \bar{\theta}^i) \text{ and } \langle \dot{\mathsf{x}}_*^i(0), u_*^i(0) \rangle \geq 0, \quad \text{for all } 0 \leq t \leq \tau\}. \tag{230}$$

Proposition 46. *Given $0 \leq \tau < \infty$ and $\mathsf{p}^i \in \mathcal{P}$, then*

$$\ell_\tau(\mathsf{p}^i) \subseteq \mathfrak{K}_\tau^*(\mathsf{p}^i) \subseteq \mathfrak{R}_\tau(\mathsf{p}^i). \tag{231}$$

Proposition 46 implies that $\mathfrak{K}_\tau^*(\mathsf{p}^i)$ provides a conservative estimate of the level set $\ell_\tau(\mathsf{p}^i)$, for a given $\tau > 0$. This conservatism is owing to the fact that regular minimizing curves may enter at some time instant $t < \tau$ the interior of the reachable set; consequently, the i–th vehicle will revisit points which can reached faster than τ units of time. More precisely, for a given $0 < \tau < \infty$, there may exist $0 < \tau_0 < \tau$ such that $\mathfrak{R}_{t \leq \tau_0}(\mathsf{p}^i) \bigcap \mathfrak{K}_\tau^*(\mathsf{p}^i) \neq \varnothing$. If $\mathsf{x} \in \mathfrak{R}_{t \leq \tau_0}(\mathsf{p}^i) \bigcap \mathfrak{K}_\tau^*(\mathsf{p}^i)$, then $\mathsf{x} \notin \ell_\tau(\mathsf{p}^i)$, given that $T_{\mathrm{f}}(\mathsf{x}; \mathsf{p}^i) \leq \tau_0 < \tau$. Therefore, in order to further refine this estimate of the level set $\ell_\tau(\mathsf{p}^i)$, we need to remove from $\mathfrak{K}_\tau^*(\mathsf{p}^i)$ those points that can be reached faster than τ units of time.

Proposition 47. *Let $\tau > 0$ and $\mathsf{p}^i \in \mathcal{P}$ be given. A point $\mathsf{x} \in \ell_\tau(\mathsf{p}^i)$ only if $\mathsf{x} \notin \mathfrak{R}_{t \leq \tau_0}(\mathsf{p}^i)$, for all $\tau_0 < \tau$.*

Figures 48 and 50 illustrate, respectively, the reachable sets $\mathfrak{K}^*_\tau(\mathsf{p}^i)$ and the level sets $\ell_\tau(\mathsf{p}^i)$ for different values of $\tau \in [0, \infty)$ and two different drift fields. For the first drift field, the computation of the set $\mathfrak{K}^*_\tau(\mathsf{p}^i)$ suffices to characterize the level set $\ell_\tau(\mathsf{p}^i)$, for a given $\tau > 0$, as is illustrated in Fig. 50(a). The situation is different for the second drift field, where the sets $\mathfrak{K}^*_\tau(\mathsf{p}^i)$, for different $\tau > 0$, may be supersets of their corresponding level sets $\ell_\tau(\mathsf{p}^i)$. In particular, for some time $\tau \geq 0$, there exist points that belong to $\mathfrak{K}^*_\tau(\mathsf{p}^i)$ and lie in the interior of the reachable set $\mathfrak{R}_{t\leq\tau}(\mathsf{p}^i)$. The situation is illustrated in Fig. 50(b), where the red dashed parts of the $\mathfrak{K}^*_\tau(\mathsf{p}^i)$ correspond to points that can be reached faster than τ units of time.

8.2.3 Topological Properties of the OP-DVD

In this section, we examine under what conditions does a generator $\mathsf{p}^i \in \mathcal{P}$ of the ZVD $\mathfrak{V} = \{\mathfrak{V}^i,\ i \in \mathcal{I}_n\}$ is an interior or a boundary point of its associated cell $\mathfrak{V}^i$, when the drift field has the structure given in (205). The following two propositions present sufficient conditions for p^i to be, respectively, an interior and a boundary point of its associated Voronoi cell $\mathfrak{V}^i$.

Proposition 48. *Given $\tau > 0$ and let $\mathfrak{V} := \{\mathfrak{V}^i,\ i \in \mathcal{I}_n\}$ be the ZVD generated by the set $\mathcal{P}$. If the system* (204) *is small-time locally controllable at p^i, then $\mathsf{p}^i \in \operatorname{int} \mathfrak{V}^i$.*

Proof. From small-time local controllability, $\mathsf{p}^i \in \operatorname{int} \mathfrak{R}_{t\leq\tau}(\mathsf{p}^i)$ for all $\tau \geq 0$ [7, p. 34]. Therefore, there exists $\varepsilon = \varepsilon(\tau) > 0$, such that $B_\varepsilon(\mathsf{p}^i) := \{\mathsf{x} : |\mathsf{x} - \mathsf{p}^i| < \varepsilon\} \subset \mathfrak{R}_{t\leq\tau}(\mathsf{p}^i)$. Assume that $\mathsf{p}^i \in \mathfrak{R}_{t\leq\tau}(\mathsf{p}^j)$, for $j \in \mathcal{J} \subset \mathcal{I}_n$ and $i \neq j$. Then $B_\varepsilon(\mathsf{p}^i) \cap \mathfrak{R}_{t\leq\tau}(\mathsf{p}^j) \neq \varnothing$, for $j \in \mathcal{J}$. By hypothesis, $\mathcal{P}$ consists of distinct points, which implies that for sufficient small ε, $\mathsf{p}^j \notin B_\varepsilon(\mathsf{p}^i)$, for all $j \in \mathcal{J}$. We wish to show that there exists $\varepsilon' > 0$, such that, for all $\mathsf{x} \in B_{\varepsilon'}(\mathsf{p}^i) \cap \mathfrak{R}_{t\leq\tau}(\mathsf{p}^j)$, $T_{\mathrm{f}}(\mathsf{x}; \mathsf{p}^j) > T_{\mathrm{f}}(\mathsf{x}; \mathsf{p}^i)$, for $j \in \mathcal{J}$. Let $\bar{\tau} := \min_{j\in\mathcal{J}} \inf\{T_{\mathrm{f}}(\mathsf{x}; \mathsf{p}^i) : \mathsf{x} \in B_\varepsilon(\mathsf{p}^i) \cap \mathfrak{R}_{t\leq\tau}(\mathsf{p}^j)\}$. From small-time local controllability, it follows that, for every $\tau' < \bar{\tau}$, there exists sufficient small $\varepsilon' = \varepsilon'(\tau') > 0$ such that $B_{\varepsilon'}(\mathsf{p}^i) \subset \mathfrak{R}_{t\leq\tau'}(\mathsf{p}^i)$. Therefore, by construction, $T_{\mathrm{f}}(\mathsf{x}; \mathsf{p}^i) < \bar{\tau}$, for all $\mathsf{x} \in B_{\varepsilon'}(\mathsf{p}^i)$, thus

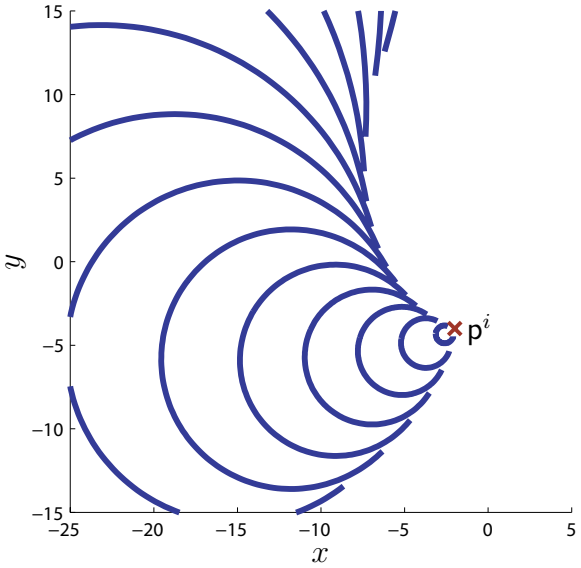

(a) $\ell_t(\mathsf{p}^i) = \mathfrak{K}^*_\tau(\mathsf{p}^i)$.

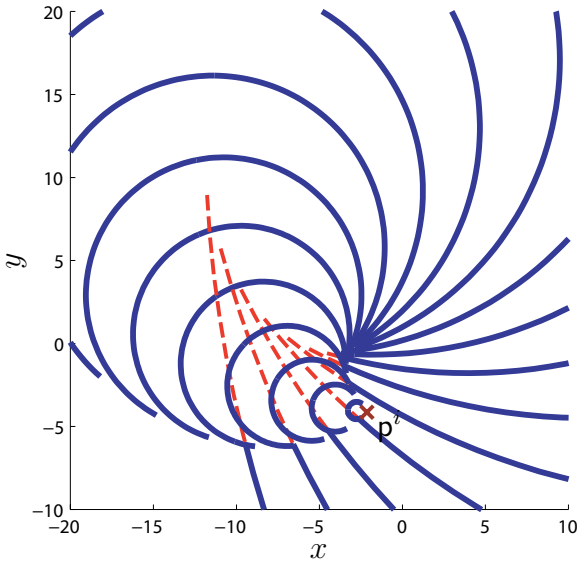

(b) $\ell_t(\mathsf{p}^i) \subseteq \mathfrak{K}^*_\tau(\mathsf{p}^i)$.

Figure 50: The level sets $\ell_\tau(\mathsf{p}^i)$ are, in general, a subset of the set $\mathfrak{K}^*_\tau(\mathsf{p}^i)$.

completing the proof. □

Proposition 49. *Let $\tau > 0$, and let $\mathfrak{V} := \{\mathfrak{V}^i,\ i \in \mathcal{I}_n\}$ be the ZVD generated by the set $\mathcal{P}$. If $\mathsf{p}^i \in \mathrm{bd}\mathfrak{R}_{t\leq\tau}(\mathsf{p}^i)$, then $\mathsf{p}^i \in \mathrm{bd}\mathfrak{V}^i$.*

Proof. The proof follows readily from the fact that $\mathrm{bd}\mathfrak{R}_{t\leq\tau}(\mathsf{p}^i) \cap \mathfrak{V}^i \ni \mathsf{p}^i$ is non-empty and $\mathfrak{V}^i \subseteq \mathfrak{R}_{t\leq\tau}(\mathsf{p}^i)$. □

Remark 13 It is possible that there might exist $\tau_0 < \tau$ such that $\mathsf{p}^i \in \mathrm{bd}\mathfrak{R}_{t\leq\tau_0}(\mathsf{p}^i)$ but $\mathsf{p}^i \in \mathrm{int}\mathfrak{R}_{t\leq\tau}(\mathsf{p}^i)$. This scenario is illustrated in Fig. 50(b). In this case, it is not clear whether a generator $\mathsf{p}^i \in \mathcal{P}$ will be an interior or a boundary point of its associated cell of the ZVD generated by $\mathcal{P}$.

8.3 Simulation Results

In this section, we present simulation results to better illustrate the previous analysis. In particular, Figure 51 illustrates the ZVD generated by a point-set of nine generators for two different drift fields having the structure given in (205). In particular, for the first drift field we use the following simulation data: $\mathsf{A} = \left[\begin{smallmatrix} 0.1 & 0.05 \\ -0.05 & 0.1 \end{smallmatrix}\right]$, $\nu = [0.2,\ 0.4]^{\mathsf{T}}$, whereas for the second drift field, we assume that $\mathsf{A} = \left[\begin{smallmatrix} 0.12 & 0.11 \\ -0.04 & -0.07 \end{smallmatrix}\right]$, $\nu = [0.3,\ -0.2]^{\mathsf{T}}$.

Furthermore, Figure 52 illustrates the interpretation of the ZVD as the projection of the surface $\mathcal{S}_i$ of minimum time-to-go from each generator $\mathsf{p}^i \in \mathcal{P}$ with their common lower envelope surface $\mathcal{S}_{\mathcal{P}}$.

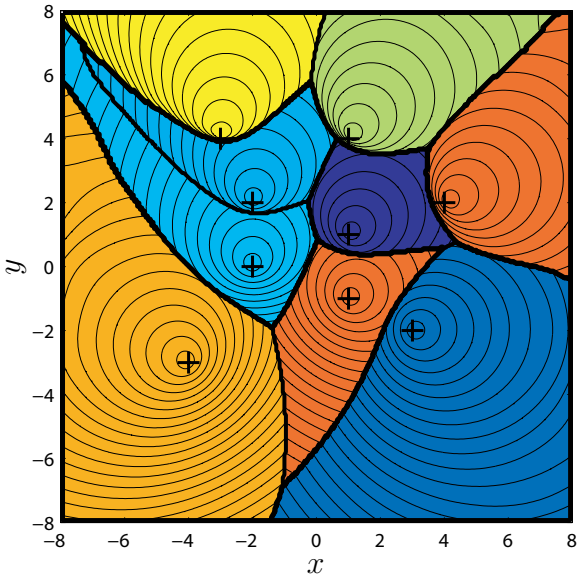

(a) First scenario

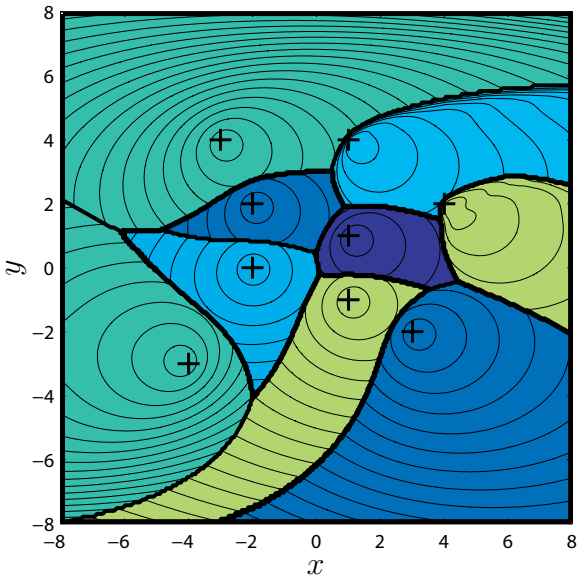

(b) Second scenario

Figure 51: The Zermelo-Voronoi diagram generated by a set of nine generators.

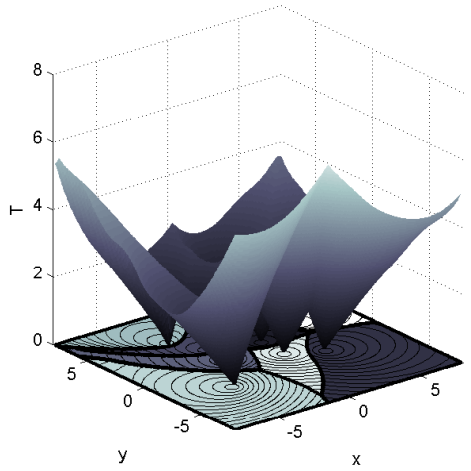

(a) First scenario

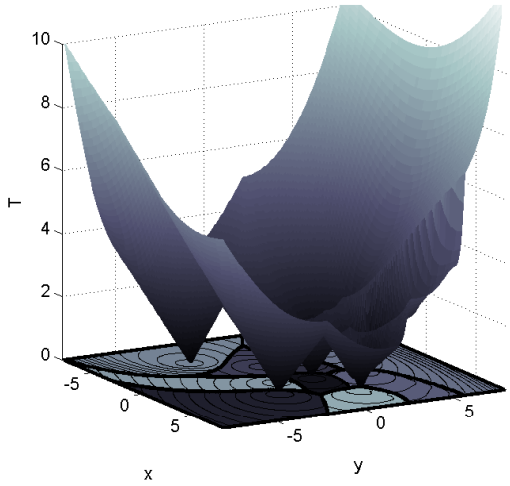

(b) Second scenario

Figure 52: The Zermelo-Voronoi diagram generated by a set of nine generators interpreted as the projection of the intersection of the surfaces of the minimum time-to-go function for each generator with their common lower envelope.

CHAPTER IX

OPTIMAL PURSUER AND MOVING TARGET ASSIGNMENT USING DYNAMIC VORONOI DIAGRAMS

The material presented in this chapter builds on the results in [13, 17].

9.1 Introduction

In this chapter, we address a Voronoi-like partitioning problem for a set of pursuers (moving generators) whose objective is to capture moving targets in the plane. The solution of this problem furnishes a scheme that assigns a pursuer from a given team of pursuers to a moving target with respect to a generalized proximity metric, namely the minimum capture time (rather than with the Euclidean distance metric as in the standard Voronoi diagram problem). The problem considered in this chapter can be put under the umbrella of dynamic Voronoi diagram problems, that is, Voronoi-like partitioning problems where the generators are moving points in the plane [141, 168, 69, 70, 2, 85, 14, 43]. Specifically, we consider the following partitioning problem: Given a team of n vehicles (pursuers), which are distributed over n distinct locations in the plane, partition the plane into n "capture zones," such that each pursuer is assigned to a unique capture zone. The rule that assigns each pursuer to a capture zone is the following: a pursuer associated with a particular capture zone can capture a moving target traveling within the same zone at a given instant of time faster than any other pursuer from the given set of pursuers. In our problem formulation, we do not constraint the moving target to follow a prescribed trajectory, as it is usually assumed in the literature [69, 70]. Instead, the target can apply an "evading" strategy

in response to the actions of its pursuer. The target's strategy is a feedback control law that depends only on the relative position between the moving target and its pursuer.

9.2 Formulation of the Optimal Pursuit Problem

Consider a team of n pursuers located, at time $t = 0$, at n distinct points in the plane, denoted by $\mathcal{P} := \{\bar{\mathsf{x}}^i_{\mathcal{P}} \in \mathbb{R}^2, i \in \mathcal{I}\}$, where $\mathcal{I}_n := \{1, \ldots, n\}$. It is assumed that the kinematics of the i^{th} pursuer starting at point $\bar{\mathsf{x}}^i_{\mathcal{P}} \in \mathcal{P}$ are given by

$$\dot{\mathsf{x}}^i_{\mathcal{P}} = u^i_{\mathcal{P}}, \quad \mathsf{x}^i_{\mathcal{P}}(0) = \bar{\mathsf{x}}^i_{\mathcal{P}}, \tag{232}$$

where $\mathsf{x}^i_{\mathcal{P}} := (x^i_{\mathcal{P}}, y^i_{\mathcal{P}}) \in \mathbb{R}^2$ and $\bar{\mathsf{x}}^i_{\mathcal{P}} := (\bar{x}^i_{\mathcal{P}}, \bar{y}^i_{\mathcal{P}}) \in \mathbb{R}^2$ denote the position vectors of the i^{th} pursuer at time t and $t = 0$, respectively, and $u^i_{\mathcal{P}}$ is the control input (velocity vector) of the i^{th} pursuer. We assume that $u^i_{\mathcal{P}} \in \mathcal{U}_{\mathcal{P}}$, where $\mathcal{U}_{\mathcal{P}}$ consists of all piecewise continuous functions taking values in the set $U_{\mathcal{P}} = \{\mathsf{z} \in \mathbb{R}^2 : |\mathsf{z}| \leq \bar{u}_{\mathcal{P}}\}$, where $\bar{u}_{\mathcal{P}}$ is a positive constant (maximum allowable speed of the pursuers). The goal of each pursuer, which is initially located at a point in $\mathcal{P}$, is to capture a moving target detected in its vicinity. It is assumed that the kinematics of such a moving target are described by

$$\dot{\mathsf{x}}_{\mathcal{T}} = u_{\mathcal{T}}, \quad \mathsf{x}_{\mathcal{T}}(0) = \bar{\mathsf{x}}_{\mathcal{T}}, \tag{233}$$

where $\mathsf{x}_{\mathcal{T}} := (x_{\mathcal{T}}, y_{\mathcal{T}}) \in \mathbb{R}^2$ and $\bar{\mathsf{x}}_{\mathcal{T}} := (\bar{x}_{\mathcal{T}}, \bar{y}_{\mathcal{T}}) \in \mathbb{R}^2$ denote the target's position vectors at time t and $t = 0$, respectively, and $u_{\mathcal{T}}$ is the control input (velocity vector) of the target. It is further assumed that the moving target can employ an evading strategy in response to the pursuer's actions. In particular, $u_{\mathcal{T}}$ is a feedback control law, which depends on the relative position of the target from the i^{th} pursuer, that is, $u_{\mathcal{T}} = u_{\mathcal{T}}(\mathsf{x}_{\mathcal{T}} - \mathsf{x}^i_{\mathcal{P}})$.

Assumption 1. *There exists a Lipschitz continuous function* $f : \mathbb{R}_+ \mapsto \mathbb{R}$ *such that the evading strategy* $u_{\mathcal{T}}$ *of the target satisfies the following condition*

$$\langle u_{\mathcal{T}}, \mathsf{x}_{\mathcal{T}} - \mathsf{x}^i_{\mathcal{P}} \rangle = f(|\mathsf{x}_{\mathcal{T}} - \mathsf{x}^i_{\mathcal{P}}|). \tag{234}$$

The interpretation of Assumption 1 is as follows: The projection of the velocity vector of the maneuvering target on the relative position vector between the target and the i^{th} pursuer depends only on the relative distance between the two. This is a reasonable assumption for problems of pursuit when only measurements of the relative position between the pursuer and the target are available to both of them. In addition, in this work we do not explicitly assume that the maximum allowable speed of the target is strictly less than the speed of the pursuer. Note that if we were dealing with a problem of pursuit-evasion [99, 93, 82], rather than a problem of pursuit of a moving/maneuvering target, then the assumption that the evader may travel faster than its pursuer would automatically mean that the evader can always escape capture [93]. Capture for the case of a faster target can occur only if the target follows a suboptimal evading strategy. In such a case, capture may (but not necessarily) still occur for some initial conditions that belong to a non-trivial subset of $\mathbb{R}^2$. In Section 9.3 we characterize the *winning set* of the i^{th} pursuer, that is, the set of initial positions of the maneuvering target from which the i^{th} pursuer can capture the target in finite time. As we shall see in more detail later in the paper, under Assumption 1 along with the following condition

$$f(\mathsf{z}) \leq \bar{f}(\mathsf{z}), \quad \text{for all} \quad \mathsf{z} \geq \epsilon_c, \tag{235}$$

where $\bar{f} : [\epsilon_c, \infty) \mapsto \mathbb{R}$ is a continuous function that is known to all of the pursuers, we will be able to estimate the winning set of the i^{th} pursuer. Note that the winning set against a slower target is always the whole $\mathbb{R}^2$, regardless of whether the target plays optimally or suboptimally.

Let $\mathsf{x}_{\mathcal{T}}(\cdot; u_{\mathcal{T}}, \bar{\mathsf{x}}_{\mathcal{T}})$ and $\mathsf{x}^i_{\mathcal{P}}(\cdot; u^i_{\mathcal{P}}, \bar{\mathsf{x}}^i_{\mathcal{P}})$ denote the trajectories of the target and the i^{th} pursuer generated by $u_{\mathcal{T}}$ and $u^i_{\mathcal{P}}$ and originating from $\bar{\mathsf{x}}_{\mathcal{T}}$ and $\bar{\mathsf{x}}^i_{\mathcal{P}}$, respectively. The objective of each pursuer is to determine an admissible pursuit strategy that minimizes the time T_{f} such that $|\mathsf{x}_{\mathcal{T}}(t; u_{\mathcal{T}}, \bar{\mathsf{x}}_{\mathcal{T}}) - \mathsf{x}^i_{\mathcal{P}}(t; u^i_{\mathcal{P}}, \bar{\mathsf{x}}^i_{\mathcal{P}})| > \epsilon_c$ for all $t < T_{\text{f}}$ (*time of first capture*), for a sufficiently small $\epsilon_c > 0$, where ϵ_c is the *capturability radius* of the pursuit problem.

To this end, let us consider the state transformation $\mathsf{y}^i := \mathsf{x}_{\mathcal{T}} - \mathsf{x}^i_{\mathcal{P}}$. Equation (232) can then be written in the following compact form

$$\dot{\mathsf{y}}^i = \mathsf{u}^i + u_{\mathcal{T}}(\mathsf{y}^i), \quad \mathsf{y}^i(0) = \bar{\mathsf{y}}^i := \bar{\mathsf{x}}_{\mathcal{T}} - \bar{\mathsf{x}}^i_{\mathcal{P}}, \tag{236}$$

where $\mathsf{u}^i := -u^i_{\mathcal{P}}$. Thus, the optimal pursuit strategy of the i^{th} pursuer follows from the solution of the following minimum-time problem.

Problem 14 (i^{th} MTP)**.** *Let the system described by equation* (236)*, and let* $u_{\mathcal{T}}$ *satisfy Assumption 1. Determine the control input* $\mathsf{u}^i \in \mathcal{U}_{\mathcal{P}}$ *such that*

i. The trajectory $\mathsf{y}^i_* : [0, T_{\text{f}}] \mapsto \mathbb{R}^2$ *generated by the control* u^i_* *satisfies the boundary conditions*

$$\mathsf{y}^i_*(0) = \bar{\mathsf{y}}^i, \quad |\mathsf{y}^i_*(T_{\text{f}})| \leq \epsilon_c. \tag{237}$$

ii. The control u^i_* *minimizes, along the trajectory* y^i_**, the cost functional* $J(\mathsf{u}^i) := T_{\text{f}} = T_{\text{f}}(\bar{\mathsf{y}}^i)$.

Problem 14 can be interpreted as a problem of steering an integrator from $\bar{\mathsf{y}}^i$ to a ball of radius ϵ_c centered at the origin, in the presence of a spatially-varying drift $u_{\mathcal{T}}(\mathsf{y}^i)$ in minimum-time. If the function $u_{\mathcal{T}}$ is perfectly known to the pursuers, then Problem 14 can be reduced to a special case of Zermelo's navigation problem. Here we employ, however, a different approach that will allow us to characterize the unique, global solution of Problem 14 in closed form, which does not follow directly from the solution of the ZNP. The following proposition gives the solution of Problem 14.

Proposition 50. *If Problem 14 is feasible, then its solution is unique, and it is given in feedback form as follows*

$$\mathsf{u}^i_* = -\bar{u}_{\mathcal{P}} \frac{\mathsf{y}^i_*}{|\mathsf{y}^i_*|}. \tag{238}$$

Proof. Let $|\mathsf{y}^i|^2 = \langle \mathsf{y}^i, \mathsf{y}^i \rangle$ and suppose that y^i is a trajectory generated from some admissible control u^i on $[0, T_\mathrm{f}]$. Then

$$\frac{\mathrm{d}}{\mathrm{d}t}|\mathsf{y}^i|^2 = \frac{\mathrm{d}}{\mathrm{d}t}\langle \mathsf{y}^i, \mathsf{y}^i \rangle = 2\langle \mathsf{y}^i, \mathsf{u}^i + u^i_{\mathcal{T}}(\mathsf{y}^i) \rangle. \tag{239}$$

In light of Assumption 1, and equations (236) and (239), it follows that, for all $t \in [0, T_\mathrm{f}]$,

$$\dot{\eta}^i = \frac{f(\eta^i)}{\eta^i} + v^i, \quad \eta^i(0) = \bar{\eta}^i := |\bar{\mathsf{y}}^i|, \tag{240}$$

where $\eta^i := |\mathsf{y}^i|$ and v^i is a new scalar control input given by

$$v^i := \frac{\langle \mathsf{u}^i, \mathsf{y}^i \rangle}{\eta^i}. \tag{241}$$

First, we show that $\eta^i(t) = |\mathsf{y}^i(t)| > 0$ for all $t \in [0, T_\mathrm{f}]$. Indeed, let us assume that $|\bar{\mathsf{y}}^i| > \epsilon_c$ (if $|\bar{\mathsf{y}}^i| \leq \epsilon_c$, then the i^{th} MTP admits a trivial solution and $T_\mathrm{f} = 0$). By continuity, if $\eta^i(t_1) = 0$ for some $t_1 > 0$, then there exists $t_2 < t_1$ such that $\eta^i(t_2) = \epsilon_c$. By definition, $T_\mathrm{f} = \inf\{\tau : \eta^i(\tau) = \epsilon_c\}$. It follows that $T_\mathrm{f} \leq t_2 < t_1$, and hence $\eta^i(t) \geq \epsilon_c > 0$, for all $t \in [0, T_\mathrm{f}]$. It follows that the rhs of equation (240) is well-defined, and $\dot{\eta}^i(t)$ exists for all $t \in [0, T_\mathrm{f}]$.

By virtue of the Cauchy-Schwartz inequality, it follows from (241) that $|v^i| \leq \bar{u}_{\mathcal{P}}$. Therefore, Problem 14 reduces to the problem of determining a scalar control v^i_* with $|v^i_*| \leq \bar{u}_{\mathcal{P}}$ that will steer the scalar system described by equation (240) to the interval $[0, \epsilon_c]$ in minimum time. In [4], it is shown that the solution of this scalar min-time problem is given by $v^i_* = -\bar{u}_{\mathcal{P}}$. Therefore, (241) implies that

$$\langle \mathsf{u}^i_*, \mathsf{y}^i_* \rangle = -\bar{u}_{\mathcal{P}} \eta^i_*, \tag{242}$$

which implies that u^i_* is a vector of length $\bar{u}_{\mathcal{P}}$ parallel to the unit vector $-\mathsf{y}^i_*/|\mathsf{y}^i_*|$, thus completing the proof. □

Proposition 50 implies, in particular, that the solution of the optimal control Problem 14 is independent of the evading strategy of the target, $u_{\mathcal{T}}$. However, as we shall see next, the characterization of the winning set of the i^{th} pursuer depends on the evading strategy of the target, hence on f as well.

9.3 The Winning Sets of the Pursuers

Next, we examine the feasibility of Problem 14 for a given $\bar{\mathsf{y}}^i \in \mathbb{R}^2$. This will allow us to characterize the winning set of the i^{th} pursuer, that is, the set of the initial positions of the target from which it can be captured by the i^{th} pursuer in finite time. In other words, the winning set of the i^{th} pursuer is given by

$$\mathcal{W}_f(\bar{\mathsf{x}}^i_{\mathcal{P}}) := \{\mathsf{x} \in \mathbb{R}^2 : T_{\text{f}}(\mathsf{x} - \bar{\mathsf{x}}^i_{\mathcal{P}}) < \infty\}, \tag{243}$$

where $T_{\text{f}}(\mathsf{x} - \bar{\mathsf{x}}^i_{\mathcal{P}})$ is the time of capture of the target by the i^{th} pursuer, when $\bar{\mathsf{x}}_{\mathcal{T}} = \mathsf{x}$. First, note that if $|\bar{\mathsf{y}}^i| \leq \epsilon_c$, then capture occurs trivially at $t = 0$. Hence, the set $\{\mathsf{x} \in \mathbb{R}^2 : |\mathsf{x} - \bar{\mathsf{x}}^i_{\mathcal{P}}| \leq \epsilon_c\}$ is necessarily a subset of the winning set for each pursuer, regardless of the dynamics of the pursuer or the target. Next, we compute the winning set for the non-trivial case $|\bar{\mathsf{y}}^i| > \epsilon_c$.

Proposition 51. *Let $\epsilon_c > 0$. Then Problem 14 is feasible for the i^{th} pursuer for all $|\bar{\mathsf{y}}^i| > \epsilon_c$ if and only if*

$$f(\mathsf{z}) < \bar{u}_{\mathcal{P}}\mathsf{z}, \quad \text{forall} \quad \epsilon_c \leq \mathsf{z} \leq |\bar{\mathsf{y}}^i|. \tag{244}$$

Proof. Proposition 50 implies that the closed loop dynamics of (236) can be written in terms of $\eta^i = |\mathsf{y}^i|$ as follows

$$\dot{\eta}^i = \frac{f(\eta^i)}{\eta^i} - \bar{u}_{\mathcal{P}}, \quad \eta^i(0) = \bar{\eta}^i. \tag{245}$$

Condition (244) implies that

$$\dot{\eta}^i = \frac{f(\eta^i)}{\eta^i} - \bar{u}_{\mathcal{P}} < 0, \quad \text{for all} \quad \epsilon_c \leq \eta^i \leq |\bar{\mathsf{y}}^i|. \tag{246}$$

From (246) it follows that the set $\{\mathsf{z} : 0 < \mathsf{z} \leq \epsilon_c\}$ is an attractive invariant set for (245) for all initial conditions $\eta^i(0) > \epsilon_c$. Furthermore, $\dot{\eta}^i < 0$ for $\eta^i = \epsilon_c$. It follows that there exists $T = T(\epsilon_c)$, such that $\eta^i(t) \leq \epsilon_c$ for $t \geq T(\epsilon_c)$, thus showing feasibility of the Problem 14.

Conversely, suppose there exists $\tilde{\eta}^i = |\tilde{\mathsf{y}}|$, where $\tilde{\mathsf{y}} \in \mathbb{R}^2$, such that $\epsilon_c \leq \tilde{\eta}^i \leq |\bar{\mathsf{y}}^i|$ and

$$f(\tilde{\eta}^i) \geq \bar{u}_{\mathcal{P}} \tilde{\eta}^i. \tag{247}$$

Notice that the set $S := \{\mathsf{z} : \mathsf{z} \geq \tilde{\eta}^i\}$ is positively invariant for (245) since $f(\mathsf{z})/\mathsf{z} - \bar{u}_{\mathcal{P}} \geq 0$ for all $\mathsf{z} \in \mathrm{bd}S$. Since $\eta^i(0) \in S$, it follows that $\eta^i(t) \geq \tilde{\eta}^i$, for all $t \geq 0$, which implies that the Problem 14 is not feasible for $\epsilon_c < \tilde{\eta}^i$. If, on the other hand, $\epsilon_c = \tilde{\eta}^i$, then either $f(\epsilon_c) > \bar{u}_{\mathcal{P}} \epsilon_c$ or $f(\epsilon_c) = \bar{u}_{\mathcal{P}} \epsilon_c$. In the first case, any trajectory starting from $\eta^i(0) > \epsilon_c$ can never reach the set $\{\mathsf{z} : \ 0 \leq \mathsf{z} \leq \epsilon_c\}$. In the second case, $\eta^i = \epsilon_c$ is an equilibrium solution for (245). Since the right hand side of (245) is Lipschitz continuous at $\eta^i = \epsilon_c$, this equilibrium can only be reached asymptotically [31]. In both cases, Problem 14 is infeasible. □

Henceforth, we refer to (244) as the *capturability condition* of Problem 14. In order to characterize the winning set of the i^{th} pursuer, let

$$\bar{\eta}_f := \inf\{\mathsf{z} \in [\epsilon_c, \infty) : f(\mathsf{z}) \geq \bar{u}_{\mathcal{P}} \mathsf{z}\}. \tag{248}$$

Note that $\bar{\eta}_f \geq \epsilon_c$. If $f(\mathsf{z}) < \bar{u}_{\mathcal{P}} \mathsf{z}$ for all $\mathsf{z} \in [\epsilon_c, \infty)$, we take $\bar{\eta}_f := \infty$, and hence $\mathcal{W}_f(\bar{\mathsf{x}}^i_{\mathcal{P}}) = \mathbb{R}^2$. If $f(\mathsf{z}) \geq \bar{u}_{\mathcal{P}} \mathsf{z}$ for all $\mathsf{z} \in [\epsilon_c, \infty)$, then $\bar{\eta}_f = \epsilon_c$, and hence $\mathcal{W}_f(\bar{\mathsf{x}}^i_{\mathcal{P}}) = \{\mathsf{x} \in \mathbb{R}^2 : \ |\bar{\mathsf{x}}^i_{\mathcal{P}} - \mathsf{x}| \leq \epsilon_c\}$. Finally, if $\epsilon_c < \bar{\eta}_f < \infty$, then it follows readily from (248) that $f(\mathsf{z}) < \bar{u}_{\mathcal{P}} \mathsf{z}$ for all $\epsilon_c \leq \mathsf{z} < \bar{\eta}_f$ and hence, in light of Proposition 51, $\mathcal{W}_f(\bar{\mathsf{x}}^i_{\mathcal{P}}) := \{\mathsf{x} \in \mathbb{R}^2 : \ |\bar{\mathsf{x}}^i_{\mathcal{P}} - \mathsf{x}| < \bar{\eta}_f\}$. For all cases, the winning set of the i^{th} pursuer can be defined compactly as

$$\mathcal{W}_f(\bar{\mathsf{x}}^i_{\mathcal{P}}) := \{\mathsf{x} : \ |\bar{\mathsf{x}}^i_{\mathcal{P}} - \mathsf{x}| < \bar{\eta}_f\} \cup \{\mathsf{x} : \ |\bar{\mathsf{x}}^i_{\mathcal{P}} - \mathsf{x}| \leq \epsilon_c\}. \tag{249}$$

Note, however, that the i^{th} pursuer does not know exactly its winning set, since it has only partial knowledge of f, and consequently of $\bar{\eta}_f$ as well. As a result, each pursuer can only compute an approximation of its actual winning set. To this end, let

$$\bar{\eta}_{\bar{f}} := \inf\{\mathsf{z} \in [\epsilon_c, \infty) : \bar{f}(\mathsf{z}) \geq \bar{u}_{\mathcal{P}}\mathsf{z}\}. \tag{250}$$

In light of (235), it follows that $\bar{\eta}_{\bar{f}} \leq \bar{\eta}_f$. Let

$$\mathcal{W}_{\bar{f}}(\bar{\mathsf{x}}^i_{\mathcal{P}}) := \{\mathsf{x} : \ |\bar{\mathsf{x}}^i_{\mathcal{P}} - \mathsf{x}| < \bar{\eta}_{\bar{f}}\} \cup \{\mathsf{x} : |\bar{\mathsf{x}}^i_{\mathcal{P}} - \mathsf{x}| \leq \epsilon_c\}. \tag{251}$$

Clearly, $\mathcal{W}_{\bar{f}}(\bar{\mathsf{x}}^i_{\mathcal{P}}) \subseteq \mathcal{W}_f(\bar{\mathsf{x}}^i_{\mathcal{P}})$. Hence, $\mathcal{W}_{\bar{f}}(\bar{\mathsf{x}}^i_{\mathcal{P}})$ is a conservative approximation of the winning set $\mathcal{W}_f(\bar{\mathsf{x}}^i_{\mathcal{P}})$. Note that, contrary to $\mathcal{W}_f(\bar{\mathsf{x}}^i_{\mathcal{P}})$, the i^{th} pursuer has perfect knowledge of $\mathcal{W}_{\bar{f}}(\bar{\mathsf{x}}^i_{\mathcal{P}})$. Furthermore, the closeness of the approximation of the winning set of the i^{th} pursuer with $\mathcal{W}_{\bar{f}}(\bar{\mathsf{x}}^i_{\mathcal{P}})$ depends on the difference $\bar{\eta}_f - \bar{\eta}_{\bar{f}}$.

9.4 The Dynamic Voronoi Partitioning Problem

Next, we formulate a dynamic Voronoi-like partitioning problem based on the minimum time-to-go of the i^{th} MTP, which will allow us to assign a pursuer starting from a point in $\mathcal{P}$ to a moving target traveling in the plane. The space we wish to partition, denoted henceforth as $\mathcal{W}$, is the union of all $\mathcal{W}_{\bar{\eta}_f}(\bar{\mathsf{x}}^i_{\mathcal{P}})$, where $i \in \mathcal{I}_n$.

Problem 15. *Given a collection of n pursuers, initially located at distinct points in $\mathcal{P}$, and the cost function*

$$c^i(\mathsf{x}, \bar{\mathsf{x}}^i_{\mathcal{P}}) := T_{\text{f}}(\mathsf{x} - \bar{\mathsf{x}}^i_{\mathcal{P}}), \tag{252}$$

where T_{f} is the minimum time from the solution of Problem 14, determine a partition $\mathcal{V} = \{\mathcal{V}^i : i \in \mathcal{I}\}$ of $\mathcal{V}$ such that

i. $\mathcal{W} = \bigcup_{i\in\mathcal{I}} \mathcal{V}_i$

ii. for all $\mathsf{x} \in \mathcal{V}^i$, $c(\bar{\mathsf{x}}^i_{\mathcal{P}}, \mathsf{x}) < \infty$

iii. $c(\bar{\mathsf{x}}^i_{\mathcal{P}}, \mathsf{x}) \leq c(\bar{\mathsf{x}}^j_{\mathcal{P}}, \mathsf{x})$ *for* $i, j \in \mathcal{I}_n$ *with* $j \neq i$.

Henceforth, we shall refer to the solution of Problem 15 as the Optimal Pursuit Dynamic Voronoi Diagram (OP-DVD). The set $\mathcal{V}^i$, constitutes a Voronoi cell (Dirichlet domain) of the OP-DVD. We say that the i^{th} and j^{th} pursuers, where $i,\, j \in \mathcal{I}_n$, are neighbors if and only if the set $\mathcal{V}^i \cap \mathcal{V}^j$ is neither non-empty nor a singleton. Because the evading strategy of any moving target is not perfectly known, we can only provide approximate solutions to Problem 15, as it is discussed next.

9.5 Construction of an Approximate OP-DVD

In order to construct an approximate OP-DVD, we will first investigate whether the minimum time-to-go of Problem 14 belongs to a class of generalized metrics that are associated with Voronoi-like partitions, for which efficient computational techniques exist in the literature [141].

To this end, observe that direct integration of equation (245) yields

$$T_{\text{f}}(\bar{\text{y}}^i) := \begin{cases} 0, & \text{if } 0 \leq |\bar{\text{y}}^i| \leq \epsilon_c, \\ \displaystyle\int_{\epsilon_c}^{|\bar{\text{y}}^i|} \frac{\mu \, \mathrm{d}\mu}{\bar{u}_{\mathcal{P}}\mu - f(\mu)}, & \text{if } \epsilon_c < |\bar{\text{y}}^i| < \bar{\eta}_f, \\ \infty, & \text{otherwise.} \end{cases} \tag{253}$$

The following result will be useful in the subsequent analysis

Proposition 52. *Let $\bar{\eta}_f > \epsilon_c$. Given two points $\xi, \psi \in \mathbb{R}^2$, with $|\xi|, |\psi| \in (\epsilon_c, \bar{\eta}_f)$, the minimum-time of Problem 14 satisfies*

$$\epsilon_c < |\xi| < |\psi| < \bar{\eta}_f \Leftrightarrow 0 < T_{\text{f}}(\xi) < T_{\text{f}}(\psi) < \infty, \tag{254}$$

and, furthermore,

$$\epsilon_c < |\xi| = |\psi| < \bar{\eta}_f \Leftrightarrow 0 < T_{\text{f}}(\xi) = T_{\text{f}}(\psi) < \infty. \tag{255}$$

Proof. First, notice that the minimum-time of Problem 14 satisfies

$$T_{\text{f}}(\psi) - T_{\text{f}}(\xi) = \int_{|\xi|}^{|\psi|} \phi(\mu) \, \mathrm{d}\mu, \quad \phi(\mu) := \frac{\mu}{\bar{u}_{\mathcal{P}}\mu - f(\mu)}.$$

The function $\phi : (\epsilon_c, \bar{\eta}_f) \mapsto \mathbb{R}$ is continuous and strictly positive on $(\epsilon_c, \bar{\eta}_f)$. From the mean value theorem for Riemann integrals [26], it follows that there exists $\epsilon_c < |\xi| \leq \zeta \leq |\psi| < \bar{\eta}_f$ such that

$$T_{\mathrm{f}}(\psi) - T_{\mathrm{f}}(\xi) = \int_{|\xi|}^{|\psi|} \phi(\mu)\, \mathrm{d}\mu = \phi(\zeta)(|\psi| - |\xi|). \tag{256}$$

Since $\phi(\zeta) > 0$ for all $\epsilon_c < \zeta < \bar{\eta}_f$, the result follows readily. □

Corollary 5. *Let $\bar{\eta}_f > \epsilon_c$ and let ξ, ψ be two given points in $\mathbb{R}^2$. Then the minimum-time of Problem 14 satisfies*

$$|\xi| \leq |\psi| \Rightarrow T_{\mathrm{f}}(\xi) \leq T_{\mathrm{f}}(\psi). \tag{257}$$

Proof. The statement of the corollary for the case when $\epsilon_c < |\xi| \leq |\psi| < \bar{\eta}_f$ has already been proved in Proposition 52. The proof for the other cases, namely, when $|\xi| \leq \epsilon_c < |\psi| < \bar{\eta}_f$, or $|\xi| \leq |\psi| \leq \epsilon_c$, or $\epsilon_c < |\xi| < \bar{\eta}_f \leq |\psi|$, and $\bar{\eta}_f \leq |\xi| \leq |\psi|$ follows trivially from (253). □

Next, we present the solution of Problem 15.

Theorem 3. *Let $V := \{V^i, i \in \mathcal{I}_n\}$ be the standard Voronoi partition generated by the set $\mathcal{P}$, and assume that $\bar{\eta}_f > \epsilon_c$. The solution of Problem 15 is given by*

$$\mathcal{V}^i = V^i \cap \mathcal{W}_f(\bar{\mathsf{x}}^i_{\mathcal{P}}), \quad i \in \mathcal{I}_n, \tag{258}$$

where $\mathcal{W}_f(\bar{\mathsf{x}}^i_{\mathcal{P}})$ is the winning set of the i^{th} pursuer, given by (249).

Proof. Let $\mathsf{x} \in V^i \cap \mathcal{W}_f(\bar{\mathsf{x}}^i_{\mathcal{P}})$. In particular, $\mathsf{x} \in V^i$ if and only if $|\mathsf{x} - \bar{\mathsf{x}}^i_{\mathcal{P}}| \leq |\mathsf{x} - \bar{\mathsf{x}}^j_{\mathcal{P}}|$, for all $j \neq i$, which implies, in light of Corollary 5, that $T_{\mathrm{f}}(\mathsf{x} - \bar{\mathsf{x}}^i_{\mathcal{P}}) \leq T_{\mathrm{f}}(\mathsf{x} - \bar{\mathsf{x}}^j_{\mathcal{P}})$ for all $i \neq j$. Furthermore, if $\mathsf{x} \in \mathcal{W}_f(\bar{\mathsf{x}}^i_{\mathcal{P}})$ then $T_{\mathrm{f}}(\mathsf{x} - \bar{\mathsf{x}}^i_{\mathcal{P}}) < \infty$. It follows that $\mathsf{x} \in \mathcal{V}^i$ and hence $V^i \cap \mathcal{W}_f(\bar{\mathsf{x}}^i_{\mathcal{P}}) \subseteq \mathcal{V}^i$ for all $i \in \mathcal{I}_n$.

Next, assume $\mathsf{x} \in \mathcal{V}^i$. By the definition of $\mathcal{V}^i$, it follows that $T_{\mathrm{f}}(\mathsf{x} - \bar{\mathsf{x}}^i_{\mathcal{P}}) < \infty$ and $T_{\mathrm{f}}(\mathsf{x} - \bar{\mathsf{x}}^i_{\mathcal{P}}) \leq T_{\mathrm{f}}(\mathsf{x} - \bar{\mathsf{x}}^j_{\mathcal{P}})$, for all $j \neq i$. If $0 < T_{\mathrm{f}}(\mathsf{x} - \bar{\mathsf{x}}^i_{\mathcal{P}}) \leq T_{\mathrm{f}}(\mathsf{x} - \bar{\mathsf{x}}^j_{\mathcal{P}}) < \infty$, it

follows from Proposition 52 that $|\mathsf{x} - \bar{\mathsf{x}}^i_{\mathcal{P}}| \leq |\mathsf{x} - \bar{\mathsf{x}}^j_{\mathcal{P}}|$, for all $j \neq i$. In addition, it follows readily that $T_{\mathrm{f}}(\mathsf{x} - \bar{\mathsf{x}}^i_{\mathcal{P}}) \leq T_{\mathrm{f}}(\mathsf{x} - \bar{\mathsf{x}}^j_{\mathcal{P}})$ implies that $|\mathsf{x} - \bar{\mathsf{x}}^i_{\mathcal{P}}| \leq |\mathsf{x} - \bar{\mathsf{x}}^j_{\mathcal{P}}|$, for all $j \neq i$ and $\mathsf{x} \in \mathcal{V}^i$, when $T_{\mathrm{f}}(\mathsf{x} - \bar{\mathsf{x}}^j_{\mathcal{P}}) = 0$ and $T_{\mathrm{f}}(\mathsf{x} - \bar{\mathsf{x}}^j_{\mathcal{P}}) = \infty$ as well. Thus $\mathsf{x} \in V^i$. Furthermore, since $T_{\mathrm{f}}(\mathsf{x} - \bar{\mathsf{x}}^i_{\mathcal{P}}) < \infty$, then $\mathsf{x} \in \mathcal{W}_f(\bar{\mathsf{x}}^i_{\mathcal{P}})$. Hence $\mathsf{x} \in V^i \cap \mathcal{W}_f(\bar{\mathsf{x}}^i_{\mathcal{P}})$ and $\mathcal{V}^i \subseteq V^i \cap \mathcal{W}_f(\bar{\mathsf{x}}^i_{\mathcal{P}})$ for $i \in \mathcal{I}_n$. □

Theorem 3 suggests that the i^{th} element of the partition that solves Problem 15 is the intersection of the winning set of the i^{th} pursuer with the cell of the standard Voronoi diagram generated by the set $\mathcal{P}$ that is associated with the generator $\bar{\mathsf{x}}^i_{\mathcal{P}}$. Note that the OP-DVD encodes the proximity relations between a target and the pursuers with respect to time of capture, for all pursuers in $\mathcal{P}$.

The following proposition deals with the neighboring relations between the set of pursuers in $\mathcal{V}$.

Proposition 53. *Let $V := \{V^i : i \in \mathcal{I}_n\}$ be the standard Voronoi partition generated by the set $\mathcal{P}$ and let $i, j \in \mathcal{I}_n$ with $i \neq j$. Then the i^{th} pursuer is a neighbor of the j^{th} pursuer in the OP-DVD if and only if*

i) The generators $\bar{\mathsf{x}}^i_{\mathcal{P}}$ and $\bar{\mathsf{x}}^j_{\mathcal{P}}$ correspond to two neighboring nodes of the dual Delaunay graph of V.

ii) $|\bar{\mathsf{x}}^i_{\mathcal{P}} - \bar{\mathsf{x}}^j_{\mathcal{P}}| \leq 2\bar{\eta}_f$.

Proof. The proof follows immediately from Theorem 3 and the definition of $\bar{\eta}_f$, and it is thus omitted. □

Theorem 3 provides an efficient way for the construction of the exact OP-DVD provided, however, that the sets $\mathcal{W}_{\bar{\eta}_f}(\bar{\mathsf{x}}^i_{\mathcal{P}})$, where $i \in \mathcal{I}_n$, are perfectly known. The following corollary, which follows readily from Theorem 3, furnishes an approximate solution to Problem 15.

Corollary 6. *Let $V := \{V^i : i \in \mathcal{I}_n\}$ be the standard Voronoi partition generated by the set $\mathcal{P}$. An approximate solution of Problem 15 is given by*

$$\widetilde{\mathcal{V}} := \{\widetilde{\mathcal{V}}^i,\ i \in \mathcal{I}_n\}, \quad \widetilde{\mathcal{V}}^i = V^i \cap \mathcal{W}_{\bar{\eta}_{\bar{f}}}(\bar{\mathsf{x}}^i_{\mathcal{P}}), \quad i \in \mathcal{I}_n. \tag{259}$$

One important question that arises in the context of the previous discussion is whether the approximate OP-DVD can provide us with reliable information regarding the actual proximity relations among the pursuers in $\mathcal{P}$ (this information is encoded in the exact OP-DVD).

Proposition 54. *Let $V := \{V^i : i \in \mathcal{I}_n\}$ be the standard Voronoi partition generated by the set $\mathcal{P}$. The i^{th} pursuer is a neighbor of the j^{th} pursuer if*

i. the generators $\bar{\mathsf{x}}^i_{\mathcal{P}}$ and $\bar{\mathsf{x}}^j_{\mathcal{P}}$ correspond to two neighboring nodes of the dual Delaunay graph of V

ii. $|\bar{\mathsf{x}}^i_{\mathcal{P}} - \bar{\mathsf{x}}^j_{\mathcal{P}}| \leq 2\bar{\eta}_{\bar{f}}$.

Proof. The proof follows readily from Proposition 53 and the definition of $\bar{\eta}_{\bar{f}}$ and $\bar{\eta}_f$. □

9.6 Simulation Results

In this section, we present simulation results to illustrate the previous developments. We consider a scenario where the maneuvering target is faster than the i^{th} pursuer, but the winning set of the i^{th} pursuer is non-empty as a result of the information pattern employed in Section 9.2. In particular, it is assumed that the target has a constant speed and its evading strategy is given by

$$u_{\mathcal{T}}(\mathsf{y}^i) = \begin{cases} \alpha \mathsf{y}^i + \rho(\mathsf{y}^i)\mathsf{S}\mathsf{y}^i, & \text{for } \epsilon_c \leq |\mathsf{y}^i| \leq \dfrac{M}{\alpha}, \\ M\dfrac{\mathsf{y}^i}{|\mathsf{y}^i|}, & \text{for } |\mathsf{y}^i| > \dfrac{M}{\alpha}, \end{cases} \tag{260}$$

where M and α are some positive constants with $M > \max\{\bar{u}_{\mathcal{P}}, \alpha\}$, S is a nonzero skew symmetric matrix in $\mathbb{R}^{2\times 2}$, and $\rho(\mathsf{y}^i) := \sqrt{M^2 - \alpha^2|\mathsf{y}^i|^2}/|\mathsf{S}\mathsf{y}^i|$. Note that

$$f(\mathsf{y}^i) := \langle u_{\mathcal{T}}, \mathsf{y}^i \rangle = \begin{cases} \alpha|\mathsf{y}^i|^2, & \text{for } \epsilon_c \leq |\mathsf{y}^i| \leq \dfrac{M}{\alpha}, \\ M|\mathsf{y}^i| & \text{for } |\mathsf{y}^i| > \dfrac{M}{\alpha}, \end{cases} \tag{261}$$

satisfies Assumption 1.

The intuition behind the evading strategy (260) is as follows: Let $\mathsf{e}_1(\mathsf{y}^i) := \mathsf{y}^i/|\mathsf{y}^i|$ be the unit vector along the line connecting the target and the i^{th} pursuer ("line-of-sight" direction), and let $\mathsf{e}_2(\mathsf{y}^i)$ be the unit vector orthogonal to $\mathsf{e}_1(\mathsf{y}^i)$ ("tangential" direction). The strategy of the target is to allocate its velocity vector, which has a constant magnitude $M > u_{\mathcal{P}}$, along the directions $\mathsf{e}_1(\mathsf{y}^i)$ and $\mathsf{e}_2(\mathsf{y}^i)$ so that it moves with constant speed M along the line-of-sight direction when it is sufficiently far away from the pursuer and uses an increasingly larger tangential component as its distance from the pursuer decreases, in an effort to maneuver away or confuse its pursuer.

Assume for this example that the set $\mathcal{P}$ consists of ten locations, and let $\bar{f}$ be defined as f modulo the replacement of α by $\bar{\alpha}$, where $\bar{\alpha}$ is a positive scalar with $\alpha \leq \bar{\alpha} < M$. In this case, the capturability condition (244) reduces to $\eta^i(0) < \bar{u}_{\mathcal{P}}/\alpha$, which implies that $\bar{\eta}_f = \bar{u}_{\mathcal{P}}/\alpha < M/\alpha$ and $\bar{\eta}_{\bar{f}} = \bar{u}_{\mathcal{P}}/\bar{\alpha} < M/\bar{\alpha}$. Furthermore, it is easy to show that for $\epsilon_c < |\bar{\mathsf{y}}^i| < \bar{\eta}_f$ the minimum-time to capture for Problem 14 is given by

$$T_{\text{f}}(\bar{\mathsf{y}}^i) = -\frac{1}{\alpha} \ln\left(\frac{\bar{u}_{\mathcal{P}} - \alpha|\bar{\mathsf{y}}^i|}{\bar{u}_{\mathcal{P}} - \alpha\epsilon_c}\right). \tag{262}$$

Figure 53(a) illustrates the exact OP-DVD along with the level sets of $T_{\text{f}}(\bar{\mathsf{y}}^i)$ for $\alpha = 0.7$, $\epsilon_c = 0.05$ and $\bar{u}_{\mathcal{P}} = 1.2$. An approximation of the OP-DVD for $\bar{\alpha} = 0.95$ is illustrated in Fig. 53(b).

Next, we examine the discrepancies between the neighboring relations among the pursuers of the exact and the approximate OP-DVDs. In light of Proposition 54, given $i, j \in \mathcal{I}_n$ with $i \neq j$, the i^{th} and j^{th} pursuers are neighbors provided that the generators

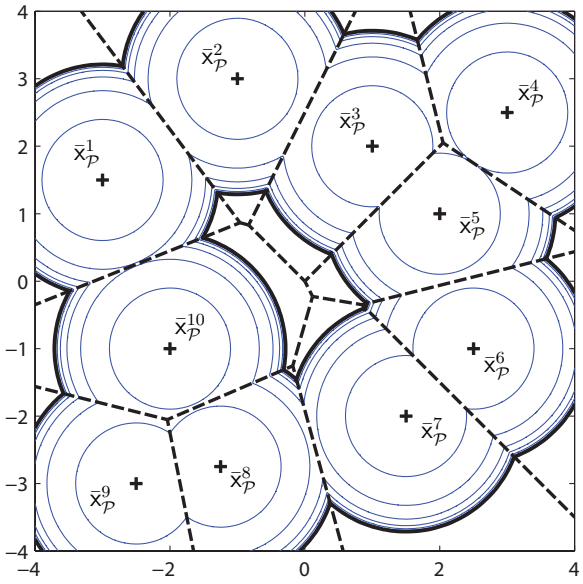

(a) Minimum-time wave fronts for Problem 14.

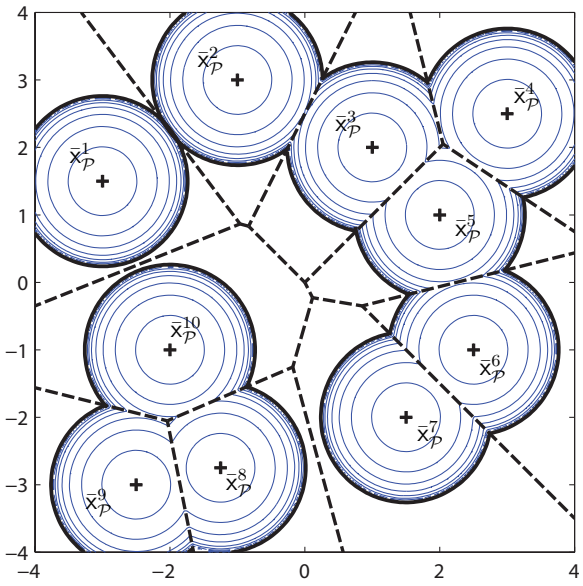

(b) Approximate minimum-time wave fronts for Problem 14.

Figure 53: The exact and an approximate solution of Problem 15 for a team of ten pursuers.

$\bar{\mathsf{x}}^i_{\mathcal{P}}$, $\bar{\mathsf{x}}^j_{\mathcal{P}} \in \mathcal{P}$ correspond to two neighboring nodes of the dual Delaunay graph of the standard Voronoi diagram generated by the set $\mathcal{P}$ and $|\bar{\mathsf{x}}^i_{\mathcal{P}} - \bar{\mathsf{x}}^j_{\mathcal{P}}| < 2\bar{\eta}_{\bar{f}} = 2\bar{u}_{\mathcal{P}}/\bar{\alpha}$. For this particular example, we can explicitly compute a lower bound of $\Delta\bar{\eta} := \bar{\eta}_f - \bar{\eta}_{\bar{f}}$ as a function of the error $\Delta\alpha := \bar{\alpha} - \alpha$. Specifically, $\Delta\bar{\eta} = \bar{u}_{\mathcal{P}}/\alpha - \bar{u}_{\mathcal{P}}/\bar{\alpha} = \bar{u}_{\mathcal{P}}\Delta\alpha/\bar{\alpha}\alpha$, which implies that $\Delta\bar{\eta} \geq \bar{u}_{\mathcal{P}}\Delta\alpha/\bar{\alpha}^2$. It follows readily from Propositions 53 and 54 that if $|\bar{\mathsf{x}}^i_{\mathcal{P}} - \bar{\mathsf{x}}^j_{\mathcal{P}}| < 2\bar{\eta}_{\bar{f}} + 2\bar{u}_{\mathcal{P}}\Delta\alpha/\bar{\alpha}^2 \leq 2\bar{\eta}_f$, then the i^{th} and j^{th} pursuers are neighbors of the exact OP-DVD although they may not be neighbors of the approximate OP-DVD. Consequently, the accuracy of the knowledge about the neighboring relations between the pursuers of the exact OP-DVD is contingent upon the smallness of the error $\Delta\alpha$. The situation is illustrated in Figs. 53(a)-53(b), where the approximate OP-DVD conceals the fact that the 1^{st} and the 10^{th}, and the 7^{th} and the 8^{th} are neighboring pursuers of the exact OP-DVD.

CHAPTER X

ON THE RELAY PURSUIT OF A MANEUVERING TARGET BY A GROUP OF PURSUERS

The material presented in this chapter builds upon the results presented in [17, 19].

10.1 Introduction

In this chapter, we present a pursuit strategy for the capture of a maneuvering target by a group of pursuers distributed in the plane. Typically, problems of group pursuit of a moving target (or an evader) are dealt with by employing cooperative or non-cooperative pursuit strategies, which are based on local or global information [154, 162, 106, 208, 32, 152, 33, 42, 43, 92]. One common theme in all these approaches is that more than one pursuer is actively participating in the process of simultaneously capturing the target. However, in many applications involving groups of agents, a more "frugal" assignment of tasks within the group may constitute a more prudent strategy. For example, in the problem of pursuit of a moving target by a group of agents guarding a certain area, the guards may be required to remain close to their initial positions to account for possible deceptive strategies, decoy targets, etc.

In this chapter, we propose a *relay pursuit* scheme to address the group pursuit problem. In particular, we consider the following problem: Given a team of pursuers, which are distributed in the plane, we wish to find a scheme such that, at every instant of time, only one pursuer is assigned the task of capturing the moving target, whereas the rest of the pursuers remain stationary. During the course of the pursuit, the scheme dynamically selects the appropriate pursuer in the group aiming to minimize the overall capture time.

10.2 The Dynamic Pursuer-Target Assignment Problem and Relay-Pursuit

10.2.1 Problem Formulation

Consider a team of n pursuers located at time $t = 0$ at n distinct points in the plane, denoted by $\mathcal{P} := \{\bar{\mathsf{x}}^i_{\mathcal{P}} \in \mathbb{R}^2, i \in \mathcal{I}_n\}$, where $\mathcal{I}_n := \{1, \ldots, n\}$. It is assumed that the kinematics of the i^{th} pursuer starting at point $\bar{\mathsf{x}}^i_{\mathcal{P}} \in \mathcal{P}$ are given by (232) and its winning set is defined in (243). In addition, it is assumed that the kinematics of the moving target, that the pursuers wish to capture are described by (233). Let us consider again the state transformation $\mathsf{y}^i := \mathsf{x}_{\mathcal{T}} - \mathsf{x}^i_{\mathcal{P}}$. Next, we formulate the dynamic pursuer-target assignment problem. To this end, assume that $\bar{\mathsf{x}}_{\mathcal{T}} \in \mathcal{W}$. Without loss of generality[1], let $\bar{\mathsf{x}}_{\mathcal{T}} \in \operatorname{int} \mathcal{V}^i$ for some $i \in \mathcal{I}$. Let $\mathcal{S}$ be the family of right continuous, piecewise constant signals $\sigma : [0, \infty) \mapsto \mathcal{I}_n$, such that $\sigma(t) = i$ implies that the i^{th} pursuer, at time $t \geq 0$, is the (only) active pursuer; subsequently, we write $\mathsf{x}^i_{\mathcal{P}} \overset{t}{\rightsquigarrow} \mathsf{x}_{\mathcal{T}}$ to denote this fact. The dynamics of the pursuit problem can then be described by the following switched system [113]

$$\dot{\mathsf{y}}^{\sigma(t)} = -\bar{u}_{\mathcal{P}} \frac{\mathsf{y}^{\sigma(t)}}{|\mathsf{y}^{\sigma(t)}|} + u_{\mathcal{T}}(\mathsf{y}^{\sigma(t)}), \quad \mathsf{y}^{\sigma(0)}(0) = \bar{\mathsf{y}}^{\sigma(0)}, \tag{263}$$

$$\dot{\mathsf{y}}^j = 0, \qquad \mathsf{y}^j(0) = \bar{\mathsf{y}}^j, \quad j \neq \sigma(t), \tag{264}$$

where $\sigma(0) = \operatorname{argmin}_{i \in \mathcal{I}_n} T_{\mathrm{f}}(\bar{\mathsf{y}}^i)$. If, in addition, $0 < \tau_1 < \cdots < \tau_k < \cdots < \infty$ are the switching times of the signal σ, then $\mathsf{y}^{i_k}(\tau_k) = \mathsf{y}^{i_k}(\tau_k^-)$ where $i_k := \sigma(\tau_k) = \sigma(\tau_k^+)$.

We will restrict the family of acceptable switching signals to a subset of $\mathcal{S}$, which includes all those signals in $\mathcal{S}$ that satisfy the following switching condition.

Switching Condition *Let $\sigma \in \mathcal{S}$ and let $\tau > 0$ be a switching time, such that $i = \sigma(\tau^-)$ and $j = \sigma(\tau^+) = \sigma(\tau)$, where $j \neq i$. Then $\sigma \in \Sigma$ if the following conditions hold:*

[1] If $\bar{\mathsf{x}}_{\mathcal{T}} \in \bigcap_{i \in \mathcal{J}} \mathcal{V}^i$, where $\mathcal{J} \subseteq \mathcal{I}_n$, we may assign as the initial pursuer any one of the elements of $\mathcal{J}$.

i) $\mathsf{x}_{\mathcal{T}}(\tau) \in \operatorname{int} \mathcal{V}^j$.

ii) $\mathrm{T}(\tau, \mathsf{y}^j(\tau); \sigma) < \mathrm{T}(\tau, \mathsf{y}^i(\tau); \tilde{\sigma})$, *where*

$$\tilde{\sigma}(t) = \begin{cases} \sigma(t), & t \in [0, \tau), \\ i, & t \geq \tau. \end{cases}$$

The previous condition can be interpreted as follows: For any $\sigma \in \Sigma$, the assignment $\mathsf{x}_{\mathcal{P}}^i \overset{t}{\rightsquigarrow} \mathsf{x}_{\mathcal{T}}$, for $t \geq 0$, is updated only if during the course of the pursuit, the target reaches a position from which, say, the j^{th} pursuer, where $j \neq i$, can capture the target faster than the i^{th} pursuer.

Next, we formulate the dynamic pursuer-moving target assignment problem.

Problem 16. *Let* $\mathcal{V} = \{\mathcal{V}^i,\ i \in \mathcal{I}_n\}$ *denote the OP-DVD generated by the set* $\mathcal{P}$ *and assume that* $\bar{\mathsf{x}}_{\mathcal{T}} \in \operatorname{int} \mathcal{V}^i$ *for some* $i \in \mathcal{I}_n$. *Determine a switching signal* $\sigma_\star \in \Sigma$ *(if one exists) such that* $\mathrm{T}(0, \bar{\mathsf{y}}^i, \sigma_\star) < T_{\mathrm{f}}(\bar{\mathsf{y}}^i) = \mathrm{T}(0, \bar{\mathsf{y}}^i; i)$.

10.2.2 Analysis of the Pursuer-Target Assignment Problem

Before proceeding to a detailed discussion on the characterization of a solution of Problem 16, we need to introduce a few geometric concepts. In particular, let $\chi_t^{i,j} \subseteq \mathbb{R}^2$ be the moving line in the plane, defined for $t \geq 0$, as follows

$$\begin{aligned} \chi_t^{i,j} &:= \left\{ \mathsf{x} : |\mathsf{x} - \mathsf{x}_{\mathcal{P}}^i(t)| = |\mathsf{x} - \mathsf{x}_{\mathcal{P}}^j(t)| \right\} \\ &= \left\{ \mathsf{x} : 2\langle \mathsf{x}_{\mathcal{P}}^j(t) - \mathsf{x}_{\mathcal{P}}^i(t), \mathsf{x} \rangle = |\mathsf{x}_{\mathcal{P}}^j(t)|^2 - |\mathsf{x}_{\mathcal{P}}^i(t)|^2 \right\}. \end{aligned}$$

At every time instant $t \geq 0$ the line $\chi_t^{i,j}$ divides $\mathbb{R}^2$ into two open half-planes, namely,

$$\begin{aligned} H_t^i(\mathsf{x}_{\mathcal{P}}^i(t), \mathsf{x}_{\mathcal{P}}^j(t)) &:= \{\mathsf{x} : |\mathsf{x} - \mathsf{x}_{\mathcal{P}}^i(t)| < |\mathsf{x} - \mathsf{x}_{\mathcal{P}}^j(t)|\}, \\ H_t^j(\mathsf{x}_{\mathcal{P}}^i(t), \mathsf{x}_{\mathcal{P}}^j(t)) &:= \{\mathsf{x} : |\mathsf{x} - \mathsf{x}_{\mathcal{P}}^i(t)| > |\mathsf{x} - \mathsf{x}_{\mathcal{P}}^j(t)|\}. \end{aligned}$$

The following proposition provides a necessary and sufficient condition for the existence of a solution to Problem 16.

Proposition 55. *Let $\mathcal{V} = \{\mathcal{V}^i,\ i \in \mathcal{I}_n\}$ denote the OP-DVD generated by the set $\mathcal{P}$, and assume that $\bar{\mathsf{x}}_{\mathcal{T}} \in \operatorname{int} \mathcal{V}^i$ for some $i \in \mathcal{I}_n$. Then $\mathrm{T}(0, \bar{\mathsf{y}}^i; \sigma) \geq T_{\mathrm{f}}(\bar{\mathsf{y}}^i)$ for all $\sigma \in \Sigma$, if and only if $\mathsf{x}_{\mathcal{T}}(t) \notin H_t^j(\mathsf{x}_{\mathcal{P}}^i(t), \mathsf{x}_{\mathcal{P}}^j(t)) \cap \operatorname{int} \mathcal{V}^j$ for all $j \neq i$ and all $t \geq 0$.*

Proof. First we show sufficiency. Let us assume, on the contrary, that there exists a switching signal $\sigma_\star \in \Sigma$ such that $\mathrm{T}(0, \bar{\mathsf{y}}^i; \sigma_\star) < T_{\mathrm{f}}(\bar{\mathsf{y}}^i)$. Clearly, $\sigma_\star \not\equiv i$. If $t_1 > 0$ is the first switching time of the signal $\sigma_\star$, then, in light of the Switching Condition, there exists $j \neq i$, such that $\mathsf{x}_{\mathcal{T}}(t_1) \in \operatorname{int} \mathcal{V}^j$ and $\mathrm{T}(t_1, \mathsf{y}^j(t_1); \tilde{\sigma}) < \mathrm{T}(t_1, \mathsf{y}^i(t_1); i)$, where $\tilde{\sigma}(t) = \sigma_\star(t) = i$ for $t \in [0, t_1)$ and $\tilde{\sigma}(t) = j$ for $t \geq t_1$. Using a similar argument as in the proof of the converse part of Theorem 3, it follows that $|\mathsf{x}_{\mathcal{T}}(t_1) - \mathsf{x}_{\mathcal{P}}^j(t_1)| < |\mathsf{x}_{\mathcal{T}}(t_1) - \mathsf{x}_{\mathcal{P}}^i(t_1)|$. Hence, $\mathsf{x}_{\mathcal{T}}(t_1) \in H_{t_1}^j(\mathsf{x}_{\mathcal{P}}^i(t_1), \mathsf{x}_{\mathcal{P}}^j(t_1))$, leading to a contradiction.

Conversely, given that $\mathrm{T}(0, \bar{\mathsf{y}}^i; \sigma) \geq T_{\mathrm{f}}(\bar{\mathsf{y}}^i)$, for all $\sigma \in \Sigma$, we wish to show that $\mathsf{x}_{\mathcal{T}}(t) \notin H_t^j(\mathsf{x}_{\mathcal{P}}^i(t), \mathsf{x}_{\mathcal{P}}^j(t)) \cap \operatorname{int} \mathcal{V}^j$, for all $j \neq i$ and $t \geq 0$. Let assume, on the contrary, that there exists $j \neq i$ and $0 < t_1 < T_{\mathrm{f}}(\bar{\mathsf{y}}^i)$ such that $\mathsf{x}_{\mathcal{T}}(t_1) \in H_{t_1}^j(\mathsf{x}_{\mathcal{P}}^i(t_1), \mathsf{x}_{\mathcal{P}}^j(t_1)) \cap \operatorname{int} \mathcal{V}^j$ and let the signal $\sigma_\star \in \Sigma$ be defined such that $\sigma_\star(t) = i$ for $t \in [0, t_1)$ and $\sigma_\star(t) = j$ for $t \geq t_1$. Since $\mathsf{x}_{\mathcal{T}}(t_1) \in H_{t_1}^j(\mathsf{x}_{\mathcal{P}}^i(t_1), \mathsf{x}_{\mathcal{P}}^j(t_1))$, it follows that $|\mathsf{x}_{\mathcal{T}}(t_1) - \mathsf{x}_{\mathcal{P}}^j(t_1)| < |\mathsf{x}_{\mathcal{T}}(t_1) - \mathsf{x}_{\mathcal{P}}^i(t_1)|$. Note that necessarily $|\mathsf{x}_{\mathcal{T}}(t_1) - \mathsf{x}_{\mathcal{P}}^j(t_1)| > \epsilon_c$, otherwise capture would occur at $t_1 < T_{\mathrm{f}}(\bar{\mathsf{y}}^i)$, contradicting the assumption that $\mathrm{T}(0, \bar{\mathsf{y}}^i; \sigma) \geq T_{\mathrm{f}}(\bar{\mathsf{y}}^i)$ for all $\sigma \in \Sigma$. Furthermore, by the definition of the OP-DVD, $\mathsf{x}_{\mathcal{T}}(t_1) \in \operatorname{int} \mathcal{V}^j$ implies that $|\mathsf{x}_{\mathcal{T}}(t_1) - \mathsf{x}_{\mathcal{P}}^j(t_1)| < \bar{\eta}_f$. Note that if $\epsilon_c < |\mathsf{x}_{\mathcal{T}}(t_1) - \mathsf{x}_{\mathcal{P}}^j(t_1)| < \bar{\eta}_f$ and $\epsilon_c < |\mathsf{x}_{\mathcal{T}}(t_1) - \mathsf{x}_{\mathcal{P}}^i(t_1)| < \bar{\eta}_f$, then it follows via Corollary 5 that $\mathrm{T}(t_1, \mathsf{y}^j(t_1); \sigma_\star) < \mathrm{T}(t_1, \mathsf{y}^i(t_1); i)$. Similarly, if $|\mathsf{x}_{\mathcal{T}}(t_1) - \mathsf{x}_{\mathcal{P}}^i(t_1)| > \bar{\eta}_f$, then it follows from (253) that $\mathrm{T}(t_1, \mathsf{y}^i(t_1); i) = \infty$. Since $\mathsf{x}_{\mathcal{T}}(t_1) \in \operatorname{int} \mathcal{V}^j$, it follows that $\mathrm{T}(t_1, \mathsf{y}^j(t_1); \sigma_\star) < \infty$. Therefore, in both cases $|\mathsf{x}_{\mathcal{T}}(t_1) - \mathsf{x}_{\mathcal{P}}^j(t_1)| < |\mathsf{x}_{\mathcal{T}}(t_1) - \mathsf{x}_{\mathcal{P}}^i(t_1)|$ implies that $\mathrm{T}(t_1, \mathsf{y}^j(t_1); \sigma_\star) < \mathrm{T}(t_1, \mathsf{y}^i(t_1); i)$ for $j \neq i$, where $\mathsf{x}_{\mathcal{T}}(t_1) \in H_{t_1}^j(\mathsf{x}_{\mathcal{P}}^i(t_1), \mathsf{x}_{\mathcal{P}}^j(t_1)) \cap \operatorname{int} \mathcal{V}^j$. Therefore, the signal $\sigma_\star \in \Sigma$ satisfies $\mathrm{T}(0, \bar{\mathsf{y}}^i; \sigma_\star) = t_1 + \mathrm{T}(t_1, \mathsf{y}^j(t_1); \sigma_\star) < t_1 + \mathrm{T}(t_1, \mathsf{y}^i(t_1); i) = \mathrm{T}(0, \bar{\mathsf{y}}^i; i) = T_{\mathrm{f}}(\bar{\mathsf{y}}^i)$. Hence there exists $\sigma_\star \in \Sigma$ such that $\mathrm{T}(0, \bar{\mathsf{y}}^i; \sigma_\star) < T_{\mathrm{f}}(\bar{\mathsf{y}}^i)$, leading to a contradiction. ■ □

Figures 54-55 illustrate some of the cases that may appear during the pursuit

of a target in the special case when $\mathcal{P} = \{\bar{\mathsf{x}}^i_{\mathcal{P}}, \bar{\mathsf{x}}^j_{\mathcal{P}}\}$ and $\bar{\mathsf{x}}_{\mathcal{T}} \in \operatorname{int} \mathcal{V}^i$. In particular, Fig. 54(a) illustrates the scenario in which the i^{th} pursuer captures the target at some point in $\mathcal{V}^i$, whereas Fig. 54(b) illustrates the case when capture occurs at some point in $(\mathcal{V}^i \cup \mathcal{V}^j)^c$. Note that in both cases shown in Fig. 54, the initial pursuer-target assignment does not change since the requirements of the Switching Condition are not met. Figure 55 illustrates the case when, during the course of the pursuit, the target enters $\mathcal{V}^j$, and subsequently reaches a position within this cell from which it can be captured by the j^{th} pursuer faster than the i^{th} pursuer.

10.2.3 Implementation and Analysis of the Relay Pursuit Strategy

Next, we present a simple algorithm that will allow us to solve Problem 16 by dynamically updating the pursuer-target assignment. In particular, we propose the following scheme. First, we construct the OP-DVD generated by the set $\mathcal{P}$, and determine the cell $\mathcal{V}^i$ of the OP-DVD such that $\bar{\mathsf{x}}_{\mathcal{T}} \in \operatorname{int} \mathcal{V}^i$, and let $\mathsf{x}^i_{\mathcal{P}} \overset{t}{\rightsquigarrow} \mathsf{x}_{\mathcal{T}}$ for $t \in [0, T_{\text{f}}(\bar{\mathsf{y}}^i)]$. If, during the course of the pursuit, the target never enters $\operatorname{int} \mathcal{V}^j$, for all $j \neq i$, then it follows that $\mathrm{T}(0, \bar{\mathsf{y}}^i; \sigma) \geq T_{\text{f}}(\bar{\mathsf{y}}^i)$, for all $\sigma \in \Sigma$. Hence, the pursuer target assignment is not updated. If there exists $t_1 > 0$ and $j \neq i$ such that $\mathsf{x}_{\mathcal{T}}(t_1) \in \operatorname{int} \mathcal{V}^j \cap H^j_{t_1}(\mathsf{x}^i_{\mathcal{P}}(t_1), \mathsf{x}^j_{\mathcal{P}}(t_1))$, where $\mathsf{x}^j_{\mathcal{P}}(t_1) = \bar{\mathsf{x}}^j_{\mathcal{P}}$, then the signal σ with $\sigma(t) = i$ for $t \in [0, t_1)$ and $\sigma(t) = j$ for $t \geq t_1$ satisfies $\mathrm{T}(t_1, \mathsf{y}^j(t_1); \sigma) < \mathrm{T}(t_1, \mathsf{y}^i(t_1); i)$. Therefore, by taking $\mathsf{x}^j_{\mathcal{P}} \overset{t}{\rightsquigarrow} \mathsf{x}_{\mathcal{T}}$, for $t \geq t_1$, it follows that capture can be achieved after $t_1 + \mathrm{T}(t_1, \mathsf{y}^j(t_1); \sigma) < t_1 + \mathrm{T}(t_1, \mathsf{y}^i(t_1); i) = T_{\text{f}}(\bar{\mathsf{y}}^i)$ units of time.

The previous procedure is repeated every time the target enters a different cell of the OP-DVD during the course of its pursuit. Note that if the pursuer-target assignment is updated at some time t_1, one needs to construct the OP-DVD of the set comprised of the positions of the pursuers at time t_1, so that the previously described pursuer-target assignment scheme can be applied mutatis mutandis until capture occurs. In particular, one needs to compute the OP-DVD generated by the

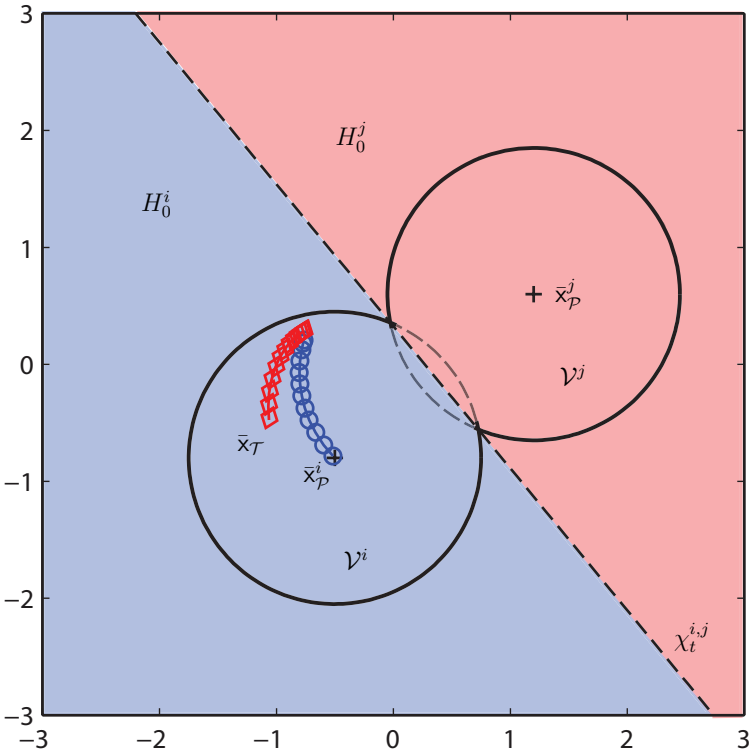

(a) Capture occurs in $\mathcal{V}^i$.

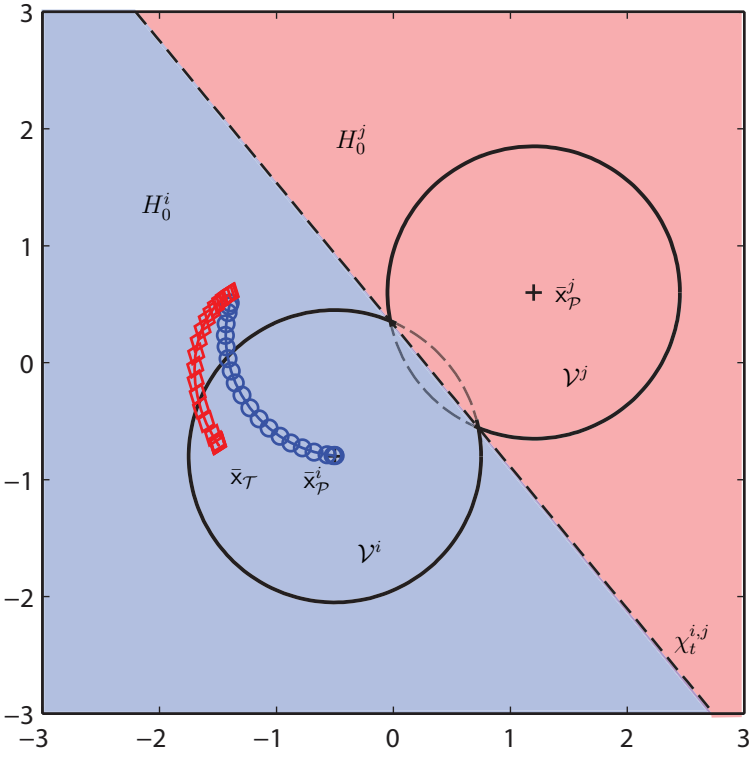

(b) Capture occurs in $(\mathcal{V}^i \cup \mathcal{V}^j)^c$.

Figure 54: If $\mathsf{x}_{\mathcal{P}}^i \overset{t}{\rightsquigarrow} \mathsf{x}_{\mathcal{T}}$ and $\mathsf{x}_{\mathcal{T}}(t) \notin \mathcal{V}^j$ for all $t \geq 0$, then $\mathrm{T}(0, \bar{\mathsf{y}}^i; \sigma) \geq T_{\mathrm{f}}(\bar{\mathsf{y}}^i)$ for all $\sigma \in \Sigma$.

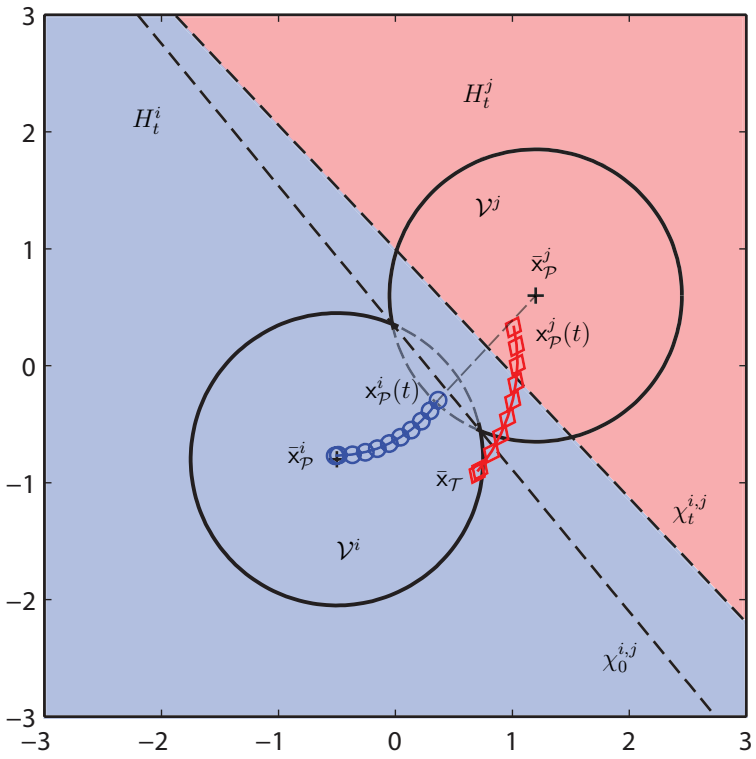

Figure 55: If $\mathsf{x}_{\mathcal{P}}^i \overset{0}{\rightsquigarrow} \mathsf{x}_{\mathcal{T}}$ and there exists $t > 0$ such that $\mathsf{x}_{\mathcal{T}}(t) \in \operatorname{int} \mathcal{V}^j \cap H_t^j(\mathsf{x}_{\mathcal{P}}^i(t), \mathsf{x}_{\mathcal{P}}^j(t))$, where $\mathsf{x}_{\mathcal{P}}^j(t) = \bar{\mathsf{x}}_{\mathcal{P}}^j$, then the j^{th} pursuer will capture the target faster than $\mathrm{T}(t, \mathsf{y}^i(t); i)$. Thus $\mathsf{x}_{\mathcal{P}}^j \overset{t}{\rightsquigarrow} \mathsf{x}_{\mathcal{T}}$.

point-set $\mathcal{P}_{t_1} := (\mathcal{P} \cup \{\mathsf{x}^i_{\mathcal{P}}(t_1)\}) \setminus \{\bar{\mathsf{x}}^i_{\mathcal{P}}\}$ at time t_1. Note that the standard Voronoi diagram generated by the new set of generators can be easily constructed from the Voronoi diagram generated by the set $\mathcal{P}$ by means of well-known local/incremental algorithms [168, 91, 195, 137].

The previous scheme may be difficult to be implemented in practice due to the indeterminacy of the pursuer-target assignment scheme when the target lies on the switching line $\chi^{i,j}_t$ at some time $t \geq 0$. This is a well known problem in the theory of switched systems [113], which can be addressed by simply redefining the sets $\chi^{i,j}_t$, H^i_t, H^j_t as follows $\chi^{i,j}_{t,\varepsilon} := \big\{\mathsf{x} : \big||\mathsf{x} - \mathsf{x}^i_{\mathcal{P}}(t)| - |\mathsf{x} - \mathsf{x}^j_{\mathcal{P}}(t)|\big| \leq \varepsilon\big\}$, and

$$H^i_{t,\varepsilon}(\mathsf{x}^i_{\mathcal{P}}(t), \mathsf{x}^j_{\mathcal{P}}(t)) := \{\mathsf{x} : |\mathsf{x} - \mathsf{x}^i_{\mathcal{P}}(t)| < |\mathsf{x} - \mathsf{x}^j_{\mathcal{P}}(t)| - \varepsilon\},$$
$$H^j_{t,\varepsilon}(\mathsf{x}^i_{\mathcal{P}}(t), \mathsf{x}^j_{\mathcal{P}}(t)) := \{\mathsf{x} : |\mathsf{x} - \mathsf{x}^i_{\mathcal{P}}(t)| > |\mathsf{x} - \mathsf{x}^j_{\mathcal{P}}(t)| + \varepsilon\},$$

where $\varepsilon > 0$ is a *hysteresis* constant. Note that after the target is assigned to, say, the i^{th} pursuer at time $t = 0$, based on the proximity relations encoded in the OP-DVD generated by $\mathcal{P}$, then the pursuer-target assignment cannot be updated as long as the target remains inside the set $H^i_{t,\varepsilon}(\mathsf{x}^i_{\mathcal{P}}(t), \mathsf{x}^j_{\mathcal{P}}(t)) \cup \chi^{i,j}_{t,\varepsilon}$, for $t > 0$ and for all $j \neq i$. In other words, if $\mathsf{x}^i_{\mathcal{P}} \overset{t_0}{\rightsquigarrow} \mathsf{x}_{\mathcal{T}}$ for some $t_0 \geq 0$, then the signal σ is allowed to switch at time $t_1 > t_0$ from $i = \sigma(t_0)$ to some $j \neq i$ with $j = \sigma(t_1)$ only if $\mathrm{T}(t_1, \mathsf{y}^j(t_1); \sigma)$ is "sufficiently" smaller than $\mathrm{T}(t_1, \mathsf{y}^i(t_1); \tilde{\sigma})$, where the signal $\tilde{\sigma}$ is defined such that $\tilde{\sigma}(t) = \sigma(t)$ for $t \in [0, t_1)$ and $\tilde{\sigma}(t) = i$, for $t \geq t_1$. The threshold difference between $\mathrm{T}(t_1, \mathsf{y}^j(t_1); \sigma)$ and $\mathrm{T}(t_1, \mathsf{y}^i(t_1); \tilde{\sigma})$ depends on the hysteresis constant ε.

Next, we determine a lower bound on the decrease of the capture time of the target that can be achieved by employing the previous dynamic pursuer-target assignment scheme when compared to a static pursuit scheme. In addition, we determine an upper bound on the number of switches of the signal $\sigma_\star \in \Sigma$ that solves Problem 16.

Proposition 56. *Let $\mathcal{V} = \{\mathcal{V}^i, i \in \mathcal{I}_n\}$ denote the OP-DVD generated by the set $\mathcal{P}$, and assume that $\bar{\mathsf{x}}_{\mathcal{T}} \in \operatorname{int} \mathcal{V}^i$ for some $i \in \mathcal{I}_n$. In addition, let $\sigma_\star \in \Sigma$ be a solution of*

Problem 16 and let $N(\sigma_\star)$ denote the number of switches of $\sigma_\star$. If $\bar{\eta}_f > \epsilon_c$, then

$$\mathrm{T}(0, \bar{\mathsf{y}}^i; \sigma_\star) < T_{\mathrm{f}}(\bar{\mathsf{y}}^i) - N(\sigma_\star)\bar{\phi}\varepsilon, \tag{265}$$

where $\bar{\phi} := \inf_{[\epsilon_c, \bar{\eta}_f)} \mathsf{z}/(\bar{u}_{\mathcal{P}}\mathsf{z} - f(\mathsf{z}))$. In particular,

$$N(\sigma_\star) < \frac{T_{\mathrm{f}}(\bar{\mathsf{y}}^i)}{\varepsilon\bar{\phi}}. \tag{266}$$

Proof. Let τ_k be the k^{th} switching time of $\sigma_\star$, such that $\sigma_\star(\tau_k^-) = \ell_k$ and $\sigma_\star(\tau_k^+) = \sigma_\star(\tau_k) = \ell_{k+1}$, where $\ell_k, \ell_{k+1} \in \mathcal{I}_n$. Furthermore, let σ^k be the switching signal defined such that $\sigma^k(t) = \sigma_\star(t)$ for $t \in [0, t_k)$ and $\sigma^k(t) = \ell_k$ for $t \geq t_k$. Note that $i \equiv \ell_1$ and $\sigma^1 \equiv i$. By hypothesis, $\mathsf{x}_{\mathcal{T}}(\tau_k) \in H^{\ell_{k+1}}_{\tau_k,\varepsilon}(\mathsf{x}^{\ell_k}_{\mathcal{P}}(\tau_k), \mathsf{x}^{\ell_{k+1}}_{\mathcal{P}}(\tau_k)) \cap \operatorname{int} \mathcal{V}^{\ell_{k+1}}$ which implies that $\epsilon_c < |\mathsf{y}^{\ell_{k+1}}(\tau_k)| + \varepsilon < |\mathsf{y}^{\ell_k}(\tau_k)| < \bar{\eta}_f$, where $\mathsf{y}^{\ell_{k+1}}(\tau_k) := \mathsf{x}_{\mathcal{T}}(\tau_k) - \mathsf{x}^{\ell_{k+1}}_{\mathcal{P}}(\tau_k)$ and $\mathsf{y}^{\ell_k}(\tau_k) := \mathsf{x}_{\mathcal{T}}(\tau_k) - \mathsf{x}^{\ell_k}_{\mathcal{P}}(\tau_k)$. Furthermore,

$$\mathrm{T}(\tau_k, \mathsf{y}^{\ell_k}(\tau_k); \sigma^k) - \mathrm{T}(\tau_k, \mathsf{y}^{\ell_{k+1}}(\tau_k); \sigma^{k+1}) = \int_{|\mathsf{y}^{\ell_{k+1}}(\tau_k)|}^{|\mathsf{y}^{\ell_k}(\tau_k)|} \phi(\mathsf{z})\,\mathrm{d}\mathsf{z}, \tag{267}$$

where $\phi(\mathsf{z}) := \mathsf{z}/(\bar{u}_{\mathcal{P}}\mathsf{z} - f(\mathsf{z}))$. By virtue of the mean value theorem for Riemann integrals, there exists $\epsilon_c < |\mathsf{y}^{\ell_{k+1}}(\tau_k)| \leq \zeta \leq |\mathsf{y}^{\ell_k}(\tau_k)| < \bar{\eta}_f$, such that

$$\begin{aligned} &\mathrm{T}(\tau_k, \mathsf{y}^{\ell_k}(\tau_k); \sigma^k) - \mathrm{T}(\tau_k, \mathsf{y}^{\ell_{k+1}}(\tau_k); \sigma^{k+1}) = \\ &\qquad \phi(\zeta)(|\mathsf{y}^{\ell_k}(\tau_k)| - |\mathsf{y}^{\ell_{k+1}}(\tau_k)|) > \phi(\zeta)\varepsilon. \end{aligned} \tag{268}$$

Note that the function ϕ is continuous and strictly positive for all $\mathsf{z} \in [\epsilon_c, \bar{\eta}_f)$. Furthermore, $\lim_{\mathsf{z}\to\bar{\eta}_f} \mathsf{z}/(\bar{u}_{\mathcal{P}}\mathsf{z} - f(\mathsf{z})) = \infty$. Therefore, $\bar{\phi} := \inf_{[\epsilon_c, \bar{\eta}_f)} \mathsf{z}/(\bar{u}_{\mathcal{P}}\mathsf{z} - f(\mathsf{z})) > 0$. Then (268) gives $\mathrm{T}(\tau_k, \mathsf{y}^{\ell_k}(\tau_k); \sigma^k) - \mathrm{T}(\tau_k, \mathsf{y}^{\ell_{k+1}}(\tau_k); \sigma^{k+1}) > \bar{\phi}\varepsilon$, which, furthermore,

implies that

$$\begin{aligned} T_{\mathrm{f}}(\bar{\mathsf{y}}^i) &= \tau_1 + \mathrm{T}(\tau_1, \mathsf{y}^{\ell_1}(\tau_1); \sigma^1) \\ &> \tau_1 + \mathrm{T}(\tau_1, \mathsf{y}^{\ell_2}(\tau_1); \sigma^2) + \bar{\phi}\varepsilon \\ &= \tau_1 + (\tau_2 - \tau_1) + \mathrm{T}(\tau_2, \mathsf{y}^{\ell_2}(\tau_2); \sigma^2) + \bar{\phi}\varepsilon \\ &> \tau_2 + \mathrm{T}(\tau_2, \mathsf{y}^{\ell_3}(\tau_2); \sigma^3) + 2\bar{\phi}\varepsilon \\ &\;\;\vdots \\ &> \tau_k + \mathrm{T}(\tau_k, \mathsf{y}^{\ell_{k+1}}(\tau_k); \sigma^{k+1}) + k\bar{\phi}\varepsilon. \end{aligned} \tag{269}$$

Therefore, $T_{\mathrm{f}}(\bar{\mathsf{y}}^i) > k\bar{\phi}\varepsilon$, for all $k \geq 1$, which implies that the maximum number of switches, N is bounded. Furthermore, the previous inequality yields

$$\begin{aligned} T_{\mathrm{f}}(\bar{\mathsf{y}}^i) &> \tau_N + \mathrm{T}(\tau_N, \mathsf{y}^{\ell_{N+1}}(\tau_N); \sigma_\star) + N\bar{\phi}\,\varepsilon \\ &= \mathrm{T}(0, \bar{\mathsf{y}}^i; \sigma_\star) + N\bar{\phi}\,\varepsilon. \end{aligned}$$

Thus (265) follows readily. Finally, (266) follows immediately from the fact that $\mathrm{T}(0, \bar{\mathsf{y}}^i; \sigma_\star) > 0$. □

10.3 Heterogeneous Team of Pursuers

The previous discussion assumes that all pursuers are identical. Under this assumption, we have shown that the ranking of a group of pursuers with respect to minimum capture time is identical to the ranking according to their relative distance to the target as long as the target lies in the intersection of the winning sets of these pursuers (see Proposition 4 and Corollary 1 of [17]). This is the key observation that allows one to use standard Voronoi partitions, which, in conjunction with the knowledge of the winning sets, provides a rather simple solution to the relay pursuit problem. The situation is much more complicated for the case of a heterogenous team of pursuers. In this case, Proposition 4 and Corollary 1 of [17] are no longer valid, and one needs to compute Voronoi-like partitions with respect to minimum-time capture (for

a related discussion, see [13]). In particular, in this case proximity relationships with respect to the Euclidean distance can be misleading when ranking the pursuers. This is easily shown, for instance, for the case when the pursuers do not necessarily satisfy a uniform maximum speed constraint.

Next, we give a short proof of the previous claim for the case of two pursuers. To this end, let i and j be the indices of the two pursuers and, without loss of generality, assume that $\bar{u}^i_{\mathcal{P}} > \bar{u}^j_{\mathcal{P}}$. Let also

$$\bar{\eta}^\ell_f := \inf\{\mathsf{z} \in [\epsilon_c, \infty) : f(\mathsf{z}) \geq \bar{u}^\ell_{\mathcal{P}}\mathsf{z}\}, \qquad \ell \in \{i, j\}. \tag{270}$$

It follows readily that

$$\{\mathsf{z} \in [\epsilon_c, \infty) : f(\mathsf{z}) \geq \bar{u}^i_{\mathcal{P}}\mathsf{z}\} \subseteq \{\mathsf{z} \in [\epsilon_c, \infty) : f(\mathsf{z}) \geq \bar{u}^j_{\mathcal{P}}\mathsf{z}\},$$

and hence $\bar{\eta}^i_f \geq \bar{\eta}^j_f$. Furthermore, let

$$T^\ell_{\mathrm{f}}(\bar{\mathsf{y}}^\ell) := \int_{\epsilon_c}^{|\bar{\mathsf{y}}^\ell|} \phi^\ell(\mathsf{z})\,\mathrm{d}\mathsf{z}, \quad \phi^\ell(\mathsf{z}) := \frac{\mathsf{z}}{\bar{u}^\ell_{\mathcal{P}}\mathsf{z} - f(\mathsf{z})}, \tag{271}$$

where $\ell \in \{i, j\}$, and $|\bar{\mathsf{y}}^\ell| \in [\epsilon_c, \bar{\eta}^\ell_f)$.

Proposition 57. *Let $\bar{u}^i_{\mathcal{P}} > \bar{u}^j_{\mathcal{P}}$, where $i \neq j$, and assume that $\bar{\mathsf{x}}_{\mathcal{T}} \in \mathcal{W}_{\bar{\eta}^i_f}(\bar{\mathsf{x}}^i_{\mathcal{P}}) \cap \mathcal{W}_{\bar{\eta}^j_f}(\bar{\mathsf{x}}^j_{\mathcal{P}})$. Furthermore, assume that $\Delta\bar{\mathsf{y}} := |\bar{\mathsf{y}}^i| - |\bar{\mathsf{y}}^j| > 0$. Then*

$$T^i_{\mathrm{f}}(\bar{\mathsf{y}}^i) < T^j_{\mathrm{f}}(\bar{\mathsf{y}}^j), \tag{272}$$

for all $\Delta\bar{\mathsf{y}} < M(|\bar{\mathsf{y}}^j|; \epsilon_c, m)$, where

$$M(|\bar{\mathsf{y}}^j|; \epsilon_c, m) := \frac{\min_{\epsilon_c \leq \mathsf{z} \leq |\bar{\mathsf{y}}^j|}(\phi^j(\mathsf{z}) - \phi^i(\mathsf{z}))}{\max_{|\bar{\mathsf{y}}^j| \leq \mathsf{z} \leq m} \phi^i(\mathsf{z})}(|\bar{\mathsf{y}}^j| - \epsilon_c),$$

and where $|\bar{\mathsf{y}}^i| \leq m < \bar{\eta}^i_f$.

Proof. We have that

$$\begin{aligned} T^i_{\mathrm{f}}(\bar{\mathsf{y}}^i) - T^j_{\mathrm{f}}(\bar{\mathsf{y}}^j) &= \int_{\epsilon_c}^{|\bar{\mathsf{y}}^i|} \phi^i(\mathsf{z})\mathrm{d}\mathsf{z} - \int_{\epsilon_c}^{|\bar{\mathsf{y}}^j|} \phi^j(\mathsf{z})\mathrm{d}\mathsf{z} \\ &= \int_{\epsilon_c}^{|\bar{\mathsf{y}}^i|} \phi^i(\mathsf{z})\mathrm{d}\mathsf{z} - \int_{\epsilon_c}^{|\bar{\mathsf{y}}^j|} \phi^j(\mathsf{z})\mathrm{d}\mathsf{z} \\ &= \int_{|\bar{\mathsf{y}}^j|}^{|\bar{\mathsf{y}}^i|} \phi^i(\mathsf{z})\mathrm{d}\mathsf{z} + \int_{\epsilon_c}^{|\bar{\mathsf{y}}^j|} (\phi^i(\mathsf{z}) - \phi^j(\mathsf{z}))\mathrm{d}\mathsf{z}. \end{aligned}$$

It follows from the mean value theorem for Riemann integrals that there exist $\mathsf{z}_1 \in [|\bar{\mathsf{y}}^j|, |\bar{\mathsf{y}}^i|]$ and $\mathsf{z}_2 \in [\epsilon_c, |\bar{\mathsf{y}}^j|]$ such that

$$T_{\mathrm{f}}^i(\bar{\mathsf{y}}^i) - T_{\mathrm{f}}^j(\bar{\mathsf{y}}^j) = \phi^i(\mathsf{z}_1)\Delta\bar{\mathsf{y}} + (\phi^i(\mathsf{z}_2) - \phi^j(\mathsf{z}_2))(|\bar{\mathsf{y}}^j| - \epsilon_c). \tag{273}$$

Furthermore, $\mathsf{z}_1 \in [|\bar{\mathsf{y}}^j|, |\bar{\mathsf{y}}^i|] \subset [\epsilon_c, m]$ implies that $\phi^i(\mathsf{z}_1) \geq \min_{|\bar{\mathsf{y}}^j| \leq \mathsf{z} \leq |\bar{\mathsf{y}}^i|} \phi^i(\mathsf{z}) \geq \min_{\epsilon_c \leq \mathsf{z} \leq m} \phi^i(\mathsf{z}) > 0$. In addition,

$$\phi^i(\mathsf{z}_2) - \phi^j(\mathsf{z}_2) = \frac{\mathsf{z}_2^2(\bar{u}_{\mathcal{P}}^j - \bar{u}_{\mathcal{P}}^i)}{(\bar{u}_{\mathcal{P}}^i \mathsf{z}_2 - f(\mathsf{z}_2))(\bar{u}_{\mathcal{P}}^j \mathsf{z}_2 - f(\mathsf{z}_2))}, \tag{274}$$

which implies that $\phi^i(\mathsf{z}_2) - \phi^j(\mathsf{z}_2) < 0$ given that $\mathsf{z}_2 \in [\epsilon_c, |\bar{\mathsf{y}}^j|] \subset [\epsilon_c, \bar{\eta}_f^j) \subseteq [\epsilon_c, \bar{\eta}_f^i)$ and $\bar{u}_{\mathcal{P}}^j < \bar{u}_{\mathcal{P}}^i$. Hence, in light of (273), it follows that $T_{\mathrm{f}}^i(\bar{\mathsf{y}}^i) < T_{\mathrm{f}}^j(\bar{\mathsf{y}}^j)$ is equivalent to

$$\Delta\bar{\mathsf{y}} < \frac{\phi^j(\mathsf{z}_2) - \phi^i(\mathsf{z}_2)}{\phi^i(\mathsf{z}_1)}(|\bar{\mathsf{y}}^j| - \epsilon_c). \tag{275}$$

Since $\phi(\mathsf{z}_1)$ and $\phi^j(\mathsf{z}_2) - \phi^i(\mathsf{z}_2)$ are continuous functions for $\mathsf{z}_1 \in [|\bar{\mathsf{y}}^j|, |\bar{\mathsf{y}}^j| + m] \supseteq [|\bar{\mathsf{y}}^j|, |\bar{\mathsf{y}}^i|]$ and $\mathsf{z}_2 \in [\epsilon_c, |\bar{\mathsf{y}}^j|]$, respectively, it follows that

$$\phi^i(\mathsf{z}_1) \leq \max_{|\bar{\mathsf{y}}^j| \leq \mathsf{z} \leq |\bar{\mathsf{y}}^i|} \phi^i(\mathsf{z}) \leq \max_{|\bar{\mathsf{y}}^j| \leq \mathsf{z} \leq m} \phi^i(\mathsf{z}), \tag{276}$$

$$\phi^j(\mathsf{z}_2) - \phi^i(\mathsf{z}_2) \geq \min_{\epsilon_c \leq \mathsf{z} \leq |\bar{\mathsf{y}}^j|} (\phi^j(\mathsf{z}) - \phi^i(\mathsf{z})). \tag{277}$$

Therefore,

$$\begin{aligned}
\Delta\bar{\mathsf{y}} &\leq \frac{\min_{\epsilon_c \leq \mathsf{z} \leq |\bar{\mathsf{y}}^j|}\{\phi^j(\mathsf{z}) - \phi^i(\mathsf{z})\}}{\max_{|\bar{\mathsf{y}}^j| \leq \mathsf{z} \leq m}\{\phi^i(\mathsf{z})\}}(|\bar{\mathsf{y}}^j| - \epsilon_c) \\
&\leq \frac{\min_{\epsilon_c \leq \mathsf{z} \leq |\bar{\mathsf{y}}^j|}\{\phi^j(\mathsf{z}) - \phi^i(\mathsf{z})\}}{\max_{|\bar{\mathsf{y}}^j| \leq \mathsf{z} \leq |\bar{\mathsf{y}}^i|}\{\phi^i(\mathsf{z})\}}(|\bar{\mathsf{y}}^j| - \epsilon_c) \\
&\leq \frac{\phi^j(\mathsf{z}_2) - \phi^i(\mathsf{z}_2)}{\phi^i(\mathsf{z}_1)}(|\bar{\mathsf{y}}^j| - \epsilon_c),
\end{aligned} \tag{278}$$

implies that $T_{\mathrm{f}}^i(\bar{\mathsf{y}}^i) < T_{\mathrm{f}}^j(\bar{\mathsf{y}}^j)$, and thus completing the proof. □

Proposition 57 implies that the i^{th} pursuer can reach the target faster than the j^{th} pursuer although at time $t = 0$ the latter is closer to the target than the former.

10.4 Simulation Results

In this section, we present simulation results to illustrate the previous developments. We consider a scenario where the maneuvering target is faster than the i^{th} pursuer, but the winning set of the i^{th} pursuer is non-empty as a result of the information pattern employed in Section 9.2. In particular, it is assumed that the target has a constant speed and its evading strategy is given by

$$u_{\mathcal{T}}(\mathsf{y}^i) = \begin{cases} \alpha \mathsf{y}^i + \rho(\mathsf{y}^i)\mathsf{S}\mathsf{y}^i, & \text{for } \epsilon_c \le |\mathsf{y}^i| \le \dfrac{M}{\alpha}, \\ M\dfrac{\mathsf{y}^i}{|\mathsf{y}^i|}, & \text{for } |\mathsf{y}^i| > \dfrac{M}{\alpha}, \end{cases} \tag{279}$$

where M and α are some positive constants with $M > \max\{\bar{u}_{\mathcal{P}}, \alpha\}$, S is a nonzero skew symmetric matrix in $\mathbb{R}^{2\times 2}$, and

$$\rho(\mathsf{y}^i) := \frac{\sqrt{M^2 - \alpha^2|\mathsf{y}^i|^2}}{|\mathsf{S}\mathsf{y}^i|}. \tag{280}$$

Note that

$$f(\mathsf{y}^i) := \langle u_{\mathcal{T}}, \mathsf{y}^i \rangle = \begin{cases} \alpha|\mathsf{y}^i|^2, & \text{for } \epsilon_c \le |\mathsf{y}^i| \le \dfrac{M}{\alpha}, \\ M|\mathsf{y}^i| & \text{for } |\mathsf{y}^i| > \dfrac{M}{\alpha}, \end{cases} \tag{281}$$

satisfies Assumption 1.

The intuition behind the evading strategy (279) is as follows: Let $\mathsf{e}_1(\mathsf{y}^i) := \mathsf{y}^i/|\mathsf{y}^i|$ be the unit vector along the line connecting the target and the i^{th} pursuer ("line-of-sight" direction), and let $\mathsf{e}_2(\mathsf{y}^i)$ be the unit vector orthogonal to $\mathsf{e}_1(\mathsf{y}^i)$ ("tangential" direction). The strategy of the target is to allocate its velocity vector, which has a constant magnitude $M > u_{\mathcal{P}}$, along the directions $\mathsf{e}_1(\mathsf{y}^i)$ and $\mathsf{e}_2(\mathsf{y}^i)$ so that it moves with constant speed M along the line-of-sight direction when it is sufficiently far away from the pursuer, and it uses an increasingly larger tangential component as its distance from the pursuer decreases, in an effort to maneuver away or confuse its pursuer.

Assume for this example that the set $\mathcal{P}$ consists of ten locations, and let

$$\bar{f}(\mathsf{y}^i) := \begin{cases} \bar{\alpha}|\mathsf{y}^i|^2, & \text{for } \epsilon_c \leq |\mathsf{y}^i| \leq \dfrac{M}{\bar{\alpha}}, \\ M|\mathsf{y}^i| & \text{for } |\mathsf{y}^i| > \dfrac{M}{\bar{\alpha}}, \end{cases} \tag{282}$$

where $\bar{\alpha}$ is a positive scalar with $\alpha \leq \bar{\alpha} < M$. In this case, the capturability condition reduces to $\eta^i(0) < \bar{u}_{\mathcal{P}}/\alpha$, which implies that $\bar{\eta}_f = \bar{u}_{\mathcal{P}}/\alpha < M/\alpha$ and $\bar{\eta}_{\bar{f}} = \bar{u}_{\mathcal{P}}/\bar{\alpha} < M/\bar{\alpha}$. Furthermore, it is easy to show that, in light of (253), the minimum-time of the optimal pursuit problem, for $\epsilon_c < |\bar{\mathsf{y}}^i| < \bar{\eta}_f$, is given by

$$T_{\mathrm{f}}(\bar{\mathsf{y}}^i) = -\frac{1}{\alpha} \ln \left(\frac{\bar{u}_{\mathcal{P}} - \alpha|\bar{\mathsf{y}}^i|}{\bar{u}_{\mathcal{P}} - \alpha\epsilon_c} \right). \tag{283}$$

Next, we present simulation results of the relay-pursuit scheme introduced in Section 10.2.3. In particular, Fig. 56 illustrates the trajectories of the active pursuers and the moving target during the course of the relay pursuit for $\mathsf{S} = \left[\begin{smallmatrix} 0 & 1.5 \\ -1.5 & 0 \end{smallmatrix}\right]$, $\varepsilon = 0.2$, and $M = 3$. It is assumed that $\bar{\mathsf{x}}_{\mathcal{T}} \in \mathcal{W}_f(\bar{\mathsf{x}}^7_{\mathcal{P}})$. Specifically, Fig. 56(a) illustrates the trajectories of the target and the 7^{th} pursuer, which is assigned to the target at $t = 0$, until $t = \tau_1$, when $\mathsf{x}_{\mathcal{T}}(\tau_1) \in \operatorname{int} \mathcal{V}^5 \cap H^5_{\tau_1,\varepsilon}(\mathsf{x}^7_{\mathcal{P}}(\tau_1), \bar{\mathsf{x}}^5_{\mathcal{P}})$ and the target is assigned to the 5^{th} pursuer. Figure 56(b) illustrates the trajectories of the target and the 5^{th} pursuer, for $\tau_1 \leq t < \tau_2$, where τ_2 is the second switching time when the target is assigned to the 3^{rd} pursuer. Note that $\mathsf{x}_{\mathcal{T}}(\tau_1)$ resides in the interior of the cell of the OP-DVD generated by the locations of all the pursuers at time $t = \tau_1$, that is, the set $\mathcal{P}_{\tau_1} := (\mathcal{P} \cup \{\mathsf{x}^7_{\mathcal{P}}(\tau_1)\}) \setminus \{\bar{\mathsf{x}}^7_{\mathcal{P}}\}$, that is associated with the 5^{th} pursuer. Figure 56(c) illustrates the trajectories of the target and the 3^{rd} pursuer for $t \geq \tau_2$. Again, we observe that at time $t = \tau_2$ the target resides inside the cell of the OP-DVD generated by the locations of the pursuers at time $t = \tau_2$, that is, the set $\mathcal{P}_{\tau_2} := (\mathcal{P} \cup \{\mathsf{x}^7_{\mathcal{P}}(\tau_1)\} \cup \{\mathsf{x}^5_{\mathcal{P}}(\tau_2)\}) \setminus (\{\bar{\mathsf{x}}^7_{\mathcal{P}}\} \cup \{\bar{\mathsf{x}}^5_{\mathcal{P}}\})$, that is associated with the 3^{rd} pursuer. Moreover, we observe that although at some time instant $\tau_3 > \tau_2$ the target enters the cell associated with the 2^{nd} pursuer at time $t = \tau_2$, the 3^{rd} pursuer

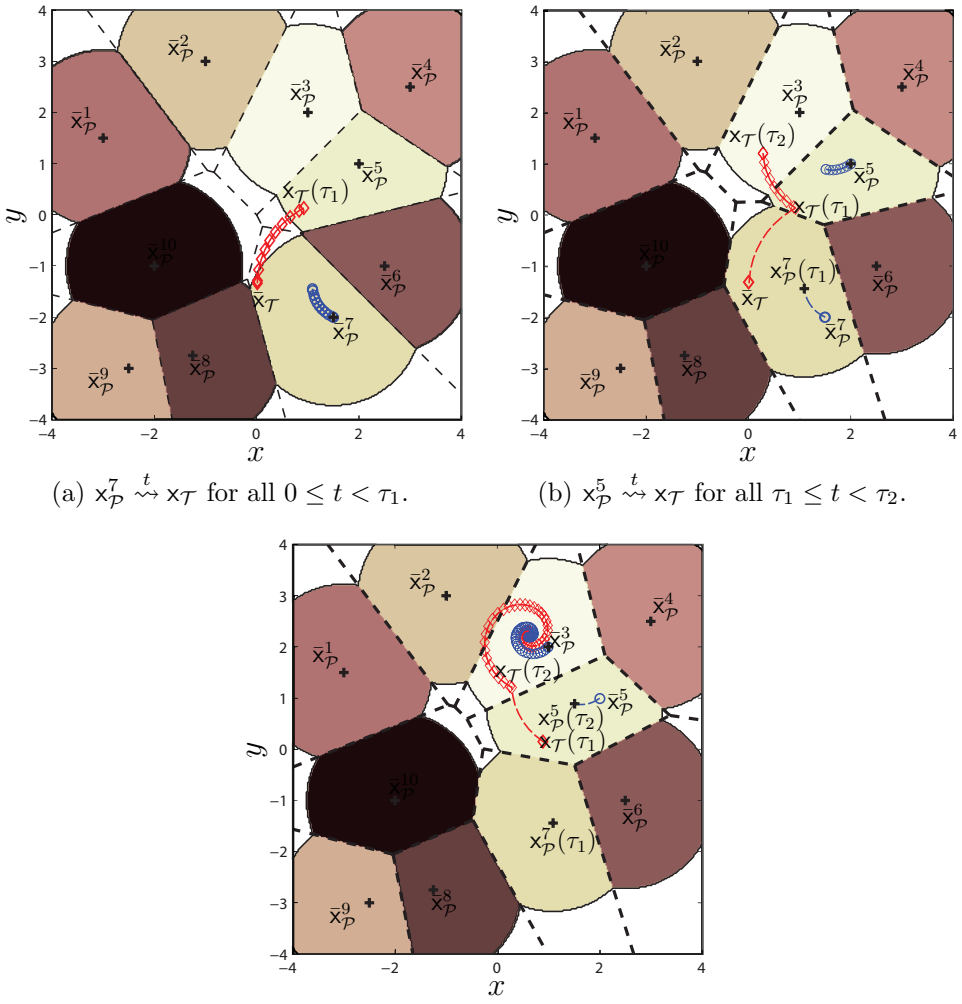

(a) $x_{\mathcal{P}}^7 \overset{t}{\rightsquigarrow} x_{\mathcal{T}}$ for all $0 \leq t < \tau_1$.

(b) $x_{\mathcal{P}}^5 \overset{t}{\rightsquigarrow} x_{\mathcal{T}}$ for all $\tau_1 \leq t < \tau_2$.

(c) $x_{\mathcal{P}}^3 \overset{t}{\rightsquigarrow} x_{\mathcal{T}}$ for all $t \geq \tau_2$.

Figure 56: Trajectories of the active pursuers and the moving target during the course of the relay pursuit for the first scenario.

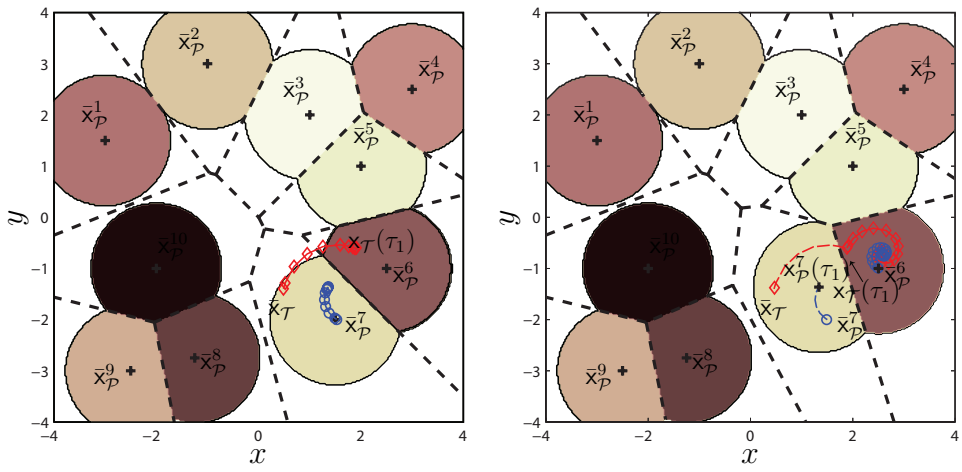

(a) $\mathsf{x}_{\mathcal{P}}^{7} \overset{t}{\rightsquigarrow} \mathsf{x}_{\mathcal{T}}$ for all $0 \leq t < \tau_1$. (b) $\mathsf{x}_{\mathcal{P}}^{6} \overset{t}{\rightsquigarrow} \mathsf{x}_{\mathcal{T}}$ for all $t \geq \tau_1$.

Figure 57: Trajectories of the active pursuers and the moving target during the course of the relay pursuit for the second scenario.

remains closer to the target than the 2nd pursuer for all $t \geq \tau_3$. Thus the pursuer-target assignment does not change for $t \geq \tau_2$, and thus the 3rd pursuer will eventually capture the target. It is interesting to observe that for this particular scenario a relay pursuit strategy induced by the approximate rather than the exact OP-DVD generated by $\mathcal{P}$ cannot solve Problem 16 since $\bar{\mathsf{x}}_{\mathcal{T}} \notin \mathcal{W}_{\bar{f}}(\bar{\mathsf{x}}_{\mathcal{P}}^{i})$, for all $i \in \mathcal{I}_n$. Next, we examine a scenario for which $\bar{\mathsf{x}}_{\mathcal{T}} \in \mathcal{W}_{\bar{f}}(\bar{\mathsf{x}}_{\mathcal{P}}^{7})$. The trajectories of the active pursuers and the maneuvering target are illustrated in Figs. 57(a)-57(b). It is interesting to note that the relay pursuit strategies induced by the exact and the approximate OP-DVD for the second scenario turn out to be exactly the same.

CHAPTER XI

CONCLUDING REMARKS AND FUTURE WORK

11.1 Synopsis of the Thesis and Concluding Remarks

In this thesis, we addressed a wide spectrum of problems ranging from steering problems involving a single planar vehicle in the presence of differential constraints and/or vehicle-environment interactions induced by local winds/currents to partitioning problems involving teams of autonomous vehicles. We started our discussion on steering problems for a single vehicle by first examining the optimal synthesis of different variations of the classical Markov-Dubins problem. In particular, we have addressed the optimal synthesis problem for a single planar vehicle, whose kinematics are similar to those of the Isaacs-Dubins car, when its maneuverability is either affected/compromised by mechanical failures and/or environment-vehicle interactions induced by local winds/currents. Another variation of the MD problem we have examined is the problem of steering the ID car with angular acceleration control. Using angular acceleration as the control input results in paths with continuous curvature profiles, which are more suited for path tracking applications. Subsequently, we examined a realistic variation of the classical Zermelo's navigation problem, namely the navigation problem in a both temporally and spatially varying flow field, when the vehicle has only local and uncertain information about the drift in its vicinity.

After having discussed several steering problems involving a single vehicle, we subsequently, addressed problems involving teams of spatially distributed vehicles. In particular, we have touched upon problems of assigning tasks among the different members of a team of autonomous vehicles by associating them with Voronoi-like

partitioning problems with respect to state-dependent (generalized) distance functions. We have argued that state-dependent Voronoi-like partition may encode more relevant information for multi-vehicle applications than standard Voronoi partitions. The so-called Zermelo-Voronoi diagram played a key role in illustrating the potential of the proposed new concept of state-dependent Voronoi-like partition for real world applications. In particular, we coined the term "Zermelo-Voronoi diagram" in order to describe a Voronoi-like diagram with respect to the minimum time-to-go/to-come of the Zermelo's navigation problem. Based on the duality between the navigation problem and a special case of the problem of pursuit of a maneuvering target, we used similar techniques with those proposed for the solution of the Zermelo-Voronoi diagram to construct state-dependent Voronoi-like partitions with respect to the minimum capture time for applications involving teams of spatially distributed pursuers.

Finally, we have illustrated how the concept of the state-dependent Voronoi diagram can serve as a "vehicle" for designing local control schemes for problems involving teams of spatially distributed vehicles by examining a group pursuit problem. In particular, we have formulated a prototypical sequential pursuit problem involving a team of spatially distributed pursuers such that, at every instant of time, only one pursuer can be assigned with the task of capturing the maneuvering target. We have addressed this problem by employing a switching architecture that was induced, in turn, by the solution of a generalized partitioning problem with respect to the minimum capture time of the maneuvering target by each pursuer.

Next, we highlight some potential directions for future research that build upon some of the results we presented in this research effort.

11.2 Optimal Steering in the Presence of Differential Constraints and Environment-Agents Interactions

First, we briefly introduce a number of interesting path-planning/steering problems involving a single vehicle, whose motion is described by a relatively simple kinematic

model. Although the literature on steering problems for mobile vehicles, whose kinematics are described by non-holonomic models, is considerably rich, there are many interesting problems that remain open. Perhaps a steering problem with a significant potential for practical applications is the minimum-time path planning problem in a three-dimensional space. For example, the optimal synthesis of the three-dimensional version of the Markov-Dubins problem remains until today an open problem (for a preliminary treatment of this problem, the reader may refer to [196]). The kinematic model of the three-dimensional version of the Isaacs-Dubins car is described by the following set of equations [196]

$$\dot{\mathsf{x}} = v, \qquad \dot{v} = \omega \times v \tag{284}$$

where $\mathsf{x} := (x, y, z) \in \mathbb{R}^3$ are the coordinates of the position of a reference point of the vehicle, $v \in \mathbb{S}^2$ is the velocity vector (a vector of constant unit length), the symbol $\times$ denote the cross product operator, and ω is the angular velocity vector (input). It is assumed that ω is a piecewise continuous function and $|\omega| \leq \bar{\omega}$, where $\bar{\omega}$ is the maximum norm that the angular velocity can attain.

Another interesting problem, especially for applications involving UAVs and AUVs, is the characterization of the time-optimal synthesis of the steering problem of a aerial/marine vehicle with kinematics similar to those of the Isaacs-Dubins car in the presence an arbitrary spatiotemporal flow-field, that is, the Zermelo-Markov-Dubins problem for an arbitrary drift field that varies both temporally and spatially. The kinematics of the vehicle for this steering problem are described by the following equations

$$\dot{x} = \cos\theta + w_x(t, x, y), \qquad \dot{y} = \cos\theta + w_y(t, x, y), \qquad \dot{\theta} = u/\rho, \tag{285}$$

where $(x, y, \theta) \in \mathbb{R}^2 \times \mathbb{S}^1$ as in Eq. (1), u is the control input with $|u(t)| \in [-1, 1]$, for all $t \geq 0$, and $w_x(t, x, y)$ and $w_y(t, x, y)$ are the components of the drift expressed with respect to an inertial frame. A complete analytical treatment of this problem is

doubtful. Therefore alternative approaches must be proposed. A promising approach is to relax the hard input constraint $|u(t)| \in [-1, 1]$, for all $t \geq 0$, by considering the following cost function

$$J_{\text{soft}}(u) = T_{\text{f}} + \beta \int_0^{T_{\text{f}}} u^2(t) \mathrm{d}t, \tag{286}$$

where β is a positive parameter to be chosen such that the input satisfies, if possible, the hard constraint $|u(t)| \in [-1, 1]$, for all $t \geq 0$, a posteriori.

Another interesting research problem within the same context is the characterization of feedback steering laws for the system described by Eq. (285), when the drift field is uncertain and is only known in the vicinity of the vehicle. This problem falls under the umbrella of steering problems for systems driven by non-anticipative control laws, which do not require global information about the future interactions between the vehicle and its operating environment. Another characteristic example of this category of steering problems is the characterization of control laws to safely steer a vehicle in an environment populated by obstacles, the exact positions of which along with their geometries are not a priori known but are reconstructed "on the fly" as the vehicle collects information about its operating environment using standard perception mechanisms.

11.3 State-Dependent Voronoi-like Partitions for Teams of Vehicles with Higher Order Kinematics

The paradigms that we have used in this dissertation in order to illustrate the concept of state-dependent Voronoi-like partition and its applications were based on simplifying assumptions that allowed us to characterize elegant solutions of particular partitioning problems. The application of the ideas presented in this dissertation to more challenging real world problems require significant modifications as well as further research. It is likely that in the majority of practical applications, the construction of state-dependent Voronoi-like partitions would require, at some extent, the

use of numerical techniques for the propagation of the level sets of the generalized, state-dependent metric of the partition.

Next, we sketch the general steps of a straightforward technique for the construction of a Voronoi-like partition with respect to a state-dependent metric for applications involving teams of spatially distributed vehicles, whose motions are described from higher order kinematic/dynamic models. In particular, let us assume that the system is described by the following equation

$$\dot{\mathsf{x}} = f(\mathsf{x}, u), \quad \mathsf{x}(0) \in \mathcal{P} := \{\bar{\mathsf{x}}^i, \quad i \in \mathcal{I}_n\} \tag{287}$$

where $\mathsf{x} \in \mathcal{X}$ is the system state, u is the control input, and $\mathcal{I}_n := \{1, \ldots, n\}$ is the index set associated with the set of generators $\mathcal{P}$. Let assume that u takes values in a convex, compact set $U \subset \mathbb{R}^m$, where m is some positive integer. Our objective is to construct a partition $\mathfrak{V} := \{\mathfrak{V}^i, \ i \in \mathcal{I}_n\}$ of the state space $\mathcal{X}$ with respect to a cost function $c(\mathsf{x}; \bar{\mathsf{x}}^i)$, which is associated, in turn, with the transition of the system (287) from $\bar{\mathsf{x}}^i \in \mathcal{P}$ to an arbitrary state $\mathsf{x} \in \mathcal{X}$, for $i \in \mathcal{I}_n$. Now let $\mathcal{S}_i := \{(\mathsf{x}, z), \ \mathsf{x} \in \mathbb{R}^2 \text{ and } z = c(\mathsf{x}; \bar{\mathsf{x}}^i)\}$ denote the cost surface associated with the minimum cost-to-go from the generator $\bar{\mathsf{x}}^i \in \mathcal{P}$, for $i \in \mathcal{I}_n$. Furthermore, the cost surface associated with the minimum cost-to-go function from the set $\mathcal{P}$ is defined as follows $\mathcal{S}_{\mathcal{P}} := \{(\mathsf{x}, z), \ \mathsf{x} \in \mathcal{X} \text{ and } z = \min_{\bar{\mathsf{x}}_i \in \mathcal{P}} c(\mathsf{x}, \bar{\mathsf{x}}^i)\}$. In addition, let us consider the following projection operator $\mathbf{P} : \mathcal{X} \times [0, \infty) \mapsto \mathcal{X}$, where $\mathbf{P}(\mathsf{x}, z) = \mathsf{x}$. It can be shown that the cell $\mathfrak{V}^i \in \mathfrak{V}$ associated with the generator $\bar{\mathsf{x}}^i \in \mathcal{P}$ can be computed as follows

$$\mathfrak{V}^i = \{\mathsf{x} \in \mathcal{X} : \ \mathsf{x} = \mathbf{P}(\mathsf{x}, z), \quad (\mathsf{x}, z) \in \mathcal{S}_{\mathcal{P}} \cap \mathcal{S}_i\}. \tag{288}$$

Figure 58 illustrates the Voronoi-like partition with respect to the minimum time of the Markov-Dunins problem for a set of four generators that are placed on the vertices of a square, which is obtained after applying the previously described method.

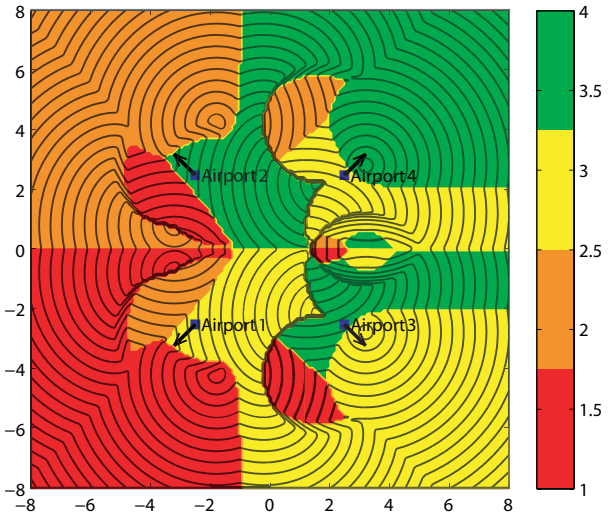

(a) Voronoi partitions for different final headings.

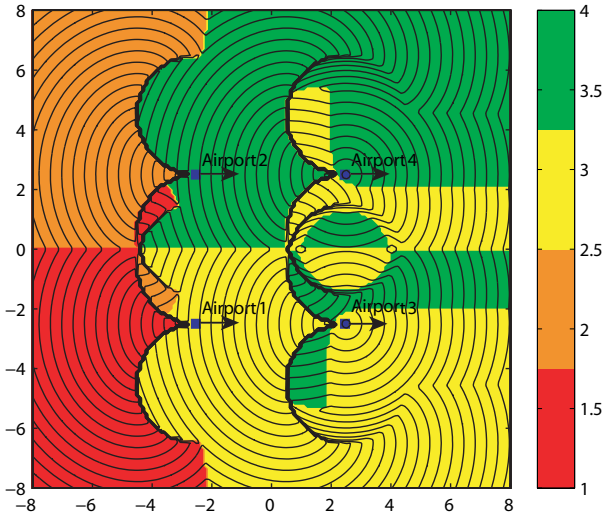

(b) Voronoi partition for equal final headings.

Figure 58: Voronoi partition with respect to the time-to-come function of the Isaacs-Dubins car for a set of generators (targets to be reached in minimum time) placed on a co-circular formation when the final headings associated with each generator are either all the same or multiples of $\pi/4$. Note that in both cases the Voronoi-like partitions consist of disconnected domains.

11.4 State-Dependent Voronoi-like Partitions with Local Information

An interesting direction for future research is the construction of the state-dependent Voronoi-like partitions for problems involving teams of autonomous vehicle when the vehicles do not have global information about their operating environment. An example of this class of problems is a variation of the Zermelo-Voronoi diagram problem, when there is no sufficient information about global spatial distribution of the winds/currents available to all the vehicles of the network. It is assumed instead that each vehicle, which can sense the locations of the other vehicles (or those within some sensing distance from it), has its own estimation of the winds/currents in its vicinity. Under the previous assumptions, each vehicle can construct its own "myopic" solution of the Zermelo-Voronoi diagram problem based on its own knowledge of the drift field in its vicinity. The situation is illustrated in Fig. 59. In particular, three vehicles are located at p_1, p_2 and p_3 where they obtain, respectively, measurements w_1, w_2, and w_3 of the local drift field. For simplicity, let us assume that each vehicle, based on its own estimation and measuring mechanisms, considers the drift field to be constant everywhere. In particular, the vehicle located at p_1 considers the drift to be constant everywhere and equal to w_1, whereas the vehicles located at p_2 and p_3 consider the drift to be constant and equal to w_2 and w_3, respectively. Consequently, there may exist regions for which there is no consensus among the vehicles on which vehicle should these regions be assigned to. Thus, the problem of assigning a point to a vehicle may not be well posed. For example, the points in the intersection of the red and the blue cells in Fig. 59 are considered from the vehicle located at p_1 to be "closer", with respect to the minimum time-to-go function, to itself than to the vehicle at p_2, and vice versa. To avoid these confusing situations, each vehicle has to propagate the information about their local measurements of the winds / currents to their neighbors. In this way, the drift field at every point in the plane is assigned

to a single, "negotiated" value which is globally known to every vehicle. One possibility is to approximate the drift field by a piece-constant field, where the drift is constant in every cell of, say, a polygonal subdivision of the plane. The solution of the navigation problem in a piecewise constant drift, which will allow us to determine the propagation of the level sets of the minimum time-to-go, was presented in our previous work [12]. Based on this negotiated, "artificial" drift field, the vehicles can agree on a common non-overlapping partition of the space.

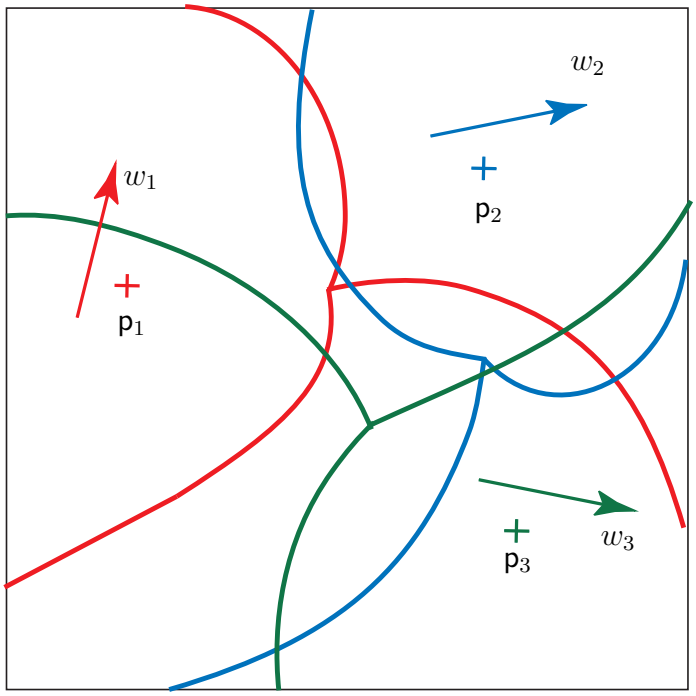

Figure 59: If the vehicles do not exchange information regarding the drift in their vicinity with each other, then each vehicle will compute its own, myopic solution of the ZVDP. If the vehicles exchange information, then a common partition, which is based on a "negotiated" estimation of the global spatial distribution of the drift field, can be constructed.

11.5 The Group Pursuit Problem Using Sequential Pursuit Strategies Along with Deception and Cooperation

The idea of sequential pursuit presented in Chapter 10 can find many interesting extensions. One possible direction is to consider group pursuit scenarios where the

motions of the pursuers and the target are described by the kinematics of the Isaacs-Dubins car. A different possibility is to consider the problem when more than one pursuers are allowed to participate in the process of pursuing the target. In particular, neighboring pursuers may be allowed to cooperate in order to incorporate the element of deception in their joint strategies leading to, for example, faster capture of the target or capture of a target that cannot be captured by a single pursuer. An interesting research topic would be the analysis of the sequential pursuit problem from a game theoretic perspective. In particular, the relay pursuit problem can be alternatively formulated as a game involving multiple players, and a global objective, namely the capture of the target by at least one pursuer from the group.

APPENDIX A

THE EQUATIONS OF THE OPTIMAL SYNTHESIS OF THE ASDMD PROBLEM

In this appendix, we provide the details for the solution of the equations for the synthesis problem of the ASDMD problem.

A.1 $\mathsf{b}^+_\alpha\mathsf{s}_\beta\mathsf{b}^+_\gamma$ *and* $\mathsf{b}^-_\alpha\mathsf{s}_\beta\mathsf{b}^-_\gamma$ *Paths*

The coordinates of a point in $\mathfrak{R}_{\theta_\mathrm{f}}(\mathsf{b}^+\mathsf{s}\mathsf{b}^+)$ $[\mathfrak{R}_{\theta_\mathrm{f}}(\mathsf{b}^-\mathsf{s}\mathsf{b}^-)]$ as a function of the parameters α and β are given by

$$x_\mathrm{f} = \rho\big[-\varrho\big]\sin\theta_\mathrm{f} + \beta\cos\frac{\alpha}{\rho\big[\varrho\big]}, \tag{289}$$

$$y_\mathrm{f} = \rho\big[-\varrho\big] + \big[-\big]\beta\sin\frac{\alpha}{\rho\big[\varrho\big]} - \rho\big[+\varrho\big]\cos\theta_\mathrm{f}. \tag{290}$$

Conversely, the parameters $\alpha \in \mathcal{I}_\alpha(\mathsf{b}^+\mathsf{s}\mathsf{b}^+)$ $[\mathcal{I}_\alpha(\mathsf{b}^-\mathsf{s}\mathsf{b}^-)]$ and $\beta \in \mathcal{I}_\beta(\mathsf{b}^+\mathsf{s}\mathsf{b}^+)$ $[\mathcal{I}_\beta(\mathsf{b}^-\mathsf{s}\mathsf{b}^-)]$ satisfy

$$\alpha = \rho\big[\varrho\big]\,\mathrm{atan2}(B, A), \qquad \beta = \sqrt{A^2 + B^2}, \tag{291}$$

where $A = x_\mathrm{f} - \rho\big[+\varrho\big]\sin\theta_\mathrm{f}$ and $B = \big[-\big]y_\mathrm{f} + \rho\big[\varrho\big]\cos\theta_\mathrm{f} - \rho\big[\varrho\big]$.

A.2 $\mathsf{b}^+_\alpha\mathsf{s}_\beta\mathsf{b}^-_\gamma$ *and* $\mathsf{b}^-_\alpha\mathsf{s}_\beta\mathsf{b}^+_\gamma$ *Paths*

The coordinates of a point in $\mathfrak{R}_{\theta_\mathrm{f}}(\mathsf{b}^+\mathsf{s}\mathsf{b}^-)$ as a function of the parameters α and β are given by

$$x_\mathrm{f} = (\varrho+\rho)\sin\frac{\alpha}{\rho\big[\varrho\big]} + \beta\cos\frac{\alpha}{\rho\big[\varrho\big]} - \varrho\big[+\rho\big]\sin\theta_\mathrm{f}, \tag{292}$$

$$y_\mathrm{f} = \rho\big[-\varrho\big] - \big[+\big](\varrho+\rho)\cos\frac{\alpha}{\rho\big[\varrho\big]} + \big[-\big]\beta\sin\frac{\alpha}{\rho\big[\varrho\big]} + \varrho\big[-\rho\big]\cos\theta_\mathrm{f}, \tag{293}$$

Conversely, the parameters $\alpha \in \mathcal{I}_\alpha(\mathsf{b}^+\mathsf{sb}^-)$ $[\mathcal{I}_\alpha(\mathsf{b}^-\mathsf{sb}^+)$ and $\beta \in \mathcal{I}_\beta(\mathsf{b}^+\mathsf{sb}^-)$ $[\mathcal{I}_\beta(\mathsf{b}^-\mathsf{sb}^+)]$ satisfy

$$\alpha = \rho\big[\varrho\big]\operatorname{atan2}\left((\rho+\varrho)A - B\beta, (\rho+\varrho)B + A\beta\right), \qquad \beta = \sqrt{A^2+B^2-(\varrho+\rho)^2}, \tag{294}$$

where $A = x_\mathrm{f} + \varrho\big[-\rho\big]\sin\theta_\mathrm{f}$ and $B = \rho\big[\varrho\big] - \big[+\big]y_\mathrm{f} + \varrho\big[\rho\big]\cos\theta_\mathrm{f}$.

A.3 $\mathsf{b}^+_\alpha\mathsf{b}^-_\beta\mathsf{b}^+_\gamma$ *and* $\mathsf{b}^-_\alpha\mathsf{b}^+_\beta\mathsf{b}^-_\gamma$ *Paths*

The coordinates of a point in $\mathfrak{R}_{\theta_\mathrm{f}}(\mathsf{b}^+\mathsf{b}^-\mathsf{b}^+)$ as a function of the parameters α and β are given by

$$x_\mathrm{f} = (\varrho+\rho)\sin\frac{\alpha}{\rho\big[\varrho\big]} + (\varrho+\rho)\sin\left(\frac{\beta}{\varrho\big[\rho\big]} - \frac{\alpha}{\rho\big[\varrho\big]}\right) + \rho\big[-\varrho\big]\sin\theta_\mathrm{f}, \tag{295}$$

$$\begin{aligned} y_\mathrm{f} = {} & \rho\big[-\varrho\big] - \big[+\big](\varrho+\rho)\cos\frac{\alpha}{\rho\big[\varrho\big]} \\ & + \big[-\big](\varrho+\rho)\cos\left(\frac{\beta}{\varrho\big[\rho\big]} - \frac{\alpha}{\rho\big[\varrho\big]}\right) - \rho\big[+\varrho\big]\cos\theta_\mathrm{f}, \end{aligned} \tag{296}$$

Conversely, the parameters $\alpha \in \mathcal{I}_\alpha(\mathsf{b}^+\mathsf{b}^-\mathsf{b}^+)$ $[\mathcal{I}_\alpha(\mathsf{b}^-\mathsf{b}^+\mathsf{b}^-)]$ and $\beta \in \mathcal{I}_\beta(\mathsf{b}^+\mathsf{b}^-\mathsf{b}^+)$ $[\mathcal{I}_\beta(\mathsf{b}^-\mathsf{b}^+\mathsf{b}^-)]$ satisfy

$$\alpha = \rho\big[\varrho\big]\operatorname{atan2}\left(\Gamma, \Delta\right), \tag{297}$$

$$\beta = \varrho\big[\rho\big]\arccos\left(1 - \frac{A^2+B^2}{2(\rho+\varrho)^2}\right), \tag{298}$$

where

$$\begin{aligned} A(x_\mathrm{f},\theta_\mathrm{f}) &= x_\mathrm{f} - \rho\big[+\varrho\big]\sin\theta_\mathrm{f}, \\ B(y_\mathrm{f},\theta_\mathrm{f}) &= y_\mathrm{f} - \rho\big[+\varrho\big] + \rho\big[-\varrho\big]\cos\theta_\mathrm{f}, \\ \Gamma(x_\mathrm{f},y_\mathrm{f},\theta_\mathrm{f}) &= A(x_\mathrm{f},\theta_\mathrm{f})\left(1-\cos\frac{\beta}{\varrho\big[\rho\big]}\right) + \big[-\big]B(y_\mathrm{f},\theta_\mathrm{f})\sin\frac{\beta}{\varrho\big[\rho\big]} \\ \Delta(x_\mathrm{f},y_\mathrm{f},\theta_\mathrm{f}) &= -\big[+\big]B(y_\mathrm{f},\theta_\mathrm{f})\left(1-\cos\frac{\beta}{\varrho\big[\rho\big]}\right) + A(x_\mathrm{f},\theta_\mathrm{f})\sin\frac{\beta}{\varrho\big[\rho\big]} \end{aligned}$$

and where $\arccos : \mathbb{R} \mapsto [\pi, 2\pi]$ is the inverse cosine function.

APPENDIX B

THE EQUATIONS OF THE OPTIMAL SYNTHESIS OF THE ZMD PROBLEM

In this appendix, we provide the details for the solution of the equations for the synthesis problem of the ZMD problem.

B.1 $\mathsf{b}^+_\alpha \mathsf{s}_\beta \mathsf{b}^+_\gamma$ *and* $\mathsf{b}^-_\alpha \mathsf{s}_\beta \mathsf{b}^-_\gamma$ *Paths*

The coordinates x_f, y_f of a configuration in $\mathfrak{R}_{\theta_\mathrm{f}}(\mathsf{b}^+\mathsf{s}\mathsf{b}^+)\Big[\mathfrak{R}_{\theta_\mathrm{f}}(\mathsf{b}^-\mathsf{s}\mathsf{b}^-)\Big]$, can be expressed as functions of the parameters α and β as follows

$$x_\mathrm{f} = [-]\rho \sin\theta_\mathrm{f} + \beta\cos\frac{\alpha}{\rho} + w_x T_\mathrm{f}, \tag{299}$$

$$y_\mathrm{f} = [-]\rho(1-\cos\theta_\mathrm{f}) + [-]\beta\sin\frac{\alpha}{\rho} + w_y T_\mathrm{f}, \tag{300}$$

where $T_\mathrm{f} = \alpha+\beta+\gamma$, and $\gamma/\rho = (\theta_\mathrm{f} - \alpha/\rho) \bmod 2\pi$ $\big[\gamma/\rho = (2\pi - \theta_\mathrm{f} - \alpha/\rho) \bmod 2\pi\big]$.

Conversely, given a state $(x_\mathrm{f}, y_\mathrm{f}, \theta_\mathrm{f}) \in \mathfrak{R}_{\theta_\mathrm{f}}(\mathsf{b}^+\mathsf{s}\mathsf{b}^+)$ $[\mathfrak{R}_{\theta_\mathrm{f}}(\mathsf{b}^-\mathsf{s}\mathsf{b}^-)]$, we can determine $(\alpha,\beta) \in [0, 2\pi\rho] \times [0,\infty)$. In particular, after some algebraic manipulation, it follows that β satisfies the following, decoupled from α quadratic equation

$$(1-\nu^2)\beta^2 + [-]2(A(x_\mathrm{f},\theta_\mathrm{f})w_x + B(y_\mathrm{f},\theta_\mathrm{f})w_y)\beta - (A^2(x_\mathrm{f},\theta_\mathrm{f}) + B^2(y_\mathrm{f},\theta_\mathrm{f})w_y)) = 0, \tag{301}$$

where $A(x_\mathrm{f},\theta_\mathrm{f}) = x_\mathrm{f} - [+]\rho\sin\theta_\mathrm{f} - w_x\rho\hat{\theta}_\mathrm{f}$, $B(y_\mathrm{f},\theta_\mathrm{f}) = [-]y_\mathrm{f} + \rho(\cos\theta_\mathrm{f} - 1) - [+]w_y\rho\hat{\theta}_\mathrm{f}$, and

$$\hat{\theta}_\mathrm{f} = \begin{cases} \theta_\mathrm{f} \quad [2\pi - \theta_\mathrm{f}], & \text{if} \quad \alpha \le \rho\theta_\mathrm{f} \quad [\alpha \le (2\pi-\theta_\mathrm{f})\rho], \\ (2\pi+\theta_\mathrm{f})\rho \quad [(4\pi-\theta_\mathrm{f})\rho], & \text{if} \quad \alpha > \rho\theta_\mathrm{f} \quad [\alpha > (2\pi-\theta_\mathrm{f})\rho]. \end{cases} \tag{302}$$

Note that for each $(x_\mathrm{f}, y_\mathrm{f}, \theta_\mathrm{f}) \in \mathfrak{R}_{\theta_\mathrm{f}}(\mathsf{b}^+\mathsf{s}\mathsf{b}^+)\Big[\mathfrak{R}_{\theta_\mathrm{f}}(\mathsf{b}^-\mathsf{s}\mathsf{b}^-)\Big]$, there exist at most two solutions of (301). If β is one solution of (301), then α is determined with back

substitution in Eqs. (299)-(300). In particular, after some algebraic manipulation, it follows that $\alpha = \hat{\alpha}\rho$, where $\hat{\alpha} \in [0, 2\pi]$ satisfies

$$\cos\hat{\alpha} = \frac{A(x_{\rm f}, \theta_{\rm f})}{\beta} - w_x, \qquad \sin\hat{\alpha} = \frac{B(y_{\rm f}, \theta_{\rm f})}{\beta} - [+]w_y, \tag{303}$$

when $\beta \neq 0$, whereas $\alpha = \rho\theta_{\rm f}$ $[\rho(2\pi - \theta_{\rm f})]$, otherwise. In this way, for a given $(x_{\rm f}, y_{\rm f}, \theta_{\rm f}) \in P_{\theta_{\rm f}}$, we find pairs (α, β) and the corresponding final time

$$T_{\rm f}(\mathsf{b}^{+}\mathsf{s}\mathsf{b}^{+})[T_{\rm f}(\mathsf{b}^{-}\mathsf{s}\mathsf{b}^{-})] = \alpha + \beta + \gamma(\alpha),$$

and subsequently, we associate the configuration $(x_{\rm f}, y_{\rm f}, \theta_{\rm f}) \in P_{\theta_{\rm f}}$ with the pair (α^*, β^*) that gives the minimum time $T_{\rm f}(\mathsf{b}^{+}\mathsf{s}\mathsf{b}^{+})[T_{\rm f}(\mathsf{b}^{-}\mathsf{s}\mathsf{b}^{-})]$.

B.2 $\mathsf{b}^{+}_{\alpha}\mathsf{s}_{\beta}\mathsf{b}^{-}_{\gamma}$ *and* $\mathsf{b}^{-}_{\alpha}\mathsf{s}_{\beta}\mathsf{b}^{+}_{\gamma}$ *Paths*

The coordinates $x_{\rm f}$,$y_{\rm f}$ of a configuration in $\mathfrak{R}_{\theta}(\mathsf{b}^{+}\mathsf{s}\mathsf{b}^{-})$ $\big[\mathfrak{R}_{\theta}(\mathsf{b}^{-}\mathsf{s}\mathsf{b}^{+})\big]$ are given by

$$x_{\rm f} = 2\rho\sin\frac{\alpha}{\rho} + \beta\cos\frac{\alpha}{\rho} - [+]\rho\sin\theta_{\rm f} + w_x T_{\rm f}, \tag{304}$$

$$y_{\rm f} = [-]\rho(1 + \cos\theta_{\rm f}) - [+]2\rho\cos\frac{\alpha}{\rho} + [-]\beta\sin\frac{\alpha}{\rho} + w_y T_{\rm f}, \tag{305}$$

where $T_{\rm f} = \alpha + \beta + \gamma$, $\gamma/\rho = (\alpha/\rho - \theta_{\rm f}) \bmod 2\pi$ $\big[\gamma/\rho = (\alpha/\rho + \theta_{\rm f}) \bmod 2\pi\big]$.

Given a configuration $(x_{\rm f}, y_{\rm f}, \theta_{\rm f}) \in \mathfrak{R}_{\theta_{\rm f}}(\mathsf{b}^{+}\mathsf{s}\mathsf{b}^{-})\big[\mathfrak{R}_{\theta}(\mathsf{b}^{-}\mathsf{s}\mathsf{b}^{+})\big]$, it can be shown that α satisfies the following transcendental equation (decoupled from β)

$$D(\alpha; x_{\rm f}, \theta_{\rm f})\sin\frac{\alpha}{\rho} + E(\alpha; y_{\rm f}, \theta_{\rm f})\cos\frac{\alpha}{\rho} = B(y_{\rm f}, \theta_{\rm f})w_x - [+]A(x_{\rm f}, \theta_{\rm f})w_y + 2\rho, \tag{306}$$

where, $A(x_{\rm f}, \theta_{\rm f}) = x_{\rm f} + [-]\rho\sin\theta_{\rm f} + [-]w_x\rho\hat{\theta}_{\rm f}$, $B(y_{\rm f}, \theta_{\rm f}) = [-]y_{\rm f} - \rho(\cos\theta_{\rm f} + 1) + w_y\rho\hat{\theta}_{\rm f}$, $D(\alpha; x_{\rm f}, \theta_{\rm f}) = A(x_{\rm f}, \theta_{\rm f}) - [+]2\rho(w_y + [-]w_x\alpha/\rho)$, $E(\alpha; y_{\rm f}, \theta_{\rm f}) = -B(y_{\rm f}, \theta_{\rm f}) - 2\rho(w_x - [+]w_y\alpha/\rho)$, and where

$$\hat{\theta}_{\rm f} = \begin{cases} \theta_{\rm f}, & \text{if} \quad \alpha \geq \rho\theta_{\rm f}\big[\alpha \leq \rho(2\pi - \theta_{\rm f})\big], \\ [-]2\pi + \theta_{\rm f}, & \text{if} \quad \alpha < \rho\theta_{\rm f}\big[\alpha > \rho(2\pi - \theta_{\rm f})\big]. \end{cases} \tag{307}$$

Furthermore, it can be shown that β satisfies the following equation

$$(1-\nu^2)\beta = \left(A(x_{\rm f},\theta_{\rm f}) - 2\rho\left(\sin\frac{\alpha}{\rho} + w_x\alpha\right)\right)\left(\cos\frac{\alpha}{\rho} - [+]w_x\right) + \left(B(y_{\rm f},\theta_{\rm f}) + 2\rho\left(\cos\frac{\alpha}{\rho} - [+]w_y\alpha\right)\right)\left(\sin\frac{\alpha}{\rho} - [+]w_y\right). \quad (308)$$

B.3 $\mathsf{b}^+_\alpha\mathsf{b}^-_\beta\mathsf{b}^+_\gamma$, $\mathsf{b}^-_\alpha\mathsf{b}^+_\beta\mathsf{b}^-_\gamma$, $\mathsf{b}^+_\alpha\tilde{\mathsf{b}}^-_\beta\mathsf{b}^+_\gamma$ *and* $\mathsf{b}^-_\alpha\tilde{\mathsf{b}}^+_\beta\mathsf{b}^-_\gamma$ *Paths*

If $(x_{\rm f},y_{\rm f},\theta_{\rm f}) \in \mathfrak{R}_{\theta_{\rm f}}(\mathsf{b}^+\mathsf{b}^-\mathsf{b}^+)$ [or $\mathfrak{R}_{\theta_{\rm f}}(\mathsf{b}^-\mathsf{b}^+\mathsf{b}^-)$], $\mathfrak{R}_{\theta_{\rm f}}(\mathsf{b}^+\tilde{\mathsf{b}}^-\mathsf{b}^+)$ [or $\mathfrak{R}_{\theta_{\rm f}}(\mathsf{b}^-\tilde{\mathsf{b}}^+\mathsf{b}^-)$], then

$$x_{\rm f} = 2\rho\left(\sin\frac{\alpha}{\rho} + \sin\frac{\beta-\alpha}{\rho}\right) + [-]\rho\sin\theta_{\rm f} + w_xT_{\rm f}, \quad (309)$$

$$y_{\rm f} = [-]\rho(1-\cos\theta_{\rm f}) - [+]2\rho\left(\cos\frac{\alpha}{\rho} - \cos\frac{\beta-\alpha}{\rho}\right) + w_yT_{\rm f}, \quad (310)$$

where, $T_{\rm f} = \alpha+\beta+\gamma$, $\gamma/\rho = (\theta_{\rm f} - \alpha/\rho + \beta/\rho) \bmod 2\pi$ $\big[\gamma/\rho = (-\theta_{\rm f} - \alpha/\rho + \beta/\rho) \bmod 2\pi\big]$.

Conversely, given $(x_{\rm f},y_{\rm f},\theta_{\rm f})$ in $\mathfrak{R}_{\theta_{\rm f}}(\mathsf{b}^+\mathsf{b}^-\mathsf{b}^+)$ [or $\mathfrak{R}_{\theta_{\rm f}}(\mathsf{b}^-\mathsf{b}^+\mathsf{b}^-)$], $\mathfrak{R}_{\theta_{\rm f}}(\mathsf{b}^+\tilde{\mathsf{b}}^-\mathsf{b}^+)$ [or $\mathfrak{R}_{\theta_{\rm f}}(\mathsf{b}^-\tilde{\mathsf{b}}^+\mathsf{b}^-)$], it follows after some algebra that β satisfies the following transcendental equation, which is decoupled from α,

$$K(\beta;x_{\rm f},y_{\rm f},\theta_{\rm f}) + 8\rho^2\left(\cos\frac{\beta}{\rho} - 1\right) = 0, \quad (311)$$

where

$$K(\beta;x_{\rm f},y_{\rm f},\theta_{\rm f}) = A^2(x_{\rm f},\theta_{\rm f}) + B^2(y_{\rm f},\theta_{\rm f}) + 4\nu^2\beta^2 + [-]4\beta(B(y_{\rm f},\theta_{\rm f})w_y - [+]A(x_{\rm f},\theta_{\rm f})w_x),$$

$$A(x_{\rm f},\theta_{\rm f}) = x_{\rm f} - [+]\rho\sin\theta_{\rm f} - [+]w_x\rho\hat{\theta}_{\rm f},$$

$$B(y_{\rm f},\theta_{\rm f}) = -[+]y_{\rm f} + \rho(1-\cos\theta_{\rm f}) + w_y\rho\hat{\theta}_{\rm f},$$

and

$$\hat{\theta}_{\rm f} = \begin{cases} [-]\theta_{\rm f}, & \text{if } \ 0 \le [-]\theta_{\rm f} - \dfrac{\alpha}{\rho} + \dfrac{\beta}{\rho} < 2\pi, \\ -2\pi[+4\pi] + [-]\theta_{\rm f}, & \text{if } \ 2\pi[-4\pi] \le [-]\theta_{\rm f} - \dfrac{\alpha}{\rho} + \dfrac{\beta}{\rho} < 4\pi[-2\pi], \\ 2\pi + [-]\theta_{\rm f}, & \text{if } \ -2\pi \le [-]\theta_{\rm f} - \dfrac{\alpha}{\rho} + \dfrac{\beta}{\rho} < 0. \end{cases}$$

Given $\beta \in [0, 2\pi\rho]$, it follows after some algebraic manipulation that α satisfies

$$\begin{bmatrix} M(\beta; x_{\mathrm{f}}, \theta_{\mathrm{f}}) & N(\beta; y_{\mathrm{f}}, \theta_{\mathrm{f}}) \\ -[+]N(\beta; y_{\mathrm{f}}, \theta_{\mathrm{f}}) & [-]M(\beta; x_{\mathrm{f}}, \theta_{\mathrm{f}}) \end{bmatrix} \begin{bmatrix} \sin\dfrac{\alpha}{\rho} \\ \cos\dfrac{\alpha}{\rho} \end{bmatrix} = 2\rho \begin{bmatrix} 1 - \cos\dfrac{\beta}{\rho} \\ [-]\sin\dfrac{\beta}{\rho} \end{bmatrix}, \tag{312}$$

where $M(\beta; x_{\mathrm{f}}, \theta_{\mathrm{f}}) = A(x_{\mathrm{f}}, \theta_{\mathrm{f}}) - 2\beta w_x$, $N(\beta; y_{\mathrm{f}}, \theta_{\mathrm{f}}) = B(y_{\mathrm{f}}, \theta_{\mathrm{f}}) + [-]2\beta w_y$.

APPENDIX C

LIST OF PUBLICATIONS

Next, we give the list of the contributing publications of this PhD dissertation.

C.1 Journal Publications

i. Bakolas, E. and Tsiotras, P., "The Zermelo-Voronoi diagram: a dynamic partition problem," *Automatica*, vol. 46, no. 12, pp. 2059–2067, 2010.

ii. Bakolas, E. and Tsiotras, P., "Optimal synthesis of the asymmetric sinistral/dextral Markov–Dubins problem," *Journal of Optimization Theory and Applications*, vol. 150, no. 2, pp. 233–250, 2011.

iii. Tsiotras, P., Jung, D. and Bakolas, E., "Multiresolution hierarchical path-planning using wavelet decompositions," *Journal of Intelligent & Robotic Systems*, doi:10.1007/s10846-011-9631-z (Note : Accepted, July 2011)

iv. Bakolas, E. and Tsiotras, P., "Feedback navigation in an uncertain flow-field and connections with pursuit strategies," *Journal of Guidance, Control, and Dynamics* (Note: Accepted, August 2011)

v. Bakolas, E. and Tsiotras, P., "Relay Pursuit of a Maneuvering Target Using Dynamic Voronoi Diagrams," *Automatica* (Note: In revision)

vi. Bakolas, E. and Tsiotras, P., "Optimal Synthesis of the Zermelo–Markov–Dubins Problem in a Constant Drift Field, *Journal of Optimization Theory and Applications* (Note: Under review)

C.2 Conference Publications

i. Tsiotras, P. and Bakolas, E., "A Hierarchical On-Line Path-Planning Scheme Using Wavelets," in *Proceedings of European Control Conference*, Kos, Greece, pp. 2807–2812, July 2–5, 2007.

ii. Bakolas, E. and Tsiotras, P., "Multiresolution Path-Planning Using Sector Based Decompositions from Sensor Data," in *Proceedings of AIAA Guidance and Control Conference and Exhibit*, Honolulu, HW, August 18–21, 2008.

iii. Bakolas, E. and Tsiotras, P., "On-Line, Kinodynamic Trajectory Generation through Rectangular Channels Using Path and Motion Primitives," in *Proceedings of the 47th IEEE Conference on Decision and Control*, Cancun, Mexico, pp. 3725–3730, December 9–11, 2008.

iv. Bakolas, E. and Tsiotras, P., "On the Generation of Nearly Optimal, Planar Paths of Bounded Curvature and Bounded Curvature Gradient," in *Proceedings of American Control Conference*, St. Louis, Missouri, USA, pp. 385–390, June 10–12, 2009.

v. Bakolas, E. and Tsiotras, P., "The Asymmetric Sinistral/Dextral Markov-Dubins Problem," in *Proceedings of 48th IEEE Conference on Decision and Control*, Shanghai, China, pp. 5649–5654, December 15–18, 2009.

vi. Bakolas, E. and Tsiotras, P., "Minimum-Time Paths for a Light Aircraft in the Presence of Regionally-Varying Strong Winds," in *Proceedings of AIAA Infotech "AT" Aerospace*, Atlanta, Georgia, AIAA 2010–3380, 2010.

vii. Bakolas, E. and Tsiotras, P., "Time-Optimal Synthesis for the Zermelo-Markov-Dubins Problem: The Constant Wind Case," in *Proceedings of 2010 American Control Conference*, Baltimore, MD, pp. 6163–6163, June 30–July 2, 2010.

viii. Bakolas, E. and Tsiotras, P., "The Zermelo-Voronoi Diagram: a Dynamic Partition Problem," in *Proceedings of 2010 American Control Conference*, Baltimore, MD, pp. 1320–1325, June 30–July 2, 2010.

ix. Bakolas, E. and Tsiotras, P., "Optimal Pursuit of Moving Targets using Dynamic Voronoi Diagrams," in *Proceedings of 49th IEEE Decision and Control Conference*, Atlanta, GA, pp. 7431–7436, December 15–17, 2010.

x. Bakolas, E. and Tsiotras, P., "Optimal Pursuer and Moving Target Assignment using Dynamic Voronoi Diagrams," in *Proceedings of 2011 American Control Conference*, San Francisco, CA, pp. 5444–5449 June 29–July 1, 2011.

xi. Bakolas, E. and Zhao, Y. and Tsiotras, P., "Initial Guess Generation for Aircraft Landing Trajectory Optimization," in *Proceedings of AIAA Guidance and Control Conference and Exhibit*, Portland, OR, August 8–11, 2011.

xii. Bakolas, E. and Tsiotras, P., "Relay Pursuit of a Maneuvering Target by a Group of Pursuers," in *Proceedings of 50th IEEE Conference on Decision and Control*, Orlando, FL, December 12–15, 2011 (Note: Accepted)

REFERENCES

[1] Merriam Webster Dictionary. http://www.merriam-webster.com/dictionary/.

[2] Albers, G., Guibas, L. J., Mitchell, J. S. B., and Roos, T., "Voronoi diagrams of moving points," *International Journal of Computational Geometry and Applications*, vol. 8, no. 3, pp. 365–380, 1998.

[3] Arslan, G., Marden, J. R., and Shamma, J. S., "Autonomous vehicle-target assignment: a game-theoretical formulation," *Transactions of the ASME*, vol. 129, no. 5, pp. 584–596, 2007.

[4] Athans, M. and Falb, P. L., "Time-optimal control for a class of nonlinear systems," *IEEE Transactions on Automatic Control*, vol. AC-8, no. 1, p. 379, 1963.

[5] Athans, M. and Falb, P. L., *Optimal Control, An Introduction to the Theory and Its Applications*. New York: Dover Publications, 2007.

[6] Aurenhammer, F., "Voronoi diagrams: A survey of a fundamental geometric data structure," *ACM Computing Surveys*, vol. 23, no. 3, pp. 345–405, 1991.

[7] Bacciotti, A., *Local Stabilizability of Nonlinear Control Systems*. New Jersey: World Scientific, 1992.

[8] Backer, J. and Kirkpatrick, D., "Finding curvature-constrained paths that avoid polygonal obstacles," in *SCG '07*, (Gyeongju, South Korea), pp. 66–73, June 2007.

[9] Bakolas, E. and Tsiotras, P., "On-line, kinodynamic trajectory generation through rectangular channels using path and motion primitives," in *Proceedings of 48th IEEE Conference on Decision and Control*, (Cancun, Mexico), pp. 3725–3730, Dec. 8–11, 2008.

[10] Bakolas, E. and Tsiotras, P., "The asymmetric sinistral/dextral Markov-Dubins problem," in *Proceedings of the 48th IEEE Conference on Decision and Control*, (Shanghai, China), pp. 5649–5654, Dec. 15–18, 2009.

[11] Bakolas, E. and Tsiotras, P., "On the generation of nearly optimal, planar paths of bounded curvature and bounded curvature gradient," in *Proceedings of the American Control Conference*, (St. Louis, MO), pp. 385–390, June 10–12, 2009.

[12] Bakolas, E. and Tsiotras, P., "Minimum-time paths for a light aircraft in the presence of regionally-varying strong winds," in *AIAA Infotech at Aerospace*, (Atlanta, GA), April 20–22, 2010. AIAA Paper 2010-3380.

[13] Bakolas, E. and Tsiotras, P., "Optimal pursuit of moving targets using dynamic Voronoi diagrams," in *Proceedings of IEEE International Conference on Decision and Control*, (Atlanta, GA), pp. 7431–7436, December 15–17, 2010.

[14] Bakolas, E. and Tsiotras, P., "The Zermelo-Voronoi diagram: a dynamic partition problem," *Automatica*, vol. 46, no. 12, pp. 2059–2067, 2010.

[15] Bakolas, E. and Tsiotras, P., "Time-optimal synthesis for the Zermelo-Markov-Dubins problem: the constant wind case," in *Proceedings of American Control Conference*, (Baltimore, MD), pp. 6163–6168, June 30–July 2, 2010.

[16] Bakolas, E. and Tsiotras, P., "Feedback navigation in an uncertain flowfield and connections with pursuit strategies," *Journal of Guidance, Control and Dynamics*, 2011. Accepted.

[17] Bakolas, E. and Tsiotras, P., "Optimal pursuer and moving target assignment using dynamic Voronoi diagrams," in *Proceedings of the American Control Conference*, (San Francisco, CA), pp. 5444–5449, June 29–July 1, 2011.

[18] Bakolas, E. and Tsiotras, P., "Optimal synthesis of the asymmetric sinistral/dextral Markov-Dubins problem," *Journal of Optimization Theory and Applications*, vol. 150, no. 2, pp. 233–250, 2011.

[19] Bakolas, E. and Tsiotras, P., "Relay pursuit of a maneuvering target by a group of pursuers," in *Proceeding of 50th IEEE Conference on Decision and Control*, (Orlando, FL), Dec. 12–15, 2011.

[20] Bakolas, E., Zhao, Y., and Tsiotras, "Initial guess generation for aircraft landing trajectory optimization," in *Proceeding of AIAA Guidance and Control Conference and Exhibit*, (Portland, OR), August 8–11, 2011.

[21] Balkcom, D. J. and Mason, M. T., "Time-optimal trajectories for bounded velocity differential drive vehicles," *The International Journal of Robotics Research*, vol. 21, pp. 199–217, March 2002.

[22] Balkcom, D. J. and Kavathekar, P. A. and Mason, M. T., "Time-optimal trajectories for an omni-directional vehicle," *The International Journal of Robotics Research*, vol. 25, pp. 985–999, October 2006.

[23] Bannikov, A. S., "A nonstationary group pursuit problem," *Russian Mathematics*, vol. 53, no. 5, pp. 1–9, 2009.

[24] Bardi, M., "Some applications of viscosity solutions to optimal control and differential games," *Viscosity Solutions and Applications. ser. Lecture Notes in Mathematics*, vol. 1660, pp. 44–97, 1995. I. Capuzzo-Dolcetta and P. L. Lions, Eds.

[25] Barraquand, J. and Latombe, J.-C., "Nonholonomic multibody mobile robots: Controllability and motion planning in the presence of obstacles," *Algorithmica*, vol. 10, no. 2–4, pp. 121–155, 1993.

[26] Bartle, R. G., *The Elements of Real Analysis*. New York: Wiley Sons Inc., second ed., 1976.

[27] Beard, R., McLain, T., Goodrich, M., and Anderson, E., "Coordinated target assignment and intercept for unmanned air vehicles," *IEEE Transactions on Robotics and Automation*, vol. 18, no. 6, pp. 911–922, 2002.

[28] Belta, C., Bicchi, A., Egerstedt, M., Frazzoli, E., Klavins, E., and Pappas, G. J., "Symbolic planning and control of robot motion [Grand Challenges of Robotics]," *IEEE Robotics and Automation Magazine*, vol. 14, no. 1, pp. 61–70, 2007.

[29] Bereg, S. and Kirkpatrick, D., "Curvature-bounded traversals of narrow corridors," in *Proceedings of the 21st Annual Symposium on Computational Geometry*, (Pisa, Italy), pp. 278–287, 2005.

[30] Berkovitz, L. D., "A variational approach to differential games," in *Advances in Game Theory*, (Princeton, NJ), pp. 127–174, Princeton University Press, 1964.

[31] Bhat, S. P. and Bernstein, D. S., "Continuous finite-time stabilization of the translational and rotational double integrators," *IEEE Transactions on Automatic Control*, vol. 43, no. 5, pp. 678–682, 1998.

[32] Blagodatskikh, A. I., "Group pursuit in Pontryagin's nonstationary example," *Differential Equations*, vol. 44, no. 1, pp. 40–46, 2008.

[33] Blagodatskikh, A. I., "Simultaneous multiple capture in a simple pursuit problem," *Journal of Applied Mathematics and Mechanics*, vol. 73, no. 1, pp. 36–40, 2009.

[34] Blanchini, F. and Miani, S., *Set-Theoretic Methods in Control*. New York, NY: Birkhäuser, 2008.

[35] Bloch, A. M., *Nonholonomic Mechanics and Control*. New York-Heidelberg-Berlin: Springer Verlag, 2003.

[36] Boissonnat, J.-D., "Geometric structures for three-dimensional shape representation," *ACM Transactions on Graphics*, vol. 3, no. 4, pp. 266–286, 1984.

[37] Boissonnat, J. D. and Bui, X. N., "Accessibility region for a car that only moves forward along optimal paths," Research Note 2181, Institut National de Recherche en Informatique et en Automatique, Sophia-Antipolis, France, 1994.

[38] Boissonnat, J.-D., Cérézo, A., and Leblond, J., "A note on shortest paths in the plane subject to a constraint on the derivative of the curvature," Research Note 2160, Institut National de Recherche en Informatique et en Automatique, 1994.

[39] Boissonnat, J.-D., Cérézo, A., and Leblond, J., "Shortest paths of bounded curvature in the plane," *Journal of Intelligent and Robotic Systems*, vol. 11, no. 1-2, pp. 5–20, 1994.

[40] Boissonnat, J.-D. and Yvinec, M., *Algorithmic Geometry*. Cambridge, United Kingdom: Cambridge University Press, 1998.

[41] Boissonnat, J.-D., Cérézo, A., and Leblond, J., "A note on shortest paths in the plane subject to a constraint on the derivative of the curvature," Research Report 2160, INRIA, 1994.

[42] Bopardikar, S. D., Bullo, F., and Hespanha, J. P., "A cooperative homicidal chauffeur game," *Automatica*, vol. 45, no. 7, pp. 1771–1777, 2009.

[43] Bopardikar, S. D., Smith, L. S., and Bullo, F., "Vehicle placement to intercept moving targets," in *Proceedings of the American Control Conference*, (Baltimore, MD), pp. 5538–5543, June 30–July 2, 2010.

[44] Bryson, A. E. and Ho, Y. C., *Applied Optimal Control*. Waltham, MA: Blaisdell Publication, 1969.

[45] Bui, X. N. and Boissonnat, J. D., "The shortest paths synthesis for nonholonomic robots moving forwards," Research Note 2153, Institut National de Recherche en Informatique et en Automatique, Sophia-Antipolis, France, 1993.

[46] Bui, X. N., Souères, P., Boissonnat, J. D., and Laumond, J. P., "Shortest path synthesis for Dubins nonholonomic robot," in *Proceedings of the 11th IEEE Intern. Conf. on Robotics and Automation (ICRA)*, (San Diego, California), 1994.

[47] Bullo, F., Cortés, J., and Martinez, S., *Distributed Control of Robotic Networks*. Applied Mathematics Series, Princeton, 2009.

[48] Bullo, F., Frazzoli, E., Pavone, M., Savla, K., and Smith, S. *Proceeedings of the IEEE*, vol. 99, no. 9, pp. 1482–1504.

[49] Bullo, F. and Lewis, A. D., *Geometric Control of Mechanical Systems*. New York-Heidelberg-Berlin: Springer Verlag, 2004.

[50] Carathéodory, C., *Calculus of Variations and Partial Differential Equations of First Order*. Washington DC: American Mathematical Society, third ed., 1999.

[51] Case, J. H., "Towards a theory of many player differential games," *SIAM Journal on Control and Optimization*, vol. 7, pp. 179–197, 1969.

[52] Ceccarelli, N., Enright, J. J., Frazzoli, E., Rasmussen, S. J., and Schumacher, C. J., "Micro UAV path planning for reconnaisance in wind," in *Proceedings of the 2007 American Control Conference*, (Evanston, IL), pp. 5310–5315, July 2007.

[53] Cesari, M., *Optimization - Theory and Applications. Problems with Ordinary Differential Equations*. New York: Springer-Verlag, 1983.

[54] Chang, A., Brazil, M., Rubinstein, J., and Thomas, D., "Curvature-constrained directional-cost paths in the plane," *Journal of Global Optimization*. In press.

[55] Chebotarev, P. Y. and Agaev, R. P., "Coordination in multiagent systems and Laplacian spectra of digraphs," *Autom. Remote Control*, vol. 70, pp. 469–483, March 2009.

[56] Chitour, Y. and Sigalotti, M., "Dubins' problem on surfaces. I Nonnegative curvature," *The Journal of Geometric Analysis*, vol. 15, no. 4, pp. 565–587, 2005.

[57] Chitsaz, H. and LaValle, S. M., "Time-optimal paths for a Dubins airplane," in *Proceedings of 46th IEEE Conference on Decision and Control*, (New Orleans, LA), pp. 2379–2384, Dec. 12–14, 2007.

[58] Cockayne, E. J., "Plane pursuit with curvature constraints," *SIAM Journal on Applied Mathematics*, vol. 15, no. 6, pp. 1511–1516, 1967.

[59] Cockayne, E. J. and Hall, W. C., "Plane motion of a particle subject to curvature constraints," *SIAM Journal on Control*, vol. 13, no. 1, pp. 197–220, 1975.

[60] Corpetti, T., Mémin, E., and Pérez, P., "Extraction of singular points from dense motion fields: An analytic approach," *Journal of Mathematical Imaging and Vision*, vol. 19, no. 3, pp. 175–198, 2003.

[61] Cortés, J. and Bullo, F., "Coordination and geometric optimization via distributed dynamical systems," *SIAM Journal of Optimization and Control*, vol. 44, no. 5, pp. 1543–1574, 2005.

[62] Cortés, J., Martinez, S., and Bullo, F., "Spatially-distributed coverage optimization and control with limited-range interactions," *ESAIM: COCV*, vol. 11, no. 4, pp. 691–719, 2005.

[63] Cortés, J., Martinez, S., Karatas, T., and Bullo, F., "Coverage control for mobile sensing networks," *IEEE Transactions on Robotics and Automation*, vol. 20, no. 2, pp. 243–255, 2004.

[64] Cowlagi, R. V. and Tsiotras, P., "On the existence and synthesis of curvature-bounded paths through narrow rectangular channels," in *Proceedings of the 2010 American Control Conference*, (Baltimore, MD), June, 30–July, 2 2010.

[65] Cowlagi, R. V. and Tsiotras, P., "Hierarchical motion planning with dynamical feasibility guarantees for mobile robotic vehicles," *IEEE Transactions on Robotics*, 2011. In press.

[66] Davis, R. E., Leonard, N. E., and Fratantoni, D. M., "Routing strategies for underwater gliders," *Deep Sea Research Part II: Topical Studies in Oceanography*, vol. 56, no. 3–5, pp. 173–187, 2009.

[67] Demetriou, M. A. and Hussein, I. I., "Estimation of spatially distributed processes using mobile spatially distributed sensor network," *SIAM Journal on Control and Optimization*, vol. 48, no. 1, pp. 266–291, 2009.

[68] Desai, J., Ostrowski, J., and Kumar, V., "Modeling and control of formations of nonholonomic mobile robots," *IEEE Trans. Robot. Autom.*, vol. 17, no. 6, pp. 905–908, 2001.

[69] Devillers, O. and Golin, M., "Dog bites postman: Point location in the moving Voronoi diagram and related problems," in *Proceedings of 1st Annual European Symposium on Algorithms (ESA '93)*, pp. 133–144, 1993.

[70] Devillers, O., Golin, M., Kedem, K., and Schirra, S., "Queries on Voronoi diagrams of moving points," *Computational Geometry*, vol. 6, no. 5, pp. 315–327, 1996.

[71] Dimarogonas, D. V. and Kyriakopoulos, K. J., "On the rendezvous problem for multiple nonholonomic agents," *IEEE Transactions on Automatic Control*, vol. 52, no. 5, pp. 916–922, 2007.

[72] Dirichlet, G. L., "Über die Reduktion der Positiven Quadratischen Formen mit drei Unbestimmten Ganzen Zahlen," *Journal für die Reine und Angewandte Mathematik*, vol. 40, pp. 209–227, 1850.

[73] Dolinskaya, I. S., *Optimal path finding in direction, location and time dependent environments*. Ph.D. dissertation, Industrial and operations engineering, The University of Michigan, Ann Arbor, MI, 2009.

[74] Dolinskaya, I. S. and Smith, L. R., "Fastest-path planning for direction dependent speed function," Research Note 08-02, University of Michigan, Ann Arbor, MI, 2008.

[75] Dong, H. S. and Sanjiv, S., "Path generation for robot vehicles using composite clothoid segments," Research Note CMU-RI-TR-90-312, Carnegie Mellon University, Pittsburgh, PA, 1994.

[76] Du, Q., Faber, V., and Gunzburger, M., "Centroidal Voronoi tessellations: Applications and algorithms," *SIAM Review*, vol. 41, no. 4, pp. 637–676, 1999.

[77] Dubins, L. E., "On curves of minimal length with a constraint on average curvature, and with prescribed initial and terminal positions and tangents," *American Journal of Mathematics*, vol. 79, no. 3, pp. 497–516, 1957.

[78] Ducard, G. Kulling, K. and Gering, H., "Evaluation of reduction in the performance of a small UAV after an aileron failure for an adaptive guidance system," in *Proceedings of the 2007 American Control Conference*, (New York City, N.Y.), pp. 1793–1798, July 11–13, 2007.

[79] Eun, Y. and Bang, H., "Cooperative control of multiple unmanned aerial vehicles using the potential field theory," in *Proceedings of the American Control Conference*, vol. 43, pp. 691–719, June 14–16, 2006.

[80] Fortune, S., "A sweepline algorithm for Voronoi diagrams," *Algorithmica*, vol. 2, no. 1–4, pp. 153–174, 1987.

[81] Fraichard, T. and Scheuer, A., "From Reeds and Shepp's to continuous-curvature paths," *IEEE Transactions on Robotics*, vol. 20, no. 6, pp. 1025–1035, 2004.

[82] Friedman, A., *Differential Games*. Mineola, N.Y.: Dover Publication, second ed., 2006.

[83] Furtuna, A. A. and Balkcom, D. J., "Generalizing Dubins curves: Minimum-time sequences of body-fixed rotations and translations in the plane," *The International Journal of Robotics Research*, vol. 29, pp. 703–726, May 2010.

[84] Gallier, J., *Geometric Methods and Applications: for Computer Science and Engineering*. New York, USA: Springer-Verlag, 2000.

[85] Gavrilova, M. L. and Rokne, J., "Updating the topology of the dynamic Voronoi diagram for spheres in Euclidean d-dimensional space," *Computer Aided Geometric Design*, vol. 20, no. 4, pp. 231–242, 2003.

[86] Getis, A. and Boots, B., *Models of Spatial Processes: An Approach to the Study of Point, Line and Area Patterns*. Cambridge, UK: Cambridge University Press, 1978.

[87] Giordano, P. L. and Vendittelli, M., "Shortest paths to obstacles for a polygonal Dubins car," *IEEE Transanctions on Robotics*, vol. 25, no. 5, pp. 1184–1191, 2009.

[88] Glendinning, P., "The mathematics of motion camouflage," *Proceedings of the Royal Society B*, vol. 271, no. 1538, pp. 477–481, 2004.

[89] Glizer, J. Y., "Optimal planar interception with fixed end conditions: A closed-form solution," *Journal of Optimization Theory and Applications*, vol. 88, no. 3, pp. 503–539, 1996.

[90] Glizer, J. Y., "Optimal planar interception with fixed end conditions: Approximate solutions," *Journal of Optimization Theory and Applications*, vol. 93, no. 1, pp. 1–25, 1997.

[91] Green, P. J. and Sibson, R. R., "Computing Dirichlet tessellations in the plane," *Computer Journal*, vol. 21, no. 2, pp. 168–173, 1978.

[92] Guo, J., Yan, G., and Lin, Z., "Local control strategy for moving-target-enclosing under dynamically changing network topology," *Systems & Control Letters*, vol. 59, no. 10, pp. 654–661, 2010.

[93] Hajek, O., *Pursuit Games: An Introduction to the Theory and Applications of Differential Games of Pursuit and Evasion*. Mineola, New York: Dover Publications, second ed., 2008.

[94] Hernadez, S. and Paley, D. A., "Three-dimensional motion coordination in a spatiotemporal flowfield," *IEEE Trans. Automatic Control*, vol. 55, no. 12, pp. 2805–2810, 2010.

[95] Hinote, C., "Centralized control and decentralized execution. A catchphrase in crisis?," Research Paper 2009-1, Air Force Research Institute, 2009.

[96] Ho, Y. C., Bryson, A. E. J., and Baron, S., "Differential games and optimal pursuit-evasion strategies," *IEEE Transactions on Automatic Control*, vol. AC-10, no. 4, pp. 385–389, 1965.

[97] Hwang, Y. K. and Ahuga, N., "Gross motion-planning–a survey," *ACM Computing Surveys*, vol. 24, no. 3, pp. 219–291, 1992.

[98] Isaacs, R., "Games of pursuit," RAND Report P-257, RAND Corporation, Santa Monica, CA, 1951.

[99] Isaacs, R., *Differential Games. A Mathematical Theory with Applications to Warfare and Pursuit, Control and Optimization*. New York: Dover Publication, 1999.

[100] Jadbabaie, A., Lin, J., and Morse, A. S., "Coordination of groups of mobile agents using nearest neighbor rules," *IEEE Transactions on Automatic Control*, vol. 48, no. 6, pp. 988–1001, 2003.

[101] Jin, Y., Liao, Y., Minai, A. A., and Polycarpou, M. M., "Balancing search and target response in cooperative unmanned aerial vehicle (UAV) teams," *IEEE Transactions on Systems, Man, and Cybernetics, Part B: Cybernetics*, vol. 36, no. 3, pp. 571–587, 2005.

[102] Jurdjevic, V., *Geometric Control Theory*. New York: Cambridge University Press, 1997.

[103] Justh, E. and Krishnaprasad, P., "Equilibria and steering laws for planar formations," *Systems & Control Letters*, vol. 52, no. 1, pp. 25–38, 2004.

[104] Kanayama, Y. and Miyake, N., "Trajectory generation for mobile robots," in *Robotic Research: The Third International Symposium on Robotics Research*, (Gouvieux, France), pp. 333–340, 1985.

[105] Kelly, A. and Stentz, A., "Analysis of requirements for high speed rough terrain autonomous mobility. part II: Resolution and accuracy," in *Proceedings of the International Conference on Robotics and Automation (ICRA)*, vol. 4, pp. 3326–3333, 1997.

[106] Kim, T.-H. and Sugie, T., "Cooperative control for target-capturing task based on a cyclic pursuit strategy," *Automatica*, vol. 43, no. 8, pp. 1426–1431, 2007.

[107] Kim, Y., Gu, D.-W., and Postlethwaite, I., "Real-time optimal mission scheduling and flight path selection," *IEEE Transactions on Automatic Control*, vol. 52, no. 6, pp. 1119–1123, 2007.

[108] Kopparty, S. and Ravishankar, C. V., "A framework for pursuit evasion games in Rn," *Inf. Process. Lett.*, vol. 96, no. 3, pp. 114–122, 2005.

[109] Kostov, V. P. and Degtiariova-Kostova, E. V., "The planar motion with bounded derivative of the curvature and its suboptimal paths," Research Note 2189, Institut National de Recherche en Informatique et en Automatique (INRIA), Sophia-Antipolis, France, 1994.

[110] Latombe, J.-C., *Robot Motion Planning*. Boston, MA: Kluwer Academic Publishers, 1991.

[111] Lavalle, S. M., *Planning Algorithms*. New York, NY: Cambridge University Press, 2006.

[112] Lee, E. B. and Markus, L., *Foundations of Optimal Control Theory*. Malabar, Florida: Krieger Publishing Company, second ed., 1986.

[113] Liberzon, D., *Switching in Systems and Control*. Boston, MA: Birkhäuser, 2003.

[114] Lin, Z., Broucke, M., and Francis, B., "Local control strategies for groups of mobile autonomous agents," *Systems & Control Letters*, vol. 55, no. 11, pp. 918–928, 2006.

[115] Liscano, R. and Green, D., "Trajectory generation for mobile robots," in *Proceedings of IEEE-RSJ International Conference on Intelligent Robotics and Systems*, (Tsukuba, Japan), pp. 380–385, 1989.

[116] Lloyd, S. P., "Least squares quantization in pcm," *IEEE Transactions on Information Theory*, vol. 28, no. 2, pp. 129–137, 1982.

[117] Lua, C. A., Altenburg, K., and Nygard, K. E., "Synchronized multipoint attack by autonomous reactive vehicles with simple local communication," in *Proceedings of the 2003 IEEE Swarm Intelligence Symposium (SIS '03)*, pp. 95–102, April 24–26, 2003.

[118] Luce, R. D. and Raiffa, H., *Games and Decisions*. New York, NY: John Wiley and Sons, 1957.

[119] Mannor, S. and Shamma, J. S., "Multi-agent learning for engineers," *Artif. Intell.*, vol. 171, no. 7, pp. 417–422, 2007.

[120] Martinez, S., "Distributed interpolation schemes for field estimation by mobile sensor networks," *IEEE Transactions on Control Systems Technology*, vol. 18, no. 2, pp. 491–500.

[121] Martinez, S., "Distributed representation of spatial fields through an adaptive interpolation scheme," in *Proceedings of the American Control Conference*, (New York, NY), pp. 2750–2755, June 25–27, 2007.

[122] Martinez, S., Cortés, J., and Bullo, F., "Motion coordination with distributed information," *IEEE Control Systems Magazine*, vol. 27, no. 4, pp. 75–88, 2007.

[123] McGee, T. G. and Hedrick, J. K., "Optimal path planning with a kinematic airplane model," *Journal of Guidance, Control, and Dynamics*, vol. 30, no. 2, pp. 629–633, 2007.

[124] McLain, T. W. and Beard, R. W., "Trajectory planning for coordinated rendezvous of unmanned air vehicles," in *AIAA Guidance, Navigation, and Control Conference and Exhibit*, August, 14–17 2000.

[125] McLain, T. W., Chandler, P. R., Rasmussen, S., and Pachter, M., "Cooperative control of UAV rendezvous," in *Proceedings of the American Control Conference*, (Arlington, VA), pp. 2309–2314, June 25–27, 2001.

[126] McNeely, R. L., Iyer, R. V., and Chandler, P. R., "Tour planning for an unmanned air vehicle under wind conditions," *Journal of Guidance, Control, and Dynamics*, vol. 30, no. 5, pp. 1299–1306, 2007.

[127] Meek, D. S. and Walton, D. J., "A note on finding clothoids," *Journal of Computational and Applied Mathematics*, vol. 170, no. 2, pp. 433–453, 2004.

[128] Merz, A. W., *Homicidal Chauffeur - A Differential Game*. PhD thesis, Stanford University, 1971.

[129] Merz, A. W., "The game of two identical cars," *Journal of Optimization Theory and Applications*, vol. 9, no. 5, pp. 324–343, 1972.

[130] Mesbahi, M., "On state-dependent dynamic graphs and their controllability properties," vol. 50, no. 3, pp. 387–392, 2005.

[131] Mesbahi, M. and Egerstedt, M., *Graph Theoretic Methods in Multiagent Networks*. Applied Mathematics Series, Princeton, 2010.

[132] Mitchell, J. S. B., "An algorithmic approach to some problems in terrain navigations," *Artificial Intelligence*, vol. 37, no. 1–3, pp. 171–201, 1988.

[133] Mitchell, J. S. B. and Papadimitriou, C. H., "The weighted region problem: finding shortest paths through a weighted planar subdivision," *Journal of the Association for Computing Machinery*, vol. 38, no. 1, pp. 18–73, 1991.

[134] Mittenhuber, D., "Dubins' problem is intrinsically three-dimensional," *ESAIM: Control, Optimisation and Calculus of Variations*, vol. 3, pp. 1–22, 1998.

[135] Monroy-Pérez, F., "Non-euclidean Dubins' problem," *Journal of Dynamical and Control Systems*, vol. 4, no. 2, pp. 249–272, 1998.

[136] Moreau, L., "Stability of multiagent systems with time-dependent communication links," *IEEE Transactions on Automatic Control*, vol. 50, no. 2, pp. 169–182, 2005.

[137] Mostafavi, M. A., Gold, C., and Dakowicz, M., "Delete and insert operations in Voronoi/Delaunay methods and applications," *Computers & Geosciences*, vol. 29, no. 4, pp. 523–530, 2003.

[138] Nahin, P. J., *Chases and Escapes: The Mathematics of Pursuit and Evasion*. Princeton, NJ: Princeton University Press, 2007.

[139] Nishida, T. and Sugihara, K., "Voronoi diagram in the flow field," *Lecture Notes in Computer Science*, vol. 2906/2003, pp. 26–35, 2004.

[140] Nishida, T., Sugihara, K., and Kimura, M., "Stable marker-particle method for the Voronoi diagram in a flow field," *Journal of Computational and Applied Mathematics*, vol. 202, no. 2, pp. 377–391, 2007.

[141] Okabe, A., Boots, B., Sugihara, K., and Chiu, S. N., *Spatial Tessellations: Concepts and Applications of Voronoi Diagrams*. West Sussex, England: John Wiley and Sons Ltd, second ed., 2000.

[142] Olfati-Saber, R., Fax, J. A., and Murray, R. M., "Consensus and cooperation in networked multi-agent systems," *Proceedings of the IEEE*, vol. 95, no. 1, pp. 215–233, 2007.

[143] Olfati-Saber, R. and Shamma, J. S., "Consensus filters for sensor networks and distributed sensor fusion," in *44th IEEE Conference on Decision and Control and European Control Conference*, (Sevilla, Spain), Dec. 12–15, 2005.

[144] O'Rourke, J., *Computational Geometry in C*. Cambridge University Press, 1998.

[145] Paley, D. A. and Peterson, C., "Stabilization of collective motion in a time-invariant flowfield," *Journal of Guidance, Control and Dynamics*, vol. 32, no. 3, pp. 771–779, 2009.

[146] Patsko, V. S. and Turova, V. L., "Numerical study of the "homicidal chauffeur" differential game with the reinforced pursuer," *Game Theory and Applications*, vol. 12, pp. 123–152, 2007.

[147] Pavone, M., Arsie, A., Frazzoli, E., and Bullo, F., "Distributed algorithms for environment partitioning in mobile robotic networks," *IEEE Transactions on Automatic Control*, vol. 56, no. 8, pp. 1834–1848, 2011.

[148] Peterson, C. and Paley, D. A., "Multi-vehicle coordination in an estimated time-varying flowfield," *Journal of Guidance, Control and Dynamics*, vol. 34, no. 1, pp. 177–191, 2011.

[149] Petres, C., Pailhas, Y., Patron, P., Petillot, Y., Evans, J., and Lane, D., "Path planning for autonomous underwater vehicles," *IEEE Transactions on Robotics*, vol. 23, no. 2, pp. 331–341, 2007.

[150] Petrich, J., Woosley, C. A., and Stilwell, D. J., "Planar flow identification for improved navigation of small AUVs," *Ocean Engineering*, vol. 36, no. 1, pp. 119–131, 2009.

[151] Petrosjan, L. A. and Murzov, N. V., "Game-theoretic problems in mechanics," *Litovsk. Mat. Sb.*, vol. 6, pp. 423–433, 1966.

[152] Petrov, N. N. and Shuravina, I. N., "On the "soft" capture in one group pursuit problem," *Journal of Computer and Systems Sciences International*, vol. 48, no. 4, pp. 521–526, 2009.

[153] Pinchard, O., L. A. and Pougnet, F., "Generalized polar polynomials for vehicle path generation with dynamic constraints," in *Proceedings of the IEEE International Conference on Robotics and Automation*, vol. 1, (Minneapolis MN, U.S.A.), pp. 915–920, 1996.

[154] Pittsyk, M. and Chikrii, A. A., "On a group pursuit problem," *Journal of Applied Mathematics and Mechanics*, vol. 46, no. 5, pp. 584–589, 1982.

[155] Plaku, E., Kavraki, L. E., and Vardi, M. Y., "Motion planning with dynamics by a synergistic combination of layers of planning," *IEEE Transactions on Robotics*, vol. 26, no. 3, pp. 469–482, 2011.

[156] Pontryagin, L. S., *Selected Scientific Papers*, vol. 2. Moscow: Nauka, 1988. (In Russian).

[157] Porat, B. and Nehorai, A., "Localizing vapor-emitting sources by moving sensors," *IEEE Transactions on Signal Processing*, vol. 44, no. 4, pp. 1018–1021, 1996.

[158] Prokopovich, P. V. and Chikrii, A. A., "A linear evasion problem for interacting groups of objects," *Journal of Applied Mathematics and Mechanics*, vol. 58, no. 4, pp. 583–591, 1995.

[159] Pshenichnyi, B. N., "Simple pursuit by several pursuers," *Kibernetika*, vol. 3, pp. 145–146, 1976.

[160] Qing, H. and Haddad, W. M., "Distributed nonlinear control algorithms for network consensus," *Automatica*, vol. 44, no. 9, pp. 2375–2381, 2008.

[161] Rao, A. V., Benson, D. A., Darby, C., Patterson, M. A., Francolin, C., Sanders, I., and Huntington, G. T., "Algorithm 902: GPOPS, a MATLAB software for solving multiple-phase optimal control problems using the gauss pseudospectral method," *ACM Trans. Math. Softw.*, vol. 37, no. 2, pp. 22:1–22:39, 2010.

[162] Rappoport, I. S. and Chikrii, A. A., "Guaranteed result in a differential game of group pursuit with terminal payoff function," *Journal of Applied Mathematics and Mechanics*, vol. 61, no. 4, pp. 567–576, 1997.

[163] Reeds, A. J. and Shepp, R. A., "Optimal paths for a car that goes both forward and backwards," *Pacific Journal of Mathematics*, vol. 145, no. 2, pp. 367–393, 1990.

[164] Ren, W., Beard, R., and Atkins, E., "Information consensus in multivehicle cooperative control," *IEEE Control Systems Magazine*, vol. 27, no. 2, pp. 71–82, 2007.

[165] Reynolds, C. W., "Flocks, herds, and schools: A distributed behavioral model, in computer graphics," in *Proceedings of SIGGRAPH '87*, vol. 21, pp. 25–34, 1987.

[166] Reynolds, C. W., "Steering behaviors for autonomous characters," in *Proceedings of Game Developers Conference*, 1999.

[167] Rhoads, B., Mezić, I., and Poje, A., "Minimum time feedback control of autonomous underwater vehicles," in *Proceedings of 49th IEEE Conference on Decision and Control*, (Atlanta, GA), pp. 5828–5834, December 15–17, 2010.

[168] Roos, T., "Voronoi diagrams over dynamic scenes," *Discrete Appl. Math*, vol. 43, no. 4, pp. 243–259, 1998.

[169] Rowe, N. C. and Alexander, R. S., "Finding optimal-path maps for path planning across weighted regions," *The International Journal of Robotics Research*, vol. 19, pp. 83–95, 2000.

[170] Rowe, N. C. and Richbourg, R. F., "An efficient Snell's law method for optimal-path planning across multiple two-dimensional irregular homogeneous-cost regions," *The International Journal of Robotics Research*, vol. 9, no. 6, pp. 48–66, 1990.

[171] Rowe, N. C. and Ross, R. S., "Optimal grid-free path planning across arbitrarily contoured terrain with anisotropic friction and gravity effects," *IEEE Transactions on Robotics and Automation*, vol. 6, no. 5, pp. 540–553, 1990.

[172] Rublein, G. T., "On pursuit with curvature constraints," *SIAM Journal on Control*, vol. 10, pp. 37–39, 1972.

[173] Sagan, H., *Introduction to the Calculus of Variations*, vol. 24. New York: Dover Publications, 1992.

[174] Sanfelice, R. G. and Frazzoli, E., "On the optimality of Dubins paths across heterogeneous terrain," in *HSCC '08: Proceedings of the 11th Intern. Workshop on Hybrid Systems*, (Berlin, Heidelberg), pp. 457–470, Springer-Verlag, 2008.

[175] Savla, K., Bullo, F., and Frazzoli, E., "The coverage problem for loitering Dubins vehicles," in *Proceedings of the 46th IEEE Conference on Decision and Control*, (New Orleans, LA), pp. 1398–1403, December 12–14, 2007.

[176] Scheuer, A. and Laugier, C., "Planning sub-optimal and continuous-curvature paths for car-like robots," in *Proceedings of IEEE-RSJ International Conference on Intelligent Robotics and Systems*, (Victoria BC, (Canada)), pp. 25–31, October 1998.

[177] Schollig, A., Caines, P. E., Egerstedt, M., and Malhame, R. P., "A hybrid Bellman equation for systems with regional dynamics," in *Proceedings of the 46th IEEE Conference on Decision and Control*, (New Orleans, LA), pp. 3393–3398, December 12–14, 2007.

[178] Sekhavat, S. and Laumond, J.-P., "Topological property for collision-free nonholonomic motion planning: The case of sinusoidal inputs for chained form systems," *IEEE Transactions on Robotics and Automation*, vol. 14, pp. 671–680, October 1998.

[179] Sellen, J., "Direction weighted shortest path planning," in *Proceedings of the 46th IEEE International Conference on Robotics and Automation*, (Nagoya, Aichi, Japan), pp. 1970–1975, May 21–27, 1995.

[180] Sepulchre, R., Paley, D. A., and Leonard, N. E., "Stabilization of planar collective motion: All-to-all communication," *IEEE Transactions on Automatic Control*, vol. 52, no. 5, pp. 811–824, 2007.

[181] Sepulchre, R., Paley, D. A., and Leonard, N. E., "Stabilization of planar collective motion with limited communication," *IEEE Transactions on Automatic Control*, vol. 53, no. 3, pp. 706–719, 2008.

[182] Serres, U., "On the curvature of two-dimensional optimal control systems and Zermelo's navigation problem," *Journal of Mathematical Sciences*, vol. 135, no. 4, pp. 3224–3243, 2006.

[183] Sethian, J. A., *Level Set Methods and Fast Marching Methods*. Cambridge: Cambridge University Press, second ed., 1999.

[184] Sgall, J., "Solution of David Gale's lion and man problem," *Theor. Comput. Sci.*, vol. 259, no. 1–2, pp. 663–670, 2001.

[185] Shaikh, M. S. and Caines, P. E., "On the hybrid control problem: theory and algorithms," *IEEE Transactions on Automatic Control*, vol. 52, no. 9, pp. 1587–1603, 2007.

[186] Shneydor, N. A., *Missile Guidance and Pursuit: Kinematics, Dynamics and Control*. West Sussex, England: Horwood Publishing, 1998.

[187] Shoham, Y. and Leyton-Brown, K., *Multiagent Systems: Algorithmic, Game-Theoretic, and Logical Foundations*. New York, NY: Cambridge University Press, 2009.

[188] Sigalotti, M. and Chitour, Y., "On the controllability of the Dubins' problem for surfaces. II Negative curvature," *SIAM J. Control Optim.*, vol. 45, no. 2, pp. 457–482, 2006.

[189] Singh, R. and Green, D. H., "Position based path tracking for wheeled mobile robots," in *Proceedings of IEEE-RSJ International Conference on Intelligent Robotics and Systems*, (Tsukuba, Japan), pp. 386–391, 1989.

[190] Souères, P. Fourquet, J.-Y. and Laumond, J.-P., "Set of reachable positions for a car," *IEEE Transactions on Automatic Control*, vol. 39, no. 8, pp. 1626–1630, 1994.

[191] Soulignac, M., "Feasible and optimal path planning in strong current fields," *IEEE Transactions on Robotics*, vol. 27, no. 1, pp. 89–98, 2011.

[192] Srinivasan, M. V. and Davey, M., "Strategies for active camouflage of motion," *Proceedings of the Royal Society B*, vol. 259, no. 1354, pp. 19–25, 1995.

[193] Starr, A. W. and Ho, Y. C., "Non-zero sum differential games," *Journal of Optimization Theory and Applications*, vol. 3, no. 3, pp. 183–206, 1969.

[194] Sugihara, K., "Voronoi diagrams in a river," *International Journal of Computational Geometry and Applications*, vol. 2, no. 1, pp. 29–48, 1992.

[195] Sugihara, K. and Iri, M., "Construction of the Voronoi diagram for "one million" sites in single-precision arithmetic," *Proc. IEEE*, vol. 80, no. 9, pp. 1471–1484, 1992.

[196] Sussmann, H. J., "Shortest 3-dimensional path with a prescribed curvature bound," in *Proceedings of 34th IEEE Conference on Decision and Control*, (New Orleans, LA), pp. 3306–3312, Dec. 1995.

[197] Sussmann, H. J., "Some recent results on the maximum principle of optimal control theory," *Systems and Control in the Twenty-First Century*, vol. 37, pp. 351–372, 1997.

[198] Sussmann, H. J., "The Markov-Dubins problem with angular acceleration control," in *Proceedings of 36th IEEE Conference on Decision and Control*, (San Diego, CA), pp. 2639–2643, Dec. 1997.

[199] Sussmann, H. J. and Tang, G., "Shortest paths for the Reeds-Shepp car: a worked out example of the use of geometric tecnhiques in nonlinear optimal control," Research Note SYCON-91-10, Rutgers University, New Brunswick, NJ, 1991.

[200] Techy, L. and Woosley, C. A., "Minimum-time path-planning for unmanned aerial vehicles in steady uniform winds," *Journal of Guidance, Control, and Dynamics*, vol. 32, no. 6, pp. 1736–1746, 2009.

[201] Thomaschewski, B., "Dubins' problem for the free terminal direction," *Preprint*, pp. 1–14, 2001.

[202] Ucinski, D., "Optimal sensor location for parameter estimation of distributed processes," *International Journal of Control*, vol. 73, no. 13, pp. 1235–1248, 2000.

[203] Venditelli, M., Laumond, J.-P., and Nissoux, C., "Obstacle distance for car-like robots," *IEEE Transactions on Robotics and Automation*, vol. 15, no. 4, pp. 678–691, 1999.

[204] Vincent, L. T. and Grantham, W. J., *Nonlinear and Optimal Control Systems*. New York, NY: Wiley–Interscience, 1997.

[205] Voronoi, G. F., "Nouveles applications des paramètres continus à la théorie de formas quadratiques," *Journal für die Reine und Angewandte Mathematik*, vol. 134, pp. 198–287, 1908.

[206] Šiljak, D. D., *Decentralized Control of Complex Systems*. Mathematics in Science and Engineering, San Diego, CA: Academic Press, INC., 1991.

[207] Šiljak, D. D., *Large-Scale Dynamic Systems Stability & Structure*. Mineola, NY: Dover, 2007.

[208] Wang, X., Cruz Jr, J. B., Chen, G., Pham, K., and Blasch, E., "Formation control in multi-player pursuit evasion games with superior evaders," in *SPIE's Defense Transformation and Net–Centric Systems Conference*, vol. 6578, (Orlando, FL), April 9–13, 2007.

[209] Yeung, D. W. K. and Petrosyan, L. A., *Cooperative Stochastic Differential Games*. New York, NY: Springer, 2006.

[210] Zermelo, E., "Über das Navigationproble bei ruhender oder veränderlicher Windverteilung," *Zeitschrift für Angewandte Mathematik und Mechanik*, vol. 11, no. 2, pp. 114–124, 1931.

[211] Zhang, F. and Leonard, N. E., "Cooperative filters and control for cooperative exploration," *IEEE Transactions on Automatic Control*, vol. 55, no. 3, pp. 911–922, 2010.

VITA

Efstathios Bakolas received the Diploma in Mechanical Engineering from the National Technical University of Athens, Greece, in 2004 and the MS. in Aerospace Engineering from Georgia Institute of Technology, Atlanta, in 2007. He is currently a Ph.D. candidate at the Georgia Institute of Technology. His main research interests include group pursuit-evasion games, motion planning, guidance, and control of autonomous vehicles using concepts and tools from optimal control theory, calculus of variations, analysis of nonlinear systems, and differential game theory.